Vol. 97 No. 2 April 1, 1978
Completing Vol. 97

ISSN 0003-2670

ANALYTICA CHIMICA ACTA

International journal devoted to all branches of analytical chemistry

ELSEVIER SCIENTIFIC PUBLISHING COMPANY

ANALYTICA CHIMICA ACTA

International journal devoted to all branches of analytical chemistry
Revue internationale consacrée à tous les domaines de la chimie analytique
Internationale Zeitschrift für alle Gebiete der analytischen Chemie

PUBLICATION SCHEDULE FOR 1978 (incorporating the section on Computer Techniques and Optimization).

	J	F	M	A	M	J	J	A	S	O	N	D
Analytica Chimica Acta	96/1	96/2	97/1	97/2	98/1	98/2	99/1	99/2	100	101/1	101/2	102
Section on Computer Techniques and Optimization			103/1			103/2			103/3			103/4

Scope. *Analytica Chimica Acta* publishes original papers, short communications, and reviews dealing with every aspect of modern chemical analysis, both fundamental and applied. The section on *Computer Techniques and Optimization* is devoted to new developments in chemical analysis by the application of computer techniques and by interdisciplinary approaches, including statistics, systems theory and operation research.

Submission of Papers. Manuscripts (three copies) should be submitted to:
for *Analytica Chimica Acta:* Dr. A. M. G. Macdonald, Department of Chemistry, The University, P.O. Box 363; Birmingham B15 2TT, England;
for the section on *Computer Techniques and Optimization:* Dr. J. T. Clerc, Laboratorium für Organische Chemie, Swiss Federal Institute of Technology, Universitätstrasse 16, CH-8092 Zürich, Switzerland.

Information for Authors. Papers in English, French and German are published. There are no page charges. Manuscripts should conform in layout and style to the papers published in this Volume. Authors should consult Vol. 93, p. 379 for detailed information. Reprints of this information are available from the Editors or from: Elsevier Editorial Services Ltd., Mayfield House, 256 Banbury Road, Oxford OX2 7DE (Great Britain).

Reprints. Fifty reprints will be supplied free of charge. Additional reprints (minimum 100) can be ordered. An order form containing price quotations will be sent to the authors together with the proofs of their article.

Advertisements. Advertisement rates are available from the publisher.

Subscriptions. Subscriptions should be sent to: Elsevier Scientific Publishing Company, P.O. Box 211, Amsterdam, The Netherlands. The section on *Computer Techniques and Optimization* can be subscribed to separately.

Publication. *Analytica Chimica Acta* (including the section on *Computer Techniques and Optimization*) appears in 8 volumes in 1978. The subscription for 1978 (Vols. 96–103) is Dfl. 1000.00 plus Dfl. 120.00 (postage) (Total approx. US $486.96). The subscription for the *Computer Techniques and Optimization* sections only (Vol. 103) is Dfl. 125 plus Dfl. 15.00 (postage) (Total approx. US $60.87). Journals are sent automatically by air mail to the U.S.A. and Canada at no extra cost and to Japan, Australia and New Zealand for a small additional postal charge. All earlier volumes (Vols. 1–87) are available at Dfl. 115.00 (plus postage).

Claims for issues not received should be made within three months of publication of the issue, otherwis they cannot be honoured free of charge.

Printed in The Netherlands

Statistical Treatment of Experimental Data

J. R. GREEN, *Lecturer in Computational and Statistical Science,* University of Liverpool, *and* D. MARGERISON, *Senior Lecturer in Inorganic, Physical and Industrial Chemistry, University of Liverpool.*

This book is intended for researchers wishing to analyse experimental data using statistical methods. Statistical concepts and methods which may be employed, are explained, and the ideas and reasoning behind statistical methodology clarified. Formal results are illustrated by many numerical worked examples mainly taken from the laboratory. Concepts, practical methodology, and worked examples are integrated in the text.

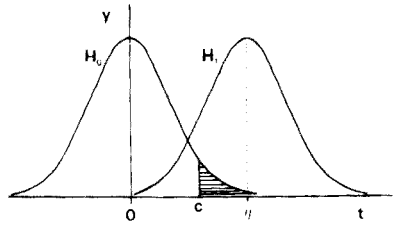

Consideration is given in this work to a large number of practical topics which are often omitted from standard texts. These include: obtaining an approximate confidence interval for a function of some unknown parameters; testing for outliers, stabilization of heterogeneous variances, and significant differences between means; estimation of parameters after performing tests; deciding what numbers of significant figures to quote for sample means and variances; straight-line and polynomial regression, through the origin or not, using weighted points, and testing the homogeneity of a set of such lines or curves.

The many examples provided throughout the text will serve as models for the various problems encountered by the readers when employing statistical methods to treat experimental data. Neither a strong mathematical background nor a prior knowledge of probability or statistics is required in order to make use of this work.

In addition to research workers in universities and industry, the book will be of use for first-year students of statistics, and will be especially suitable as the basis of a graduate course in experimental sciences.

Sept. 1977 xiv + 382 pages US $34.95/Dfl. 85.00 ISBN 0-444-41615-3

ELSEVIER

P.O. Box 211, Amsterdam
The Netherlands
52 Vanderbilt Ave
New York, N.Y. 10017

The Dutch guilder price is definitive. US $ prices are subject to exchange rate fluctuations.

7046

The Chemistry of Gold

RICHARD J. PUDDEPHATT, *Department of Inorganic, Physical and Industrial Chemistry, The University of Liverpool, U.K.*

TOPICS IN INORGANIC AND GENERAL CHEMISTRY, Monograph 16

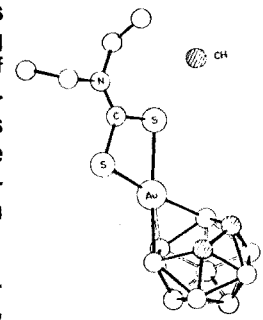

In recent years new applications of gold, such as its use in micro-electronic circuits, have been increasing rapidly. Recent developments also suggest the use of gold as a catalyst in the near future. Along with the expanding use of gold, there have been major advances in the chemistry of gold compounds. Thus, at a time when gold chemistry is undergoing an impressive renaissance, this book fills the need for a monograph covering all aspects of the subject.

This work covers gold chemistry in eleven chapters. The introductory chapter discusses the occurrence, isolation and properties of the element, the isotopes of gold, and the general principles which help to systematise gold chemistry. The second chapter deals with the binary compounds of gold. The co-ordination chemistry of gold is given thorough, up-to-date coverage in chapters on gold (I), gold (II), gold (III) and gold (V) complexes.

Separate chapters are devoted to organometallic compounds, metal-gold compounds, reaction mechanisms, and spectroscopic studies of gold because of the great interest shown toward these topics in recent years. The final chapter covers analytical methods for examining gold, as well as the various applications of gold compounds. The book is completed by an appendix which contains a compilation of gold-element bond lengths.

This work will serve as a reference source, not only for researchers in gold chemistry but also for all those interested in the applications of gold. In addition, it will be of value as a textbook for final year and post-graduate students following courses in inorganic chemistry.

CONTENTS: Chapters: 1. Introduction to the Chemistry of Gold. 2. Binary Compounds of Gold. 3. Gold (I) Complexes. 4. Gold (II) Complexes. 5. Gold (III) Complexes. 6. Gold (V) Complexes. 7. Organogold Complexes. 8. Compounds with Gold-Metal Bonds. 9. Reaction Mechanisms in Gold Chemistry. 10. Spectroscopic Studies of Gold Complexes. 11. Analysis and Applications of Gold Complexes. Appendix. Subject Index.

March 1978 x + 276 pages US $49.75/Dfl. 119.00 ISBN 0-444-41624-2

ELSEVIER

P.O. Box 211, Amsterdam
The Netherlands
52 Vanderbilt Ave
New York, N.Y. 10017

The Dutch guilder price is definitive. US $ prices are subject to exchange rate fluctuations.

7084

Analytica Chimica Acta, 97 (1978) 221—228

ELECTROCHEMICAL OXIDATION OF REDUCED NICOTINAMIDE ADENINE DINUCLEOTIDE DIRECTLY AND AFTER REDUCTION IN AN ENZYME REACTOR

HANS JAEGFELDT, ARNE TORSTENSSON and GILLIS JOHANSSON*

Analytical Chemistry, Chemical Center, University of Lund, P.O. Box 740, S-220 07 Lund (Sweden)

(Received 5th October 1977)

SUMMARY

Reduced nicotinamide adenine dinucleotide (NADH) was oxidized coulometrically at a rotating platinum gauze electrode at 0.7 V vs. SCE at pH 9. The NAD^+ formed was reduced enzymatically in a reactor containing immobilized alcohol dehydrogenase. Several recyclings were made with the same lot of NADH. The coulometric results were in reasonable agreement with spectrophotometric measurements. The overall conversion to enzymatically active NAD^+ showed a current efficiency of 99.3%. The electrode pretreatment described is essential for high current efficiency. A continuous method of oxidation of alcohol with electrolytic regeneration of cofactor and removal of aldehyde by dialysis was tested.

Regeneration of cofactors is of some importance both in enzyme technology and for analytical purposes. Two enzymatic reactions, one for the reduction and one for the oxidation of the cofactors, can be coupled to facilitate regeneration of expensive cofactors. For technical purposes, the disadvantage of this method is that the product is mixed with the reagents and products for the regeneration cycle. For analytical purposes, the regenerating system must be chosen so that selective detection is possible, and the equilibrium conditions must be favourable for the desired reaction. An electrolytic regeneration should have advantages in both applications.

Preliminary experiments by Burnett and Underwood [1] showed quantitative recovery of nicotinamide adenine dinucleotide (NAD^+) upon electrolytic oxidation of NADH. However, it was found later [2] that the electrode surface became fouled by accumulation of unknown oxidation products. Aizawa et al. [3] studied the voltammetric properties at platinum electrodes and also performed coulometric oxidations at 0.7 V vs. SCE. The electrolytic cell was also incorporated into a continuous-flow reactor system [4]. A slow adsorption was reported and the current efficiency was 95% [4] for reoxidation. The voltammetric and coulometric oxidation of NADH and other cofactors at glassy carbon electrodes was studied by Braun et al. [5]. An n value of 1.5 was found with controlled potential coulometry

(which corresponds to 75% current efficiency), in contrast to the value of 2.0 found from voltammetric measurements. Blaedel and Jenkins [6, 7] used steady-state voltammetry to study the conditions for direct amperometric determination of NADH in micromolar concentrations. This method was selected as it had been found impossible to oxidize NADH cleanly in aqueous systems by conventional voltammetry. It was concluded [7] that platinum was not quite as suitable as glassy carbon for studies of NADH oxidation; it was also shown that even small amounts of Tris buffer blocked the electron transfer. Thomas and Christian [8] devised an amperometric method for alcohol determination using electrochemical oxidation of NADH. Wallace et al. [9] used NADH oxidation for enzyme determinations in a flow system. Blaedel and Jenkins [10] described a lactate electrode in which the NADH was regenerated electrochemically.

In most of the references cited some difficulties have been encountered in the oxidation, and various methods of electrode pretreatment have been devised. The reasons for the lack of electrode reproducibility are not well understood although adsorption may be of some importance. Why a given pretreatment should change the adsorption behaviour is not easy to understand.

The present investigation is a continuation of the investigation by Aizawa et al. [3] and the condition of the electrolysis is similar. In addition to the spectrophotometric method used by these workers, a coulometric method capable of high precision is included in the present study. The continuous regeneration unit also follows a design described earlier [4] but the conditions used in this work allowed a simultaneous and precise coulometric measurement.

EXPERIMENTAL

Electrochemical oxidation of NADH was done in a three-compartment cell as shown in Fig. 1. Sample was added to the working electrode compartment which contained a rotating platinum-gauze electrode; the gauze was 36 mesh and the electrode diameter was 35 mm, the rotating speed was 550 r.p.m. A mercury contact was provided at the top of the axis. A calomel reference electrode (Radiometer K 401) was placed as close as possible to the rotating electrode. The volume of the chamber was about 20 ml but usually only 15 ml of solution was dispensed into it. Electrolytic connection to the auxiliary electrode was made through two clay-filters with an intermediate chamber in between. The cell was connected to a three-electrode potentiostat with electronic integration and direct read-out of the current—time integral on a digital voltmeter.

The electrolyte was either 0.1 M or 0.05 M sodium pyrophosphate which was adjusted to pH 9.00 with 5 M HCl. Various amounts of NADH (Sigma Chemicals Company, Cat. No. N-8129) were added to the solution in the working electrode compartment. In some experiments ethanol was present and in this case an ethanolic buffer was used in all three compartments.

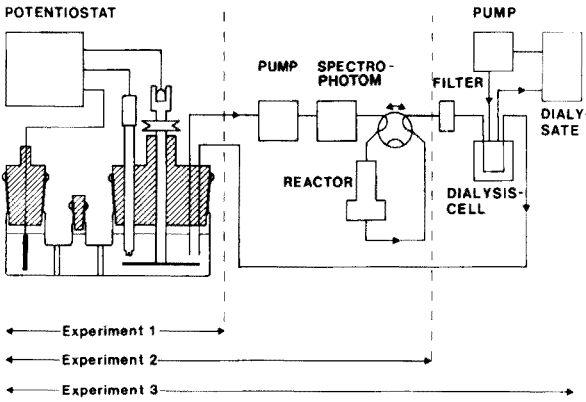

Fig. 1. Diagram of experimental arrangement showing which parts were used during the three reported reactions.

Figure 1 shows the experimental arrangement. The first series of coulometric oxidations was made in the cell, the left part of Fig. 1, with no external devices connected. In the next series of experiments, an enzyme reactor containing immobilized alcohol dehydrogenase was added in an external loop. A peristaltic pump (LKB 12000 Varioperpex) pumped the solution at a flow rate of 5 ml min^{-1}. A flow-through 10-mm spectrophotometric cell was also inserted into the loop. The spectrophotometer was a Zeiss PMQ II. The enzyme reactor could be bypassed by switching a sample loop (Altex Rotary Valves, Series 202) which had a volume of 2.7 ml. The third arrangement included a hollow-fiber dialysis cell (Bio-Rad Laboratories, model Bio-Fiber 20 Beaker) with a cut-off at 200D. The dialysate consisted of 1100 ml of exactly the same buffer solution as that filled into the loop and electrolysis cell except that no NADH was present in the dialysing solution. The solution was pumped through the hollow-fiber unit at 10 ml min^{-1}. The volume of the external cell loop was increased by about 4 ml when the dialysis cell was inserted. The loop also contained a Millipore filter unit (Swinnex-13 model) with a 5-μm cellulose acetate filter to prevent clogging of the hollow fibers.

The alcohol dehydrogenase (Sigma Chemical Company, Cat. No. A-7011) was immobilized on porous glass (CPG-10/700 Å, 80—120 mesh, pore diameter 654 Å; Serva Feinbiochemica) with glutaraldehyde as described earlier [11]. The immobilized enzyme was filled into a reactor (i.d. 5 mm, length 55 mm) and held with 5-μm Millipore filter discs at the lower end. The porous glass was not an ideal support and the reactor became deactivated several times. Alumina would probably have been a better support [4].

RESULTS

Single-pass electrolysis

NADH was dissolved in 0.1 M sodium pyrophosphate to give a stock solution of about 0.15 mM. A more exact determination of the concentration was made spectrophotometrically, based on a molar absorptivity of 6220 $l\ mol^{-1}\ cm^{-1}$ [12]. An aliquot of the stock solution was added to the coulometric cell and oxidized at 0.70 V vs. SCE. The results are shown in Table 1. Some experiments were also made in which a smaller aliquot was taken; the volume was made up with buffer. It can be seen that the coulometric and the spectrophotometric determinations give the same result within 1.3% or better. This shows that a coulometric oxidation of NADH can be made quantitatively, in contrast to some earlier reports [1, 4, 5].

In order to obtain these results, it was necessary to pretreat the working electrode by first washing it in warm, concentrated nitric acid for about 10 min, then rinsing thoroughly in water, and preelectrolysing in 0.1 M pyrophosphate buffer at 0.7 V until the residual current decreased to a value of 10—20 μA. The pretreatment changed the oxidation behaviour drastically. The electrolysis current in both cases followed the equation

$$i_t = i_0\, e^{-\beta \cdot t} \qquad (1)$$

in which i_t is the current at the time t, e the natural logarithm base, and β and i_0 are constants. After preelectrolysis, values of β were around $8 \times 10^{-3}\ s^{-1}$, but without the pretreatment the value of β varied, often being much lower, down to $1 \times 10^{-3}\ s^{-1}$. The determinations made after pretreatment indicated 100% current efficiency, i.e. the amount of NADH calculated from the current integral was equal to the amount determined spectrophotometrically. Without pretreatment the current efficiency varied; values of 65%, 116%, 110% as well as some around 100% were obtained.

TABLE 1

Comparison of spectrophotometric (340 nm, ϵ = 6220 $l\ mol^{-1}\ cm^{-1}$) and coulometric (Pt, pH 9.0 pyrophosphate, +0.70 V vs. SCE) determination of NADH

NADH (μmol)		Number of runs	Difference Δ%
Spectrophotometric	Coulometric		
0.79	0.78	1	1.3
0.83	0.82	1	1.2
1.57	1.58	4	−0.6
1.61	1.61	3	0
1.63	1.63	2	0
1.65	1.65	3	0
2.47	2.45	2	0.8

Electrolysis and enzymatic regeneration

For a successful electrolytic oxidation of a cofactor the oxidation product must necessarily be enzymatically active. Alcohol dehydrogenase is dependent on NAD^+ for the reaction

$$CH_3CH_2OH + NAD^+ \xrightarrow{ADH} CH_3CHO + NADH + H^+ \quad (2)$$

By adding immobilized ADH in a side loop it should be possible to regenerate NADH quantitatively from NAD^+. Oxidation products other than NAD^+ should not be reduced and it should therefore be possible to achieve a quantitative measure of the inactive side products. In order to increase the accuracy of the measurement, the set-up was arranged so that the same lot of NADH could be electrolytically oxidized, enzymatically reduced, electrolytically oxidized etc. Figure 2 shows the results obtained during such a recycling when the original concentration of ethanol was 0.53 M in 0.1 M pyrophosphate, pH 9.0. The circles give the amount of NADH oxidized as a percentage of the amount (107 μmol) originally present.

There is a steady decrease of the amount of NADH which is regenerated. It is known that NAD^+ is unstable in alkaline solution whereas NADH is more stable. The rate of this non-electrolytic decomposition was measured separately by storing a solution of buffer-NAD^+ at pH 9.0 (see below). A complete regeneration of NADH will also be prevented if the acetaldehyde concentration increases. The equilibrium constant of eqn. (2) is known [4]; it was taken to be 2.31×10^{-2} when the H^+ concentration is included. The concentration of NADH after the ith oxidation will then be

$$[NADH]_i = -X + (X^2 + Y)^{\frac{1}{2}} \quad (3)$$

$$X = ([EtOH]_i + [NAD^+] + [CH_3CHO]_i/2.31 \times 10^{-2})/84.6$$

$$Y = [EtOH]_i[NAD^+]_i/42.3$$

The acetaldehyde present as an impurity in the alcohol was estimated to be 80 μM at the start; the amount was determined by gas chromatography (Varian Aerograph 2700, FID, 4-m column, i.d. 2 mm, 15% PEG on Chromosorb, 65°C). Equation (3) was evaluated by computer with the 80 μM start concentration of aldehyde and the result is given in Fig. 2, curve A. Obviously equilibrium considerations alone cannot explain the experimental results.

The non-electrolytic decomposition of NAD^+, measured spectrophotometrically, as above, was found to be 6.1×10^{-5} min^{-1}. Each cycle took 52 min and therefore the decomposition can be approximated by the equation

$$[NAD^+]_i = [NAD^+]_0 (1 - ki) \quad (4)$$

where $k = 1.6 \times 10^{-3}$. Curve B, Fig. 2, shows the result when both the non-electrolytic decomposition and the equilibrium were taken into account.

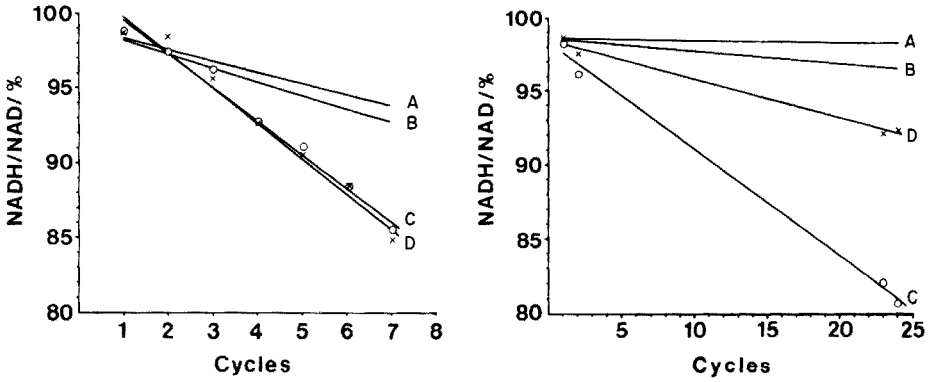

Fig. 2. Recovery of NADH vs. the number of oxidation cycles. Experiment 2. (A) Calculated from equilibrium data. (B) As for A but including pH-dependent non-electrolytic decomposition of NAD^+. (C) Measured coulometrically (○). (D) Measured spectrophotometrically (×).

Fig. 3. Recovery of NADH vs. number of reoxidations when dialysis was used. Experiment 3. Legends to curves A—D as in Fig. 2.

Curves C and D represent the least-squares lines through the experimental points. The difference between curves B and C and line D is thus a measure of decomposition at the electrode which is estimated to be 1% per cycle.

Recycling with dialysis

To reduce the concentration of acetaldehyde to such a low value that eqn. (2) can be considered to proceed almost completely to the right, a dialysis cell was included in the loop (Fig. 1). The products which could pass the hollow fibers were diluted to a total volume of 1100 ml as compared to the 17 ml in the electrolysis cell, the loop and the hollow fiber unit. The acetaldehyde was thus diluted 65 times compared to the experiment reported above. Some low-molecular-weight products, probably decomposition products from the cofactor, also passed into the dialysate. It is not known if those affect the oxidation. The external solution was periodically checked for the presence of NAD^+ and NADH with a spectrophotometer (McPherson model EU-707-11). No NAD^+ or NADH could be found with the method which had a detection limit of 0.08 μmol corresponding to a 6% loss during a run of 9 h 22 min. The sensitivity of the test was thus too low to detect minor losses.

Figure 3 shows the results obtained when 1.34 μmol of NADH was dissolved in 0.05 M pyrophosphate buffer, pH 9.0, containing 0.53 M ethanol and 80 μm acetaldehyde as an impurity. The total volume was 17 ml. First a complete oxidation was performed with the enzyme reactor bypassed (cycle 1). The enzyme reactor was then used to reduce the NAD^+ completely with the potentiostat switched to stand-by, and the oxidation cycle was then repeated once more (cycle 2). Then the valve was switched

to allow continuous operation. The current integral was taken as a measure of the number of recyclings. After about twenty passes the system was switched back to discontinuous operation to obtain the amount of active cofactor.

Curve C in Fig. 3 is drawn through the points obtained by coulometry and curve D through those obtained spectrophotometrically. Curve A gives the amount expected when the equilibrium constant is taken into account as described above. The line is practically parallel (0.2%/24 cycles) to the abscissa but less than 100% because of the acetaldehyde impurity. Curve B includes also the non-electrolytic decomposition of NAD^+ at pH 9, obtained as above but with a mean cycle time of 23 min during the time of continuous operation.

The two methods give different values. The reason for this lies probably in the different modes of operation. The spectrophotometric method measures a concentration whereas the coulometric method primarily measures an amount (of electricity). Any decrease in volume, e.g. by reverse osmosis through the hollow fibers, could give such a discrepancy with the coulometric method producing the lower value. It was difficult to measure the volume precisely.

The overall result is that NADH can be oxidized electrolytically to enzymatically active NAD^+ with an overall efficiency of 99.3%. This value is obtained when the results from the coulometric method (curve C, Fig. 3) are used.

DISCUSSION

The present results indicate that a quantitative reoxidation of NADH to NAD^+ is possible with a very high current efficiency in a two-electron process; and the product is enzymatically active. These results contrast with some earlier reports in which substantially lower current efficiency was found. Electrode fouling has also been reported [2, 9] as well as adsorption and different behaviour on successive sweeps in voltammetry [3]. The oxidation peak in voltammetry appears at +0.7 V but the half-wave potential for reduction occurs in two steps, 0.9 and 1.7 V [1] at the DME. This indicates a complex electrochemical behaviour.

The pretreatment of the platinum electrode was absolutely essential in order to obtain reproducible and accurate results. The condition of the electrode surface must therefore be an essential factor for the quantitative oxidation of NADH. Probably the condition of the surface affects the adsorption behaviour but the exact mechanism has not been studied further. Another factor which might influence the result is the mass transfer at the working electrode. In the cell used, the platinum gauze was rotated at high speed. A violent turbulence is created around each wire in the mesh and the Nernst diffusion layer is therefore very thin. Any byproducts from the oxidation will thus be transferred into the bulk of the solution very rapidly.

The concentration of active products at the electrode surface will therefore be much lower than if the electrolysis were performed at a stationary or plane electrode. This may be a factor in explaining why no electrode fouling was observed even after very long repeated oxidation.

The accuracy of the coulometric measurements is rather astonishing when the procedure is considered. Diffusion of reactant will normally take place through the filters and during a long run an appreciable loss can occur [13]. The cofactor could diffuse into the intermediate chamber and the counter electrode compartment. The intermediate chamber was occasionally analyzed spectrophotometrically and in all cases the amounts of NAD^+ and NADH were negligible. Both NAD^+ and NADH have a negative overall charge and therefore the migration counteracts diffusion. This effect should be small, however, as the electrolyte concentration is fairly high. Possibly the clay filters are charged so that exclusion takes place and the charge is transported by positive ions.

Financial support from the Swedish Natural Research Council is gratefully acknowledged.

REFERENCES

1 J. N. Burnett and A. L. Underwood, Biochemistry, 4 (1965) 2060.
2 R. G. Haas, Electrochemical Oxidation of NADH Analogs, Ph.D. Thesis, University of Wisconsin, Madison, 1970.
3 M. Aizawa, R. W. Coughlin and M. Charles, Biochim. Biophys. Acta, 385 (1975) 362.
4 R. W. Coughlin, M. Aizawa, B. F. Alexander and M. Charles, Biotechnol. Bioeng., 17 (1975) 515.
5 R. D. Braun, K. S. V. Santhanam and P. J. Elving, J. Am. Chem. Soc., 97 (1975) 2591.
6 W. J. Blaedel and R. A. Jenkins, Anal. Chem., 46 (1974) 1952.
7 W. J. Blaedel and R. A. Jenkins, Anal. Chem., 47 (1975) 1337.
8 L. C. Thomas and G. D. Christian, Anal. Chim. Acta, 78 (1975) 271.
9 T. C. Wallace, M. B. Leh and R. W. Coughlin, Biotechnol. Bioeng., 19 (1977) 901.
10 W. J. Blaedel and R. A. Jenkins, Anal. Chem., 48 (1976) 1240.
11 G. Johansson and L. Ögren, Anal. Chim. Acta, 84 (1976) 23.
12 A. D. Winer, J. Biol. Chem., 239 (1964) 3598.
13 J. Lindberg, J. Electroanal. Chem., 40 (1972) 265.

Analytica Chimica Acta, 97 (1978) 229—236

GLUCOSE AND L-AMINO ACID ELECTRODES BASED ON ENZYME MEMBRANES

G. J. LUBRANO and G. G. GUILBAULT*

Department of Chemistry, University of New Orleans, New Orleans, Louisiana 70122 (U.S.A.)

(Received 26th October 1977)

SUMMARY

Membranes containing immobilized glucose oxidase have been constructed in a simple, easily reproduced procedure. The enzyme is co-crosslinked with bovine serum albumin using the bifunctional agent, glutaraldehyde. Amperometric enzyme electrodes have been constructed using these membranes and the effect of membrane thickness and enzyme activity studied.

In the past, enzyme electrodes have generally been formed by (1) trapping solubilized enzyme over an electrode with some type of membrane layer(s) [1, 2]; (2) trapping enzyme in a synthetic organic gel matrix over an electrode [1, 3—5]; and (3) chemically insolubilizing enzyme on porous organic polymer or with a bifunctional reagent and holding a thin layer over an electrode with some type of membrane(s) [1, 6, 7]. The first procedure is simple, but has all the disadvantages of solubilized enzyme systems. The second procedure is relatively simple, but the enzyme is only trapped and electrode life is not nearly as good as for electrodes based on chemically insolubilized enzymes. The third procedure produces enzyme electrodes that have the long-term stability associated with insolubilized enzyme systems, but the preparation of the insolubilized enzyme and electrode is often poor in terms of convenience and reproducibility. It is often difficult to reproduce the enzyme layer thickness and the enzyme activity present in each electrode. Reproducibility from electrode to electrode is poor and difficult to obtain.

Broun et al. have formed artificial enzyme membranes on cellophane [8], and glass [9—11], by crosslinking the enzyme with an inactive protein by means of the bifunctional agent, glutaraldehyde. Tran-Minh and Broun have applied these techniques to electrodes by coating a cation electrode with an enzyme membrane and by placing enzyme membranes over pO_2 and pCO_2 gas electrodes [12]. Blaedel and Jenkins [13] immobilized LDH and NAD on cellophane and applied this to a glassy carbon electrode to form a reagentless lactate electrode. These techniques appear to be the solution to most of the problems associated with forming simple, cheap and reproducible enzyme electrodes on a large or small scale.

This technique of glutaraldehyde coupling can be applied to the construction of amperometric enzyme electrodes for glucose and L-amino acids. The effects of membrane thickness and enzyme activity on electrode response are investigated. Some advantages of using enzyme membranes rather than gels or other non-membrane techniques are discussed.

EXPERIMENTAL

Reagents

Phosphate buffers were prepared at an ionic strength of 0.1, and at pH 6.6 for glucose studies and 7.8 for amino acid studies. Stock solutions of glucose were prepared with β-D(+) glucose (Sigma Chemical Co.) in buffer and allowed to equilibrate overnight. Dilutions were made in buffer. L-Phenylalanine (reagent-grade; Sigma Chemical Co.) solutions were prepared daily in buffer. Glucose oxidase (E.C. 1.1.3.4) was purified from *Aspergillus niger* (Sigma Chemical Co., Type II, 19.4 Units/mg). L-Amino acid oxidase (E.C. 1.4.3.2) was from *Crotalus adamentus* venom (Sigma Chemical Co., Type I, 0.9 Units/mg). Bovine serum albumin (BSA) powder was 96—99% albumin (Sigma Chemical Co., fraction V). Glutaraldehyde was an aqueous 25% solution (Sigma Chemical Co., Grade IV).

Preparation of enzyme membranes

A small volume of enzyme/BSA solution in buffer was spread on a 3 × 1-in. glass microscope slide. Another small volume of 2.5% glutaraldehyde in buffer was added to the center of the slide. The two solutions were then mixed rapidly with a small glass rod of ca. 1.5-mm diameter. The membranes were allowed to form at room temperature and open to the atmosphere for up to 3 h, at which time the water had completely evaporated. The membranes were then washed several times in buffer and stored in buffer at room temperature. Membranes were easily removed from the glass slide either by light pressure with a glass rod or by scraping with a razor blade. The compositions of various membranes are given in Tables 1 and 2 for glucose oxidase and L-amino acid oxidase, respectively.

Preparation of enzyme electrodes

Membranes were cut with a razor blade to the size of an electrode face and trapped over the platinum face of the electrode with a layer of cellophane (Will Scientific, Inc.), which was in turn held on with a rubber O-ring.

Apparatus

A Heath polarograph module (Model EUA-19-2) combined with a Heath operational amplifier system (Model EUW-19A) was used as a two-electrode polarograph at a constant potential of 0.6 V (vs. SCE) for the glucose studies and at 0.35 V (vs. SCE) for the L-amino acid studies. The platinum electrode was of the inlay disc type (Beckman No. 39273). A side-arm

TABLE 1

Glucose oxidase membranes

Membrane code	Glucose[a] oxidase (mg)	Glucose[b] oxidase-BSA solution (μl)	Glutaraldehyde[c] solution (μl)	Glucose[d] oxidase/electrode (m Units)
G1	0.25	250	50	12.3
G2	0.50	250	50	24.6
G3	1.0	250	50	49.1
G4	5.0	250	50	245.0
G5	10.0	250	50	491.0
G6	20.0	250	50	983.0
G7	1.0	500	100	98.2
G8	5.0	500	100	419.0
G9	10.0	500	100	983.0
G10	0.25	125	25	6.15
G11	0.50	125	25	12.3
G12	1.0	125	25	24.6

[a]mg Glucose oxidase per ml of BSA solution (50 mg BSA/ml buffer). [b]μl Glucose oxidase—BSA solution per slide. [c]μl Glutaraldehyde solution per slide. [d]mUnits of glucose oxidase in membrane over platinum disc of electrode.

TABLE 2

L-Amino acid oxidase membranes
(All mixtures contained 250 μl of L-amino acid oxidase—BSA solution and 50 μl of glutaraldehyde solution.)

Membrane code	L-AA Ox[a] (mg)	BSA[b] (mg)	L-AA Ox[c]/electrode (mUnits)
A1	1	50	2.28
A2	5	50	11.4
A3	10	50	22.8
A4	20	50	45.5
A5	40	50	90.0
A6	5	45	11.4
A7	10	40	22.8
A8	20	30	45.5
A9	40	10	90.0

[a]mg of L-Amino acid oxidase per ml of BSA solution in buffer. [b]mg of BSA per ml of L-AA Ox-BSA solution. [c]mUnits of L-AA Ox in membrane over platinum disc of electrode.

saturated calomel electrode [14] was placed in contact with the enzyme electrode just below the O-ring to allow application of a potential when the electrode is out of solution. The current was recorded on a strip-chart recorder.

Substrate measurements

Before the electrodes were placed in the test solution, they were pretreated by applying a potential of 0.6 V (vs. SCE) for the glucose electrodes or 0.35 V (vs. SCE) for the L-amino acid electrodes, until the current decayed to a low value. The electrode was then submerged in the test solution and the resulting current monitored on the strip-chart recorder. The electrode was then removed from the solution and rinsed with buffer until the current again decayed to a low value. Rates of reaction were measured within 3—12 s; steady-state currents were obtained after 1—2 min.

RESULTS AND DISCUSSION

A typical response curve for the glucose electrode is given in Fig. 1, which shows the response of a glucose electrode to 5×10^{-3} M glucose. A similar response curve was obtained with L-amino acid electrodes. The initial rate is linear and maximal within the first 3—12 s. The steady-state current is reached within 1—2 min. Typical rate and steady-state calibration curves for the glucose electrodes are given in Fig. 2. All the glucose electrodes studied had similar curves with respect to both general shape and slopes. Curves were merely displaced up or down along the vertical axis. The rate curves were linear from 5×10^{-4} M to 10^{-2} M and then curved downward slightly at higher concentrations. The steady-state curves were linear to only 5×10^{-3} M and leveled off sharply at higher concentrations.

To test the magnitude of the effect of the cellophane membrane on the response of the electrodes, response curves were recorded for a 5×10^{-3} M glucose solution with a typical glucose electrode and with the same electrode with an additional cellophane membrane (Fig. 1). With the additional membrane, the steady-state response was halved and the initial rate was lowered by a factor of five.

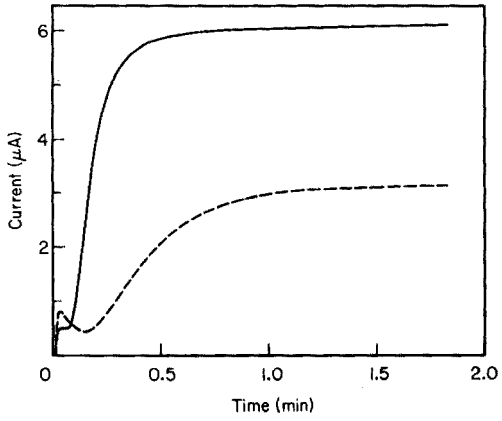

Fig. 1. Response curves for glucose electrode. —— Typical electrode. ---------- Effect of an additional cellophane membrane.

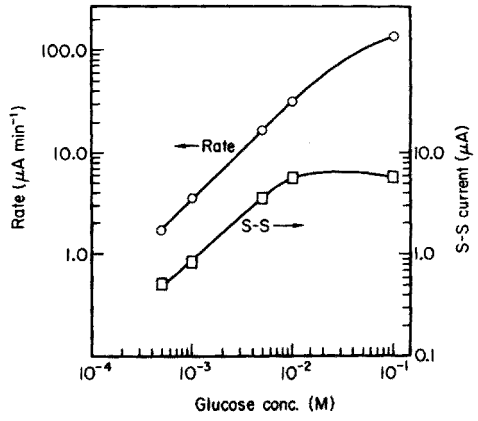

Fig. 2. Calibration curves for glucose electrode. ○ Rate. □ Steady-state.

Figure 3 shows the rate and steady-state response of various glucose electrodes to 5×10^{-3} M glucose. The lines drawn indicate constant membrane volume, BSA and glutaraldehyde concentrations, and thus are membrane thickness isograms for the three membrane thicknesses studied. The glucose oxidase activity added to the membrane is given on the abscissa as enzyme units per electrode. Only at the highest enzyme activities is the protein content of the added glucose oxidase significant compared to that of the BSA present in the membranes. As expected, the highest response was obtained with a combination of high enzyme activity and thin membrane. High activity in the thick or medium membranes caused a lowering of response. The medium membrane had peak responses at approximately 49 and 25 mUnits/electrode for the rate and steady-state responses, respectively.

Electrodes and membranes were stored in buffer at room temperature when not in use. Long-term stabilities of glucose electrodes were studied by

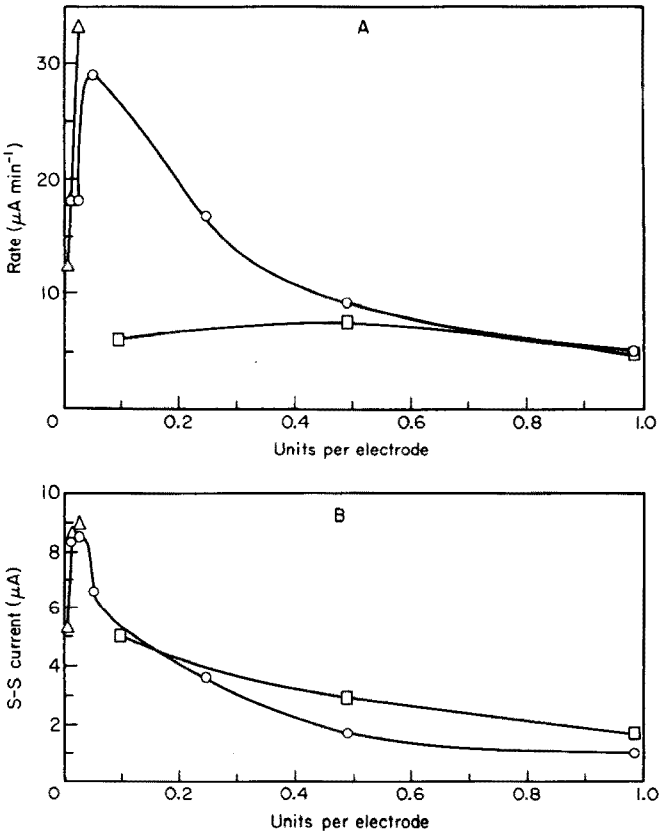

Fig. 3. Membrane thickness isograms for glucose electrode. A, Rate detection. B, Steady-state detection. △ Thin membranes (G10-G12). ○ Medium membranes (G1-G6). □ Thick membranes (G7-G9).

periodically testing their response to 5×10^{-3} M glucose. Curves similar to those in Fig. 4 were generally obtained; there was an increase in response from several days to several weeks. This behavior has been observed in the past [1] with enzyme electrodes and possible explanations were given: (a) the establishment of diffusion channels in the matrix, and (b) changes in conformation of the fraction of enzyme immobilized in an inactive conformation to the more stable and preferred active conformation. Although these explanations may be valid, the results given in Fig. 3 suggest and prove a third explanation. In a membrane of constant thickness, composition and porosity, if enzyme activity over and above that needed for maximum response is present, then as activity is naturally lost with time, the response of the electrode increases until the maximum response for that particular membrane is reached. Only then will the electrode response begin to decrease.

The term "maximum" response is used above, and not "optimum" response. When an enzyme electrode is constructed, more enzyme activity than is required for maximum response should generally be added. In this way, as the electrode ages, its response will be useful for a period of time very much longer than if the electrode had been constructed for immediate maximum response. One should not add so much activity, however, that initial response is too poor. This applies, of course, only to membranes of finite thickness where membrane diffusion plays a significant role in response.

L-Amino acid oxidase membranes were prepared, based on the results of the glucose oxidase membranes, with varying activity, and with constant volume and BSA and glutaraldehyde concentrations. A direct comparison with the glucose oxidase membranes is hindered because the L-amino acid oxidase used had an activity approximately twenty times lower than the glucose oxidase used, and the protein in the membrane arising from the added L-amino acid oxidase was often significant compared to the protein from the BSA.

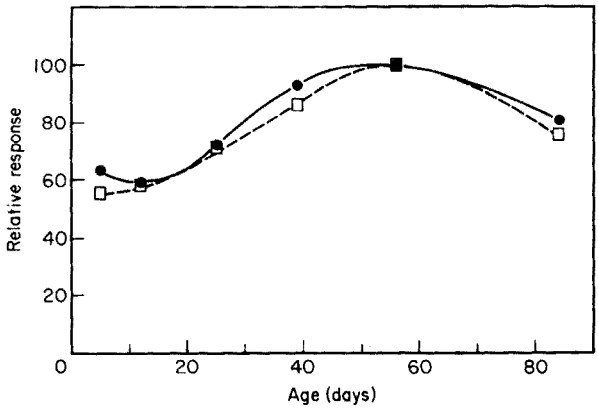

Fig. 4. Typical long-term stability of glucose electrodes for 5×10^{-3} M glucose solutions. • Rate detection. □ Steady-state detection.

The response of these membranes to 5×10^{-4} M L-phenylalanine is given in Fig. 5; the rate and steady-state methods are shown. As with the glucose oxidase membranes of similar thickness, maximum rate response occurs with an activity of approximately 50 mUnits/electrode. The steady-state response, however, did not peak at the activities tested.

In order to determine the effect of the greater proportion of protein to glutaraldehyde in the L-amino acid membranes, membranes were prepared with varying activity and constant protein weight (i.e., constant BSA plus enzyme). The response to 5×10^{-4} M L-phenylalanine is given in Fig. 5 for the rate and steady-state methods. Again, the rate peaked at an activity of approximately 50 mUnits/electrode. This time, however, the steady-state response peaked at approximately 25 mUnits/electrode, as did the glucose oxidase membranes.

Several attempts were made to form membranes with glucose oxidase in a similar manner directly on cellophane, to ease storage and handling. The results were partially successful. The response could never be made as high as when the membrane was formed first on glass and then held on by the cellophane, and reproducibility problems could not be achieved. Work in this direction is continuing.

The technique of forming enzyme membranes and electrodes described here affords many advantages over the previous techniques utilizing thin layers of enzyme chemically insolubilized in bulk on organic polymers or with bifunctional reagents. Only the common reagents, BSA, glutaraldehyde and buffer are required for membrane formation. Insolubilization and membrane formation involves only a simple, fast mixing of reagents and a

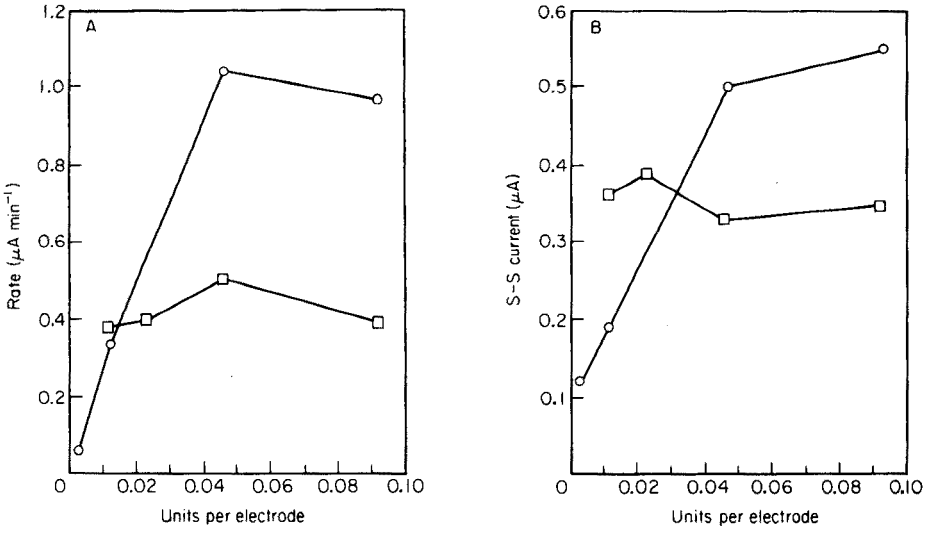

Fig. 5. Membrane isograms for the response of L-amino acid oxidase electrodes to L-phenylalanine. A, Rate detection. B, Steady-state detection. ○ Constant BSA. □ Constant protein.

short wait, as opposed to a sequence based on several steps of reaction and washing with one or more uncommon and generally expensive reagents. Large-scale preparation is a simple matter of scaling up volumes and formation area. The simplicity, rapidity and gentleness of enzyme membrane formation make this technique inherently easier to reproduce. Membranes of constant thickness and containing a particular level of enzyme activity are easily and rapidly formed. As a result of the use of enzyme membranes, enzyme electrodes can be produced on a large or small scale in a manner, which is cheaper, faster, simpler and more reproducible.

The financial assistance of the National Institutes of Health, Grant No. RO1 GM 17268, is gratefully acknowledged.

REFERENCES

1 G. G. Guilbault and G. J. Lubrano, Anal. Chim. Acta, 64 (1973) 439.
2 L. C. Clark, U.S. Patent No. 3,539,455 (1970).
3 G. G. Guilbault and J. G. Montalvo, J. Am. Chem. Soc., 91 (1969) 264.
4 G. J. Papariello, A. K. Mukherji and C. M. Shearer, Anal. Chem., 45 (1973) 790.
5 R. A. Llenado and G. A. Rechnitz, Anal. Chem., 43 (1971) 1457.
6 G. G. Guilbault and G. J. Lubrano, Anal. Chim. Acta, 69 (1974) 183.
7 G. Nagy, L. H. Von Storp and G. G. Guilbault, Anal. Chim. Acta, 66 (1973) 443.
8 G. Broun, E. Selegny, S. Avrameas and D. Thomas, Biochim. Biophys. Acta, 185 (1969) 260.
9 G. Broun, D. Thomas, G. Gellf, D. Dommado, A. M. Berjonneau and C. Guillon, Biotech. Bioeng., 15 (1973) 359.
10 D. Thomas and G. Broun, Methods Enzymol., 44 (1976) 901.
11 G. Broun, Methods Enzymol., 44 (1976) 263.
12 C. Tran-Minh and G. Broun, Anal. Chem., 47 (1975) 1359.
13 W. J. Blaedel and R. A. Jenkins, Anal. Chem., 48 (1976) 1240.
14 R. N. Adams, Electrochemistry at Solid Electrodes, M. Dekker, New York, 1969, p. 288.

Analytica Chimica Acta, 97 (1978) 237—244

EVALUATION OF MEASURING RANGE AND INTERFERENCES FOR GAS-SENSING POTENTIOMETRIC PROBES

MARCO MASCINI* and CARLO CREMISINI

Istituto di Chimica Analitica, Università di Roma (Italy)

(Received 17th August 1977)

SUMMARY

The experimental limit of detection and the interferences for any assembled gas sensor are the analytical features of greatest interest. Theoretical and practical studies of CO_2 and SO_2 gas sensors are reported. In the measurement of CO_2, the sample should not be buffered at too acidic a value, although the rate of diffusion at e.g. pH 6.8, may be slower than at low pH. Choice of sample pH can also be used to limit interfering effects. The conditions must be selected on the basis of the required rate of analysis and the selectivity attainable.

Gas-sensing potentiometric probes have been widely applied, but little has been published on their analytical evaluation, i.e. the measuring range and the interferences of other gaseous species. Recently, a graphical method has been reported for evaluating the measuring range [1]. The method is simple but is far from solving the complexity of the behaviour of gas sensors. Bailey and Riley [2] have criticized the graphical method and have proposed an alternative theoretical treatment based on different assumptions, in order to obtain the limit of detection of gas-sensing probes. In the present paper, theoretical and experimental data are reported for the measuring ranges and the interferences of gaseous species for several sensors. Methods of eliminating interferences are discussed.

All experiments were done with a gas-sensing probe assembled as reported previously [3] and with analytical-grade reagents.

LIMIT OF DETECTION

The gas-sensing probes generally comprise a pH electrode (glass or antimony [3]) coupled with a reference electrode through a thin layer of electrolyte. The pH of the electrolyte changes when gas from the sample diffuses through a porous membrane which separates the sample solution from the electrolytic film. The composition of the electrolyte is chosen so that an equilibrium is achieved with the gas for which the electrode is assembled. For example, for the ammonia electrode, 0.1 M ammonium chloride is the

internal electrolyte, and the pH of the electrolyte film is given by

$$pH_f = pk_a - \log [NH_4^+]_f + [NH_3]_f \quad (1)$$

where the suffix f denotes the film of electrolyte solution. The last term is a function of the ammonia concentration in the sample solution (with suffix s) and the relation then becomes

$$pH_f = pk_a - \log [NH_4^+]_f + [NH_3]_s + \log p \quad (2)$$

where p is the partition coefficient. From a Hägg diagram [4], Hansen and Larsen [1] calculated the calibration curve of the system and established a theoretical lower sensitivity limit for a given electrolyte concentration. The hypothesis was that when the sample solution has an ammonia concentration, $[NH_3]_s$, lower than the ammonia concentration in the bulk electrolyte, $[NH_3]_e$, or in the electrolyte film, $[NH_3]_f$, then the concentration of ammonia in the film is no longer proportional to the ammonia concentration of the sample but becomes

$$[NH_3]_f = [NH_3]_e = [H_3O^+]_e \quad (3)$$

This hypothesis is not always valid (and indeed this could depend on the construction of the probe), as has been suggested by Bailey and Riley, and as is indicated by Figs. 1 and 2.

These Figures show the theoretical calibration curves derived from Hägg diagrams by the method of Hansen and Larsen [1], the theoretical curves derived by the method of Bailey and Riley [2] and the experimental curves.

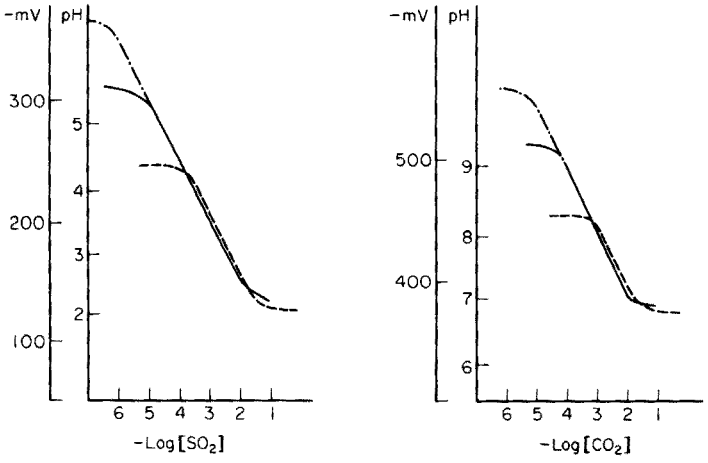

Fig. 1. Experimental (——) and theoretical calibration curves for a SO_2 sensor. (---) Curve obtained by the method of Hansen and Larsen [1]. (·—·—·) Curve obtained by the method of Bailey and Riley [2]. The internal solution was 0.1 M $NaHSO_3$.

Fig. 2. Theoretical and experimental calibration curves for a CO_2 sensor. The theoretical curves are designated in the same way as for Fig. 1. The internal solution was 0.1 M $NaHCO_3$.

The method of Hansen and Larsen is based on the assumptions that the limit of detection is the concentration of the gaseous species in the bulk electrolyte, and that the gaseous species cannot diffuse from the electrolyte film to the sample solution, because of the continuous feed of internal electrolyte to the electrolyte film. In contrast, in the Bailey and Riley treatment, it is assumed that the electrolyte film is separated from the internal electrolyte and is not fed by the bulk electrolyte; the concentration of the gaseous species in the film can follow the concentration of the gaseous species in the sample solution even when it is lower than the internal electrolyte value. This means that the relationship $[NH_3]_f = [NH_3]_s$ is valid even when $[NH_3]_s < [NH_3]_e$; the limit of sensitivity does not depend on the latter value. In the present work, in many cases the pH of the electrolyte shifted from the hydrolysis value obtained when the electrode was assembled, to an equilibrium value depending on two kinetic factors: the diffusion rate of the gaseous species from the electrolytic film to the external sample solution, and the diffusion rate from the internal electrolyte to the electrolyte film. Such effects will depend on the pH of the sample solution because of the diffusion of the gaseous species from the electrolyte film to the sample solution. Figure 3 shows the experimental change of some assembled ammonia sensors to an equilibrium value. This effect has been reported [5] for a methylamine electrode and attributed to carbon dioxide desorption from the electrolyte film. However, in this case, also, it seems simpler to explain the matter as diffusion of methylamine from the electrolyte film to the sample solution. This would explain how, when the sample solution

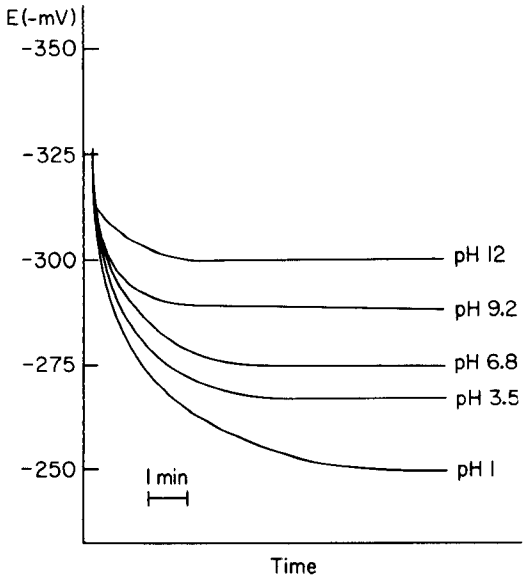

Fig. 3. Equilibrium potentials for an ammonia sensor after assembly. The sensor was dipped in samples buffered at different pH values and not containing ammonia.

is more alkaline, the pH of the electrolyte film is higher, because the diffusion rate of the gaseous base will be lower; when the sample solution is more acidic, the diffusion of the gaseous base will be enhanced and the resulting pH of the electrolyte film will be lower. This is clear from Fig. 3, which shows that the pH of the internal solution always decreases, reaching a lower equilibrium value when the sample solution is more acidic, and a higher equilibrium value when the sample solution is alkaline. If a desorption of carbon dioxide were involved, then the pH variation with time towards the equilibrium value should be in the opposite direction. The conclusion from such experiments is that the linear range depends on those experimental factors which influence the kinetics of the diffusion of the gaseous species and, more importantly, on the pH of the sample solution. Often the sample solution is made completely acidic (ca. pH 1) or alkaline (ca. pH 13) to ensure the conversion of the acid or base to the gaseous form, but this precaution can sometimes be harmful because it decreases the diffusion rate of the gaseous form from the electrolyte film.

SELECTIVITY

A gas membrane probe suffers direct interferences from dissolved gaseous species that can produce pH variations in the thin electrolyte film in contact with the pH electrode. If two acidic volatile species, HA and HB, are present in solution and the sensor is assembled for the measurement of HB, i.e. the internal solution contains B^-, the following equilibrium will be established

$$HA + B^- \rightleftharpoons HB + A^- \qquad (4)$$

with an equilibrium constant $k = k_A/k_B$, where k_A and k_B are the protolysis constants of HA and HB, respectively, Thus

$$k = [HB]_f[A^-]_f/[HA]_f[B^-]_f$$

where the suffix f indicates the electrolytic film.

Provided that the sample is acidic enough to ensure that the species in the sample are both converted to their volatile forms and that the membrane is an air gap or a membrane such as Teflon which does not discriminate between the two different acidic species, then $[HA]_f$ and $[HB]_f$ can be assumed equal to the corresponding concentrations in the sample, i.e. $[HB_s]/[HA]_s = [HB]_f/[HA]_f = r$.

It can be established that if this ratio r is more than 10 times the value of k, the species HA does not interfere because the reaction will not be shifted to the right and the $[B^-]_f$ concentration in the electrolyte film will not change appreciably. The system HB—B^- will determine the pH of the electrolyte film. However, when the ratio r becomes smaller than 0.1 k, the HA—A^- system will determine the pH. Between 10 k and 0.1 k, both systems will determine the pH of the electrolyte film. For example, if $k_B = 10^{-6}$ and $k_A = 10^{-3}$, the value of k will be 10^3, and the sensor assembled for determining the species HB will respond to this species with ratios $[HB]/[HA] \geqslant 10^4$.

However, if $k_B = 10^{-3}$ and $k_A = 10^{-6}$, the k value is 10^{-3} and the sensor assembled for determining the species HB will respond to this species for ratios $[HB]/[HA] \geqslant 10^{-2}$.

Figure 4 shows how the selectivity varies with different pairs of acids. In practice, when the ratio is smaller than 0.1 k, reaction (4) lies far to the right in solution and B^- is completelv converted to A^-; that is, the electrolyte film concentration changes and the sensor behaves as if it had been assembled for the measurement of HA.

However, it is possible to limit the interference by raising the pH of the sample solution. In fact, in some cases, the stronger acid will not be completely converted to the volatile form. The concentration of the acid in the electrolyte layer $[HA]_f$ will not then be the same as the formal (or total) concentration in the sample solution $[HA]_s^\circ$ but only a fraction of it. For example, if the protolysis constants of HA and HB, i.e. k_A and k_B, are 10^{-3} and 10^{-7}, respectively, and if the pH of the sample is about 7, then

$$[HA]_f = [HA]_s = [H^+]\,[A^-]/k_A \simeq 10^{-7}\,[HA]_s^\circ/10^{-3} = 10^{-4}\,[HA]_s^\circ \qquad (5)$$

and

$$[HB]_f = [HB]_s = [HB]_s^\circ/2 \qquad (6)$$

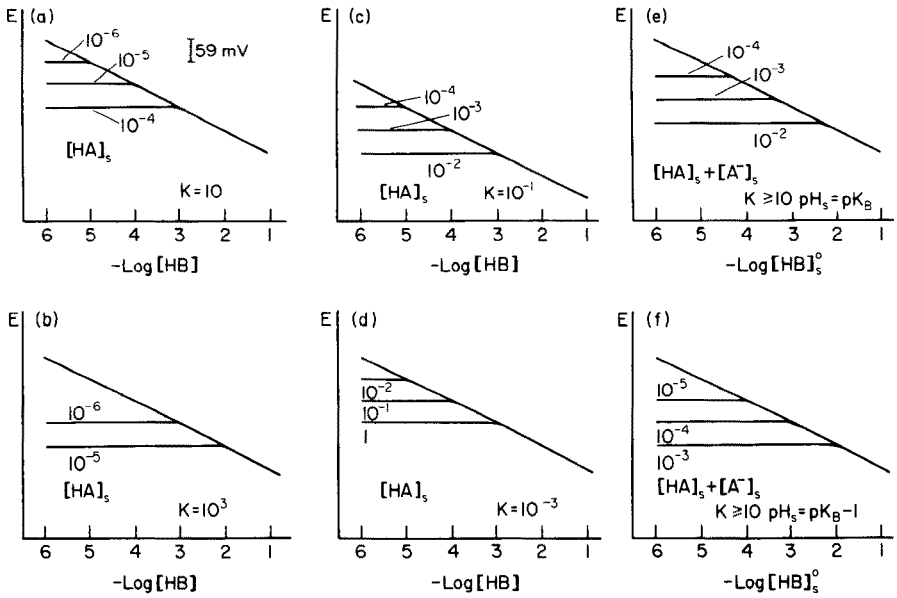

Fig. 4. Theoretical calibration curves for the gaseous species HB in the presence of an interferent HA. The electrode is considered to be assembled for HB, i.e. containing a 0.1 M B^- solution. Plots (a—d) refer to complete conversion of the species HA and HB to their volatile forms and for different value of the k ratio of the acid constants k_A and k_B; in (a) and (b) HA is the stronger acid, in (c) and (d) HB is the stronger. The plots (e) and (f) are the calibration curves when HA is stronger than HB, but the pH of the sample solution does not allow complete conversion of both acids to the volatile forms, thus limiting the interference.

Then

$$k = 10^4 = [HB]_f[A^-]_f/[HA]_f\,[B^-]_f = [HB]_s^\circ \cdot 10^4 \cdot [A^-]_f/2[HA]_s^\circ\,[B^-]_f$$

or

$$[HB]_s^\circ\,[A^-]_f/[HA]_s^\circ\,[B^-]_f = 10^4 \cdot 2/10^4 = 2$$

If $r = [HB]_s^\circ/[HA]_s^\circ \geqslant 20$, then selective response of the gas sensor is ensured for the volatile species HB; in acidic solution the ratio r should exceed 10^5 to obtain a selective response to the weak volatile acid HB. This is shown in Fig. 4 (e and f). This result was confirmed experimentally; Figs. 5—7 show the determination of CO_2 in the presence of SO_2 at pH 6 and calibration plots for CO_2 in the presence of several interfering gaseous species, SO_2, acetic acid and HF. All are stronger acids than CO_2 and the interferences are greatly reduced by buffering the sample at pH 6.8. Figure 8 shows the results obtained when the SO_2 sensor was calibrated in the presence of CO_2, acetic acid and HF. Sulphur dioxide is a stronger acid than the other interferents, and in this case the sample pH must be low, otherwise the interference effects are enhanced. The interferences occur only with high concentrations of interferents.

These measurements were obtained by assembling the sensor for each measurement and by recording the potential value after a constant time of 15 min. At the end of this time, for low interfering effects, the potential values changed slowly and continuously, by a few mV per h, whereas for high interfering effects, the potential values were very stable.

The agreement between theoretical and experimental curves generally

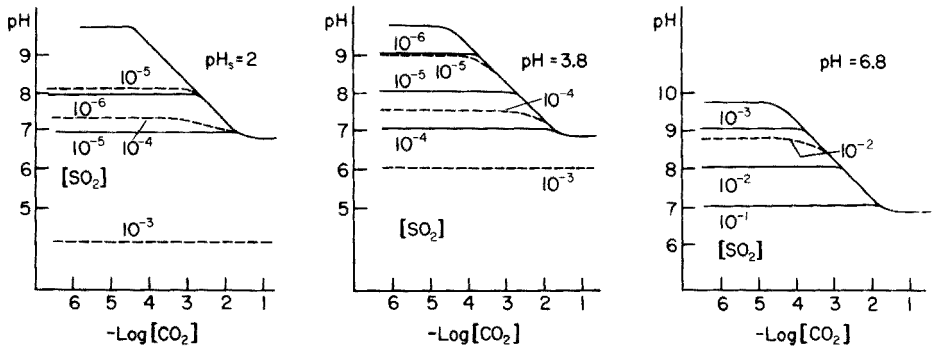

Fig. 5. Theoretical and experimental calibration curves for CO_2 in the presence of SO_2 as interferent. Dashed lines are the experimental curves, and solid lines the theoretical curves. The upper curve is the CO_2 calibration (experimental) in the absence of interferences. The concentration of the interferent is labelled on the right for experimental curves and on the left for theoretical curves. The three plots were obtained by buffering the sample solution at different pH values to obtain complete and partial conversion for the SO_2 species.

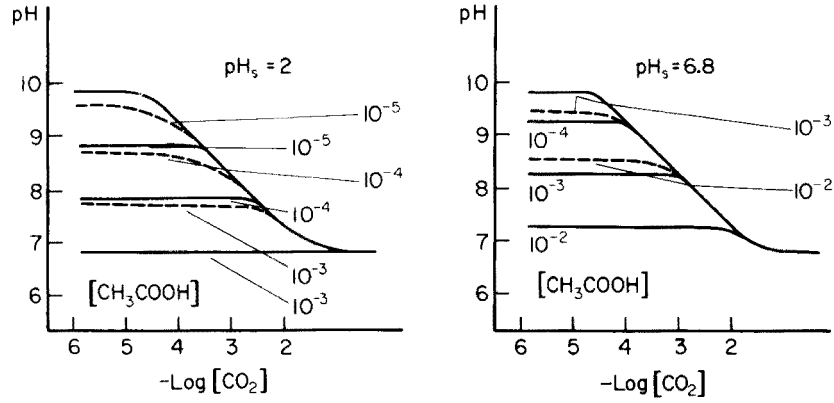

Fig. 6. Theoretical and experimental calibration curves for CO_2 in the presence of acetic acid as interferent. Dashed lines are the experimental curves; solid lines are theoretical curves. The upper curve is the CO_2 calibration without interference. The numbers on the curves have the same meaning as in Fig. 5. The two plots were obtained by buffering the sample solution at different pH values to obtain complete and partial conversion for the acetic acid species.

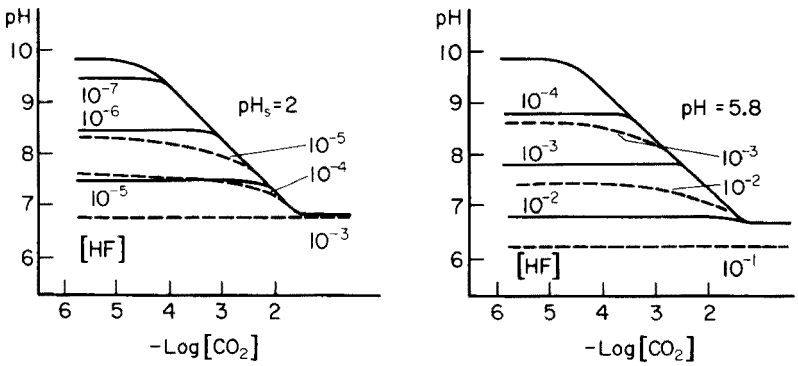

Fig. 7. Theoretical and experimental calibration curves for CO_2 in the presence of HF as interferent. Dashed lines are the experimental curves; solid lines are theoretical curves. The upper curve is the CO_2 calibration without interference. The numbers on the curves have the same meaning as in Fig. 5. The two plots were obtained by buffering the sample solution at different pH values to obtain complete and partial conversion for the HF species.

follows the trend expected theoretically. From a strict quantitative point of view, the experimental curves show lower interfering effects than the theoretical; this depends on two factors. The first is that equilibrium between the species analyzed and the interfering species is not completely obtained in the film. The second is the continuous diffusion of the species analyzed to the film from the electrolyte bulk. Thus the experimental curves can be considered as working curves for practical purposes. Such curves make it possible to

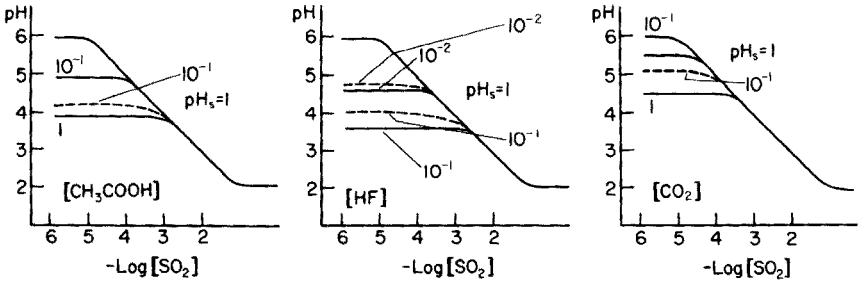

Fig. 8. Theoretical and experimental calibration curves for SO_2 in the presence of CO_2, CH_3COOH, HF as interferents. Dashed lines are the experimental curves; solid lines are theoretical curves. The upper curve is the SO_2 calibration without interference. The numbers on the curves have the same meaning as in Fig. 5. All the plots were obtained at a sample pH low enough to ensure conversion of both acids. SO_2 is the stronger acid and a high pH should enhance the interfering effect.

establish if an analytical problem involving interfering species can be solved. In fact, they were obtained for this purpose more than as a theoretical exercise.

REFERENCES

1 E. H. Hansen and N. R. Larsen, Anal. Chim. Acta, 78 (1975) 459.
2 P. L. Bailey and M. Riley, Analyst, 102 (1977) 212.
3 M. Mascini and C. Cremisini, Anal. Chim. Acta, 92 (1977) 277.
4 G. Hägg, Kemisk Reactionslära, Almqvist and Wiksell AB Stockholm, 1969, pp. 70—72.
5 K. P. Hsiung, S. S. Kuan and G. G. Guilbault, Anal. Chim. Acta, 84 (1976) 15.

Analytica Chimica Acta, 97 (1978) 245—252

THE LIMITS OF DETECTION OF GAS-SENSING PROBES. APPLICATION TO THE AMMONIA SENSOR

F. VAN DER POL

Department of Soils and Fertilizers, Agricultural University, Wageningen (The Netherlands)

(Received 29th September 1977)

SUMMARY

A theory is proposed for the estimation of the limits of detection of the ammonia air-gap or membrane sensor. This theory is also applicable to other gas-sensing probes. The limits of detection depend both on the linearity of the equilibrium response and on the velocity with which the equilibrium is reached. Mathematical expressions are given for both characteristics as a function of the concentration of the inner electrolyte and the partial pressure of CO_2 in the system. Based on these expressions, the detection limits of the electrode are calculated for different conditions.

In a recent paper on the limits of detection of gas-sensing probes, Bailey and Riley [1] compare theoretically derived limits with experimentally obtained limits. They query, rightly, the correctness of the graphical method presented by Hansen et al. [2, 3], which leads to the conclusion that the lower limit of detection for the ammonia air-gap electrode is equal to the concentration of ammonia in the ammonium chloride used as the internal electrolyte. Bailey and Riley [1] calculated the pH response in the electrolyte film as a function of the equilibrium concentration of ammonia in this film, the former being directly related to the electrode response, and the latter to the concentration of ammonia in the sample. Their calculations are based on substitution of the appropriate equilibrium relations into the electroneutrality equation that holds for the film. In this way, the equilibrium response of the electrode and its linearity with respect to $\log[NH_3]$ can be calculated.

In the present paper, it is shown that, in most cases, it is not the lower limit of linearity that determines the limit of detection, but the fact that below a certain ammonia level the velocity with which equilibrium is reached decreases rapidly to zero. Fortuitously enough, this level is situated at the same ammonia concentration in the internal electrolyte as is mentioned by Hansen and Larsen [3]. The influence of CO_2 on the limit of detection of the ammonia sensor is also discussed.

EQUILIBRIUM RESPONSE OF THE SENSOR

The theory of Bailey and Riley is summarized below; to improve exactitude, differences between concentrations and activities are not neglected.

The sensor assembly consists of a glass electrode which responds to the pH of the electrolyte film on its sensitive surface according to Nernst's law, and of an Ag/AgCl reference electrode in an internal electrolyte solution which is in contact with the film of the same composition. The potential difference between these two electrodes can be written as

$$E = E_g^0 - E_{AgCl}^0 + \frac{RT}{F} \ln (Cl^-)_{electrolyte} + \frac{RT}{F} \ln (H^+)_{film} \quad (1)$$

The H^+ activity is related to the ammonia activity in the film by the equilibrium constant for the dissociation of ammonium ion [4]

$$NH_4^+ \rightleftharpoons NH_3 + H^+; \quad K_a = 5.5 \times 10^{-10} \quad (2)$$

giving the relationship

$$(NH_3)_{film} = K_a \cdot (NH_4^+)_{film} \times (H^+)_{film}^{-1} \quad (3)$$

As long as the NH_4^+ activity in the film remains constant, the relationship between the electrode potential and $\ln(NH_3)_{film}$ will be linear. For inspection of the limits of linear response, the exact behaviour of this NH_4^+ activity can be calculated from the charge balance that holds in the film

$$[NH_4^+] + [H^+] = [Cl^-] + [OH^-] \quad (4)$$

or

$$f_{NH_4^+}^{-1} \cdot (NH_4^+) = [Cl^-] + f_{OH^-}^{-1} \cdot \frac{K_w}{(H^+)} - f_{H^+}^{-1} \cdot (H^+) \quad (5)$$

where ( ) represent activities and [ ] concentrations, the two being related by activity coefficients (f). Substitution of the NH_4^+ activity resulting from the charge balance in eqn. (3) gives the following relationship between NH_3 and H^+ activity in the film

$$(NH_3) = K_a \cdot \left\{ f_{NH_4^+} \cdot [Cl^-] + \frac{A}{(H^+)} - \frac{f_{NH_4^+}}{f_{H^+}} (H^+) \right\} \cdot (H^+)^{-1} \quad (6)$$

where $A = K_w f_{NH_4^+}/f_{OH^-}$. The relation between (NH_3), (NH_4^+) and (H^+) in the film is calculated from eqn. (6). Activity coefficients are computed from the Debye—Hückel equation [5]

$$-\log f_i = 0.51 z_i^2 I^{\frac{1}{2}}/(1 + 0.33 \mathring{a}_i I^{\frac{1}{2}}) \quad (7)$$

For univalent ions $z = 1$; I is the ionic strength of the film which is assumed to be kept at 0.1 M by addition of inert supporting electrolyte if low NH_4Cl concentrations are used in the electrode. The mean diameters ($\mathring{a}$) of the solvated NH_4^+, OH^- and H^+ ions were assumed to be 3, 3 and 9 Å, respectively.

The results are given in Fig. 1. It can be concluded that: (1) the lower limit of linearity is not dependent on the electrolyte concentration; (2) the range of linearity is larger for higher electrolyte concentrations; and (3) the same NH_3 activity corresponds to a smaller change in pH of the film if a higher electrolyte concentration is used.

RESPONSE TIME OF THE SENSOR

The time of response of the sensor will be determined by the time required to build up a concentration of ammonia in the film in equilibrium with the partial pressure (p_{NH_3}) of the sample. This time depends on the readiness with which the gas is liberated from the sample, the velocity of ammonia transport through the gas phase and the readiness with which the gas dissolves in the film; all these effects govern the final flux of NH_3 through the film or air-gap interface. However, not all the ammonia entering the film will be used to build up the concentration of ammonia. Part of it reacts with H^+ to form NH_4^+, thus causing the change in pH of the film which is registered by the sensitive surface of the glass electrode. This means that the response time also depends on the fraction (F) of the NH_3 flux used to change the NH_3 concentration in the film. This fraction, which may be called the efficiency of the flux, can be written as the change in the NH_3 concentration caused by this flux during a very short period of time, divided by the change in the total concentration of $NH_3 + NH_4^+$ during this period, or

$$F = \frac{d[NH_3]}{d[NH_4^+] + d[NH_3]} = \left\{\left(\frac{d[NH_3]}{d[NH_4^+]}\right)^{-1} + 1\right\}^{-1} = \{G^{-1} + 1\}^{-1} \qquad (8)$$

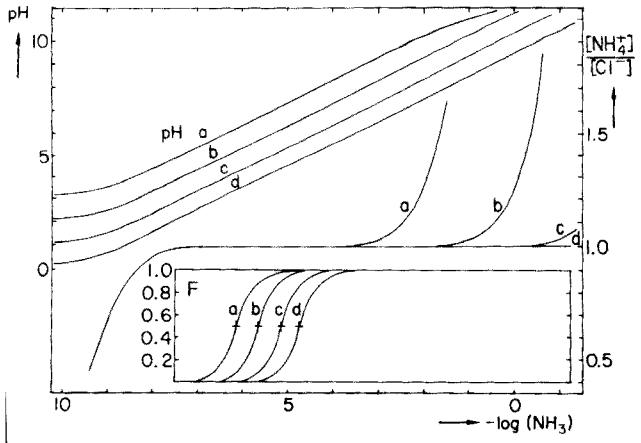

Fig. 1. pH response of the film and linearity of the response (represented as $[NH_4^+]/[Cl^-]$ in the film) and NH_3 flux efficiency (F) as a function of the NH_3 concentration in the film. Inner electrolyte concentrations 0.001 M (a), 0.01 M (b), 0.1 M (c), 1 M (d). Symbol + indicates the NH_3 concentration of the electrolyte itself by hydrolysis.

where

$$G = \frac{d[NH_3]}{d[NH_4^+]} = \frac{K_a}{f_{NH_4^+}^{-1}} \cdot \frac{d(NH_4^+)\,(H^+)^{-1}}{d(NH_4^+)} = K_a \left\{ \frac{(H^+)^{-1}}{f_{NH_4^+}^{-1}} - \frac{(NH_4^+)\,(H^+)^{-2}}{f_{NH_4^+}^{-1}} \cdot \frac{d(H^+)}{d(NH_4^+)} \right\} \tag{9}$$

and all concentrations and activities refer to the film.

From the charge balance in the film (eqn. 5),

$$f_{NH_4^+}^{-1}\, d(NH_4^+) = d\,\frac{A}{(H^+)} - f_{H^+}^{-1}\, d(H^+) = -\{A \cdot (H^+)^{-2} + f_{H^+}^{-1}\}\, d(H^+) \tag{10}$$

or

$$\frac{d(H^+)}{f_{NH_4^+}^{-1} \cdot d(NH_4^+)} = -\{A \cdot (H^+)^{-2} + f_{H^+}^{-1}\}^{-1}$$

and after substitution in eqn. (9)

$$G = K_a\,(H^+)^{-1} \left\{ f_{NH_4^+} + (NH_4^+) \Big/ \left[\frac{A}{(H^+)} + \frac{(H^+)}{f_{H^+}} \right] \right\} \tag{11}$$

Graphs of the ammonia flux efficiency, calculated from eqns. (8) and (11) are shown in Fig. 1 as a function of the concentration of ammonia in the film. These plots show that the efficiency approaches 1 at high NH_3 concentrations, but decreases rapidly at concentrations lower than the concentration of NH_3 in the electrolyte itself. In fact, at this latter concentration the efficiency is about 0.5, which can also be derived from eqn. (11). If, at the low pH in the pure electrolyte, $A/(H^+)$ is neglected with respect to (H^+), and if $(NH_4^+) \gg (H^+)$, then $G \approx K_a\,(NH_4^+)/(H^+)^2$. Since the pH of the pure electrolyte is given by $(H^+) = \{K_a \cdot (NH_4^+)\}^{\frac{1}{2}}$, then $G \approx 1$, which indicates 50% efficiency.

Furthermore, when the equilibrium concentration of NH_3 is only 3 times lower than the initial NH_3 concentration in the film, the efficiency decreases to about 10%, so that the response time for this low concentration is at least ten times longer than for high concentrations. If, in order to obtain the final response in a reasonable time, a minimum efficiency of 25% is accepted, then it can be concluded from Fig. 1 that the lower limit of detection is determined not by the non-linear response of the electrode, but by the time needed to obtain the response.

The influence of the flux efficiency on the rate of equilibration can be illustrated by an experiment with an air-gap electrode which was prepared as described by Hansen and Růžička [2]. After equilibration for 10 min above a 0.5 M H_2SO_4 solution of zero NH_3 activity, the electrode was put above an alkaline solution with $[NH_3] = 2 \times 10^{-3}$ M, and the response—time curve was recorded (Fig. 2). If the flux efficiency had no effect, dE/dt would be expected to decrease gradually with time. However, at $[NH_3]_{film} \approx [NH_3]_{0.1\ M\ NH_4Cl}$, dE/dt increases with time as a result of the rapidly increasing flux efficiency.

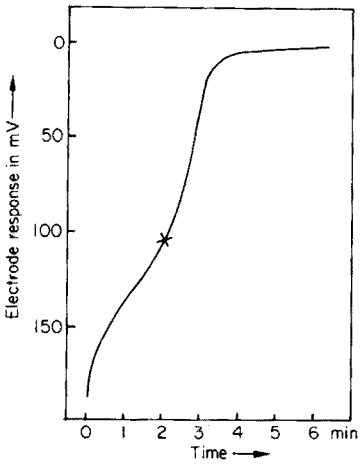

Fig. 2. Recorded electrode response after transfer from a sample with $[NH_3] = 0$ to a sample with $[NH_3] = 2 \times 10^{-3}$. The cross marks the response corresponding to the NH_3 activity of NH_4Cl itself.

INTERFERENCE OF CARBON DIOXIDE

When the so-called total conversion method is used, the NH_3 in the air gap is measured above solutions which are made strongly alkaline. In that case, the influence of CO_2 will be negligible as the partial pressure of CO_2 at equilibrium approaches zero because of the formation of carbonates in the sample. Natural samples may have a much higher p_{CO_2} value at equilibrium because of buffering by considerable quantities of hydrogencarbonate and carbonate. The CO_2 will also dissolve in the film on the glass electrode to a concentration that is in equilibrium with the p_{CO_2} in the air gap. If the pH in the film is low (pH < 4.5), there will be no influence, but at higher pH the formation of hydrogencarbonates and eventually of carbonates will buffer the pH in the film and affect the NH_3 response. Since the effect increases with pH, it will be more pronounced at higher NH_3 activities and at lower electrolyte concentrations of NH_4Cl.

The exact influence of CO_2 can be calculated by means of the equilibrium constants for hydrogencarbonate and carbonate formation [5]

$$CO_2 + H_2O \rightleftharpoons H^+ + HCO_3^-, \quad K_1 = 10^{-7.81} \text{ mol l}^{-1} \text{ bar}^{-1}$$

$$HCO_3^- \rightleftharpoons H^+ + CO_3^{2-}; \quad K_2 = 10^{-10.33} \text{ mol l}^{-1}$$

leading to the relations

$$(HCO_3^-) = K_1 (H^+)^{-1} p_{CO_2}$$

and

$$(CO_3^{2-}) = K_1 K_2 (H^+)^{-2} p_{CO_2}$$

Introduction of the latter expressions into the charge balance of the film

$$[NH_4^+] + [H^+] = [Cl^-] + [OH^-] + [HCO_3^-] + 2\,[CO_3^{2-}]$$

results again in the relation between the NH_3 and H^+ activities in the film. The result is identical to eqn. (6) derived earlier but here with

$$A = K_w\, f_{NH_4^+}\, f_{OH^-}^{-1} + p_{CO_2}\, K_1\, f_{NH_4^+}\, \{f_{HCO_3^-}^{-1} + 2K_2\,(H^+)^{-1}\, f_{CO_3^{2-}}^{-1}\} \qquad (12)$$

Equations (6) and (12) were used to recalculate the relation between (NH_3), (NH_4^+) and (H^+) for two values of p_{CO_2}. The partial pressure in normal air (p_{CO_2} = 0.3 mbar) was chosen as the first value. The second value was p_{CO_2} = 30 mbar, which is commonly encountered in soils. The results are

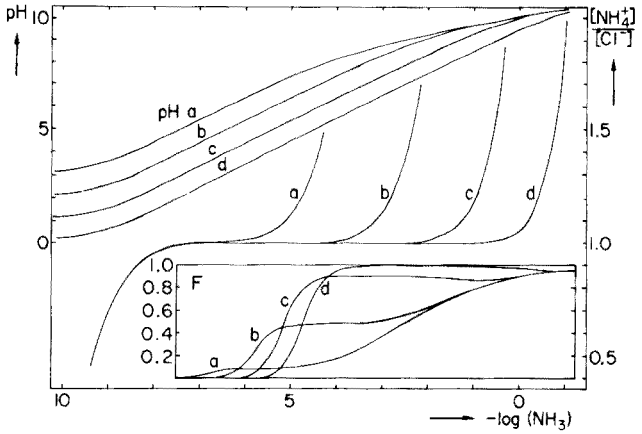

Fig. 3. The functions described are the same as in Fig. 1, but the system is in equilibrium with normal air (p_{CO_2} = 0.3 mbar).

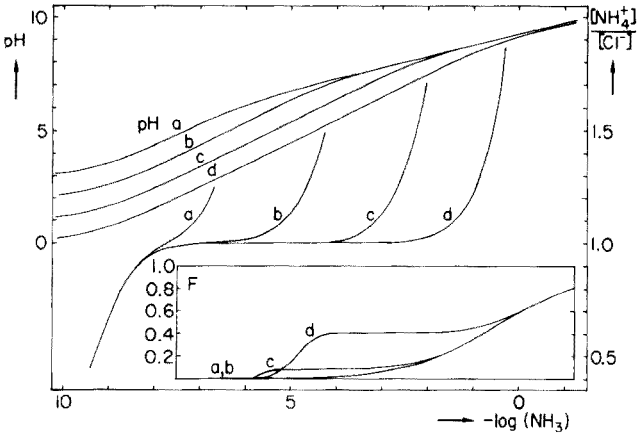

Fig. 4. The functions described are the same as in Fig. 1, but the system is in equilibrium with air of high CO_2 content (p_{CO_2} = 30 mbar).

shown in Figs. 3 and 4. (The activity coefficients of HCO_3^- and CO_3^{2-} were calculated from eqn. (7), with $\mathring{a}$ = 4 and 5 Å, respectively [5].)

The efficiency of the NH_3 flux was derived by following the same route as that described under Response Time. The only difference lies in the term $d\{A/(H^+)\}$ in eqn. (10) which becomes $B(H^+)^{-2}$ instead of $A(H^+)^{-2}$, where

$$B = A + 2K_1K_2 p_{CO_2} (H^+)^{-1} f_{NH_4^+} f_{CO_3^{2-}}^{-1} \quad (13)$$

The second term in eqn. (13) represents the pH-dependence of A, thus

$$G = K_a (H^+)^{-1} \left\{ f_{NH_4^+} + (NH_4^+) \Big/ \left[\frac{B}{(H^+)} + \frac{(H^+)}{f_{H^+}} \right] \right\} \quad (14)$$

from which the NH_3 flux efficiencies in Figs. 3 and 4 were calculated. It can be seen that both the linearity and the efficiency of the sensor are significantly decreased when CO_2 is present, especially for low inner electrolyte concentrations. At a given concentration of NH_3, depending on the inner electrolyte concentration and the partial pressure of CO_2 in the system, the sensitivity of the sensor can change from ±60 mV/decade to ±30 mV/decade. In the transition region, the flux efficiency decreases to a lower level when the inner electrolyte concentration is lower.

DISCUSSION

If it is assumed that the deviation from linearity should be less than 15% and that the flux efficiency should be better than 25%, the detectable ranges mentioned in Table 1 are obtained. These ranges are in fair agreement with those quoted by Hansen and Larsen [3] and with the experimental limits summarized by Bailey and Riley [1].

The minimum flux efficiency of 25% is chosen quite arbitrarily; it depends on the construction of the electrode. The higher the NH_3 flux, the lower the minimum flux efficiency required; this efficiency is also determined by the stability of the electrode and of the system to be measured. However, one cannot work with a significantly lower flux efficiency: with a sample/film volume ratio of 1000:1 and a flux efficiency of 1:1000, a change in the

TABLE 1

Limits of detection of the ammonia electrode, in mol l^{-1}, for different inner electrolyte concentrations and partial CO_2 pressures

p_{CO_2} (mbar)	$[NH_4Cl]_{film}$			
	0.001 M	0.01 M	0.1 M	1 M
0	5×10^{-7}—5×10^{-3}	10^{-6}—0.5	5×10^{-6}—> 2	10^{-5}—> 2
0.3	—	2×10^{-6}—10^{-3}	5×10^{-6}—10^{-1}	10^{-5}—2
30	—[a]	—[a]	—[a]	2×10^{-5}—5×10^{-2}

[a] > 0.03 M with a sensitivity of only 30 mV/decade.

NH_3 concentration in the film would cause a change of the same magnitude in the sample but in the opposite direction. Thus the assumption that the sample concentration remains unchanged when the sensor is introduced becomes false.

Because of the influence of CO_2, the limits of detection depend on the method of determination used, either the total conversion method in strongly alkaline solutions or the partial conversion method. The optimum concentration of the inner electrolyte can be chosen in accordance with the concentrations that should be measured. For low concentrations, an inner electrolyte concentration of 0.001 M NH_4^+ or even lower might be selected, but the system should then be free of CO_2. For most purposes, 0.01 M NH_4^+ seems an acceptable concentration, but for work in natural systems with high CO_2 content, the inner electrolyte concentrations should be between 0.1 and 1 M NH_4^+.

I thank Ir. J. Ch. van Schouwenburg for helpful and stimulating discussions and for critical reading of the manuscript.

REFERENCES

1 P. L. Bailey and M. Riley, Analyst, 102 (1977) 213.
2 E. H. Hansen and J. Růžička, Anal. Chim. Acta, 72 (1974) 353.
3 E. H. Hansen and N. R. Larsen, Anal. Chim. Acta, 78 (1975) 459.
4 W. J. Blaedel and V. W. Meloche, Elementary Quantitative Analysis, Harper & Row, N.Y., 1964, p. 923.
5 G. H. Bolt and M. G. M. Bruggenwert (Ed.), Soil Chemistry A. Basic Elements, Elsevier, Amsterdam, pp. 17, 97.

Analytica Chimica Acta, 97 (1978) 253—258

RELATIVKONDUKTOMETRISCHE BESTIMMUNG DER DURCHSCHNITTLICHEN SCHICHTDICKE ORGANISCHER FILME AUF ALUMINIUMFOLIEN

H. MALISSA*, R. KELLNER und G. GIDÁLY

Institut für Analytische Chemie und Mikrochemie der Technischen Universität Wien, A-1060 Wien (Österreich)

(Eingegangen den 7. November 1977)

ZUSAMMENFASSUNG

Die Anwendbarkeit der relativkonduktometrischen Kohlenstoffbestimmung zur Bestimmung der Schichtdicke dünner organischer Schichten auf Aluminiumfolien wurde untersucht. Die organischen Schichten wurden direkt auf der Aluminiumfolie bei 1000°C im Sauerstoffstrom verbrannt und das aus der Schicht entstandene CO_2 relativkonduktometrisch bestimmt. Die gefundene Menge Substanz wurde auf die Probenoberfläche bezogen und so die mittlere Schichtdicke erhalten. Ein großer Vorteil dieser Methode ist der geringe Zeitbedarf von ca. 2 Min. pro Bestimmung. Die relative Standardabweichung der Methode betrug für die untersuchten Proben 5,2% bei einer Schichtdicke von 3 g m^{-2} (1 g m^{-2} ist 1 μm bei einer Dichte der Schicht von 1 g cm^{-3}). Die der Probenfläche verkehrt proportionale Nachweisgrenze wurde mit 0,0354 g m^{-2} bei 1 cm^2 Probenoberfläche bestimmt.

SUMMARY

The relative-conductometric determination of thin plastic films on aluminium foil

The relative-conductometric carbon determination can be applied to the determination of the thickness of thin plastic films on aluminium foils. The organic cover is decomposed directly on the aluminium foil in a stream of oxygen at 1000°C, and the CO_2 formed is determined by relative conductometry. The amount of organic material is correlated to the surface area of the sample, and the film thickness calculated. A single determination requires not more than 2 min. For the samples studied, the relative standard deviation is 5.2% for a film thickness of 3 g m^{-2} (1 g m^{-2} corresponds to a thickness of 1 μm if the density is 1 g cm^{-3}). The detection limit, which is inversely proportional to the surface area of the sample, is 0.0354 g m^{-2} for 1-cm^2 samples.

Kunststoffbeschichtete Aluminiumfolien finden eine sich ständig ausweitende Verwendung in der Verpackungsindustrie. Bei der Analyse dieser organischen Schichten ist neben der qualitativen und quantitativen Zusammensetzung auch die Menge der Substanz pro Fläche oder die Schichtdicke zu bestimmen, da diese neben der Oberflächenstruktur des Metalles ein wesentliches Kriterium für die Haftfähigkeit weiterer Beschichtungen darstellt.

Die Schichtdicke ist mit der Menge Substanz pro Flächeneinheit über die Dichte der Schicht verbunden, die aber wegen Porosität und Inselstruktur nicht

mit der Dichte der Substanz identisch ist. Daher wird in dieser Arbeit die als Belegung bezeichnete Menge Substanz pro Flächeneinheit in g m^{-2} angegeben. Wird durch ein Analysenverfahren die Menge Substanz pro Flächeneinheit bestimmt, so läßt sich daraus unter Annahme einer gleichmäßigen Verteilung die durchschnittliche Schichtdicke berechnen, bei einer Dichte der Schicht von 1 g cm^{-3} entspricht eine Belegung von 1 g m^{-2} einer durchschnittlichen Schichtdicke von 1 μm. Initiiert durch die Halbleitertechnologie wurden gute Schichtdickenbestimmungsmethoden ausgearbeitet, die sich jedoch fast ausnahmslos nur für schichten anorganischer Stoffe (Metalle und Metalloxide) einsetzen lassen [1].

Für Schichten organischer Stoffe gibt es nur wenige anwendbare Verfahren. Einige davon sind:

a. Interferometrische Bestimmung der Schichtdicke. Dazu muß die Schicht gut reflektierende Phasengrenzen besitzen und es wird nur die Schichtdicke bestimmt [2].

b. IR-ATR-Spektroskopische Bestimmung der Belegung. Neben der Belegung läßt sich mit dieser Methode auch die qualitative und quantitative Zusammensetzung der Schicht bestimmen. Es können Schichtdicken in einem Bereich von ca. 1 bis 1000 nm bestimmt werden [3].

c. Gravimetrische Bestimmung der Belegung. Die Schicht wird mit einem Lösungsmittel abgewaschen und der Gewichtsverlust durch Wägen bestimmt. Die Einsatzgrenze der gravimetrischen Methode liegt bei etwa 0,1 g m^{-2} Schicht auf Aluminiumfolien (20—50 mg cm^{-2}), darunter läßt sich trotz Vergrößerung der Probenfläche nur schwer eine Bestimmung durchführen, da das Gewichtsverhältnis Schicht zu Trägerfolie zu ungünstig wird.

d. Bestimmung der Belegung durch relativkonduktometrische Bestimmung der Verbrennungsprodukte. Grundgedanke zu dieser Methode war, die zeitraubende, gravimetrische Bestimmung durch eine schnellere Methode zu ersetzen, die auch noch empfindlicher sein sollte.

Ist die quantitative Zusammensetzung der Schichtsubstanz, oder zumindest ihr Kohlenstoffgehalt, bekannt, so läßt sich sehr schnell und genau durch Verbrennung der beschichteten Probe im Sauerstoffstrom bei sehr hohen Temperaturen und relativkonduktometrischer Bestimmung des Verbrennungsproduktes CO_2 die Menge bestimmen [4]. Die untersuchte Schicht darf nur auf einer Seite der Folie sein, oder muß auf beiden Seiten gleich sein. Die gefundene Menge Substanz wird dann auf die Probenfläche bezogen.

EXPERIMENTELLES

Probenmaterial

Probenserie A. Es lagen mit Vinylite (PVC-PVA) beschichtete Aluminiumfolien in sieben verschiedenen Belegungen von 1,31 bis 4,68 g m^{-2} vor. 1,29 gm^{-2} Vinylite sind 1 μm bei idealer Schicht.

Probenserie B. Um den untersuchten Bereich in Richtung dünner Schichten zu erweitern, wurde Vinylite in Äthylmethylketon gelöst und definierte Volumina mit einer Mikroliterspritze auf Aluminiumfähnchen von 2-cm² Fläche aufgetragen und möglichst gleichmäßig verteilt. Die mittlere Belegung dieser Proben ergibt sich aus der aufgetragenen Menge pro Flächeneinheit.

Meßprinzip

Die Proben wurden in ausgeglühten Porzellanschiffchen bei 1000°C im reinen Sauerstoffstrom verbrannt, das aus dem Vinylite entstehende HCl wurde durch einen Silberwolle-Kontakt absorbiert und das Kohlendioxid relativkonduktometrisch mit einem Analysenautomaten Wösthoff "Carmhomat" bestimmt [4].

Der Gehalt an Kohlenstoff im Vinylite wurde auf gleiche Weise bestimmt und die Digitalanzeige des Analysenautomaten in mg Vinylite geeicht. Aus 5 Bestimmungen ergab sich ein Mittelwert von 3689 Skaleneinheiten pro mg Vinylite mit einer relativen Standardabweichung von 3,79%.

Messung der Belegung der Proben der Serie B

Die Probengröße betrug 2 cm², vom Ergebnis wurde der Blindwert der zur Beschichtung verwendeten Aluminiumfolien (25,16 Skaleneinheiten) abgezogen. Die Ergebnisse zeigt die Tabelle 1. Der Ausgleich nach kleinsten Quadraten für die 55 Meßwerte ergibt für die Ausgleichsgerade einen Ordinatenabschnitt von −0,00166 und eine Steigung von 1,0524 bei einem Bestimmtheitsmaß r^2 von 0,997.

Messung der Proben der Serie A

Zur Überprüfung der angegebenen Belegungen wurde eine gravimetrische Bestimmung der Belegung durchgeführt, indem Proben der Größe 14,5 × 35 mm vor und nach dem Waschen mit Äthylmethylketon gewogen wurden. Die

TABELLE 1

Ergebnis der relativkonduktometrischen Bestimmung der Belegung der Proben der Serie B (Eichproben). (Probengröße: 2 cm², Schicht einseitig.)

Aufgetragen (g m^{-2})	Anzahl der Bestimmungen	Gefunden[a]	
		(g m^{-2})	s_r (%)
0,108	7	0,115	8,73
0,216	7	0,221	3,47
0,431	7	0,461	4,99
0,647	6	0,658	8,07
1,08	7	1,17	2,98
1,62	7	1,73	3,36
2,16	7	2,18	5,17
3,24	7	3,44	1,10

[a]Mittelwerte.

TABELLE 2

Ergebnis der gravimetrischen Überprüfung und relativkonduktometrischen Bestimmung der Belegung der Proben der Serie A

Angegeben	Gravimetrisch[a]		Relativkonduktometrisch[c]		
	Gefunden[b]		Anzahl der Bestimmungen	Gefunden[d]	
($g\ m^{-2}$)	($g\ m^{-2}$)	s_r (%)		($g\ m^{-2}$)	s_r (%)
1,31	1,25	3,06	10	1,38	14,45
2,01	1,89	2,14	6	1,88	6,57
2,68	2,65	6,24	6	2,73	4,18
3,24	3,07	2,25	7	3,12	8,67
3,41	3,37	6,44	6	3,38	7,30
4,05	4,31	3,08	6	4,34	2,22
4,68	4,93	0,67	6	5,00	7,13

[a]Probengröße: 14,5 × 35 mm, Schicht einseitig.
[b]Mittelwerte der 3 Bestimmungen.
[c]Probengröße: 9,5 × 17,5 mm, Schicht einseitig.
[d]Mittelwerte.

Ergebnisse zeigt die Tabelle 2. Für die 21 Meßwerte ergibt sich eine Standardabweichung von 0,120 g m^{-2}, bezogen auf den Wert 3,07 g m^{-2} eine relative Standardabweichung von 3,91%.

Die relativkonduktometrische Bestimmung der Belegung wurde mit Proben der Größe 9,5 × 17,5 mm durchgeführt, die mit einer Schablone ausgeschnitten wurden. Die Meßwerte zeigt ebenfalls Tabelle 2. Der Ausgleich nach kleinsten Quadraten für die 47 Meßwerte ergibt für die Ausgleichsgerade der relativkonduktometrisch gefundenen Belegung gegen die gravimetrisch gefundene Belegung einen Ordinatenabschnitt von 0,0633 und eine Steigung von 1,007 bei einem Bestimmtheitsmaß r^2 von 0,971.

Führt man für alle 102 Meßwerte der beiden Meßreihen den Ausgleich nach kleinsten Quadraten durch, so erhält man für die Ausgleichsgerade einen Ordinatenabschnitt von 0,00276 und eine Steigung von 1,022 bei einem Bestimmtheitsmaß r^2 von 0,989. Für alle 102 Meßwerte wurde eine Standardabweichung von 0,155 g m^{-2} erhalten, bezogen auf eine Schichtdicke von 3 g m^{-2} ergibt sich eine relative Standardabweichung von 5,2%. Die graphische Darstellung aller Meßwerte zeigt die Abb. 1.

Bestimmung der Nachweisgrenze

Die Nachweisgrenze ist gegeben durch die Beziehung [5]

$$NG = x_{Bl} + 6 \times s_{Bl}$$

x_{Bl} ist der Mittelwert und s_{Bl} die Standardabweichung des Blindwertes. Der Blindwert des Schiffchens und der Trägerfolie läßt sich bestimmen und von den Meßwerten subtrahieren. Die Beziehung für die Nachweisgrenze reduziert sich auf: $NG = 6 \times s_{Bl}$. Mit 2-cm^2 großen Proben der unbeschichteten

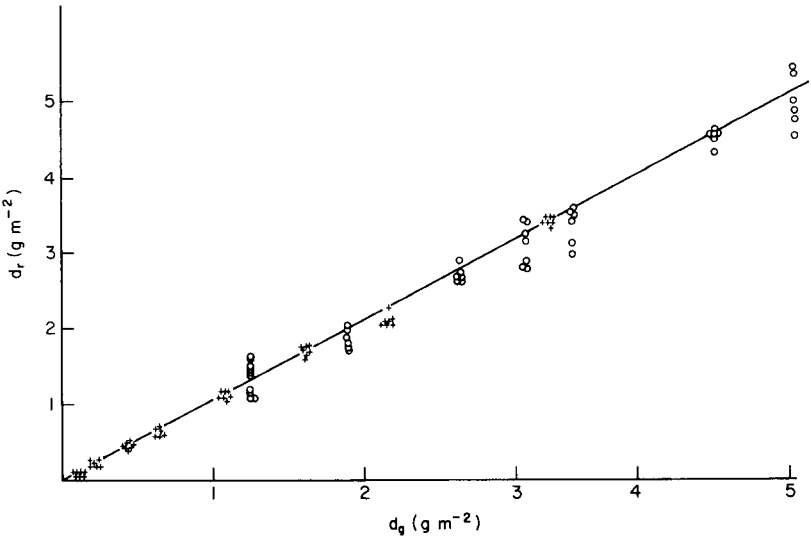

Abb. 1. Relativkonduktometrisch bestimmte Belegung (d_r) in Abhängigkeit von der gravimetrisch bestimmten oder durch Auftragung vorgegebenen Belegung (d_g).
○ Probenserie A, + Probenserie B. Ausgleichsgerade: $k = 1{,}022$; $d = 0{,}00276$; $r^2 = 0{,}989$.

Aluminiumfolie wurde der Blindwert x_{Bl} mit 25,16 Skalenteilen, entsprechend 0,0068 mg Vinylite mit einer Standardabweichung von 0,000591 mg Vinylite bestimmt. Die sechfache Standardabweichung 0,00354 mg Vinylite entspricht bei 1-cm² Probenfläche 0,0354 g m^{-2}, drückt man die Nachweisgrenze in g m^{-2} aus so ergibt sich: NG = $0{,}0354/F$ g m^{-2} (F = Probenfläche in cm²).

DISKUSSION

Die statistische Auswertung der Meßergebnisse ergab einen linearen Zusammenhang mit einem Bestimmtheitsmaß r^2 von 0,989 zwischen gemessener CO_2-Menge und der Belegung der Probe. Vorteil der Methode ist ihre einfache Durchführung und ihr geringer Zeitbedarf von etwa 2 Min. pro Probe. Die relative Standardabweichung betrug für die untersuchten Proben im Bereich von 0,1 bis 5 g m^{-2} 5,2% bezogen auf 3 g m^{-2}.

Für die umständlichere und wesentlich zeitaufwendigere gravimetrische Methode wurde mit dengleichen Proben ein relative Standardabweichung von 3,91%, bezogen auf 3 g m^{-2}, bestimmt. Die Nachweisgrenze der gravimetrischen Methode hängt weitgehend von der verwendeten Waage ab, bei Verwendung einer Mikrowaage und einem Foliengewicht von ca. 20 mg cm^{-2} liegt sie im nm-Bereich. Diese Methode ist jedoch durch ihre umständliche, zeitraubende Probenvorbereitung (Konditionierung) in ihrer praktischen Anwendbarkeit stark eingeschränkt.

Die Nachweisgrenze für die relativkonduktometrische Bestimmung wurde mit 0,0354 g m^{-2} bei 1-cm² Probenoberfläche bestimmt. Diese der Proben-

oberfläche verkehrt proportionale Nachweisgrenze läßt sich durch Vergrößerung der Probenfläche noch absenken. Laufende Arbeiten zeigen auch eine gute Übereinstimmung mit der unter 1.b erwähnten IR-ATR-Methode [6].

LITERATUR

1 R. W. Berry, P. M. Hall und M. T. Harris, Thin Film Technology, Van Nostrand, Princeton, N.J., 1968.
2 N. J. Harrick, Appl. Opt., 10 (1971) 2344.
3 R. Kellner und G. Gidály, Mikrochim. Acta, im Druck.
4 H. Malissa, Mikrochim. Acta, 1 (1960) 127; Z. Anal. Chem., 181 (1961) 39.
5 K. Doerffel, Beurteilung von Analysenverfahren und -Ergebnissen, Springer-Verlag, 1962.
6 R. Kellner und G. Gidály, in Vorbereitung.

Analytica Chimica Acta, 97 (1978) 259—267

SINGLE-POINT TITRATIONS
Part III. Experimental Determination of Acids

OVE ÅSTRÖM

Department of Analytical Chemistry, University of Umeå, S-901 87 Umeå (Sweden)

(Received 12th September 1977)

SUMMARY

The single-point technique is used for the determination of acids and acid mixtures with basic buffer mixtures. The method is based on the titration of buffer mixtures with strong acid. A linear decrease in pH with concentration is obtained. Compositions of two buffer mixtures, covering different concentration ranges, are given. Determinations of strong acids in the range 0.025—0.25 M are reported. Methods for the determination of mixtures of acids as well as the determination of mono-, di- and tribasic acid solutions are described. The advantages of computed buffer mixtures over diluted ones, and the influence of buffer samples are reported.

When acids and mixtures of acids must be determined, titrations are most commonly chosen on the basis of accuracy and speed. Although it is possible to determine acids by direct potentiometry, the method is normally rejected because of its poor accuracy and uncertainty concerning the degree of protolysis of the acids.

One of the most commonly used methods of evaluation is to linearize the data according to a mathematical model which has been treated theoretically by several authors [1—7]. The linear plot has the advantage over the traditional potentiometric titration method, that several experimental points are used to evaluate the result; it also permits the use of statistical methods. However, the linearization procedures are very laborious and time-consuming, since the experimental data must be stored and calculations must be done on a computer either partly, to evaluate the result from a plot, or completely.

The method used in the present work [8, 9] has certain similarities with linear titration plots. The linearization is done before the titration and need not be repeated for every titration. The time saving is very advantageous in control laboratories or in routine analyses.

When this technique is used for the determination of acids, a mixture of bases is prepared such that when it is titrated with a strong acid a linear relationship is obtained between pH and amount of acid added. Prideaux [10, 11] and Britton and Robinson [12] described buffer solutions where pH is a linear function of base added (the so-called universal buffer solutions), but these were never employed for quantitative analysis.

In this paper it is shown that determinations of strong and weak acids as well as mixtures of acids are possible by using an alkaline buffer mixture and applying the single-point titration technique.

EXPERIMENTAL

Calculations

The FORTRAN program [9] used earlier was revised both to fit the new computer Cyber 172 and to calculate the base concentrations of the mixture. The computer time was reduced considerably from 10—20 min to 10—20 s by the newer and faster computer and by the change in the library routines. The coefficients in eqn. (23) in ref. 8 were evaluated by a program written in BASIC for an Alpha LSI minicomputer. The final calculation of eqn. (23) was performed on an HP9810 calculator.

The conditional constants were evaluated as described earlier [9]. Owing to very small errors in the calculations which were discovered when the alkaline buffer solution was made, minor corrections had to be applied to the constants.

Apparatus and pH measurements

The titration equipment and electrodes were essentially the same as those described previously [9]. Buffer mixture and strong acid were delivered to the titration vessel by motor-driven burettes. The vessel was thermostated at 25.0 ± 0.1 °C. After reaction, the pH was read from an Orion 801 digital pH meter. Values were usually taken within 5 min. Owing to the basic properties of the mixture, carbon dioxide must be excluded; this was ensured by a nitrogen inlet to the vessel. To maintain the silver—silver chloride reference electrode in good condition, it was renewed every two weeks and the outer solution was changed every week.

Standardization

Standardizations of acids and bases in the buffer mixtures were done as described previously [9]. Solutions were prepared with boiled-out water to avoid bubble formation in the burette tubes and to remove dissolved carbon dioxide. Ascarite tubes were attached to burettes to exclude carbon dioxide. From the calculated values of the bases in mixture, a stock buffer mixture of twice this strength was prepared. Equal volumes of that mixture and water were added to the vessel and titrated with hydrochloric acid with the apparatus described earlier [9]. The two buffer mixtures shown in Table 1 were made from the same chemicals as the acidic buffer solution described in Part 2 [9].

RESULTS AND DISCUSSION

By changing the sign of the symbol b in eqn. (1) in ref. 8 and by fulfilling the consequences of that change throughout every equation, it was possible to

TABLE 1

Calculated buffer mixtures for single-point titration of acids

Buffer composition	Conc. (M) stronger solution	Conc. (M) weaker solution
Hydrochloric acid	−0.133508[a]	−0.064267[a]
Formic acid	0.022544	0.010083
Acetic acid	0.014955	0.009753
Malonic acid	0.012843	0.004489
Piperazine	0.021809	0.011470
Bis-tris[b]	0.014375	0.006816
N-Methylmorpholine	0.022611	0.011482
N-Methyldiethanolamine	0.022317	0.011019
Sodium chloride	1.0	1.0
Calculated linear pH range	2.05—8.85	2.35—8.85
Buffer capacity (mM/pH)	20	10
Mean dev. in the range 0—10% (M)	0.00037	0.00019
10—90% (M)	0.00018	0.00011
90—100% (M)	0.00021	0.00011
whole interval (M)	0.00020	0.00012

[a]Negative sign of HCl means addition of NaOH instead of HCl. The program calculates as if all participating compounds were acids. In the stronger solution, the final value for NaOH will be 0.030587 M.
[b]$(HOCH_2CH_2)_2NC(CH_2OH)_3$

calculate the composition of a solution containing a mixture of bases by the procedure described earlier. The solution evaluated by the computer will be presented as if all the components included were acids, and a negative sign on the strong acid will correspond to a strong base.

Two buffer mixtures with linear pH ranges 2.05—8.85 and 2.35—8.85, respectively, were calculated on the basis of earlier experience with the buffer mixture for determining bases. (Identical chemicals were used both from the practical point of view and to avoid standardization difficulties.) The advantage of using stock chemicals for acidic as well as alkaline buffer mixtures is clearly evident when the user wishes to make both, e.g. the standardization procedures are reduced considerably. The stronger buffer mixture was made with buffer strength 20 mM pH^{-1} and the weaker with half that strength (Table 1). The following relationships are valid for the two mixtures, respectively,

$$pH = 8.850 - 50\,c \text{ (stronger solution)} \quad (1)$$

$$pH = 8.850 - 100\,c \text{ (weaker solution)} \quad (2)$$

If the linear pH range data from Table 1 are introduced into eqns. (1) and (2), the two mixtures are found to cover the ranges 0—0.27 M and 0—0.14 M,

respectively. The value will actually be twice that calculated because, for measurements, the buffer mixtures (Table 1) are made with twice the strength tabulated and mixed with an equal amount of sample. The equations are valid only for mixtures with the compositions given in Table 1.

As expected, the mean error is much less in the weaker buffer mixture. It is evident from Table 1, but more easily seen in Fig. 1, that the titration curve for the buffer mixture starts to deviate from the straight line in the boundary regions. A good fit is obtained over the greater part of the curve and the buffer mixture is therefore useful analytically.

Table 2 shows the results of measurements of some strong acids. The concentrations were calculated from eqn. (1) and referred to the mixed solution.

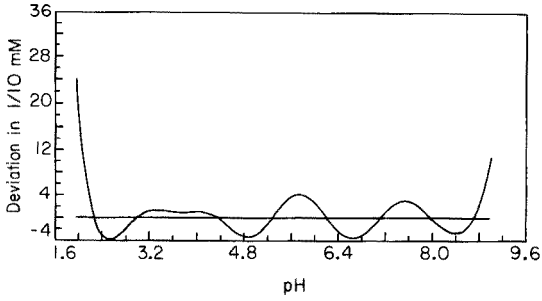

Fig. 1. Theoretical deviation for the stronger (see Table 1) buffer mixture from the predicted straight line.

TABLE 2

Determination of the concentration of some strong acid solutions with the stronger buffer mixture

Compound	$[H^+]$ taken (M)	$[H^+]$ found (mean value) (M)	pH expected	pH found (mean value)	ΔpH
HCl	0.0500	0.05021	6.348	6.340	0.008
	0.1001	0.0998	3.846	3.858	0.012
	0.1251	0.12503	2.595	2.599	0.004
H_2SO_4	0.02490	0.0248	7.605	7.609	0.004
	0.04979	0.05011	6.360	6.345	0.015
	0.07469	0.0751	5.116	5.095	0.021
	0.09959	0.09980	3.870	3.860	0.010
	0.12448	0.12391	2.626	2.654	0.028
HNO_3	0.02470	0.02467	7.615	7.617	0.002
	0.04939	0.04944	6.380	6.378	0.002
	0.07409	0.07407	5.145	5.146	0.001
	0.09879	0.09891	3.911	3.904	0.007
	0.1235	0.1230	2.676	2.700	0.024

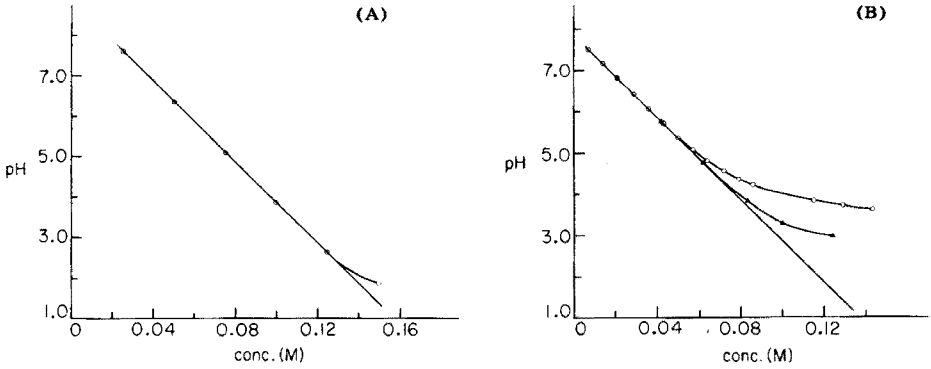

Fig. 2. pH as a function of concentration for different acids. A. Sulphuric acid. B. Acetic acid (○) and formic acid (▲). The straight line is the theoretical line for a strong acid.

The agreement between the values taken and found is very good. The last value for sulphuric acid gives an indication of the slight deviation from the expected value at higher concentrations. The increase in this deviation with concentration is clearly seen in Fig. 2A. Sulphuric acid, usually regarded as a strong acid, shows here the effect of having a second pK_a around pH 1 in 1 M media [13].

Table 2 deals with concentrations of 0.025—0.12 M. If lower concentrations are required, the weak buffer solution is preferred. Table 3 shows the results obtained for hydrochloric acid with this buffer; the concentrations were calculated from eqn. (2). Even here, the experimental values fall close to those expected. The use of the weaker buffer mixture for low concentrations has the advantage that a greater part of the pH range is used per concentration unit, so that errors in the pH measurement have less effect on the final result. For example, a deviation of 0.02 pH units corresponds to an error of 0.0002 M for the weaker buffer and an error of 0.0004 M for the stronger buffer.

The results for the determination of acetic and formic acids are shown in Fig. 2B. The hydrogen ion concentrations of the weak acids are plotted as if they were completely dissociated over the whole pH range. As expected from the pK_a values of the acids, the curve for formic acid follows the predicted straight line to a lower pH than acetic acid. The pK_a values for acetic and formic acids are respectively, 4.45 and 3.40 in the acidic mixture [9], and the starting points of deviation from the straight line show a difference of one pH unit in Fig. 2B. The deviations start at around 1.8—2.0 pH unit from the pK_a and this can be used to give a rough estimate of the pK_a. Similar behaviour is shown by malonic and citric acids (Fig. 3); the two curves almost coincide, probably because the last pK_a values of the dibasic and tribasic acids are very close to each other. The results in Figs. 2 and 3 indicate the possibility of determining the acid strengths of mono-, di- and tribasic acid solutions, provided that the pK_a of the acid sample is known. This problem might be decreased if the linear range of the buffer mixture were extended

TABLE 3

Determination of the concentration of some hydrochloric acid solutions with the weaker buffer mixture

Compound	$[H^+]$ taken (M)	$[H^+]$ found (mean value) (M)	pH expected	pH found (mean value)	ΔpH
HCl	0.01251	0.01245	7.599	7.605	0.006
	0.02502	0.02517	6.348	6.333	0.015
	0.03753	0.03778	5.097	5.072	0.025
	0.05004	0.04998	3.846	3.853	0.007
	0.06255	0.06268	2.595	2.582	0.013

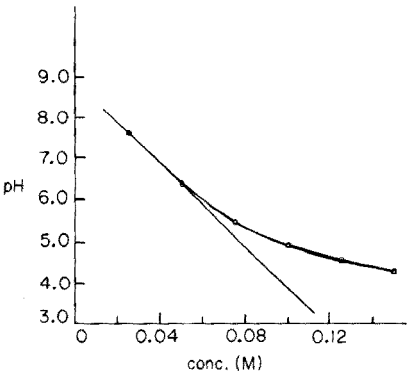

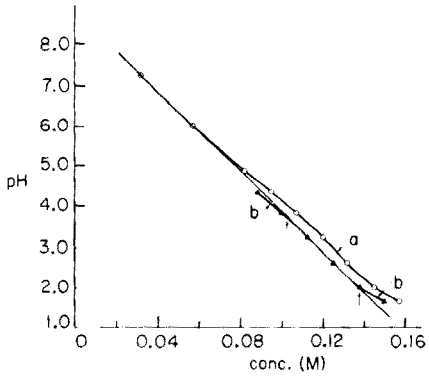

Fig. 3. pH as a function of concentration for malonic acid (○) and citric acid (△). The straight line is the theoretical line for a strong acid.

Fig. 4. pH as a function of concentration for the sum of acetic and hydrochloric acids (○) (upper curve a) and hydrochloric acid alone (▲) (lower curve b). The straight line is the theoretical line for a strong acid. The arrows are explained in the text.

further into the alkaline region. Solutions of mono-, di- and tribasic acids were measured with the stronger buffer mixture; the results are shown in Table 4.

Acetic acid was measured at very close concentration intervals to show the good consistency between the observed and taken values for the pH range lying about 2 pH units above the pK_a value. The last values for the other acids in Table 4 show approximately the highest concentration range measurable with any good agreement. For example, when the measured concentration of formic acid was ca. 0.1 M, the deviation of 0.6 pH read corresponded to an error of ca. 13%.

Figure 4 shows the result for the sum of the concentrations of hydrochloric and acetic acids (upper line a). When the concentrations were calculated as if only hydrochloric acid were present, the lower curve (b) was obtained. The upper curve starts to deviate from the straight line at around the same value as that for acetic acid (Fig. 2B) but the deviation is less pronounced, because the curve was obtained by keeping the acetic acid strength constant and

TABLE 4

Determination of the acid strength of some weak mono-, di- and tribasic acid solutions with the stronger buffer solution

Compound	$[H^+]$ taken (M)	$[H^+]$ found (mean value) (M)	pH expected	pH found (mean value)	ΔpH
Acetic acid	0.007162	0.007120	8.492	8.494	0.002
	0.014325	0.014280	8.134	8.136	0.002
	0.021487	0.021160	7.776	7.792	0.016
	0.028649	0.028430	7.418	7.429	0.011
	0.035812	0.035860	7.059	7.057	0.002
	0.042974	0.043040	6.701	6.698	0.003
	0.050136	0.049640	6.343	6.368	0.025
Formic acid	0.020727	0.020500	7.814	7.825	0.011
	0.062180	0.062380	5.741	5.731	0.010
Malonic acid	0.025000	0.024490	7.600	7.626	0.026
	0.050000	0.049910	6.350	6.355	0.005
Citric acid	0.025000	0.024573	7.600	7.621	0.021
	0.050000	0.048920	6.350	6.404	0.054

varying the hydrochloric acid strength. The lower curve coincides with the straight line over a certain range. The contribution from acetic acid vanishes in the presence of hydrochloric acid; it is possible to evaluate both the total concentration and the concentration of the hydrochloric acid alone, if the measurement is made in a suitable range. The bending of the curves shows that the buffer mixture is inappropriate below pH 2.05.

Table 5 summarizes some measurements on mixtures of hydrochloric and acetic acids. By taking suitable amounts of sample, conditions can be chosen such that the measured pH falls within the range, indicated by arrows on the lower curve (b) in Fig. 4, which coincides with the theoretical straight line. These measurements will give the hydrochloric acid concentration. After diluting the samples to the pH region where curve (a) coincides with the straight line, new measurements are made which will give the total concentration.

Figure 5 shows the influence of an acetate buffer. Stock solutions of buffer were made equimolar with respect to acetic acid and sodium acetate. For comparison, the curve for acetic acid has been included. Although the sample is a buffer, the acidic component can be determined provided that the measurement is made in that part of the curve which coincides with the straight line. The contribution from sodium acetate will be observed in the same region as the curve of acetic acid starts to deviate from the straight line. By using the same procedure

TABLE 5

Determination of the concentrations for some mixtures of hydrochloric acid and acetic acid.

Solution	[HAc + HCl] taken (M)	[HAc + HCl] found (M)	[HCl] taken (M)	[HCl] found (M)
A	0.2116	0.2112	0.2002	0.2016
B	0.2517	0.2490	0.2402	0.2396
C	0.2574	0.2542	0.2402	0.2397
D	0.2660	0.2650	0.2602	0.2604

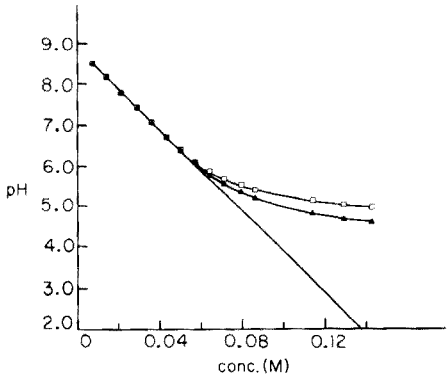

Fig. 5. pH as a function of concentration for acetic acid (▲) and acetate buffer (□). The straight line is the theoretical line for a strong acid.

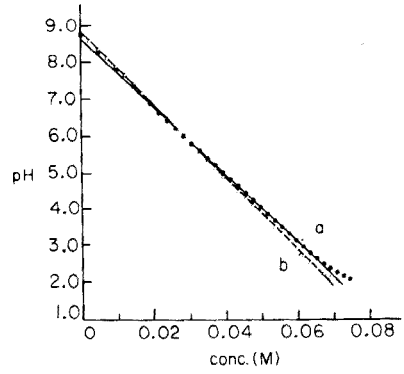

Fig. 6. pH as a function of acid concentration. Experimental points for weaker buffer solution (△) and for stronger buffer solution (•) diluted to half strength. Lines a and b are explained in the text.

for the basic component and employing the acidic buffer mixture [9], it would be possible to determine the buffer capacity of the samples.

The effect of dilution of the stronger buffer mixture (Table 1) to half strength on the titration curve is shown in Fig. 6. For comparison, the titration curve for the weaker buffer mixture in Table 1 is also included. Line b is that predicted for the weak buffer solution with a slope of -100 pH M^{-1}; line a is that obtained for the central part of the titration curve of the diluted mixture. The fit of the experimental points for the calculated mixture is much better than for the diluted case. The slope will not be doubled, as pointed out earlier, when the buffer is diluted to half strength. The linear range will, however, be reduced and the accuracy decreased. Nevertheless, the diluted buffer mixture could still be used after calibration.

The author thanks Kerstin Palmgren for great help with the experiments, and Dr. Michael Sharp for linguistic revision of the manuscript.

REFERENCES

1 G. Gran, Acta Chem. Scand., 4 (1950) 559.
2 G. Gran, Analyst, 77 (1952) 661.
3 B. H. J. Hofstee, Science, 131 (1960) 39.
4 F. Ingman and E. Still, Talanta, 13 (1966) 1431.
5 C. McCallum and D. Midgley, Anal. Chim. Acta, 65 (1973) 155.
6 D. Midgley and C. McCallum, Talanta, 21 (1974) 723.
7 T. N. Briggs and J. E. Stuehr, Anal. Chem., 46 (1974) 1517.
8 G. Johansson and W. Backén, Anal. Chim. Acta, 69 (1974) 415.
9 O. Åström, Anal. Chim. Acta, 88 (1977) 17.
10 E. B. R. Prideaux, Proc. Roy. Soc. London, Ser. A, 92 (1916) 403.
11 E. B. R. Prideaux and A. T. Ward, J. Chem. Soc., 125 (1924) 426.
12 H. T. S. Britton and R. A. Robinson, J. Chem. Soc., (1931) 1456.
13 L. G. Sillén and A. Martell, Stability Constants of Metal-Ion Complexes, Special Publication No. 17, Chemical Society, London, 1964.

Analytica Chimica Acta, 97 (1978) 269—274

BESTIMMUNG VON IRIDIUM(IV) MIT ADSORPTIONS-POLARISIERTEN ELEKTRODEN [1]

U. BARTELS und F. UMLAND*

Anorganisch-Chemisches Institut, Lehrstuhl für Anorganisch-Analytische Chemie, der Westfälischen Wilhelms-Universität Münster, Gievenbecker Weg 9-11, D-Münster/Westf. (Bundesrepublik Deutschland)

(Eingegangen den 2. November 1977)

ZUSAMMENFASSUNG

Adsorptionspolarisierte Elektroden (platiniertes und glattes Platinblech) sind geeignet, die Titration von Mikrogrammengen Iridium(IV) potentiometrisch zu indizieren. In 0,5—1 M H_2SO_4 oder 2—4 M $HClO_4$ ist die direkte Umsetzung von Iridium(IV) mit Kaliumjodid möglich. Für die Titration von 1 mg Iridium(IV) in 20 ml Lösung ergibt sich eine relative Standardabweichung von 2% (n = 12), für 40 μg Ir(IV) von 7% (n = 12). Genauer und empfindlicher ist die indirekte jodimetrische Titration mit Thiosulfat. Sie wird am besten in HCl, H_2SO_4 oder $HClO_4$ bei pH 2—3 durchgeführt. Iridium(IV) (100μg) lassen sich in 20 ml Lösung mit einer relativen Standardabweichung von 1,8% (n = 12) bestimmen, 2 μg Ir(IV) noch mit 10% (n = 12)

SUMMARY

The titration of iridium(IV) with adsorption-polarized electrodes

Adsorption-polarized electrodes (platinized and bright platinum foil) are suitable for end-point indication in the titration of microgram amounts of iridium(IV). Direct titration of iridium(IV) with iodide is possible in 0.5—1 M H_2SO_4 or 2—4 M $HClO_4$ media. For 1 mg of iridium in 20 ml of solution, the relative standard deviation is 2% (n = 12), and for 40 μg 7% (n = 12). The indirect iodimetric titration with thiosulfate after addition of iodide is more sensitive. In HCl, H_2SO_4 or $HClO_4$ solutions (20 ml) at pH 2—3, 100 μg Ir(IV) can be determined with a relative standard deviation (s_r) of 1.8% (n = 12); for 2 μg Ir(IV) s_r = 10% (n = 12).

Das Standardnormalpotential des Redoxgleichgewichts $IrCl_6^{2-}/IrCl_6^{3-}$ beträgt in salzsaurer Lösung + 1.02 V [3]. Prinzipiell ist es also möglich, Iridium(IV) durch Umsetzung mit Kaliumjodid zu bestimmen. Erste Versuche dieser Art gehen auf Delépine [2] sowie Sho-Chow Woo und Yost [3] zurück, die Iridiat mit einem Überschuß Jodid versetzen und das freigesetzte Jod mit Thiosulfat unter Zusatz von Stärke als Indikator zurücktitrieren. Beamish [4] äußert allerdings Bedenken zu dieser Methode, ohne seine Einwände näher zu erläutern. Erst kürzlich teilten Zacharov u.a. [5] eine amperometrische Methode der direkten Titration mit Kaliumjodid mit.

Eine Mitteilung über eine potentiometrische Bestimmung liegt nicht vor.

Wir haben nun untersucht, inwieweit die Titration unter Anwendung adsorptionspolarisierter Elektroden (APE) möglich ist. Über den Mechanismus und die Anwendung adsorptionspolarisierter Elektroden bei Redoxreaktionen ist bereits früher [1, 6] berichtet worden.

EXPERIMENTELLES

Geräte und Chemikalien; Metrohm-Potentiographen E 536 und E 436 mit automatischer Bürette; Metrohm Universalgefäß mit Magnetrührung; pH-Meter mit Glaselektrode; Metrohm-Platindoppelblechelektroden, davon wurde ein Blech ca. 30 s bei 1 A mit Platinmohr beschichtet. Diese oberflächengestörte Elektrode wurde als Indikatorelektrode geschaltet.

Methoden

Die Titrationen erfolgten in einem Gesamtvolumen von ca. 20 ml bei 22 ± 1°C und einer Geschwindigkeit von 3 min ml^{-1}. Die Probelösung wurde ständig von einem schwachen Stickstoffstrom durchspült, um eine Reaktion des Jodids mit Luftsauerstoff zu verhindern.

Methode 1. Die Probelösung (0.5—1 M H_2SO_4 oder 2—4 M $HClO_4$) wird direkt mit 0,01 M oder 0,001 M KJ-Lösung titriert.

Methode 2. Die Probelösung, pH 3, wird mit kleinem Überschuß an KJ (1 ml 0,1 M KJ-Lösung) versetzt und unmittelbar mit 0,01, 0,001 oder 0,0001 M $Na_2S_2O_3$-Lösung titriert.

Die verdünnten Lösungen wurden täglich frisch hergestellt. Für die Eichung der Methoden wurden Lösungen mit 1000 bzw. 100 ppm Iridium(IV) in 1 M HCl hergestellt aus $(NH_4)_2$ $[IrCl_6]$ (43,42% Ir) der Firma DEGUSSA.

ERGEBNISSE

Methode 1. Die direkte Titration von Iridium(IV) mit Jodid

Abbildung 1 zeigt eine Serie von Potentiogrammen in H_2SO_4-Lösungen zwischen pH 6.5 und 6 M H_2SO_4. Der Bereich des Äquivalenzpunktes wird durch einen Peak angezeigt, dessen Potentialrichtung von der Säurestärke abhängt. Bei pH 1 ist sie — bezogen auf die platinierte Elektrode — negativ, bei pH 1 dagegen positiv. Es gibt also einen ausgezeichneten pH-Wert, bei dem keine Potentialdifferenz zwischen der gestörten und der ungestörten Elektrode auftritt.

Die Höhe des Peaks steigt mit zunehmender Säurestärke stark an. Für die analytische Anwendung ist von Bedeutung, daß die Lage des Peaks nur in einem schmalen Säurebereich exakt mit dem theoretischen Äquivalenzpunkt zusammenfällt. Dieses ist der Fall in Lösungen von 0,5 bis 1 M H_2SO_4 oder von 2 bis 4M $HClO_4$.

Das Verhalten des Elektrodenpaares beruht auf dem unterschiedlichen Ansprechen der beiden in ihrer Oberflächenbeschaffenheit ungleichen Elektroden auf die Reduktion des Iridiums. Deutlich wird dieser Effekt, wenn

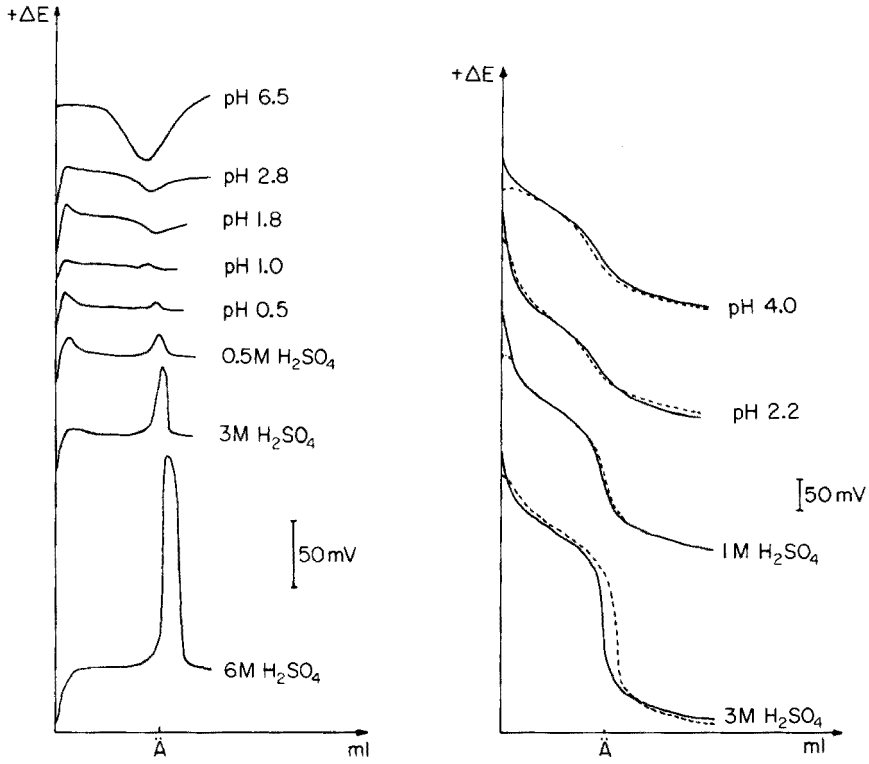

Abb. 1. Titrationen von 1 ml 0,01M Ir(IV) mit 0,01M KJ in Lösungen verschiedener H_2SO_4-Konzentration. Elektroden: $Pt_{platiniert}/Pt_{glatt}$.

Abb. 2. Titration von 1 ml 0,01M Ir(IV) mit 0,01M KJ in Lösungen verschiedener H_2SO_4-Konzentration. Elektroden: Pt_{glatt}/ges.AgCl (————); $Pt_{platiniert}$/ges.AgCl (----------).

man die beiden Elektroden für sich gegen eine Referenzelektrode schaltet und die Einzelpotentiale während der Titration mit gleichbleibender Geschwindigkeit verfolgt. Abbildung 2 zeigt, daß das platinierte Pt-Blech in saurer Lösung unter pH 1 wesentlich langsamer als das glatte auf die Reaktion anspricht, während es in schwächer sauren Lösungen umgekehrt ist. Lediglich die glatte, ungestörte Elektrode zeigt in 0,5 — 3 M H_2SO_4 den richtigen Äquivalenzpunkt an. Analytisch brauchbar ist die Kombination von glatter und platinierter Pt- Elektrode, wo die beiden Wendepunkte nahe beieinander liegen, aber nicht exakt zusammenfallen, also in 0,5— 1 M $H_2 SO_4$ und 2 — 4M $HClO_4$.

Unsere Untersuchungen deuten darauf hin, daß die Fähigkeit von platiniertem Platin, als Wasserstoffelektrode zu wirken und Wasserstoff zu adsorbieren, hier die entscheidende Rolle spielt. Ein glattes Platinblech, an dem zuvor Wasserstoff entwickelt worden war, reagiert ebenfalls zögernd wie ein platiniertes Platinblech. Adsorbierter Wasserstoff hemmt also die Gleichgewichtseinstellung auf der Elektrode. Dies ist auch bereits in anderen Fällen [6] festgestellt worden.

Wie daher zu erwarten, erhält man bei Umkehrung der Reaktion, nämlich der Titration von Jodid mit Iridium(IV) in saurer Lösung, einen negativen Peak. Auch hier spricht die oberflächengestörte Elektrode mit deutlicher Verzögerung auf die Oxidation an.

Die direkte Titration von kleinen Mengen Iridium mit Jodid eignet sich für analytische Zwecke, sofern man in einem Bereich von 0,5—1 M H_2SO_4 bzw. 2—4 M $HClO_4$ arbeitet. Nicht möglich ist sie dagegen in salzsaurer Lösung, da der Äquivalenzpunkt nicht genau genug angezeigt wird. Kleine Mengen Chlorid stören jedoch nicht. Bei der Anwendung eines Paares aus einer adsorptionspolarisierten und einer glatten Pt-Elektrode ergeben sich für die Titration in 20 ml 1M H_2SO_4 folgende Standardabweichungen (n = 12)

1 mg Ir mit 0,01 M KJ σ = 2,0%
100 μg Ir mit 0,001 M KJ σ = 3,4%
40 μg Ir mit 0,001 M KJ σ = 6,8%

Methode 2. Die indirekte Titration von Iridium(IV) mit Thiosulfat nach vorheriger Reduktion mit Kaliumjodid

Zur vollständigen und raschen Reduktion von Ir(IV) bedarf es lediglich eines geringen Überschusses an Kaliumjodid. Abbildung 3 zeigt die Titration des dabei freigesetzten Jods mit Thiosulfat bei verschiedenen pH-Werten. Der Äquivalenzpunkt wird durch einen positiven Peak indiziert, der darauf beruht, daß sich bevorzugt auf der platinierten Elektrode eine Platin-Jod-Oberflächenverbindung ausbildet [6, 1]. Im Bereich von pH 2 — 3 ist der Peak besonders scharf und für analytische Zwecke brauchbar. Die Einstellung des pH-Wertes kann dabei sowohl durch Säure/Base-Zusatz als auch durch Verwendung eines Hydrogenphthalatpuffers erfolgen. Im Gegensatz zu der direkten Titration von Ir(IV) mit Jodid kann in diesem Fall auch in salzsaurer Lösung titriert werden.

Messungen in stark verdünnten Lösungen zeigten, daß die Indikation selbst noch bei Vorlage von 2 μg Ir in ca. 20 ml Lösung (0,1 p.p.m.) mit genügender Genauigkeit möglich ist. Zwar wird der Peak mit zunehmender Verdünnung breiter (Abb. 4), doch läßt sich der Äquivalenzpunkt durch Extrapolation ermitteln. Eine Verschleppung der Peakspitze, wie z.B. bei Fällungstitrationen [7], tritt hier nicht auf.

Insgesamt erweist sich die indirekte Bestimmung als genauer und wesentlich empfindlicher als die direkte potentiometrische oder die amperometrische [5] Titration. Sie kann auch ohne Schwierigkeit zur Verbesserung des Ergebnisses bei kleinen Mengen Iridium im Anschluß an die direkte Titration (Methode 1) durchgeführt werden. Für verschiedene Mengen von Ir(IV) in 20 ml salzsaurer Lösung bei pH 3 ergaben sich als relative Standardabweichungen (n = 12)

96 μg mit 0,001 M Thiosulfat σ = 1,8%
19,2 μg mit 0,0001 M Thiosulfat σ = 2,7%
9,6 μg mit 0,0001 M Thiosulfat σ = 5,5%
1,9 μg mit 0,0001 M Thiosulfat σ = 9,9%

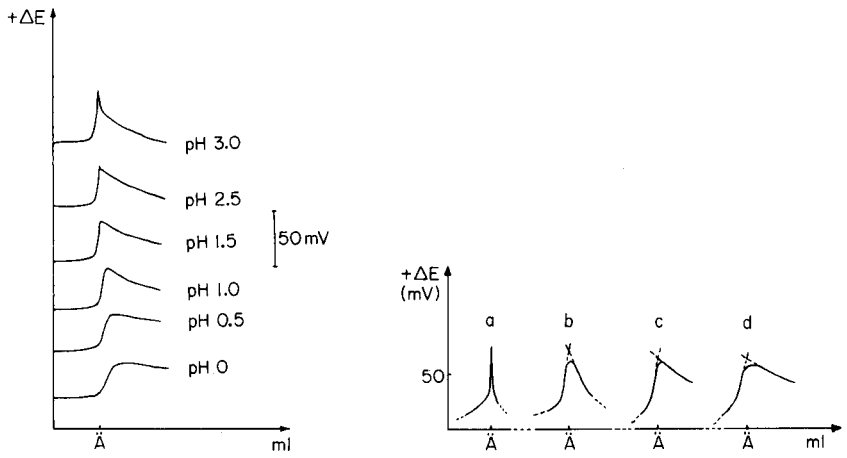

Abb. 3. Titration von 1 ml 0,01M Ir(IV), nach vorheriger Reduktion mit KJ, mit 0,01M $S_2O_3^{2-}$ in Lösungen verschiedener HCl-Konzentration. Elektroden: $Pt_{platiniert}/Pt_{glatt}$.

Abb. 4. Titration verschiedener Mengen Ir(IV) in 20 ml Lösung, pH 3, nach vorheriger Reduktion mit KJ. Elektroden: $Pt_{platiniert}/Pt_{glatt}$. (a) 96 µg Ir(IV) mit 10^{-3}M $S_2O_3^{2-}$ (b) 19,2 µg Ir(IV) mit 10^{-4}M $S_2O_3^{2-}$. (c) 3,8 µg Ir(IV) mit 10^{-4}M $S_2O_3^{2-}$. (d) 1,9 µg Ir(IV) mit 10^{-4}M $S_2O_3^{2-}$.

Störungen

Bei der direkten Titration von Ir(IV) mit KJ (Methode 1) stören auch bei großem Überschuß nicht: Rh(III), Os(IV), Ru(IV), As, Co, Ni, Al, Cu. Fe(III) stört bis zu einem 20fachen, Pt(IV) bis zu einem 3fachen Überschuß nicht. Es stören, da sie ebenfalls mit Jodid reagieren, Au(III) und Pd(II).

Bei der indirekten Titration mit Thiosulfat (Methode 2) stören auch bei großem Überschuß nicht: Rh(III), Os(IV), Ru(IV), As, Ag, Co, Ni, Al. Es stören nicht: Cu(II) bis zu einem 10fachen Überschuß, Pd(II) bis zu einem 3 fachen Überschuß sowie Pt(IV) bis zu einem 3 fachen Überschuß. Dagegen setzen Fe(III) sowie Au(III) mit KJ Jod frei.

Eisen kann durch NaF maskiert werden. Au(III) sollte — z.B. mit SO_2 — zum Element reduziert werden. Da dabei auch Ir(IV) zu Ir(III) reduziert wird, muß anschließend wieder mit HNO_3 oxidiert werden.

Palladium fällt mit KJ als PdJ_2. Titriert man eine Ir und Pd enthaltende Probe nach der ersten Methode, erhält man einen Summenpeak für beide Elemente. Bei der zweiten Methode löst sich PdJ_2 im KJ-Überschuß als PdJ_4^{2-}, das ebenfalls mit Thiosulfat reagiert. Es muß daher in jedem Fall abgetrennt werden. Im allgemeinen wird zu diesem Zwecke die Fällung mit Dimethylglyoxim empfohlen [8, 9]. Gerade aber bei Vorliegen sehr kleiner Mengen — für die die hier beschriebene Methode gedacht ist — wird keine vollständige Trennung erreicht. Auch die elektrolytische Abscheidung von Palladium ist untauglich, da Iridium leicht mit abgeschieden wird, obgleich es sich allein nur schwer elektrolytisch fällen läßt. Nach unseren Erfahrungen eignen sich zur

Trennung kleiner Mengen der Platinmetalle dagegen sehr gut Ionenaustauscher [10, 11]. Das so abgetrennte Palladium kann anschließend mit Jodid und einem Elektrodenpaar, bestehend aus einem palladinierten und einem glatten Platin-Blech, titriert werden [7].

Ebenso ist es möglich, Pt(IV) nach Zugabe eines großen Jodidüberschusses zu bestimmen. In einer mit Hydrogencarbonat gepufferten Lösung wird der entstandene $[PtJ_6]^{2-}$-Komplex bzw. das mit ihm im Gleichgewicht stehende J_2 reduziert. Bei Anwendung der in dieser Arbeit beschriebenen Elektrodenanordnung erhält man nach Methode 2 eine positive Stufe. Die Streuungen der Ergebnisse sind jedoch größer als bei der Iridiumbestimmung.

Wir danken dem Minister für Wissenschaft und Forschung des Landes Nordrhein-Westfalen, Landesamt für Forschung, sowie dem Verband der Chemischen Industrie, Fonds der Chemie, für Sachbeihilfen.

LITERATUR

1 7. Mitt. über Adsorptionspolarisierte Elektroden zur Endpunktsindikation bei der potentiometrischen Titration. 6. Mitt. F. Sefzik und F. Umland, Fresenius Z. Anal. Chem., im Druck.
2 M. Delépine, Ann. Chim. Anal., 7 (1917) 277.
3 Sho-Chow Woo und D. M. Yost, J. Am. Chem. Soc., 53 (1931) 884; Sho-Chow Woo, J. Am. Chem. Soc., 53 (1931) 469.
4 F. E. Beamish, Anal. Chim. Acta, 20 (1959) 101.
5 N. K. Zacharov, O. A. Songina und T. A. Ajtchozaeva, Z. Anal. Chem., 30 (1975) 1430.
6 U. Bartels, E. Schumacher und F. Umland, Fresenius Z. Anal. Chem., 281 (1976) 215.
7 U. Bartels und F. Umland, Fresenius Z. Anal. Chem., 284 (1977) 263.
8 R. Gilchrist und E. Wichers, J. Am. Chem. Soc., 57 (1935) 2565.
9 F. E. Beamish, Talanta, 1 (1958) 3.
10 E. Blasius und D. Rexin, Fresenius Z. Anal. Chem., 179 (1961) 105.
11 P. C. Stevenson, A. A. Franke, R. Borg und W. Nervik, J. Am. Chem. Soc., 75 (1953) 4876.

Analytica Chimica Acta, 97 (1978) 275—281

THE ANALYSIS OF SILVER BY X-RAY FLUORESCENCE SPECTROMETRY

F. T. WYBENGA and L. R. P. BUTLER*

National Physical Research Laboratory, Council for Scientific and Industrial Research, P.O. Box 395, Pretoria (South Africa)

(Received 4th October 1977)

SUMMARY

An x-ray fluorescence method is described for the analysis of silver alloys. The major element silver as well as the impurities are determined. Corrections are made for inter-element and line overlap effects. The results obtained compare favourably with wet chemical and emission spectrometric values. The method is rapid and reliable.

The value of silver has increased significantly in recent years, because of its increasingly wide usage and its relative scarcity. As with the precious metals, its assay, with regard both to purity and to the type and concentrations of impurity elements, requires the highest degree of accuracy and precision.

Assay methods based on gravimetric techniques meet these requirements, but a total chemical analysis demands several techniques and is accordingly time-consuming, especially when the precious metals need to be determined. X-ray fluorescence spectroscopy is well known for its high degree of precision and this, together with the fact that the method is non-destructive, suggested its use for the rapid analysis of silver alloys.

Various alloys of silver, where the impurities included precious metals and totalled between 1 and 5%, were obtained. A method of analysis was developed which enabled the silver and other elements to be determined with a high degree of accuracy and precision. Line overlap and interelement effects were present at the levels of impurities in the samples, and the correction methods of Lucas-Tooth and Pyne [1], Stephenson [2] and Kodama et al. [3] had to be applied.

This paper describes the method and presents the results obtained on the range of alloys available.

EXPERIMENTAL

Sample preparation

The silver samples were prepared by melting in graphite crucibles at 1100°C in an induction furnace. They were vertically cast in a special mould (Fig. 1)

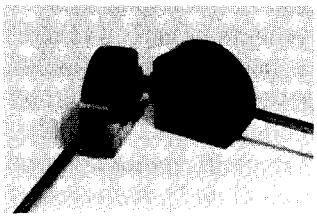

Fig. 1. Mould used for casting silver samples.

to obtain discs of 40-mm diameter and 7-mm thickness. This procedure ensured that all samples were treated in the same way, thus removing the possibility that metallurgical history would affect results. It was established by means of a scanning electron microscope that these samples were homogeneous.

Smoothing of the surfaces of the sample was done on a water-covered surfacing disc with 180 and then 800 silicon carbide paper.

Apparatus

A Philips PW 1220C sequential x-ray fluorescence spectrometer with a molybdenum anode tube was used for all the measurements. An 8K Honeywell computer was coupled to this instrument and was used to control the spectrometer as well as the automatic sample changer.

Selection of instrumental conditions

Preliminary wavelength scans of some of the samples were made to establish optimum conditions (Fig. 2). LiF (200) as well as LiF (220) crystals were tried as analysing crystals. The resolution of the instrument was improved by

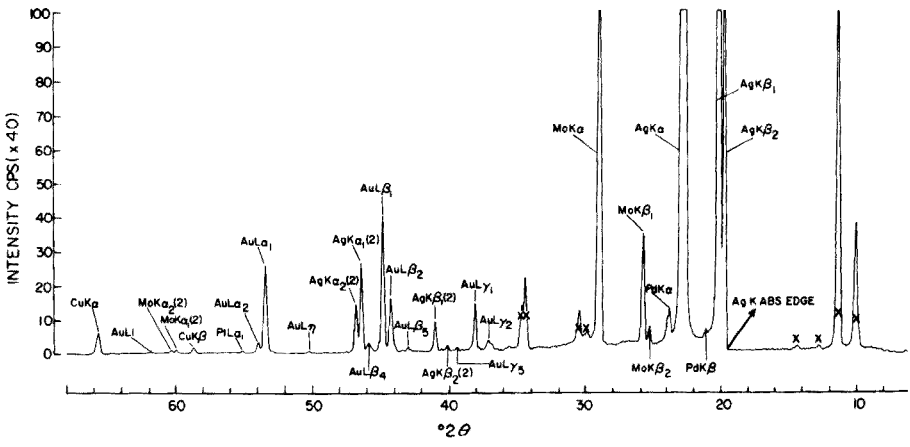

Fig. 2. Typical spectrum of silver sample. Sample S-11. Analysing crystal, LiF (220). Mo anode, 80 kV, 50 mA. Full scale, 4000 cps. × Spurious reflections.

introducing an additional auxiliary soller collimator (150-μm spacing, 100 mm long) in front of the scintillation detector. The following results were obtained in these experiments.

(i) The Pd $K\alpha$ and Ag $K\alpha$ lines were inadequately separated with the LiF (200) crystal and the auxiliary collimator. The LiF (220) crystal was therefore used. The loss in intensity was approximately 30%.

(ii) The LiF (200) analysing crystal gave adequate resolution for the separation of the Au $L\alpha$ and Pt $L\alpha$ lines, with the auxiliary collimator.

(iii) Spurious reflections do occur with the LiF (220) crystal, but fortunately not in positions where they affect the measurements.

(iv) By using the long auxiliary collimator, the intensity is reduced by a factor of six for the Ag $K\alpha$ and Pd $K\alpha$ lines. This is not serious as adequate intensity is available for these lines.

The experimental conditions for individual elements are given in Table 1.

All measurements were done in air with a fine primary soller collimator (150-μm spacing), an auxiliary soller collimator in front of the detector (150-μm spacing, 100 mm long) and a scintillation detector. Samples were loaded into the spectrometer by means of a sample changer controlled by the computer.

Correction procedure

One in every four measurements was done on a single reference standard and all values were ratioed to these reference measurements to enable correction for possible drift. All measurements were corrected for background by direct subtraction of a measurement taken close to the peak and also for dead-time losses.

TABLE 1

Measuring conditions

Element line	Crystal	°2θ	kV	mA	Counting time (s)
Ag $K\alpha$	LiF (220)	22.72	60	20	100
Background	LiF (220)	18.00	60	20	100
Pd $K\alpha$	LiF (220)	23.79	80	30	100
Background	LiF (220)	18.00	80	30	100
Mo $K\alpha$	LiF (200)	28.87	80	30	100
Mo Kα (Compton)	LiF (200)	30.00	80	30	100
Au $L\alpha$	LiF (200)	36.97	80	30	100
Background	LiF (200)	35.80	80	30	100
Pt $L\alpha$	LiF (200)	38.05	80	30	200
Background	LiF (200)	39.50	80	30	200
Cu $K\alpha$	LiF (200)	45.03	80	30	100
Background	LiF (200)	47.00	80	30	100
Pb $L\alpha$	LiF (200)	33.92	80	30	200
Background	LiF (200)	35.80	80	30	200
Bi $L\beta$	LiF (220)	39.06	80	30	100
Background	LiF (220)	42.00	80	30	100

The equation used in the correction procedure is

$$C_i = A_0 + A_i R_i + \sum_{j=1}^{n} A_j R_j + \sum_{j=1}^{n} A_{ij} R_i R_j$$

where C_i is the concentration, and R_i is the intensity of the analytical element; R_j is the intensity of the interfering element; and A_0, A_i, A_j and A_{ij} are constants.

This equation differs from the normal Lucas-Tooth equation [1] in that the term $A_j R_j$ is introduced to correct for line overlap and possible background effects. In the ideal case where no interference is present, the last two terms in the equation fall away.

Under normal circumstances only some of the elements in a specific matrix have an appreciable effect on the determination of a concentration. The stepwise multiregressional program [4] suggested by Stephenson [2] was used to establish the regression constants. In this program it is possible to specify F-levels for the inclusion or deletion of variates. Non-significant variates are not included in the model. A practical F-level is determined by the degrees of freedom. In the case of these analyses the F-level for inclusion and deletion was chosen as 2.0.

The exact forms of the regression formulae had to be determined before any analyses were attempted. A number of standards had therefore to be measured for all the elements of interest under the conditions given in Table 1. The regression equations given in Table 2 were obtained following the multiple regression method described.

TABLE 2

Regression equations

Ag	$C = 36.30043\ R_{Ag} - 1.82587\ R_{Mo} - 0.57374\ R_{Au} - 0.22638\ R_{Pt} - 0.68108\ R_{Cu} R_{Ag} + 62.60551$ Standard error of estimate = 0.0773; $r = 0.9982$.
Au	$C = 2.88256\ R_{Au} - 0.03075\ R_{Pd} - 0.60284\ R_{Mo} + 0.04073\ R_{Pt} + 0.07722\ R^2_{Au} + 0.63012$ Standard error of estimate = 0.0052; $r = 1.0000$.
Cu	$C = 1.25654\ R_{Cu} - 0.04957\ R^2_{Cu} - 0.09904$ Standard error of estimate = 0.0309; $r = 0.9984$.
Pd	$C = 0.80353\ R_{Pd} - 0.00341\ R_{Pt} - 0.01062\ R_{Pb} - 0.45910\ R_{Ag} \times R_{Pd} + 0.03386\ R_{Pb} \times R_{Pd} - 0.09389$ Standard error of estimate = 0.0010; $r = 0.9999$.
Pt	$C = 0.10894\ R_{Pt} - 0.000129\ R_{Au} + 0.01041\ R_{Cu} + 0.000989\ R_{Pt} \times R_{Pb} - 0.01558$ Standard error of estimate = 0.0007; $r = 0.9998$.

TABLE 3

Analytical results

Sample	Silver (%)			Gold (%)			Copper (%)			Palladium (%)			Platinum (p.p.m.)		
	Chem	G.d.	X.r.f.	Chem	G.d.	X.r.f.	Chem	G.d.	X.r.f.	Chem	G.d.	X.r.f.	Chem	G.d.	X.r.f.
1	98.75	98.77	98.78	0.019	0.023	0.020	1.21	1.18	1.20	0.001		—	6		—
9	98.65	98.63	98.54	0.192	0.193	0.191	1.14	1.17	1.17	0.0100	0.0108	0.0095	30	25	27
10	98.61	98.61	98.71	0.154	0.151	0.153	1.19	1.21	1.20	0.0135	0.0151	0.0146	95	94	92
11	—	98.66	98.74	0.081	0.086	0.083	1.20	1.23	1.18	0.0068	0.0072	0.0073	24	23	21
13	96.16	96.09	96.23	2.644	2.691	2.662	1.11	1.05	1.08	0.034	0.037	0.035	130	127	144
16	—	96.90	96.96	—	2.025	1.970	0.95	0.92	0.95	0.035	0.037	0.033	290	292	287
17	96.75	96.70	96.67	2.109	2.161	2.105	1.03	0.97	1.02	0.039	0.042	0.041	330	326	322
18	97.54	97.37	97.40	1.495	1.629	1.499	0.85	0.84	0.84	0.043	0.051	0.046	430	482	440
19	—	96.98	97.03	—	1.846	1.752	0.96	0.96	0.98	0.077	0.082	0.078	550	568	553
20	97.14	97.18	97.10	1.743	1.673	1.735	0.94	0.93	0.94	0.088	0.096	0.090	550	541	542
21	—	96.50	96.85	—	2.024	1.773	1.03	1.17	1.03	0.113	0.118	0.112	985	983	982
22	96.56	95.47	95.66	2.961	2.884	2.97	1.11	1.18	1.10	0.238	0.240	0.238	870	866	871
23	94.95	95.02	95.03	3.59	3.48	3.587	1.07	1.06	1.12	0.225	0.215	0.225	700	666	700
27	—	96.33	96.41	—	2.521	2.546	0.99	1.00	0.97	0.025	0.027	0.025	90	75	78
31	96.59	96.73	96.60	0.896	0.890	0.895	2.09	1.99	2.07	0.013	0.012	0.013	17	18	—
36	96.20	96.09	96.06	0.905	0.903	0.909	2.62	2.57	2.67	0.025	0.022	0.026	25	19	—

RESULTS

Accuracy

Standard values (chem), glow discharge values (g.d.) and x.r.f. values are compared for the elements, silver, gold, copper, palladium and platinum in Table 3. The chemical values were used in the multiple regression analysis. The accuracy of the method depends largely on the accuracy of the chemical values. Good agreement is found for all the elements. The x.r.f. method lends itself very well to silver determination at these high concentration levels. It is also very accurate for the minor and trace elements.

The standard errors of estimate and the regression coefficients, r, shown in Table 2 are also measures of the accuracy. Compared to the other elements, copper has the lowest relative accuracy. Although bismuth and lead were detectable on some of the samples, and could be measured, reliable values for regression analysis on these two elements were not available.

Precision

Ten individual determinations were done on 6 samples to establish the precision of the method. The results are given in Table 4.

Sensitivity and detection limits

Values for the sensitivities and detection limits of the elements gold, palladium and platinum, are given in Table 5. The lower limit of detection(s) is defined [5] as $(3/m)\ (R_B/T)^{1/2}$ %, where R_B is the counting rate on the background, T the counting time, and m the slope factor or sensitivity which is expressed in counts per second/%.

In the case of palladium the background count is strongly influenced by the closeness of the very intense Ag $K\alpha$ peak, which is responsible for the relatively poor detection limit.

CONCLUSION

The x-ray fluorescence method is well suited for the analysis of silver samples. A sophisticated computer is needed to obtain the correction parameters, but once these are available, calculations with a small on-line computer of 8K capacity is possible on routine samples. On a sequential x-ray spectrometer the time for an analysis is of the order of 30 min.

TABLE 4

Precision of x-ray results (N = 10)[a]

		Ag (%)	Au (%)	Pt (p.p.m.)	Pd (p.p.m.)	Cu (%)	Pb (p.p.m.)
R-1	M	98.76	0.0195	11	12	1.2132	107
	s	0.057	0.0024	7	8	0.0063	3
	s_r (%)	0.06	12.1	65	71	0.52	2.9
R-11	M	98.68	0.1891	30	94	1.1424	78
	s	0.049	0.0020	4	8	0.0029	4
	s_r (%)	0.05	1.1	14	8.6	0.25	4.6
R-12	M	98.59	0.1531	96	140	1.2139	65
	s	0.046	0.0018	4	7	0.0048	3
	s_r (%)	0.05	1.2	4.4	5.0	0.39	4.1
S-5	M	96.92	1.971	286	345	0.9546	119
	s	0.028	0.0052	6	13	0.0023	4
	s_r (%)	0.03	0.27	2.2	3.7	0.24	3.4
S-9	M	97.11	1.747	549	908	0.9229	264
	s	0.038	0.0058	8	10	0.0038	6
	s_r (%)	0.04	0.33	1.5	1.1	0.41	2.4
S-10	M	96.81	1.776	983	1113	1.0278	216
	s	0.035	0.0050	10	10	0.0043	5
	s_r (%)	0.04	0.28	1.1	0.9	0.41	2.3

[a]M = Mean. s = Standard deviation. s_r = Relative standard deviation.

TABLE 5

Sensitivity and detection limits of x-ray measurements

	Gold	Palladium	Platinum
Sensitivity (cps/%)	1115	2100	1160
Counting time (s)	100	100	200
Background count (cps)	35	315	29
Detection limit (p.p.m.)	16	25	10

REFERENCES

1 J. Lucas-Tooth and C. Pyne, Adv. X-ray Anal., 7 (1964) 523.
2 D. A. Stephenson, Anal. Chem., 43 (1971) 310.
3 H. Kodama, J. E. Brydon and B. C. Stone, Geochim. Cosmochim. Acta, 31 (1967) 649.
4 W. J. Dixon, BMD02R — Stepwise Regression, University of California Publications in Automatic Computation, No. 2, Biomedical Computer Programme, Univ. Calif. Press, 1967.
5 R. Jenkins and J. L. de Vries, Practical X-ray Spectrometry, 2nd. edn., Macmillan, 1970. p. 167.

Analytica Chimica Acta, 97 (1978) 283—294

ENERGY-DISPERSIVE X-RAY FLUORESCENCE OF METALS — A SIMPLE FUNDAMENTAL PARAMETERS APPROACH

P. VERBEKE, H. NULLENS and F. ADAMS*

Department of Chemistry, University of Antwerp (U.I.A.), B-2610 Wilrijk (Belgium)

(Received 19th September 1977)

SUMMARY

The merits of energy-dispersive x-ray spectrometry with secondary target set-up applied to the multi-element analysis of thick metallic specimens, are investigated. A number of measuring characteristics are examined. In the method corrections for matrix effects calculated according to the fundamental parameter technique, are utilized. Calculations are done by a computerized iterative procedure. The influence of primary energy radiation and secondary fluorescence is discussed. Thin film standards are used for standardizations. Several reference materials, for which the composition varies over a wide range, are analysed to test the accuracy of the method. For most elements accuracies better than 10% are obtained.

The accurate quantitative x-ray fluorescence analysis of thick samples requires a correction procedure that accounts for any important matrix or interelement effects. Several correction schemes have been proposed; these are based mainly on the use of experimental coefficients obtained from measurements of large numbers of reference materials with a composition similar to the unknown samples. Especially in the case of analyses of metallic samples, where the elemental concentrations can be extremely variable, this approach is hardly practical and certainly not flexible.

In order to develop a much more general and efficient method of analysis, suitable for any combination of elements, various authors [1—3] have derived mathematical formulae to obtain the matrix corrections. These algorithms contain a number of physical parameters characteristic for each element, including absorption coefficients and fluorescence yields, and the spectral distribution of the exciting radiation. In the case of polychromatic excitation sources, the calculations are rather lengthy and complicated, in so far as allowance is made for all the excitation energies above the absorption edges of the various sample elements. A simplified approach makes use of a so-called "most effective excitation energy" [4] or "equivalent wavelength" [5] for each element, which results in an important decrease in the number of parameters and hence in the computing time. In the case of energy-dispersive analysis, where pseudo-monochromatic excitation beams obtained from a secondary target set-up or a radioisotope source can be employed,

the method is intrinsically simple and no longer requires the introduction of the concept of effective excitation energy. The major remaining disadvantage of the fundamental parameter technique is the uncertainty on the parameter values, especially the absorption coefficients.

In this study, the application of the fundamental parameter technique was investigated for the analysis of metallic samples measured with an energy-dispersive apparatus with secondary target set-up. The advantages of the secondary target system are the low fluorescence radiation background and the high sensitivity obtainable [6].

INSTRUMENTATION

The apparatus consists of a Siemens Kristalloflex 2 generator, a Kevex Subsystem 0810 and a Northern Econ II multichannel spectrometer.

Sample excitation is done through the characteristic radiation of a secondary target material, irradiated by the x-ray spectrum of a tube with tungsten anode. Collimators are set between the secondary target and the sample and between the sample and the detector, making a 45° angle with the sample area. A sixteen-position sample changer allows automated sequential measurements. The fluorescence radiation is detected with a 30-mm^2 Si(Li) detector, and the pulse-processing system consists of an FET pre-amplifier, a linear amplifier with pulse pile-up rejector and a 4096-channel spectrometer. The data can be transferred to a magnetic tape unit for subsequent computer evaluation. The off-line computer system consists of a 64 K memory PDP 11/45.

Most analyses were done with molybdenum-K radiation as the primary excitation source. For low Z-elements titanium excitation is suitable, whereas tin excitation can be used for high Z-elements.

WORKING EQUATION AND DATA PROCESSING

The equation given by Criss and Birks [7] was adapted. The excitation beam is assumed to consist of the characteristic fluorescent lines of the secondary target material, usually K_α and K_β radiation. The relation between intensity and concentration for an "infinitely" thick specimen then becomes:

$$C_i = \left\{ \left(\frac{(P_i + S_i)/Zr}{P_i^{\star}/Zr^{\star}} \right) \left(\sum_{k=1}^{N_E} \frac{\mu_i(k)\, I(k)/I_{tot}}{\mu_i(k) + \mu_i(i)} \right) \right\} \Big/ \left\{ \sum_{k=1}^{N_E} \frac{\mu_i(k)\, I(k)/I_{tot}}{\mu_M(k) + \mu_M(i)} \right.$$

$$\left. \times \left[1 + \frac{1}{2\mu_i(k)} \sum_{j=i'}^{N} C_j K_j \mu_i(j) \mu_j(k)\, X \right] \right\}$$

where

$$X = \frac{1}{\mu_M(k)\sqrt{2}} \ln \left(1 + \frac{\mu_M(k)\sqrt{2}}{\mu_M(j)} \right) + \frac{1}{\mu_M(i)\sqrt{2}} \ln \left(1 + \frac{\mu_M(i)\sqrt{2}}{\mu_M(j)} \right)$$

$$K_j = \left(1 - \frac{1}{J_j}\right) R_j \omega_j$$

$$\mu_M(i) = \sum_{j=1}^{N'} C_j \mu_j(i)$$

C_i = weight fraction of element i in the sample
P_i = fluorescence intensity of element i due to primary excitation
S_i = fluorescence intensity of element i due to secondary excitation
P_i^* = fluorescence intensity of pure element i (calculated)
N_E = number of fluorescent lines in the excitation spectrum
$I(k)$ = intensity of line k in the excitation spectrum
I_{tot} = total excitation intensity
$\mu_i(k)$ = mass absorption coefficient of element i for line k
$\mu_M(k)$ = mass absorption coefficient of the matrix for line k
J_j = absorption jump ratio for element j
ω_j = fluorescence yield of element j
R_j = intensity fraction of line j in its series
i' = first line for which the energy is larger than the absorption edge of element i
N = number of fluorescent lines
N' = number of elements present
Zr, Zr^* = correction factors resulting from the use of an external reference signal (zirconium wire) during measurements [16]

The angles of incidence and emergence of the radiation have already been replaced by their actual values (cosec $\theta = \sqrt{2}$). The factors P_i^*, representing the pure element intensities, were derived from the measurement of very thin films, prepared by vacuum evaporation on mylar foil [8] and considered as "infinitely" thin for the radiation. The term between square brackets takes care of the enhancement effects of all lines of sufficiently high energy, namely above the excitation edge of the element determined. Tertiary fluorescence has not been considered since its contribution is mostly negligible [9].

Parameter values

For the description of the variation of the absorption coefficients with energy, polynomial fitting functions were employed. The fitting coefficients were taken from the compilation of mass absorption coefficients by McMaster et al. [10]. These data have been used by many authors for x-ray absorption corrections. According to the survey by Sparks [11], the data of McMaster et al. yield the most accurate results. Moreover, the use of polynomial expressions is more practical than interpolation from tables listing absorption coefficients for arbitrary energies. In the calculations, total mass absorption coefficients were employed, including coherent and incoherent scatter contributions.

The fluorescence yields were taken from the paper of Bambynek et al. [12]. The intensity ratios of the different lines in a series originate from the tabulated data of Salem [13]. For a number of elements these ratios were

checked experimentally by the measurement of pure elements, radiation absorption by air and differences in detection efficiency being taken into account; the values found compared well with the literature data (Table 1).

Data processing

For the deconvolution of the raw data, a computerized procedure based on a non-linear least-squares algorithm was employed [14]. The fitting function for a given energy range consists mainly of a polynomial background contribution and a number of Gaussian functions, for which both peak width and peak maximum position are calculated as a function of the energy. The input information for the application of the program consists of the spectrum number, the specifications of the energy regions to be fitted, and the energies of the fluorescence lines present. The data output are the peak intensities and the background contribution. The least-squares criterion provides a measure of the goodness of fit. Because of the change of the matrix absorption as a function of the photon energy, spectral constraints relying on constant intensity ratios for lines of a particular series could not be incorporated. Moreover, escape and sum peaks had to be dealt with.

Equation (1) is used to calculate the elemental weight fractions from the net fluorescence intensities. However, since it is not an explicit function for the concentration, iterative calculation is necessary. The iteration is stopped when the calculated concentrations satisfy a predetermined convergence criterion or become smaller than a preset value ϵ. The convergence criterion used is that for one iteration all calculated concentrations agree to within 0.01% with the previous one. In most cases, the calculated concentrations are scaled to 100% after each iteration step. Scaling to 100% is only acceptable, of course, when the total composition of the sample is more or less known from the measurements, i.e. when nearly all the impurities present give rise to a measurable fluorescence signal. Except for the aluminum samples discussed below, this condition was met by all the samples investigated. Difficulties could arise, however, for samples which contain variable amounts of low Z-elements (e.g. environmental-type matrices).

TABLE 1

Comparison between K_β—K_α ratios as expected from the tables of Salem [13] and experimental data

Element	Thin film		Thick sample	
	Expected	Measured	Expected	Measured
Fe	0.138	0.136	0.151	0.152
Co	0.137	0.135	0.151	0.151
Ni	0.137	0.135	0.150	0.148
Cu	0.139	0.135	0.151	0.150

Errors in the thin film thickness can easily induce inaccuracies of 5% or more [15] in the calibration factors $P_i^{\star}$. To improve the accuracy, the calibration coefficients can be smoothed by a logarithmic least-squares fit as a function of the K absorption edge. The fitted curve also allows calculation of the calibration intensity factors for elements that are not available in standards. In order to test the overall accuracy of the calibration factors obtained in this manner, several thick pure element samples were measured. Although these samples could not be considered as infinitely thick, a considerable radiation absorption had to be taken into account. Correction for the absorption effect was obtained from the equation:

$$P_i = R_i^{\star} \left\{ \sum_{k=1}^{N_E} \mu_i(k)\, I(k)/I_{tot}\, \frac{(1 - e^{-[\mu_i(k) + \mu_i(i)]\, \rho D \cdot \sqrt{2}})}{[\mu_i(k) + \mu_i(i)]\sqrt{2}} \right\} \Big/ \left\{ \sum_{k=1}^{N_E} \mu_i(k)\, I(k)/I_{tot} \right\} \tag{2}$$

where most symbols have been defined before; $R_i^{\star}$ is the calibration intensity for element i obtained from thin film measurement, and ρD is the sample thickness in g cm^{-2}. The measured intensities and the values expected from thin film calibration are shown in Table 2. The average deviation between the two modes of calibration is 4%, with a maximum of 7% for molybdenum.

Measuring characteristics

Several instrumental parameters were examined in order to avoid possible systematic errors.

Variations in total tube output were compensated for by normalizing all the intensities to the fluorescence K_α intensity from a zirconium wire placed in the pathway of the x-rays [16]. This allows automatic correction for fluctuations in excitation intensity and analysis time.

TABLE 2

Measurement of metal foils: comparison between measured intensities and intensities expected from calibration on infinitely thin films

Element	Calibration factor (counts s^{-1} g^{-1} cm^2)	Sample thickness (g cm^{-2})	Specific count rate (counts s^{-1})	
			Expected from calibration	Measured with metal foils
Fe	143753	0.0104	752	790
Co	180675	0.0098	945	959
Ni	221310	0.0117	1224	1269
Cu	265410	0.0091	1364	1400
Zn	312773	0.0104	1674	1798
Mo	194700	0.0213	1864	2003
Pb	355365	0.0154	1177	1123

The effect of variations in sample height and the effect of measurements of a sample placed in different holders of the sample changer was investigated. It appeared that a precision similar to the expected statistical variation could be attained.

Dead-time and count-rate effects were examined by measuring a sample with increasing tube current intensities up to total count rates of 10,000 cps. The observed changes in the peak width and in the position of the peak maximum are plotted in Fig. 1. The occurrence of sum peaks at high count rates was also checked, since interference with other elemental lines may arise. By using the relative sum peak intensities it was possible to calculate the resolution time of the detection system [17], which amounted to approximately 2 μs.

RESULTS AND DISCUSSION

The procedure was applied to the analysis of a number of simple alloys, in order to verify the extent of secondary fluorescence contributions. As examples, the results of the analysis of a copper—manganese—nickel alloy and a stainless steel sample, with molybdenum primary radiation are shown in Tables 3 and 4. The calculations were done with eqn. (1) and also with a simplified equation which neglects the enhancement effects (square bracket term in eqn. 1). The extent of radiation enhancement is directly apparent for both samples.

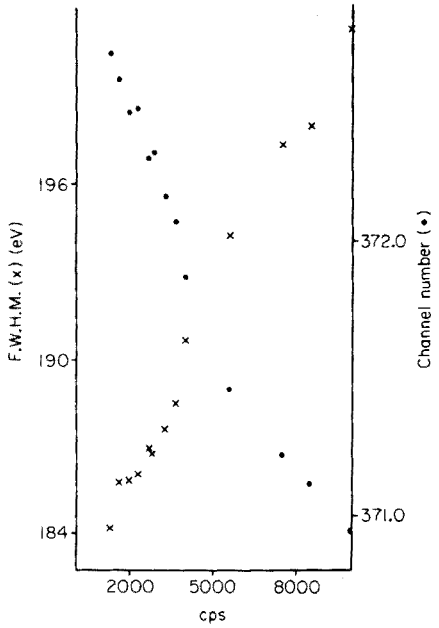

Fig. 1. Peak maximum displacement and energy resolution degradation as a function of total count rate.

TABLE 3

Analysis of a copper—manganese—nickel alloy

Element	Present (%)	Found (%)		Fluorescent signal contributions (%)					
		Eqn. (1)	Simplified eqn. (1)	Primary excitation		Enhancement contributions			
				Mo-K_α	Mo-K_β	Ni-K_α	Ni-K_β	Cu-K_α	Cu-K_β
Mn	12	11.7	19.7	40.4	6.2	1.4	0.2	46.4	5.4
Ni	2	2.5	2.6	78.0	12.1	—	—	—	9.9
Cu	86	85.8	77.7	86.3	13.7	—	—	—	—

TABLE 4

Stainless steel analysis

Element	Present (%)	Found (%)		Fluorescent signal contributions (%)					
		Eqn. (1)	Simplified eqn. (1)	Primary excitation		Enhancement contributions			
				Mo-K_α	Mo-K_β	Fe-K_α	Fe-K_β	Ni-K_α	Ni-K_β
Cr	17—20	18.9	25.7	51.3	7.7	34.4	4.3	2.1	0.3
Mn	<2	1.6	1.4	77.9	11.9	—	6.6	3.2	0.4
Fe	—	70.9	66.1	84.0	12.6	—	—	3.0	0.4
Ni	8—11	8.6	6.9	87.3	12.7	—	—	—	—

The relative contribution of the Mo K_α and K_β radiation to the fluorescence for each element and the signal contribution of the enhancement effect arising from other constituents of the samples also follow from the calculation (and are represented in the tables).

For a more complete investigation of the method, different sets of multi-element samples, available in disk or in block form, with certified concentration values were analysed. The results of the analyses of a series of aluminum alloys with up to 15% of other elements are shown in Table 5. The samples were measured using molybdenum K-radiation, and the measuring time was 2000 s at an integral count rate of 1000 cps. During the iterative approximations of the concentrations, the aluminum fraction in the sample was determined by difference because this element could not be measured precisely enough. The agreement between certified and experimental results is fair. For some elements there are significant deviations: for instance, the experimental titanium concentrations are on average 20% higher than the certified value. This deviation could be due to inaccurate calibration and is presently being studied. The precision of the procedure was checked by 6 measurements of sample 3; the data are summarized in Table 6. For concentrations above 0.01%, the precision is approximately 1—2%.

TABLE 5

Comparison between the certified values and the x.r.f. results for 10 aluminum standards (%)
(NC means not certified. The 95% confidence limits are given.)

	Certified	X.r.f.	Certified	X.r.f.	Certified	X.r.f.	Certified	X.r.f.	Certified	X.r.f.
	Sample 1		*Sample 2*		*Sample 3*		*Sample 4*		*Sample 5*	
Ti	0.32 ± 0.03	0.42	0.104 ± 0.006	0.132	0.18 ± 0.01	0.19	0.0030 ± 0.0005	<0.02	0.100 ± 0.005	0.097
Cr	0.108 ± 0.005	0.108	NC.	0.001	NC.	0.002	NC.	0.003	0.0105 ± 0.0006	0.0065
Mn	2.00 ± 0.10	1.89	0.110 ± 0.005	0.116	0.335 ± 0.015	0.341	0.31 ± 0.02	0.31	0.104 ± 0.005	0.111
Fe	0.320 ± 0.025	0.311	0.58 ± 0.03	0.59	0.78 ± 0.04	0.72	0.35 ± 0.02	0.38	0.360 ± 0.018	0.374
Ni	0.0015 ± 0.0003	0.0022	0.25 ± 0.02	0.24	0.049 ± 0.002	0.048	0.43 ± 0.03	0.45	0.105 ± 0.005	0.099
Cu	0.037 ± 0.002	0.051	8.90 ± 0.30	9.26	0.78 ± 0.03	0.81	7.10 ± 0.15	7.28	3.02 ± 0.15	3.10
Zn	0.145 ± 0.005	0.139	1.00 ± 0.05	1.09	0.46 ± 0.02	0.46	2.95 ± 0.15	3.17	0.0125 ± 0.0008	0.0198
Pb	0.11 ± 0.01	0.09	0.15 ± 0.01	0.14	0.158 ± 0.012	0.144	0.35 ± 0.03	0.25	0.060 ± 0.004	0.056
	Sample 6		*Sample 7*		*Sample 8*		*Sample 9*		*Sample 10*	
Ti	0.052 ± 0.003	0.077	0.100 ± 0.007	0.123	0.20 ± 0.01	0.23	0.100 ± 0.007	0.129	0.210 ± 0.015	0.254
Cr	NC.	0.002	NC.	0.001	NC.	0.002	0.022 ± 0.002	0.018	0.057 ± 0.006	0.052
Mn	0.630 ± 0.025	0.615	0.185 ± 0.010	0.186	0.0075 ± 0.0010	0.0045	5.70 ± 0.25	6.24	3.90 ± 0.15	3.66
Fe	0.32 ± 0.02	0.32	1.25 ± 0.05	1.17	0.21 ± 0.01	0.23	0.97 ± 0.04	1.09	0.615 ± 0.040	0.632
Ni	0.33 ± 0.01	0.34	0.140 ± 0.005	0.136	0.004	<0.008	0.098 ± 0.008	0.105	0.053 ± 0.003	0.057
Cu	0.30 ± 0.01	0.32	1.26 ± 0.05	1.26	11.00 ± 0.30	11.85	0.250 ± 0.015	0.283	0.16 ± 0.01	0.18
Zn	0.160 ± 0.007	0.154	0.78 ± 0.03	0.79	0.10 ± 0.01	0.14	0.054 ± 0.004	0.058	0.100 ± 0.005	0.114
Pb	0.063 ± 0.003	0.059	0.345 ± 0.020	0.302	0.010 ± 0.002	0.003	0.038 ± 0.006	0.040	0.086 ± 0.010	0.087

TABLE 6

Precision of measurements on aluminum sample 3

	Element							
	Ti	Cr	Mn	Fe	Ni	Cu	Zn	Pb
Mean peak intensity (c/2000 s)	1346	78	12575	42383	6204	145172	119312	40293
Background intensity	1158	947	1205	1281	1542	1429	1532	1578
Statistical deviation	60	44	122	212	96	385	350	208
Experimental standard deviation	25	52	116	441	145	1060	1036	230
Mean elemental concentration (%)	0.194	0.002	0.341	0.724	0.048	0.805	0.464	0.144
Standard deviation	0.003	0.002	0.003	0.008	0.001	0.006	0.004	0.001

A comparison between certified and determined concentrations for a set of iron and nickel alloys is given in Tables 7 and 8. Titanium was used as a secondary target for the measurement of aluminum and silicon, molybdenum for the medium Z-elements, and tin for the measurement of niobium and molybdenum. The three sets of equations resulting from these measurements were solved simultaneously, and the enhancement effect of the niobium and molybdenum L-radiation on aluminum and silicon was also taken into account. As the samples were rather complex, the spectral interferences were more serious than in the analysis of the aluminum samples, hence the net intensity values obtained by the spectral analysis were less reliable.

Significant errors for low concentration elements were induced by the high background near the most intense lines. This hampers the possibility of defining general detection limits for the analysis of metals. However, the overall agreement for the concentrations is satisfactory. Typically, accuracies of 10% or better are obtained.

The other nickel alloys were also analyzed with sample SRM 1207-1 serving as the standard. The results obtained are also summarized in Table 7. They are very similar to the data obtained by means of thin film calibration.

Conclusion

A simplified fundamental parameters approach, based on a theoretical formula for primary and secondary fluorescent x-ray intensities makes it a simple task to calculate and to correct for matrix effects. Reliable quantitative results can be obtained on multi-element samples. Application of the method to a set of aluminum alloys and to a series of six iron and nickel-base alloys shows mean deviations of 5—10% from the certified values. The

TABLE 7

Certified and measured compositions of NBS nickel alloys (%)

Element	SRM 1206-2			SRM 1207-1		SRM 1208-1		
	Certified	X.r.f.[a]		Certified	X.r.f.[a]	Certified	X.r.f.[a]	
		(1)	(2)		(1)		(1)	(2)
Al	1.7	1.4	1.2	1.26	1.5	(0.15)	0.38	0.33
Si	0.21	0.21	0.18	0.47	0.58	0.43	0.36	0.31
Ti	2.9	3.4	2.9	3.09	3.58	0.46	0.51	0.43
Cr	19.17	19.59	19.17	18.88	19.35	17.5	18.3	17.7
Mn	0.030	0.078	0.075	0.34	0.35	0.38	0.41	0.39
Fe	0.46	0.39	0.40	2.22	2.13	19.2	19.3	20.1
Co	11.5	10.9	11.6	13.0	12.35	0.82	1.01	1.07
Ni	53.3	53.2	53.9	56.1	55.5	51.9	50.6	52.6
Cu	0.04	0.02	0.06	0.026	0.010	0.14	0.13	0.35
Nb	NC	<0.002	—	NC	<0.002	5.3	5.6	—
Mo	10.3	10.7	10.5	4.50	4.62	3.2	3.4	3.4

[a](1) Calibration based on thin film standards. (2) Calibration based on SRM 1207-1.

TABLE 8

Certified and measured compositions of NBS iron alloys (%)

Element	SRM 1154		SRM 1155		SRM 1156	
	Certified	X.r.f.	Certified	X.r.f.	Certified	X.r.f.
Si	1.09	0.97	0.50	0.50	0.184	0.26
Ti	(0.48)	0.54	NC	0.013	0.21	0.23
Cr	19.58	20.48	18.4	19.2	0.20	0.20
Mn	1.74	1.77	1.63	1.66	0.21	0.13
Fe	(65.0)	64.9	(64.5)	64.0	(69.7)	70.8
Co	(0.12)	0.33	0.10	0.33	7.3	7.1
Ni	10.25	9.44	12.1	11.4	19.0	17.7
Cu	0.56	0.46	0.169	0.142	0.025	0.016
Nb	(0.26)	0.25	NC	<0.001	NC	<0.002
Mo	0.463	0.478	2.38	2.43	3.1	3.3

discrepancies in the analyses for some of the elements are probably caused by incorrect calibration or inaccurate spectral deconvolution rather than by errors in the absorption enhancement calculations. Further refinements of the computer spectrum analysis could partly overcome these difficulties. Work is in progress to utilize a refined least-squares analysis with a more realistic description of the peaks than the pure Gaussian shape [18]. The calibration factors determined from thin film standards are believed to be accurate within 5%.

The combination of the fundamental parameters technique with energy-dispersive x-ray fluorescence provides a flexible and adequate multi-element analysis of samples with extremely variable compositions.

P. V. is indebted to the "Instituut tot aanmoediging van het wetenschappelijk onderzoek in nijverheid en landbouw" for financial support. This work was also supported by the "National Fonds Voor Wetenschappelyk Onderzoek.

REFERENCES

1 E. Gilliam and H. Heal, Brit. J. Appl. Phys., 3 (1952) 353.
2 J. Sherman, Spectrochim. Acta, 7 (1955) 283.
3 T. Shiraiwa and N. Fujino, Jpn. J. Appl. Phys., 5 (1966) 886.
4 D. A. Stephenson, Anal. Chem., 43 (1971) 1761.
5 R. Tertian and R. Vié le Sage, X-Ray Spectrom., 5 (1976) 73.
6 R. Jenkins, An Introduction to X-ray Spectrometry, Heyden, London, 1976.
7 J. Criss and L. S. Birks, Anal. Chem., 40 (1968) 1080.
8 Micromatter Co., Seattle, Washington, U.S.A.
9 T. Shiraiwa and N. Fujino, X-Ray Spectrom., 3 (1974) 64.
10 W. H. McMaster, N. K. Del Grande, J. H. Mallett and J. H. Hubbell, Compilation of X-Ray Cross Sections, UCRL-50174, Sec. II, Rev. 1 (1969).
11 C. J. Sparks, Adv. X-Ray Anal., 19 (1975) 19.

12 W. Bambynek, B. Crasemann, R. W. Fink, H.-U. Freund, H. Mark, C. D. Swift, R. E. Price and P. V. Rao, Rev. Mod. Phys., 44 (1972) 716.
13 Handbook of Chemistry and Physics, R. C. Weast (Ed.), The Chemical Rubber Co., Cleveland, 1972.
14 P. Van Espen, H. Nullens and F. Adams, Nucl. Instrum. Methods, 142 (1977) 243.
15 A. R. Stiles, T. G. Dzubay, R. M. Baum, R. L. Walter, R. D. Willis, L. J. Moore, E. L. Garner, J. W. Gramlich and L. A. Machlar, Adv. X-ray Anal., 19 (1975) 473. .
16 P. J. Van Espen and F. C. Adams, Anal. Chem., 48 (1976) 1823.
17 S. L. Blatt, Nucl. Instrum. Methods, 128 (1975) 277.
18 P. Van Espen, H. Nullens and F. Adams, Nucl. Instrum. Methods, 145 (1977) 579.

Analytica Chimica Acta, 97 (1978) 295—301

THE SIMULTANEOUS DETERMINATION OF As, Cd, Co, Hg, Mo, AND Zn IN FRESH WATER BY NEUTRON ACTIVATION ANALYSIS†

K. LENVIK§ and E. STEINNES*

Institutt for atomenergi, Isotope Laboratories, Kjeller (Norway)

A. C. PAPPAS

Department of Chemistry, University of Oslo, Oslo (Norway)

(Received 19th October 1977)

SUMMARY

A radiochemical neutron activation method for the simultaneous determination of arsenic, cadmium, cobalt, mercury, molybdenum, and zinc in fresh water is described. The method is based on anion-exchange separation in hydrochloric acid media followed by simple precipitations. The determination limits, based on analysis of a 5-ml sample without preconcentration, and with a well-type NaI(Tl) detector, are as follows: As, 10^{-3} μg l^{-1}; Cd, 6×10^{-2} μg l^{-1}; Co, 4×10^{-3} μg l^{-1}; Hg, 7×10^{-3} μg l^{-1}; Mo, 10^{-1} μg l^{-1}; Zn, 2×10^{-1} μg l^{-1}. The method is adequate for the analysis of natural fresh waters.

Present awareness of the importance of trace metals in aquatic systems has prompted increased activity in the development of sensitive and accurate methods for their determination. Several analytical techniques are applicable to this type of work; one of these is neutron activation analysis, the sensitivity of which is adequate for a great number of elements at the concentration levels present in natural waters, and which is capable of simultaneous determination of a number of elements. Moreover, contamination problems are less in activation analysis than in most other techniques suitable for trace element determination in water.

Applications of n.a.a. to fresh water analysis have largely been based on radiochemical separations [1]. Some of the methods reported previously have involved the simultaneous determination of a considerable number of elements [2—4]. With the advent of solid-state detectors for γ-spectrometry, the radiochemical treatment may be considerably simplified [5, 6] or even omitted [7—10]. Even though Ge(Li) γ-spectrometry combined with computer data reduction may allow up to 40 elements to be determined in fresh water by purely instrumental n.a.a. in certain cases [10], the determination of some important trace elements is still difficult or impossible by this technique at natural concentration levels, because of interfering γ-activities or inadequate counting efficiencies of the Ge(Li) detectors available.

† Based on a thesis by K. Lenvik.

§ Present address: State Pollution Control Authority, Oslo, Norway.

Thus elements such as As, Cd, and Mo were difficult to determine quantitatively by instrumental activation analysis at actual concentration levels [10].

A radiochemical separation scheme applicable to water analysis was therefore developed. The ultimate goal of this work was to obtain separated fractions sufficiently pure for counting in a well-type NaI(Tl) detector coupled to a small multichannel analyzer. The main step of the procedure is a separation by anion exchange developed mainly on the basis of earlier information [11—14]. The method is designed for the simultaneous determination of As, Cd, Co, Hg, Mo, and Zn.

EXPERIMENTAL

Reagents

Standards. The standard solutions for cadmium, cobalt, and zinc were made by dissolution of appropriate amounts of the respective metals in nitric acid and diluting with water to a concentration of 0.1 M HNO_3. The mercury standard was made similarly by dissolving HgO in nitric acid. The arsenic and molybdenum standards were made respectively by dissolving As_2O_3 and MoO_3 in 3 M NH_4OH and diluting with water to a concentration of 0.1 M NH_4OH. The following appropriate concentrations were used: As, 30 $\mu g\ ml^{-1}$; Cd, 15 $\mu g\ ml^{-1}$; Co, 20 $\mu g\ ml^{-1}$; Hg, 30 $\mu g\ ml^{-1}$; Mo, 10 $\mu g\ ml^{-1}$; Zn, 150 $\mu g\ ml^{-1}$.

Carriers. The carriers were made by dissolving the compounds listed above in 4 M HNO_3 (Cd, Co, Hg, Zn) or 3 M NH_4OH (As, Mo). Appropriate concentrations were: As, Cd, Co, Hg, 5 mg ml^{-1}; Mo, Zn, 10 mg ml^{-1}.

Anion-exchange columns. Columns of 12-mm i.d., filled with Dowex 1-X8 (100-200 mesh, chloride form) to 55 ± 5 mm height of resin bed, were used. Before use, the columns were equilibrated with 8 M HCl. The columns were operated at free flow, corresponding to about 1.1 ml min^{-1}.

Irradiation

Samples (5 ml) were sealed for irradiation in carefully cleaned quartz ampoules. From each standard solution, ca. 1 ml was sealed in a separate quartz ampoule.

The irradiations were performed for 3 d in the JEEP-II reactor (Kjeller, Norway) at a thermal neutron flux of ca. 1.5×10^{13} n cm^{-2} s^{-1}. The cadmium ratio of gold in the position employed was about 3. The samples were left for 24 h for the decay of short-lived activities, mainly ^{31}Si from the quartz ampoules, before the start of the radiochemical separation.

Radiochemical separation

After being cleaned with warm 6 M HNO_3 to remove surface contamination, and subsequently cooled with liquid nitrogen, the ampoules are opened and the contents transferred to a 250-ml beaker containing 3 ml of concentrated nitric acid and 1-ml carrier solutions of each of the six elements

under consideration. The ampoule is washed with two 2-ml portions of 6 M HNO_3 which are added to the sample solution. After evaporation to dryness on a hot plate, 6 ml of 5% H_2O_2 and 3 drops of concentrated nitric acid are added. Upon gentle heating the residue is dissolved, and excess of H_2O_2 is boiled off. By this treatment the elements are oxidized to their highest stable valency state. The solution is evaporated down to a volume of 2 ml, and 4 ml of concentrated hydrochloric acid are added. After cooling, the sample is transferred to a pre-equilibrated anion-exchange column. The beaker is washed with two 2-ml portions of 8 M HCl which are also added to the column. The elements are then eluted successively with 5-ml portions of eluents according to the following sequence: I. As, 7 × 5 ml 8 M HCl; II. Co, 4 × 5 ml 4 M HCl; III. Mo, 9 × 5 ml 0.9 M HCl; IV. Zn, 7 × 5 ml 0.01 M HCl/10% CH_3OH; V. Cd, 11 × 5 ml H_2O; VI. Hg, 7 × 5 ml 8 M HNO_3/4 M NH_4NO_3.

A set of curves showing a typical elution sequence is shown in Fig. 1.

The different fractions from the elution are collected in 100-ml beakers, and subsequently each element is treated separately.

Arsenic. Reduction of As(V) to As(III) is brought about by adding about 100 mg of KI to the eluate. Then As_2S_3 is precipitated by the addition of ca. 100 mg of thioacetamide and heating. After centrifuging and washing with H_2O, the precipitate is collected on a blue ribbon filter paper. Before chemical yield determination, the precipitate is dissolved with 3 ml of concentrated nitric acid.

Cobalt. The eluted fraction is reduced to a volume of 3 ml by evaporation and transferred to a counting vial.

Molybdenum. The eluate is cooled to 0°C, and 10 ml of α-benzoinoxime solution (2.5% w/w in ethanol) is added. The molybdenum benzoinoximate formed is separated by extraction with 45 ml of ethyl acetate. Back-extraction is performed with 45 ml of 4 M ammonia solution. The solution is evaporated

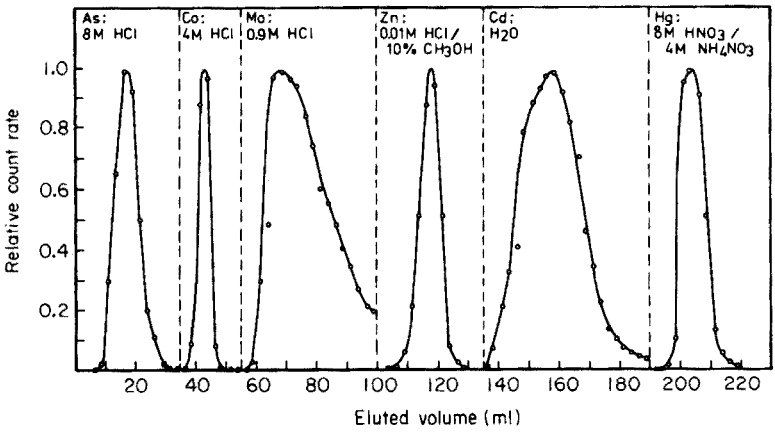

Fig. 1. Elution curves from a Dowex 1-X8 column.

down to 3-ml volume, transferred to a counting vial, and stored for 24 h before counting to permit the transient equilibrium of ^{99}Mo—^{99m}Tc to be approached.

Zinc. After heating to about 80°C, the eluate is adjusted to pH 6.5 with an aqueous solution of $(NH_4)_2HPO_4$ (150 mg ml^{-1}). The resulting precipitate ($ZnNH_4PO_4$) is filtered on a blue ribbon filter paper and washed with an acetate buffer of pH 6.5. Before chemical yield determination the precipitate is dissolved with 0.1 M HNO_3.

Cadmium. The eluate is made slightly alkaline by dropwise addition of ammonia solution. Then thioacetamide is added to pH 3—5. A yellow precipitate (CdS) is obtained on gentle heating at 90—100°C for 10—15 min. The precipitate is collected on a blue ribbon filter paper and washed with H_2O. A delay of 24 h between separation and counting is employed in order to reach the transient equilibrium ^{115}Cd—^{115m}In. Before chemical yield determination the precipitate is dissolved with 0.1 M HNO_3.

Mercury. After the eluate has been made alkaline with concentrated ammonia solution, about 200 mg of ascorbic acid are added. After a delay of 2 h, the metallic mercury precipitate is isolated by filtration through a 0.45-μm membrane filter and washed with water. Before the chemical yield determination the precipitate is dissolved in concentrated nitric acid.

Activity measurements

Two γ-spectrometry systems were used for activity measurements of the isolated fractions. The basic unit was a 3 × 3-in. well-type Na(Tl) detector connected to a 400-channel analyzer equipped with a sample changer. The determinations of As, Zn, and Hg were in many cases performed with a Ge(Li) detector (5.4% efficiency and 2.1-keV resolution, defined in the usual manner by means of ^{60}Co) with associated electronics, interfaced to a NORD-I computer (16K, 16 bit). Counting times of 10 min—2 h were used, depending on the counting system employed and the element concerned. The radionuclides and γ-energies used in the analyses are listed in Table 1.

As, Co, Zn, and Hg were measured as soon as possible after the chemical separation. Peak areas were, in most cases, calculated by the method of Covell [15]. For very small peaks, however, the method of Sterlinski [16] was preferred.

For the measurements of standards, 500-μl aliquots were withdrawn from the irradiated ampoules and diluted to a suitable volume with dilute nitric acid. From this solution a suitable volume was withdrawn for counting.

Chemical yield determination

After completion of the counting procedure, the various precipitates were dissolved as indicated above, transferred to 50-ml volumetric flasks and diluted to the mark with distilled water. The chemical yields of As, Cd, Hg, Mo, and Co were determined by re-irradiation. Suitable aliquots of the dilute sample solution were given a short irradiation at a thermal neutron

TABLE 1

Some data for the radionuclides used in the present work

Element	Target nuclide	Radionuclide formed by (n,γ) reaction	Half-life	γ-rays used (keV)	Experimental determination limits (μg l^{-1})	
					NaI(Tl) detector	Ge(Li) detector
As	^{75}As	^{76}As	26.4 h	559	0.001	0.01
Cd	^{114}Cd	$^{115}Cd/^{115m}In$	53.5 h/4.5 h	336	0.06	0.4
Co	^{59}Co	^{60}Co	5.3 y	1173, 1332	0.004	0.03
Hg	^{196}Hg	^{197}Hg	65 h	69, 78	0.007	0.08
	^{202}Hg	^{203}Hg	28 d	279	0.16	0.6
Mo	^{98}Mo	$^{99}Mo/^{99m}Tc$	66.7 h/6.0 h	140	0.1	0.8
Zn	^{64}Zn	^{65}Zn	243 d	1116	1	5
	^{68}Zn	^{69m}Zn	13.9 h	439	0.2	2

flux of ca. 1.5×10^{13} n cm^{-2} s^{-1} by means of the pneumatic-tube system of the JEEP-II reactor. An aliquot of the standard solution was irradiated simultaneously. The re-activated samples were assayed by γ-spectrometry with the Ge(Li) detector system.

In the case of Zn, the sample solution was diluted to a concentration of about 1 ppm and analyzed for chemical yield by a.a.s. with a Perkin-Elmer model 305 spectrometer with a three-slot Boling burner.

RESULTS AND DISCUSSION

Chemical yield

The chemical yields for the elements in question, obtained from five samples run simultaneously by the procedure given above, are listed in Table 2. The yield for Co is constant and nearly quantitative. The yields of Zn and Mo are also quite reproducible at levels of about 80% and 70% respectively. For As, Cd, and Hg the chemical yield values are more scattered; in most cases they fall within the range 70—90%.

Precision and accuracy

The precision of the method was studied by analyzing a synthetic water sample made by mixing appropriate amounts of the standard solutions and diluting to a concentration level similar to that observed in many polluted waters. Results from the analysis of four replicates are given in Table 3. The precision is in the range 4—15%. The most important factors contributing

TABLE 2

Chemical yields (%) for five samples run simultaneously

	As	Co	Cd	Hg	Mo	Zn
Mean value (N = 5)	77.8	96.4	83.0	81.2	70.2	81.0
Standard deviation (single value)	9.9	1.9	7.3	10.1	2.6	1.9

TABLE 3

Results obtained by analysis of a standard water sample and some natural water samples

Element	Standard sample				Natural waters[b]	
	Nominal concentration ($\mu g\ l^{-1}$)	Mean value observed[a] ($\mu g\ l^{-1}$)	R.s.d. (%)	Deviation from nominal value (%)	Typical concentration level [17] ($\mu g\ l^{-1}$)	R.s.d. from duplicate analyses (%)
As	2.39	2.56	12.9	+7.1	0.4	17.6
Cd	2.16	1.93	12.1	−10.6	0.3	20.6
Co	1.83	1.84	13.0	+0.5	0.2	—
Hg	7.63	7.78	4.7	+2.0	—	12.8
Mo	3.62	3.74	14.5	+3.3	0.2	22.5
Zn	34.2	36.1	4.1	+5.6	20	13.5

[a]Means of 5 analyses.
[b]Hg values cannot be given because of a laboratory contamination problem.

to the observed spread are presumably counting statistics and variation in the chemical yield determination. Deviations of the observed mean values from the nominal values were 10% or less, indicating that the accuracy of the method was similar to the precision in this case.

The method has been applied to a study of water samples from Norwegian rivers, the results of which will be published elsewhere [17]. In some cases duplicate determinations were carried out, and the calculated standard deviations are given in Table 3. At these very low concentration levels, counting errors are assumed to be responsible for a major part of the observed spread.

The accuracy of water analyses may be affected by several sources of systematic errors, of which the most serious are often those associated with the sampling and storage of samples, i.e. blanks, sorption phenomena, etc. Such errors are, however, in most cases independent of the analytical method used; their discussion is considered to be outside the scope of this paper.

Considering nuclear sources of error, neutron-shielding effects are insignificant in fresh water analysis. Contributions from interfering nuclear reactions are also negligible for the elements studied in this work, except for the contribution to the ^{99}Mo—^{99m}Tc activity from fission of uranium. This contribution depends on the energy spectrum of neutrons in the reactor and on the uranium content of the water samples, and must therefore be determined experimentally in each case. In the present work the presence of 1.00 ng U yielded an activity corresponding to that induced from 0.93 ng Mo. In an irradiation position with a nearly thermal neutron flux the relative uranium interference may be as much as three times higher. The uranium content of the water samples studied in connection with this work was determined by a rapid neutron activation method [18] involving the radiochemical separation of 23.5-min ^{239}U by solvent extraction in the system tributyl phosphate—nitric acid.

Spectral interferences, which are significant for several of the elements concerned in the purely instrumental activation analysis of water, were not observed in the separated fractions resulting from the present method.

Determination limits

Determination limits obtained under the present conditions for the six elements are given (Table 1) for the two detection systems employed in this work. The determination limit is defined as the amount of element yielding a measured peak area equal to three times the square root of the background under the peak in a counting period of 2 h. As evident from the figures, the sensitivity obtained with the well-type NaI(Tl) detector is about tenfold higher than that observed with the 35 cm^3 Ge(Li) detector. In the case of Zn and Hg, the use of the shorter-lived isotopes ^{69m}Zn and ^{197}Hg gives higher sensitivity than that obtained with the longer-lived counterparts.

Conclusion

The method reported is suitable for the simultaneous determination of As, Cd, Co, Hg, Mo, and Zn at the concentration levels at which these elements are present in natural fresh water. Except for Zn, where a.a.s. is slightly more sensitive, the method with the well-type NaI(Tl) detector shows practical determination limits for the elements studied that are better than those of other analytical techniques currently available.

REFERENCES

1 G. J. Lutz, R. J. Boreni, R. S. Maddock and J. Wing (Eds.), Activation Analysis: A Bibliography through 1971. National Bureau of Standards, Washington, DC, 1972.
2 R. L. Blanchard and G. W. Leddicotte, USAEC Report ORNL-2620 (1959).
3 O. Landström and C. G. Wenner, Report AE-204, AB Atomenergi, Stockholm, 1965.
4 D. P. Kharkar, K. K. Turekian and K. K. Bertine, Geochim. Cosmochim. Acta, 32 (1968) 285.
5 L. L. Thatcher and J. O. Johnson, Nuclear Techniques in Environmental Pollution, IAEA, Vienna, 1971, pp. 323—328.
6 T. M. Tanner, L. A. Rancitelli and W. A. Haller, Water, Air, Soil Pollut., 1 (1972) 132.
7 J. Schmitz, J. Schneider and H. Vogg, Gas-Wasserfach, Wasser-Abwasser, 113 (1972) 318.
8 J. Slavic, R. Draskovic, T. Tasovac and R. Radosavljevic, Isotopenpraxis, 9 (1973) 87.
9 J. Schneider and R. Geisler, Z. Anal. Chem., 267 (1973) 270.
10 B. Salbu, E. Steinnes and A. C. Pappas, Anal. Chem., 47 (1975) 1011.
11 K. A. Kraus and F. Nelson, Proc. Int. Conf. Peaceful Uses of Atomic Energy, Geneva, 7 (1956) 113.
12 E. W. Berg and J. T. Truemper, Anal. Chem., 30 (1958) 1827.
13 P. van den Winkel, A. Speecke and J. Hoste, Nuclear Activation Techniques in the Life Sciences, IAEA, Vienna, 1967, pp. 159—172.
14 O. Johansen and E. Steinnes, Talanta, 17 (1970) 407.
15 D. F. Covell, Anal. Chem., 31 (1959) 1785.
16 S. Sterlinski, Anal. Chem., 40 (1968) 1995.
17 K. Lenvik, E. Steinnes and A. C. Pappas, Nord. Hydrol., in press.
18 E. Steinnes, Radiochem. Radioanal. Lett., 16 (1973) 25.

Analytica Chimica Acta, 97 (1978) 303—310

DETERMINATION OF RARE EARTH ELEMENTS AND HEAVY METALS IN RIVER WATER BY PRECONCENTRATION ON CHELEX 100 AND NEUTRON ACTIVATION†

A. HIROSE*, K. KOBORI and D. ISHII

Department of Applied Chemistry, Faculty of Engineering, Nagoya University: Furo-cho, Chikusa-ku, Nagoya (Japan)

(Received 19th September 1977)

SUMMARY

The neutron activation determination of rare earth elements and heavy metals in river water has been studied with Chelex 100 resin as a preconcentration agent. The resin is applied directly as a support for irradiation and for radiochemical separation. The radioactive rare earth elements are recovered selectively and quantitatively from the irradiated resin by elution with hot 1 M sodium carbonate solution; radioactive heavy metals are recovered with 2 M nitric acid. Activities from each eluate are counted with a Ge(Li) detector connected to a multichannel analyzer; La, Sm, Eu, Dy, Mn, Cu and Zn can be determined. The recoveries were almost quantitative and the measurement of chemical yield was unnecessary.

Since the concentrations of trace elements in natural water samples are generally too low for direct analysis, some appropriate preconcentration or enrichment step is unavoidable even when a sensitive detection method such as neutron activation is applied [1]. Chelex 100 or Dowex A-1 chelating resin strongly adsorbs a number of elements [2—8] and have been used for the preconcentration of water samples. However, there have been few attempts to combine the technique with neutron activation; in the radioactive measurement, the irradiated resin introduces sources of interference and the radiochemical separation is complicated because the ion-exchange resin cannot be removed without ashing. To overcome such difficulties, the radionuclides of interest should be eluted selectively and quantitatively from the irradiated resin but such a method has not been tried in conjunction with neutron activation analysis.

The present work shows that the radioactive rare earth elements and heavy metals can be recovered quantitatively and selectively by elution, and the preconcentration technique with a chelating resin can be combined conveniently with neutron activation.

---

†Presented at the 18th Symposium on Radiochemistry, Sendai, October, 1974.

EXPERIMENTAL

Apparatus

The 10MW JRR-2 and -3 reactors at the Japan Atomic Research Institute were used. The former has a thermal neutron flux of 6.5×10^{13} n cm^{-2} s^{-1}, a fast (>1 MeV) neutron flux of 2×10^{12} n cm^{-2} s^{-1} and a γ-exposure dose rate of ca. 2×10^{8} r h^{-1}; the latter has thermal and fast fluxes of 2×10^{13} and 7×10^{11} n cm^{-2} s^{-1}, respectively and gamma rate of ca. 2×10^{8} r h^{-1}.

The radiation detector was a 41.5-cm^3 Ge(Li) detector connected to a 1024-channel pulse-height analyzer.

Funnels with stems of 0.65—0.8 cm i.d. × 12—15 cm length were used for the resin columns (Fig. 1). The smaller dimensions were used for sample preparation, the larger for radiochemical separation.

Reagents

Chelating resins. Chelex 100 was conditioned and purified by washing successively with 25 ml of 2 M ammonium hydroxide, 25 ml of 2 M nitric acid and 25 ml of water; this cycle was repeated. The resin was transformed into NH_4-form by washing with 0.1 M ammonium hydroxide until the pH of the effluent was greater than 6. After washing with a small amount of water, the resin was applied to preconcentration. Dowex A-1 was used for radiochemical separation without further purification.

Standard solutions. Lanthanum, samarium, europium, dysprosium and ytterbium oxides and manganese, cobalt, copper, zinc and cadmium metals were dissolved in dilute nitric acid; the solutions were diluted with water to the desired concentrations.

Radioactive tracer solutions. Rare earth oxides, or nitrates, and heavy metals were irradiated in the JRR-3 reactor for 1 h (or for 75 h with a flux of 5×10^{12} n cm^{-2} s^{-1}), and dissolved in dilute nitric acid or water; the solutions were adjusted to pH 3 with ammonia solution, if necessary, and diluted with water to the desired concentrations.

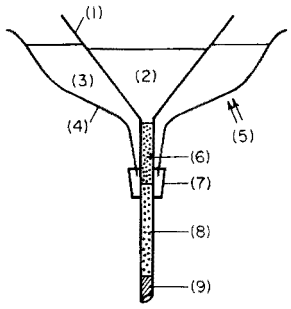

Fig. 1. Resin column used for radiochemical separation. (1) Glass funnel. (2) Hot 1 M Na_2CO_3 soln. (3) Hot water. (4) Water jacket. (5) Gas burner. (6) Irradiated resin sample. (7) Rubber stopper. (8) Dowex A-1 resin. (9) Cotton wad.

Purified 0.1 M ammonium acetate solution. Commercial ammonium acetate was dissolved in water to give 0.5 M solution which was passed through a column packed with Chelex 100 (NH_4-form) and diluted to 0.1 M.

The ammonia solution and nitric acid used in the Preparation of Sample were of "super-special" grade (Wako Pure Chemicals). All other reagents were of analytical grade. Deionized water was used throughout.

Preparation of sample, standard and blank

Immediately after collection, add nitric acid to adjust the water sample to pH 1, and filter through membrane filters to remove suspended matter. Neutralize a 500-ml aliquot with ammonia solution, and pass through the column packed with 1 g (wet basis) of Chelex 100 at 2—3 ml min^{-1}.

Wash the resin bed with 30 ml of purified 0.1 M ammonium acetate solution to eliminate sodium, and finally with a small amount of water. Transfer the resin samples into polyethylene bags, allow to dry in an oven at 75°C for 10 h, and heat-seal.

To prepare standards, drop 20 μl of a standard solution onto a 2-cm filter paper, dry at room temperature, and heat-seal in a polyethylene bag.

Prepare the resin blank by treating Chelex 100 with the same amounts of the solutions or reagents as used in the sample preparation.

Irradiation and radiochemical separation

Pack the samples, standards, and blanks into a polyethylene capsule, and irradiate in the JRR-3 reactor for 1 h. After cooling for ca. 3 h to allow the nuclides with short half-lives, especially ^{38}Cl, to decay, open the capsule and load the irradiated resin sample onto the Dowex A-1 resin bed (see Fig. 1). Wash with 50 ml of 0.1 M potassium nitrate solution at room temperature to eliminate interfering radionuclides, e.g. ^{24}Na, ^{82}Br, and ^{38}Cl.

Heat the column with a hot water jacket. Elute the radioactive rare earth elements by adding 100 ml of 1 M sodium carbonate solution that has been heated to boiling previously. Finally, elute the radioactive heavy metals with 100 ml of 2 M nitric acid solution at room temperature.

Treat the irradiated resin blanks by the procedure used for the resin sample. To prepare radioactive standards, dissolve the irradiated filter papers in a small amount of a mixture of nitric and sulfuric acids, and dilute to 100 ml with 1 M sodium carbonate or 2 M nitric acid solution.

Counting

Measure the γ-ray spectrum of each fraction, and identify the photo-peaks corresponding to nuclides or elements by determining the energies and half-lives, or relative intensities. Determine the amounts of elements by comparing the net photo-peak activities in the sample with corresponding standards.

RESULTS

Recoveries from the preconcentration step

With the procedure described, recoveries of trace elements in river water from the preconcentration step were examined by means of radioactive tracer solutions. The results obtained are listed in Table 1.

Selective elution of radioactive rare earth elements from irradiated resin

With a radiotracer solution of samarium and unirradiated chelating resin, elution of samarium was examined by adding 50 or 100 ml of 0.2, 0.5 or 1.0 M sodium carbonate solution at room temperature. Quantitative recovery was obtained when 100 ml of 1.0 M solution was used. This volume and concentration of solution were used in subsequent experiments.

Elution from the irradiated resin was examined by the procedure described under Radiochemical Separation. At room temperature the recovery was less than 60% for ^{153}Sm. The results obtained with heating are summarized in Table 2; the recoveries were satisfactory, except for ^{140}La.

The presence of radioactive heavy metals in the sodium carbonate fraction was checked. The irradiated resin was loaded on to a resin bed of 0.1 or 1.0 g

TABLE 1

Radiotracer recoveries from the pre-irradiation concentration step

Element	Tracer added (μg)	Recovery (%)	Element	Tracer added (μg)	Recovery (%)
Mn	0.2	98.5	La	0.5	98.8
Co	4	99.4	Sm	1	98.5
Cu	0.5	99.4	Eu	0.1	99.0
Zn	40	99.2	Yb	2	99.1
Cd	20	99.5			

TABLE 2

Elution of radioactive rare-earth elements from irradiated Chelex 100 with hot 1 M sodium carbonate solution

Isotope	Element added to resin (μg)	Radioactivity found in			Yield on elution (%)
		H_2O (%)	0.1 M KNO_3 (%)	Resin (%)	
^{140}La	10	0.2	0.2	5—20[a]	80—95
^{153}Sm	10	0.4	0.3	0.8	98.5
^{152m}Eu	2	0.4	0.4	0.7	98.5
^{169}Yb	25	0.1	0.3	1.0	98.6

[a]See Table 4.

of Dowex A-1, and washed. The results are shown in Table 3. When the column packed with 0.1 g of Dowex A-1 was used, the Compton contribution from the 1% of ^{56}Mn interfered with the measurement of radioactive rare earth elements. Therefore, columns containing 1.0 g of the resin are recommended.

Elution of radioactive heavy metals

After the elution of radioactive rare earth elements, the recoveries of radioactive heavy metals with 2 M nitric acid solution were examined. The results are listed in Table 4. The ^{140}La which remained in the irradiated resin after elution with hot sodium carbonate solution was quantitatively recovered in the nitric acid fraction. This nuclide has a longer half-life and emits γ-rays of higher energy than other rare-earth radionuclides, e.g. ^{153}Sm, ^{152m}Eu and ^{165}Dy, and could be measured, after cooling for 1—2 d, without interference from heavy metals.

TABLE 3

The presence of radioactive heavy metals in the 1 M sodium carbonate fraction

Isotope	Element added to resin (μg)	Heavy metals	
		Column 1[a] (%)	Column 2[a] (%)
^{56}Mn	8	1.0	0.01
^{64}Cu	27	0.62	0.25
^{69m}Zn	800	0.21	0.00

[a]Column 1 packed with 0.1 g of Dowex A-1. Column 2 packed with 1.0 g of Dowex A-1.

TABLE 4

Elution of radioactive heavy metals from irradiated Chelex 100 with 2 M nitric acid

Isotope	Element added to resin (μg)	Radioactivity found in[a]			Yield on elution (%)
		H_2O (%)	0.1 M KNO_3 (%)	Resin (%)	
^{56}Mn	8	0.2	0.3	0.9	98.6
^{64}Cu	27	1.1	0.4	0.4	97.8
^{69m}Zn	800	0.2	0.9	0.1	98.8
^{60}Co	80	0.0	1.3	0.7	98.0
^{115}Cd	800	0.3	0.0	0.4	99.3
^{140}La	10	0.2	0.2	0.3	5—19.7

[a]See Tables 2 and 3 for 1 M Na_2CO_3 fraction.

Analysis of river waters

Results for two natural river waters are listed in Table 5. Typical γ-ray spectra are shown in Figs. 2 and 3; the separation of rare earth elements and heavy metals and the elimination of interfering radionuclides are clearly satisfactory.

The blank values were: rare earth elements, not detected; Mn, 0.003 μg; Cu, 0.03 μg; Zn, 0.06 μg.

DISCUSSION

Elimination of interfering radionuclides originating from the resin

Although the conversion of Chelex 100 to its NH_4-form was useful in decreasing the sodium content, small amounts of interfering activities, e.g.

TABLE 5

Results for two river waters (ppb)

Sample		Mn	Cu	Zn	La	Sm	Eu	Dy
1		2.1	0.36	8.8	0.10	0.010	0.0034	0.0070
		1.8	0.36	7.4	0.096	0.011	0.0036	0.0072
	Av.	2.0	0.36	8.1	0.098	0.011	0.0035	0.0071
2		10	0.18	3.9	0.093	0.011	0.0054	0.0040
		9.0	0.18	3.7	0.083	0.009	0.0055	0.0036
	Av.	9.5	0.18	3.8	0.088	0.010	0.0055	0.0038

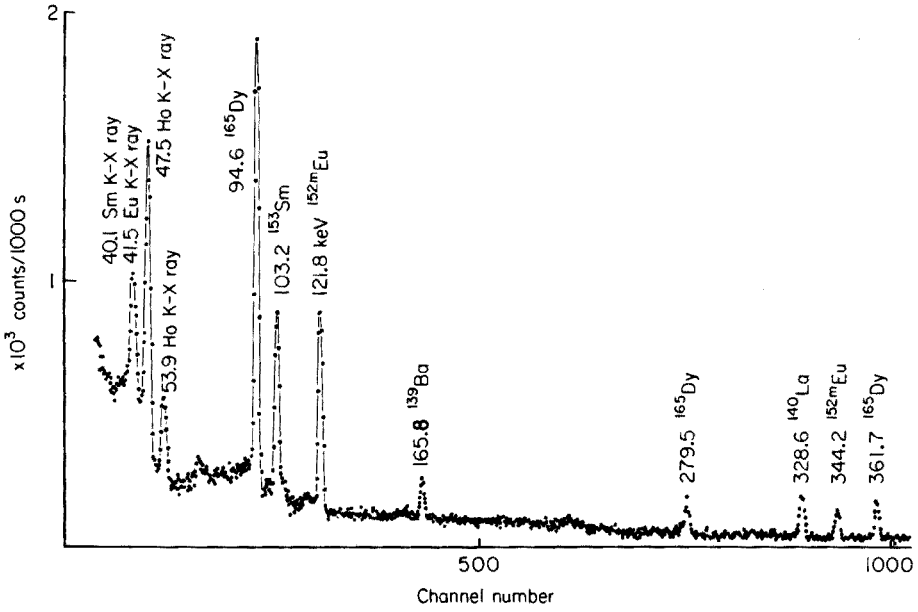

Fig. 2. γ-Ray spectrum of radioactive rare earth elements in 1 M sodium carbonate fraction, measured with Ge(Li) detector after cooling for 5.5 h.

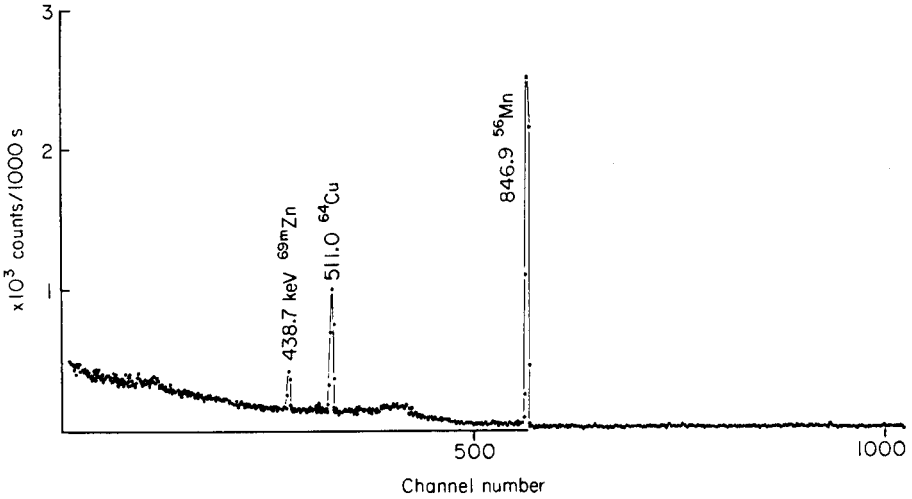

Fig. 3. γ-Ray spectrum of radioactive heavy metals in 2 M nitric acid fraction, measured with a Ge(Li) detector after cooling for 30 h.

^{24}Na, ^{82}Br, ^{38}Cl, ^{56}Mn, ^{64}Cu and ^{69m}Zn, were observed in the irradiated NH_4-form resin. The contents of sodium, bromine and chlorine in the resin were ca. 4.5, 1.0 and 750 ppm, respectively. After the post-irradiation washing with 1 M potassium nitrate solution, these were reduced to 0.03, 0.05 and 500 ppm, respectively. The amounts of the nuclides in the sodium carbonate and nitric acid fractions were decreased to negligibly small amounts, e.g. ^{24}Na, 0.005 μg; ^{82}Br, not detected; ^{38}Cl, not detected (after cooling for 3—5 h), when 1 g of the wet resin was irradiated.

Regarding the heavy metal contents, the blank values described above originated mainly from the Chelex 100 in its NH_4-form. As described previously [9] washing alternately with 2 M ammonia solution and 2 M nitric acid was effective in reducing the contents; washing twice with this cycle was recommended.

Other associated nuclides, e.g. ^{65}Zn, ^{80m}Br and ^{80}Br, did not interfere in the present measurements, because of the low activation yield or γ-ray energies.

Effects of reactor irradiation and drying of resin in air

Damage to ion-exchange resins by irradiation or by drying in air has usually been discussed in terms of decreased ion-exchange capacity [10]. In the present investigation, however, the change in yield of radioactive species eluted from irradiated resin allowed the effect of irradiation and drying in air to be examined.

Three resin samples adsorbing 25 μg of ytterbium labelled with ^{169}Yb were prepared; the first, treated with 100 ml of 1 M sodium carbonate solution at room temperature, had neither been air-dried nor irradiated. The

second sample of resin had been air-dried but not irradiated; the third had been both dried and irradiated. The recoveries of ^{169}Yb were 99.7, 95.5 and 91.9. respectively. These results indicate that both air-drying and radiation affect the yield on elution, but the effect can apparently be eliminated by elution at elevated temperature, as described under Experimental.

Irradiation in a different reactor

When the resin samples are irradiated in reactors other than the JRR-3 used, the elution yields may differ from the present results, because the reactors may have different thermal and fast neutron fluxes and γ-exposure dose rates. This problem was examined with the JRR-2 reactor. The recoveries, however, did not show any appreciable difference from the results in Tables 2 and 4 when the samples were irradiated in JRR-2 for 20 min which corresponds approximately to 60-min irradiation in the JRR-3 reactor.

REFERENCES

1 J. M. Rottschafer, R. J. Boczkowski and H. B. Mark, Jr., Talanta, 19 (1972) 163.
2 D. E. Leyden and A. L. Underwood, J. Phys. Chem., 68 (1964) 2093.
3 J. L. Sides and C. T. Kenner, Anal. Chem., 38 (1966) 707.
4 C. W. Blount, D. E. Leyden, T. L. Thomas and S. M. Guill, Anal. Chem., 45 (1973) 1045.
5 Separating Metals Using Chelex 100 Chelating Resin: The Bio-Rad Laboratories Technical Bulletin 114, May, 1972.
6 J. P. Riley and D. Taylor, Anal. Chim. Acta, 40 (1968) 479.
7 K. Kawabuchi, M. Kanke, T. Muraoka and M. Yamauchi, Bunseki Kagaku (Jpn. Anal.), 25 (1976) 213.
8 K. Ohnishi, Y. Hori and Y. Tomari, Bunseki Kagaku (Jpn. Anal.), 26 (1977) 74.
9 A. Hirose, K. Kobori and D. Ishii, Nippon Kagaku Kaishi (J. Chem. Soc. Jpn.), (1974) 900.
10 E. V. Egorov and P. D. Novikov, Action of Ionizing Radiation on Ion-Exchange Materials, Israel Program for Scientific Translations, Jerusalem, 1967.

Analytica Chimica Acta, 97 (1978) 311—316

DETERMINATION OF MERCURY IN HUMAN URINE BY NEUTRON ACTIVATION ANALYSIS, WITH LEAD DIETHYLDITHIOCARBAMATE AS A PRECONCENTRATION AGENT

J. M. LO, J. C. WEI, and S. J. YEH*

Institute of Nuclear Science, National Tsing Hua University, Hsinchu 300 (Taiwan)

(Received 17th October 1977)

SUMMARY

Lead diethyldithiocarbamate is an effective reagent for preconcentration of mercury in urine for neutron activation analysis. Sodium and bromine are removed from the sample by this procedure. As lead diethyldithiocarbamate is insensitive to neutron activation, radiochemical separation is not needed after neutron irradiation. Results from the analysis of urine collected from workers in caustic soda manufacturing plants are discussed.

The determination of elements present in the human body in extremely small amounts is necessary in the search for correlation between a particular element and a specific medical disorder [1, 2]. The content of mercury in human urine is one of the important factors for such a clinical study [3—5]. Recently a method was developed for the determination of mercury in sea water by n.a.a. in which mercury in aqueous solution was concentrated into chloroform by solvent extraction with lead diethyldithiocarbamate ($Pb(DDTC)_2$) prior to neutron irradiation [6]. This is an extension of previous work on the analysis of human urine for mercury.

EXPERIMENTAL

Reagents

$Pb(DDTC)_2$ was prepared as reported previously [6]. All reagents were of Suprapur grade (E. Merck). Sub-boiled redistilled water, as suggested by Kuehner et al. [7], was used throughout. The urine samples were collected in 50-ml screw-capped polyethylene bottles, to which 2 ml of concentrated nitric acid and 0.2 g of $K_2Cr_2O_7$ were added to prevent loss of mercury during storage before analysis [8—10].

All the containers used were immersed overnight in 8 M HNO_3, washed with distilled water and sub-boiled redistilled water successively several times, and rinsed with a solution of $Pb(DDTC)_2$ in chloroform to remove any possible contamination of mercury. Finally, traces of $Pb(DDTC)_2$ were removed by washing with $CHCl_3$.

Preconcentration procedures

Exactly 25.00 ml of the urine sample was digested in a Sjöstrand type wet-oxidation reflux apparatus [11, 12], with a mixture of concentrated HNO_3 and 30% H_2O_2, until a colorless solution was obtained. This treatment was necessary to avoid formation of colloidal mercury in the urine sample [13, 14] and to convert all organomercury species to inorganic mercury species [12, 15]. After cooling, the solution was shaken with $CHCl_3$ several times to remove bromine. After adjustment to pH 2—3 with 6 M NaOH (with cooling), the bromine was removed again with $CHCl_3$. Mercury was then extracted into 5.00 ml of 8×10^{-4} M $Pb(DDTC)_2$ solution in $CHCl_3$. The extract was washed with water several times to remove sodium. Then 1.00 ml of extract was transferred to a quartz ampoule. Chloroform was evaporated completely at room temperature before the ampoule was sealed for neutron irradiation. The mercury standard for n.a.a. was prepared in entirely the same way as the urine sample.

Neutron irradiation and radioactivity measurement

The sealed sample was irradiated, together with the standard, in the Tsing Hua Open Pool Reactor with a neutron flux of 2×10^{12} n cm^{-2} s^{-1} for 30 h. After cooling for 10 h, the surface of the irradiated quartz ampoule was washed with nitric acid to remove any radioactive contamination. Then it was frozen in dry ice and the tip was cut off. The irradiated sample was transferred to a glass-stoppered counting tube by washing successively with 2 ml of chloroform and 2 ml of aqua regia. The counting tube was shaken for 2 min and left for 10 min before counting. The 77.6-keV ^{197}Hg γ-peak was assayed with a 38-cm^3 Ge(Li) detector connected to a 4096-channel pulse-height analyzer. The detector had a high resolution of 2.2 keV (FWHM) for the 1332-keV ^{60}Co γ-ray and a peak-to-Compton-ratio of 27. The peak analysis was carried out with the Hewlett-Packard 2116C computer program. Covell's method was used for the calculation of γ-peak area [16, 17].

RESULTS AND DISCUSSION

Neutron activation analysis is one of the most sensitive methods for the determination of trace amounts of more than 75 elements in various kinds of matrices. Many elements are found at extremely low concentration levels in biological systems, and considerable difficulty may be encountered in the direct analysis of these samples by n.a.a. One possible way to solve this disadvantage is to extend the sensitivity of n.a.a. by a preconcentration technique.

$Pb(DDTC)_2$ is a very effective reagent for the preconcentration of mercury in sea water for n.a.a. [6]. Its advantages are that interfering elements, e.g. sodium, potassium, bromine, and phosphorus may be removed from the bulk; at the same time, a large volume of aqueous solution can be reduced to a small volume of organic solution, which can give a tiny amount of

solid by evaporating the organic solvent. This process is particularly convenient for n.a.a. since the excess of $Pb(DDTC)_2$ in the extract gives no interfering radioactivity under the irradiation conditions studied.

In the direct analysis of urine samples by n.a.a., Kim and Stärk [5] postulated that a rotating irradiation technique is needed to minimize the chance of a voluminous liquid sample receiving an inhomogeneous neutron flux. This kind of inconvenience can be avoided by using a preconcentration technique.

Since the primary interest of this work is to provide a reliable method for the determination of extremely small amounts of mercury in urine, special emphasis was placed on an examination of the basic aspects of the analytical method. The recovery of mercury in urine during the digestion process, tested with mercury tracer, was better than 99%, in very good agreement with the results reported by the Mercury Analysis Working Party of BITC [12].

The blank tests for mercury, performed from time to time, were 1.1 ± 0.6 ppb under the conditions studied. The reproducibility tests were made as often as possible to ensure the reliability of the method. The relative standard deviations were within 7% for Hg contents of 31 ppb, and within 10% for Hg contents of 7.1 ppb.

The mercury content in the urine of persons supposed to have very little chance of exposure to a large quantity of mercury in their daily life is shown in Table 1; the mercury content is scattered over quite a wide range, i.e., from 3 ppb to 12 ppb, and there is no apparent correlation with respect to the age and sex of the person under investigation, in agreement with the data obtained by Schaller et al. [3].

Table 2 summarizes results for the mercury content in the urine of workers in caustic soda manufacturing plant A, in which mercury is used in the electrolysis cell. The mercury content for these workers depends more

TABLE 1

Contents of Hg in the urine of persons not exposed to high concentrations of mercury daily

Group A (age 10—15 y)		Group B (age 20—30 y)		Group C (age 31—60 y)	
Sample code no.	Hg contents (ppb)	Sample code no.	Hg contents (ppb)	Sample code no.	Hg contents (ppb)
C-1	10	C-11	3	C-18	5
C-2	9	C-12	3	C-19	8
C-3	4	C-13	6	C-20	12
C-4	8	C-14	10	C-21	8
C-5	6	C-15	11	C-22	5
C-6	10	C-16	3		
C-7	9	C-17	7		
C-8	11				
C-9	5				
C-10	9				

TABLE 2

The concentration of Hg in the urine of workers in caustic soda plant A

Sample code no.	Age of workers (y)	Position held (y)	Type of work	Hg in urine (ppb)	Sample code no.	Age of workers (y)	Position held (y)	Type of work	Hg in urine (ppb)
A-1	51	30	Electrolysis operation	62	A-21	47	18	Wash and cleaning	74
A-2	47	28		79	A-22	51	8		8
A-3	52	31		75	A-23	54	29		38
A-4	45	27		32	A-24	38	8		19
A-5	48	25		55	A-25	40	23		7
A-6	47	25		29	A-26	38	20		26
A-7	49	28		83	A-27	55	10		33
A-8	46	30		20	A-28	26	4	Group leader	24
A-9	45	25		61	A-29	41	1.5		40
			Electrolysis		A-30	29	4		16
A-10	49	30	cell reconditioning	44	A-31	30	5		34
A-11	42	1.5		25	A-32	26	2	Analysis of saline	11
A-12	40	20		37	A-33	50	15		9
A-13	46	25		71	A-34	50	1.5	Soda plant	41
A-14	48	20		95	A-35	51	1.5		35
A-15	44	18		119	A-36	52	1.5		41
A-16	49	10		49	A-37	56	1.5		5
A-17	54	10		84	A-38	52	20	Repair shop	14
A-18	45	9		160	A-39	47	15		13
A-19	45	28		150	A-40	38	1		8
A-20	45	15		105	A-41	57	31	Office staff	62
					A-42	32	3		19
					A-43	41	15		18
					A-44	46	5	Plant manager	12

on the type of work, and seems to be independent of the period spent in the job held. The electrolysis cell reconditioning workers showed, on the average, higher mercury contents than the others: they have more chance of exposure to a large amount of mercury than other persons in plant A. This trend is more pronounced in plant K, in which the electrolysis cells are ca. ten times larger than those of plant A (see Table 3). The urine of workers engaged in electrolysis cell reconditioning contains extraordinarily high mercury contents; the group leaders, superintendents and plant manager show low mercury contents, comparable with the lowest level shown in Table 1.

Urinary mercury in workers is related closely to the mercury concentration in the environmental air [3—5, 18—21]. The mercury content of the air in the room containing electrolysis cells has been found to be several orders higher than the average atmosphere [22—25]; results shown in Tables 2 and 3 are in good accordance with those reported by previous authors [22—25].

The urine of some of the electrolysis cell reconditioning workers in plant K, who showed extraordinarily high mercury contents, was reexamined 6 months later; the results are compared in Table 4. The mercury content of each person was of the same order of magnitude. The content of mercury in the urine depends strongly on the environmental working conditions.

TABLE 3

The concentration of Hg in the urine of workers in caustic soda plant K

Sample code no.	Age of workers (y)	Position held (y)	Type of work	Hg in urine (ppb)	Sample code no.	Age of workers (y)	Position held (y)	Type of work	Hg in urine (ppb)
K-1	23	2	Electrolysis operation	58	K-29	47	6	Saline loop operation	28
K-2	49	6		31	K-30	48	6		8
K-3	38	4		42	K-31	49	6		37
K-4	46	5		50	K-32	24	2		32
K-5	26	1		5	K-33	26	2		16
K-6	42	6		42	K-34	43	6	Group leader	52
K-7	45	6		15	K-35	28	1		54
K-8	24	1		17	K-36	47	6	Soda plant	48
K-9	47	6		46	K-37	50	6		32
K-10	50	6		152	K-38	54	6		4
K-11	43	6		136	K-39	46	6		51
			Electrolysis		K-40	48	1.5		22
K-12	34	3	cell reconditioning	213	K-41	51	6		36
					K-42	46	6		40
K-13	39	5		376	K-43	20	5		15
K-14	18	1		182	K-44	48	6		26
K-15	45	3		195	K-45	42	6		17
K-16	36	4		113	K-46	25	2	Repair shop	55
K-17	31	1		80	K-47	58	2		25
K-18	26	2		420	K-48	53	6		48
K-19	50	6		410	K-49	49	6	Chlorine plant	67
K-20	36	3		364	K-50	43	6		11
K-21	26	2	Saline loop operation	12	K-51	47	6		7
					K-52	37	5	Group leader	3
K-22	49	6		11	K-53	30	1		6
K-23	27	3		46	K-54	29	6	Superintendent	4
K-24	24	1		21	K-55	41	2		3
K-25	23	3		32	K-56	48	5	Plant manager	3
K-26	25	2		34					
K-27	40	6		8					
K-28	29	1		39					

TABLE 4

The concentration of mercury in the urine of workers after six months

Sample code no.	Hg in urine Feb. 1977 (ppb)	Hg in urine Aug. 1977 (ppb)
K-12	213	140
K-13	376	422
K-19	410	488
K-20	364	391

REFERENCES

1 E. J. Underwood, Trace Elements in Human and Animal Nutrition, 3rd edn., Academic Press, New York, 1971.
2 W. Mertz and W. E. Cornatzer, Newer Trace Elements in Nutrition, M. Dekker, New York, 1971.
3 K. H. Schaller, P. Strasser, R. Woitowitz, and D. Szadkowski, Fresenius Z. Anal. Chem., 256 (1971) 123.
4 A. Shaner, A. Strasser, and L. Petrovic, N. Y. State J. Med., 70 (1970) 952.
5 J. I. Kim and H. Stärk, Radiochim. Acta, 13 (1970) 213.
6 J. M. Lo, J. C. Wei, and S. J. Yeh, Anal. Chem., 49 (1977) 1146.
7 E. C. Kuehner, R. Alvarez, P. J. Paulsen, and T. J. Murphy, Anal. Chem., 44 (1972) 2050.
8 C. Feldman, Anal. Chem., 46 (1974) 99.
9 J. M. Lo and C. M. Wai, Anal. Chem., 47 (1975) 1869.
10 D. R. Christmann and J. D. Ingle, Jr., Anal. Chim. Acta, 86 (1976) 53.
11 B. Sjöstrand, Anal. Chem., 36 (1964) 815.
12 Mercury Analysis Working Party of BITC, Anal. Chim. Acta, 84 (1976) 231.
13 M. H. Yang, P. Y. Chen, C. L. Tseng, S. J. Yeh, and P. S. Weng, Determination of Trace Elements by Neutron Activation Analysis Using Dinonylnaphthalene Sulfonic Acid as a Preconcentration Agent, 1976 International Conference on Modern Trends in Activation Analysis, Munich, September 13—17, 1975.
14 H. Chermette, J. F. Colonat, and J. Tousset, Anal. Chim. Acta, 80 (1975) 335.
15 J. W. Huckabee, C. Feldman, and Y. Talmi, Anal. Chim. Acta, 70 (1974) 41.
16 D. F. Covell, Anal. Chem., 31 (1959) 1785.
17 K. Heydorn and W. Lada, Anal. Chem., 44 (1972) 2313.
18 Z. G. Bell, Jr., H. B. Lovejoy, and T. R. Vizena, J. Occup. Med., 15 (1973) 501.
19 R. R. Lauwerys and J. P. Buchet, Arch. Environ. Health, 26 (1973) 65.
20 A. Taylor and V. Marks, Brit. J. Ind. Med., 30 (1973) 293.
21 A. Shandar and R. E. Simson, Med. J. Aust., 2 (1971) 1005.
22 J. H. Janssen, J. E. Van Den Enk, R. Bult, and D. C. De Groot, Anal. Chim. Acta, 84 (1976) 319.
23 S. H. Williston, J. Geophys. Res., 73 (1968) 7051.
24 R. S. Foote, Science, 177 (1972) 513.
25 S. J. Long, D. R. Scott, and R. J. Thompson, Anal. Chem., 45 (1973) 2227.

Analytica Chimica Acta, 97 (1978) 317—326

PARTICLE VOLATILIZATION AND CALIBRATION CURVATURE IN FLAME SPECTROMETRY

J. T. H. ROOS*

Department of Chemistry, University of Rhodesia, Salisbury (Rhodesia)

(Received 17th August 1977)

SUMMARY

Expressions have been derived for the shapes of analytical curves in flame spectrometry under conditions of incomplete volatilization of the sample material in the flame. Particle size distribution has been taken into consideration, as has the variation of flame temperature with observation height. The effects of changes in observation height and in flame temperature on the extent of sample volatilization within the observation zone of the flame are outlined, and calculated shapes of analytical curves are compared with those found experimentally for strontium both in an air-acetylene flame and in an air-propane/butane flame.

Various factors are known to contribute to the bending of analytical curves in atomic absorption analysis [1—7]; these include the profiles of source emission lines and self-absorption effects, the hyperfine structure of spectral lines, unequal absorption of closely-spaced emission lines from the lamp, and non-absorbable radiation from the light source impinging on the detector. Relatively little attention has, however, been paid to the effect on the shape of analytical curves of incomplete volatilization of the sample material in the flame, although it is well known that this can give rise to non-linearity [3, 8]. The flame emission studies of Leyton [9] showed that, whereas calcium chloride gave a response linear with respect to concentration, calcium phosphate gave a response which varied approximately as the 4/5th power of concentration. This was subsequently confirmed by Alkemade and Voorhuis [10]. Zeegers et al. [3] used data obtained by Schuhknecht and Schinkel [11] with a variety of flames, to illustrate the effect of incomplete solute vaporization on the shapes of analytical curves. Roos and Price [12] observed greater calibration curvature with chromium in the presence of iron than with chromium alone, and attributed this to incomplete volatilization in the former case. Alkemade [13] has discussed the important rôle that volatilization processes may play in the occurrence of interference in flame spectrometry and, more recently, has summarized the present state of knowledge relating to the processes of sample decomposition, atomization and excitation [14].

*Present address: Marlborough College, Wiltshire, England.

In a series of papers [15—17] dealing with various aspects of the overall process of atomization in flame spectrometry, Hieftje and his co-workers have reported results based on measurements of a single controlled stream of uniform droplets. Hieftje et al. [15, 16] studied desolvation of aerosol droplets, and showed that desolvation was complete only after a significant residence time in the flame. However, it has been suggested elsewhere [18] that, with conventional flame spectrometric equipment, the solvent will have evaporated by the time the aerosol has reached the flame, leaving the suspended solid particles in a gas mixture partially saturated with solvent vapour. Bastiaans and Hieftje [17] investigated the mechanism of solute vaporization, and suggested the probability of semi-dried particles undergoing explosive decomposition. Their studies showed that the total vaporization time was proportional to the original solute concentration, thus indicating that vaporization follows the same mechanism for all concentrations.

However, the only complete mathematical treatments of particle volatilization appear to be those by Li and L'vov. Li [19] approached the overall process of atom production by considering each drop individually, and produced a theoretical model which takes into account the processes of desolvation, diffusion, vaporization and ionization; he included an expression for the droplet size distribution in his mathematical model. L'vov [20] based his treatment extensively on the work of Lykov [21], and suggested that the rate of volatilization is controlled by heat transfer from the surrounding medium. Heat is absorbed in raising the temperature of the particles and vaporizing the sample material; as the temperature of a particle rises, so the rate of vaporization increases until a stationary temperature is reached when the heat absorbed by the particles is used entirely in the vaporization process. Volatilization is therefore completed at temperatures which are normally considerably lower than the temperature of the flame, especially for more volatile samples, and are frequently well below the boiling point of the substance concerned. L'vov's main concern has been with the time required to vaporize particles of solute in flames commonly employed in atomic absorption analysis, and with the effect of interfering ions on the rate of volatilization, and not with the influence of volatilization effects on the shapes of analytical curves.

L'vov's treatment is here extended by taking into account the distribution in particle (droplet) size produced by conventional pneumatic nebulizers, and equations are developed which enable the shapes of analytical curves to be calculated when these depend only on volatilization effects.

MATHEMATICAL TREATMENT OF THE VOLATILIZATION PROCESS

Using the equations for heat and mass transfer during the vaporization process, Lykov [21] has shown that the temperature T_d at the vaporization surface can be expressed by

$$T_d = T_f - (sMD/\lambda R T_f)\,(P_d - P_f) \qquad (1)$$

where T_f is the absolute temperature of the flame, s is the specific heat of vaporization of the liquid (or, sublimation of the solid, if volatilization occurs below the melting point), M is the molecular mass, D is the coefficient of diffusion of the gaseous substance at the temperature T_f, λ is the thermal conductivity of the gas, P_d is the saturated vapour pressure of the substance above the droplet surface and P_f that of the substance in the flame, and R is the gas constant.

Since the vapour pressure of the substance in the flame will be much lower than the saturated vapour pressure above the droplet surface, eqn. (1) can be re-written as follows

$$T_f - T_d = \Delta T = sMDP_d/\lambda RT_f \tag{2}$$

Lykov [21] has expressed the rate of vaporization in terms of the amount of heat acquired by the droplet

$$-dm/dt = \alpha\pi d^2 \cdot \Delta T/s \tag{3}$$

where m is the mass of unvaporized particle, t is time, d is the diameter of the particle (in m) and α is the coefficient of heat transfer. For the vaporization of small droplets [20]

$$\alpha = 2\lambda/d \tag{4}$$

hence, combining eqns. (2), (3) and (4), the rate of vaporization may be expressed by

$$-dm/dt = 2\pi MDP_d d/RT_f \tag{5}$$

The mass of substance in a particle is given by

$$m = \pi d^3\rho/6 \tag{6}$$

hence

$$d = (6/\pi\rho)^{\frac{1}{3}} m^{\frac{1}{3}} \tag{7}$$

where ρ is the density of the liquid in kg m^{-3}. By combining eqns. (5), (6) and (7), the rate expression becomes

$$-dm/dt = (48\pi^2 M^3/\rho R^3)^{\frac{1}{3}} \cdot (DP_d/T_f) \cdot m^{\frac{1}{3}} \tag{8}$$

Since D, P_d and T_f all depend on the temperature of the flame, and since this will vary with time (i.e., observation height), eqn. (8) cannot be integrated directly. Therefore

$$-dm/dt = k_1 \cdot f(t) \cdot m^{\frac{1}{3}} \tag{9}$$

where $k_1 = (48\pi^2 M^3/\rho R^3)^{\frac{1}{3}}$ and $f(t) = DP_d/T_f$.

Rearrangement of eqn. (9) gives

$$f(t) \cdot dt = -m^{-\frac{1}{3}} \cdot dm/k_1 \tag{10}$$

Integrating between the limits $t = 0$ and t and $m = m_0$ and m gives

$$I_t = \int_0^t f(t) \cdot dt = (-1.5\, m^{\frac{2}{3}}/k_1) + (1.5\, m_0^{\frac{2}{3}}/k_1) \tag{11}$$

thus

$$m^{\frac{2}{3}} = m_0^{\frac{2}{3}} - (k_1 I_t/1.5) \tag{12}$$

For a fixed observation height in the flame, t and hence I_t will be a constant, and we may write

$$m^{\frac{2}{3}} = m_0^{\frac{2}{3}} - k_2 \tag{13}$$

where $k_2 = k_1 I_t/1.5$.

In practice, m_0 will be proportional to the concentration c of the sample solution (in kg m^{-3}), and the spectrometric response will be proportional to $m_0 - m$ ($m_0 - m$ is the amount of sample material which volatilizes before reaching the observation zone in the flame).

If we define $m_0 = k_3 c$ and $m_0 - m = k_4 A$, where A is the spectrometric response such as absorbance, emission intensity, etc., then

$$m = m_0 - k_4 A = k_3 c - k_4 A$$

Substituting for m and m_0 in eqn. (13) gives

$$(k_3 c - k_4 A)^{\frac{2}{3}} = (k_3 c)^{\frac{2}{3}} - k_2 \tag{14}$$

Therefore

$$k_3 c - k_4 A = [(k_3 c)^{\frac{2}{3}} - k_2]^{\frac{3}{2}} \tag{15}$$

and

$$A = \{k_3 c - [(k_3 c)^{\frac{2}{3}} - k_2]^{\frac{3}{2}}\}/k_4 \tag{16}$$

$$= \frac{\{c - (c^{\frac{2}{3}} - k_2/k_3^{\frac{2}{3}})^{\frac{3}{2}}\}}{k_4/k_3} \tag{17}$$

In eqn. (16), $(c^{\frac{2}{3}} - k_2/k_3^{\frac{2}{3}})^{\frac{3}{2}}$ is proportional to m, the mass which does not volatilize within the time t specified by the height of the observation zone above the burner top. Thus $c - (c^{\frac{2}{3}} - k_2/k_3^{\frac{2}{3}})^{\frac{3}{2}}$ may be looked on as the "effective concentration" which gives rise to the observed response.

PARTICLE-SIZE DISTRIBUTION

It has been assumed thus far that the particles entering the flame are of uniform size, and can therefore be fully described in terms of a single diameter, d (eqns. 3—7). This is manifestly not true in practice, and several attempts have been made to measure the size distribution of the droplets produced by pneumatic nebulizers as normally employed in atomic absorption analysis [22—24]. In order to produce an accurate model of particle volatilization and its effect on the shape of atomic absorption analytical curves, it is necessary to take the drop-size distribution into

account in the mathematical treatment outlined above. The data have been taken from Stupar and Dawson [22], and it has been assumed that particles greater than 20 μm in diameter would be deposited on the walls of the mixing chamber and burner feed tube, and need not, therefore, be considered further. The drop-size distribution pattern is shown in Table 1.

For a given concentration of analyte, it may be assumed that the diameter of a dried particle before volatilization commences will be proportional to the diameter of the droplet from which that particle is derived, so that the particle-size distribution in the flame will be directly related to the drop-size distribution produced by the nebulizer/cloud-chamber system. It is also assumed that, within the concentration limits normally encountered in atomic spectrometry, the analyte concentration does not significantly influence the drop-size distribution pattern.

In any assumed distribution of drop sizes, the degree of volatilization of each individual drop may be calculated for given values of the various parameters (I_t, M, ρ, etc.) and the size of the drop, relative to the volatilization which would occur if the drops were all of uniform size such that the same volume of solution would be transported by n droplets of this size as by n droplets representative of the assumed droplet size distribution. Multiplication each time by the factor $F_i/\Sigma F_i$ (where F_i is the relative frequency of occurrence of any drop-size interval $d_i \pm \Delta d$), followed by summation over the drop-size range 0—20 μm, will give the "effective concentration" mentioned previously. Figure 1 compares the shapes of analytical curves calculated for the element strontium with and without taking drop-size distribution into account, and assuming a constant flame temperature of 2350 K. The values of the parameters used in these calculations are shown in Table 2. The observation height was taken as 0.6 cm, and volatilization was assumed to be the only factor affecting the shapes of the curves. It can be seen that curvature commences at a lower concentration when a distribution in droplet size is assumed: this is due to the effect of the (few) larger droplets which contain a relatively high proportion of the total transported sample mass, and therefore becomes more pronounced the larger the limiting droplet size. Drop-size distribution is assumed in the discussion which follows.

TABLE 1

Drop-size (diameter) distribution pattern assumed in this work

Drop-size interval (μm)	Approximate frequency (%)	Drop-size interval (μm)	Approximate frequency (%)	Drop-size interval (μm)	Approximate frequency (%)	Drop-size interval (μm)	Approximate frequency (%)
0.0—1.0	1.4	5.0—6.0	13.1	10.0—11.0	2.4	15.0—16.0	2.0
1.0—2.0	6.2	6.0—7.0	6.0	11.0—12.0	2.3	16.0—17.0	1.9
2.0—3.0	14.5	7.0—8.0	5.7	12.0—13.0	2.2	17.0—18.0	1.9
3.0—4.0	14.5	8.0—9.0	2.6	13.0—14.0	2.1	18.0—19.0	1.8
4.0—5.0	13.1	9.0—10.0	2.5	14.0—15.0	2.0	19.0—20.0	1.8

TABLE 2

Parameters for calculating volatilization curves

$s = 2.635 \times 10^6$ J kg^{-1}	Flame gas velocity = 12 m s^{-1}
$M = 0.1036$ kg mol^{-1}	$\rho = 4.5 \times 10^3$ kg m^{-3}
$D = 9.17 \times 10^{-4}$ m^2 s^{-1} at 2350 K	$\lambda = 2.18 \times 10^{-1}$ J m^{-1} s^{-1} K^{-1}
$T_f = 2350$ K and $I_t = 2.4 \times 10^{-8}$	$R = 8.314$ J K^{-1} mol^{-1}

P_d and T_d were computed by an iterative process from eqn. (2) and the expression [25]

$$\log P_d = (-0.2185\, A/T_d) + B$$

where $A = 1.34827 \times 10^5$ and $B = 14.72687$ if T_d is expressed in degrees absolute and P_d in pascals.

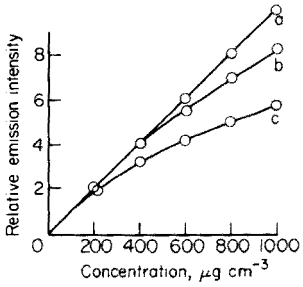

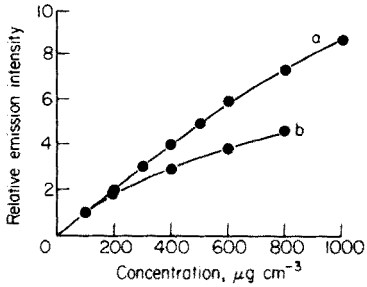

Fig. 1. Effect of particle distribution and cut-off diameter on the shape of the analytical curves. Calculated points are indicated by open circles. a: no distribution; b: distribution with cut-off at 15 μm; c: distribution, with cut-off at 20 μm.

Fig. 2. Comparison of calculated curves (unbroken lines) and measured intensities (•) for strontium at an observation height of 0.6 cm, normalized to an initial slope of 1/100. a: air-acetylene flame; b: air-propane flame.

EXPERIMENTAL AND RESULTS

As a test of the accuracy of the mathematical model, experimental analytical curves were obtained for strontium (as strontium nitrate) at an observation height of 0.6 cm both in a slightly lean air-acetylene flame and in an air-propane/butane flame with a Pye-Unicam SP90 series II atomic absorption spectrometer; all measurements were made in the emission mode at 610 nm (SrOH band) in order to eliminate (i) the influence of possible self-absorption, and (ii) effects caused by other spectral factors which could cause significant deviations from linearity in absorption measurements, such as hyperfine structure, source line profiles, etc. In order to obtain meaningful results, an aperture stop, ca. 2 mm × 2 mm, was positioned between the burner and the monochromator.

The measured curves were compared with the theoretical curves calculated for the volatilization of strontium oxide under the same conditions as were used above. (Vapour pressure data were available for strontium oxide but not

TABLE 3

Assumed effective temperature distribution in air-acetylene and air-propane flames

Obs. ht. (cm)	Flame temp. (K)	Diffusion coefficient D ($m^2\ s^{-1}$)	Vapour pressure P_d (Pa)	$I_t = \int \frac{D \cdot P_d}{T_t}$
Air-acetylene flame (gas velocity ≈ 10 m s^{-1})				
0.0	2355	9.17×10^{-4}	135	0.0
0.2	2375	9.21×10^{-4}	166	1.16×10^{-8}
0.3	2390	9.24×10^{-4}	186	1.86×10^{-8}
0.4	2404	9.26×10^{-4}	218	2.70×10^{-8}
0.6	2464	9.38×10^{-4}	363	4.72×10^{-8}
0.8	2491	9.43×10^{-4}	445	7.93×10^{-8}
0.9	2499	9.44×10^{-4}	468	9.78×10^{-8}
1.0	2505	9.46×10^{-4}	492	1.16×10^{-7}
1.2	2519	9.48×10^{-4}	541	1.51×10^{-7}
Air-propane flame (gas velocity ≈ 45 cm s^{-1})				
0.0	1900	8.2×10^{-4}	0.17	0.0
0.2	2000	8.5×10^{-4}	0.96	1.03×10^{-9}
0.4	2090	8.6×10^{-4}	4.1	5.54×10^{-9}
0.6	2150	8.8×10^{-4}	10.0	1.79×10^{-8}
0.8	2200	8.9×10^{-4}	20.2	4.42×10^{-8}

for strontium chloride; for this reason solutions of strontium nitrate were used, as this would decompose to the oxide at a temperature well below that of the flame.) I_t was evaluated by means of graphical integration, assuming the variations of flame temperature with observation height given in Table 3 [26]; the calculated values of P_d, D and I_t for strontium in the different flames are also shown. The results are shown in Fig. 2.

DISCUSSION

It is clear that uncertainty exists in the values of many of the parameters used in these calculations, such as the latent heat of vaporization of strontium oxide (calculated from vapour pressure data by means of the Clapeyron—Clausius equation [27]), the coefficient of diffusion, D, of the gaseous substance and the distribution pattern and limiting size of the droplets entering the flame. In addition, considerable uncertainty exists in the value which should be assigned to temperature variations both in the vertical and horizontal directions in the flame. Literature values quoted for the maximum temperature of the air-acetylene flame range from 2470 K to 3000 K [28]. L'vov [20] favours a value of 2400 K for the reducing air-acetylene flame, which would decrease to ca. 2350 K on aspiration of an aqueous solution. In the present work, the variation in flame temperature with observation height in an air-acetylene flame as quoted by Snelleman [26] has been used, but this is in poor agreement with

the work of Fulton [29], who measured the temperature gradient in a stoichiometric air-acetylene flame, and found a drop in temperature of some 230 K between heights of 0.4 cm and 1.2 cm in the flame, with a maximum value at ca. 0.7 cm. There is less information on temperature variations in air-propane flames. Further, the derivation does not allow for radiative heat losses by the droplets or the effect of particle size on vapour pressure [8]. Because of the scarcity of vapour pressure data, in particular, it has not been possible to test the suggested model by calculating volatilization curves for elements which might be of interest in an air-acetylene flame, other than strontium.

Nevertheless, the agreement between theory and experiment found for the strontium oxide system is most encouraging — in particular, the fact that the calculated curves have exactly the correct shape for assumed flame temperature conditions which are at least approximately correct — and enables definite conclusions to be drawn concerning the effects of (i) concentration (ii) flame temperature and (iii) observation height.

Concentration

Despite the fact that strontium oxide is relatively involatile (m.p. = 2800K, vapour pressure at 2400 K ≈ 270 Pa), it is only at very high concentrations that incomplete volatilization occurs. Accordingly, most elements normally determined in an air-acetylene flame should not show line curvature caused by volatilization effects, unless the concentration of analyte is high, or an interfering species is present which causes a considerable decrease in vapour pressure of the particles at the temperature of the flame.

Flame temperature

Reference to the emission response calculated for different flame temperatures (Fig. 3) shows that the temperature of the flame may have a considerable effect on the degree of volatilization of the sample material. It is not surprising, therefore, that the extent of chemical interference

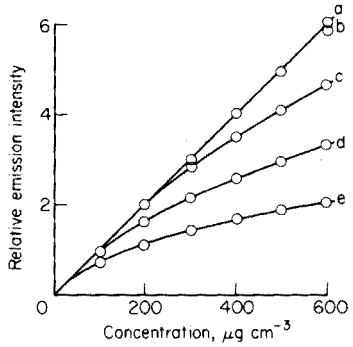

Fig. 3. Calculated influence of the "effective average flame temperature" on the analytical curves. Calculated points are shown as open circles for strontium. Observation height = 1.2 cm. a: 2300 K; b: 2250 K; c: 2200 K; d: 2150 K; e: 2100 K.

encountered in atomic absorption spectrometry generally depends markedly on the flame conditions employed [8, 12], because these will affect both the overall temperature of the flame and the variation of temperature with observation height.

Observation height

The calculated effect of observation height is summarized in Table 4. As the observation height increases, there is a general increase in the degree of volatilization of larger particles, thus increasing the linearity of the analytical curve. Small changes in the value of the observation height are predicted to have a considerable influence, so that above a value of ca. 0.8 cm the theoretical analytical curve becomes linear; no further change therefore occurs with increasing observation height. In practice, the linearity of the analytical curve is much less sensitive to changes in the observation height (Table 4). This can in part be accounted for by the fact that signals from the cooler outer region of the flame as well as the hot central region, and signals from areas in the flame other than that of the observation zone, are detected and averaged out to give the final measured response. Investigation has shown that, with the experimental arrangement used in the present work, the effective measuring zone of the flame extended 0.3 cm above and below the set observation height. (As expected, the trend of increasing volatilization higher up in the flame was observed; this is consistent with the effect of observation height on interference reported elsewhere [30].) In addition, increases in particle velocity with observation height caused by expansion of the flame gases at higher temperature have not been included in the treatment given here. Such velocity increases will mean that the time-related integral I_t (eqn. 11) is not proportional to the observation height, but increases less rapidly as the height increases.

TABLE 4

Calculated and measured effect of observation height on curvature in an air-acetylene flame

Strontium concentration ($\mu g\ cm^{-3}$)	Obs. ht. = 0.3 cm		Obs. ht. = 0.6 cm		Obs. ht. = 0.9 cm	
	Calcd.[a]	Measd.[a]	Calcd.[a]	Measd.[a]	Calcd.[a]	Measd.[a]
100	100	100	100	100	100	100
200	182	200	200	200	200	200
400	298	400	400	398	400	400
600	387	576	585	587	600	596
800	459	729	740	741	800	761
1000	523	862	876	878	1000	910

[a]Relative emission intensity, normalized to a maximum value of 1000 for a concentration of 100 $\mu g\ cm^{-3}$.

Conclusion

From the results reported here it appears that, although incomplete volatilization may lead to bending of the analytical curve, the effect is unlikely to be significant unless an interfering ion is present in the sample matrix, or concentrated analyte solutions are employed. In general, other factors are likely to have a far greater influence on the shape of the analytical curve.

REFERENCES

1 I. Rubeska and V. Svoboda, Anal. Chim. Acta, 32 (1965) 235.
2 T. J. Vickers, Anal. Chim. Acta, 36 (1966) 42.
3 P. J. T. Zeegers, R. Smith and J. D. Winefordner, Anal. Chem., 40(13) (1968) 26A.
4 L. de Galan and C. F. Samaey, Spectrochim. Acta Part B, 24 (1969) 679.
5 Z. van Gelder, Spectrochim. Acta Part B, 25 (1970) 669.
6 C. F. Bruce and P. Hannaford, Spectrochim. Acta Part B, 26 (1971) 207.
7 H. C. Wagenaar, I. Novotny and L. de Galan, Spectrochim. Acta Part B, 29 (1974) 301.
8 C. A. Baker and F. W. J. Garton, U.K. Atomic Energy Authority Report R3490, H.M. Stationery Office, London, 1960.
9 L. Leyton, Analyst, 79 (1954) 497.
10 C. T. J. Alkemade and M. H. Voorhuis, Z. Anal. Chem., 163 (1958) 91.
11 W. Schuhknecht and H. Schinkel, Z. Anal. Chem., 163 (1958) 266.
12 J. T. H. Roos and W. J. Price, Spectrochim. Acta Part B, 26 (1971) 441.
13 C. T. J. Alkemade, Anal. Chem., 38 (1966) 1252.
14 C. T. J. Alkemade, in J. A. Dean and T. C. Rains (Eds.), Flame Emission and Atomic Absorption Spectrometry, Dekker, New York, 1969.
15 G. M. Hieftje and H. V. Malmstadt, Anal. Chem., 40 (1968) 1860.
16 N. C. Clampitt and G. M. Hieftje, Anal. Chem., 44 (1972) 1211.
17 G. J. Bastiaans and G. M. Hieftje, Anal. Chem., 46 (1974) 901.
18 W. J. Price, Analytical Atomic Absorption Spectrometry, Heyden and Son, London, 1972.
19 Kuang-pang Li, Anal. Chem., 48 (1976) 2050.
20 B. V. L'vov, Atomic Absorption Spectrochemical Analysis, Adam Hilger Ltd., London 1970.
21 M. V. Lykov, Spray Drying, Pishchepromizdat, Moscow, 1955.
22 J. Stupar and J. B. Dawson, Appl. Opt., 7 (1968) 1351.
23 J. B. Willis, Spectrochim. Acta Part A, 23 (1967) 811.
24 S. R. Koirtyohann and E. E. Pickett, Anal. Chem., 38 (1966) 1087.
25 R. C. Weast (Ed.), Handbook of Chemistry and Physics, 51st. ed., C.R.C. Press, Cleveland, Ohio, 1970.
26 W. Snelleman, in J. A. Dean and T. C. Rains (Eds.), Flame Emission and Atomic Absorption Spectrometry, Dekker, New York, 1969.
27 G. W. C. Kaye and T. H. Laby, Tables of Physical and Chemical Constants, 13th ed., Longmans, London, 1966.
28 R. Mavrodineanu and H. Boiteux, Flame Spectroscopy, Wiley, New York, 1965.
29 H. A. Fulton, M.Sc. Thesis, University of South Africa, Pretoria, 1968.
30 J. T. H. Roos and W. J. Price, Spectrochim. Acta Part B, 26 (1971) 279.

Analytica Chimica Acta, 97 (1978) 327—333

RAPID DETERMINATION OF PROTEIN IN PLANT MATERIAL BY FLOW INJECTION SPECTROPHOTOMETRY WITH TRINITROBENZENESULFONIC ACID

L. SODEK[§], J. RŮŽIČKA* and J. W. B. STEWART**

Centro de Energia Nuclear na Agricultura 13400 Piracicaba, SP (Brasil)

(Received 6th October 1977)

SUMMARY

The rapid determination of protein in plant material based on spectrophotometric determination of amino acids in protein hydrolysates with trinitrobenzenesulfonic acid has been adapted to flow injection analysis. With the manifold described, a routine sampling rate of 120 samples/h is possible, though this, as well as sensitivity, can easily be varied. The method was calibrated against the Kjeldahl method and a good correlation was obtained between the two methods over a wide range of protein values for beans.

The discovery of the selective reaction of TNBS (2,4,6-trinitrobenzenesulfonic acid) with primary amine groups [1] led Satake et al. [2] to develop a colorimetric method for the determination of amino acids based on this reagent. TNBS has several advantages over other reagents used for this purpose, such as ninhydrin and 2,4-dinitrofluorobenzene. In particular, it is water-soluble and reacts with amine groups under far milder conditions.

Gehrke and Wall [3] adapted the TNBS method for the automated determination of total amino nitrogen in protein hydrolyzates, using the Technicon Autoanalyzer system, as a measure of protein in forages and grain. Currently, fast methods of analysis for protein in grains are of tremendous importance as an aid to crop improvement programs where large numbers of samples need to be analyzed for protein content. The development of the flow injection technique [4—10] as an alternative to the autoanalyzer system promises to offer a fast analytical tool with much higher sampling rates. It was the aim of the work reported here to adapt the TNBS method to the flow injection system.

Present addresses:
[§] Rothamsted Experimental Station, Harpenden, Herts AL5 2JQ, England.
*Chemistry Department A, The Technical University of Denmark, Building 207, 2800 Lyngby, Denmark.
**Dept. of Soil Science, University of Saskatchewan, Saskatoon, Canada.

EXPERIMENTAL

Instrumentation

The instrumentation used was exactly the same as reported earlier [7]. In addition all coils were immersed in a temperature-controlled water bath (Tecam, Temporar, Techne Inc., USA). The diameter of the pump tubing was such that a flow rate of 3 ml min^{-1} was generated in each of the reaction lines. The rest of the manifold was made of 1.0-mm i.d. polyethylene tubing. The TNBS reagent solution was used in the reference beam of the spectrophotometer.

Reagents and materials

NaOH — borax. 27.5 g of sodium hydroxide were dissolved in 1 l of 0.05 M borax (freshly made).

TNBS reagent. 1.5 g of 2,4,6-trinitrobenzenesulfonic acid (British Drug Houses) was dissolved in 1 l of water (freshly made).

Glycine solution. 16 mg of glycine were dissolved in 100 ml of 0.6 M hydrochloric acid.

Plant material and hydrolysis

Beans (*Phaseolus vulgaris* L.) were ground to a powder in a Wiley mill to pass a 20-mesh screen. Samples were taken for the determination of nitrogen by the standard Kjeldahl method [11] and for protein hydrolysis. Nitrogen values were transformed into protein after multiplying by the factor 6.25. Protein hydrolysis was carried out in 15 × 125 mm culture tubes fitted with Teflon-lined screw caps. Each tube contained 100 mg of powdered sample and 10 ml of (1 + 1) HCl. The tube was incubated at 110°C for 22 h. After hydrolysis the samples were allowed to cool and filtered through a glass-fiber disc under reduced pressure. A 2-ml aliquot of the filtrate was diluted to 20 ml with water and a 0.4-ml sample analyzed by the flow injection system.

Manifold design

The manifold used in the flow injection system is outlined in Fig. 1. This consisted of three pump lines: a sample-carrier line, a buffer line and reagent line. The sample was injected at point "S" into a carrier stream of 0.6 M HCl. The samples were either a solution of glycine in 0.6 M HCl or a protein hydrolyzate in 6 M HCl diluted ten times before analysis. The strength of HCl in the carrier stream therefore was comparable with that of the sample. After the injection port, a 60-cm delay coil (D) was used which was sufficient to avoid the entry of sample under injection pressure beyond the following confluence point. This ensured that the sample entered the neutralizing coil (N) solely by pump pressure. Separate tests showed that neutralization of the sample stream by the buffer stream was instantaneous and a coil of 40 cm was arbitrarily chosen for this purpose. Following the entry of the TNBS reagent line at the end of the neutralizing coil, the flow was directed

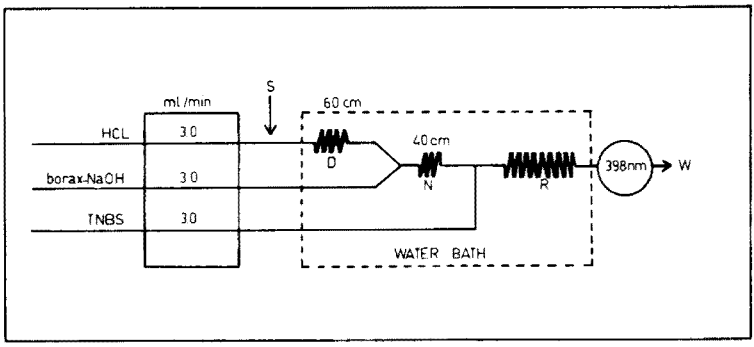

Fig. 1. Flow diagram for the flow injection spectrophotometry of amino acids. S is the point of sample injection. W = waste. The dotted line encloses the part of the manifold immersed in the water bath. D = delay coil, N = neutralizing coil, and R = reaction coil.

through a reaction coil (R) and finally to the flow-through cuvette of the spectrophotometer. This basic set-up was used to determine the influence of various parameters such as pH, line length and temperature on colour formation.

[The use of the most recently developed sample rotary valve [9] would allow an overall miniaturization of the manifold and substantial reduction of the sample volume and the pumping rates [10], provided that the flow-through cell is also small (max. 18 μl). The 60-cm delay coil (D) would then no longer be necessary.]

RESULTS AND DISCUSSION

Effect of pH

The influence of pH on the trinitrophenylation reaction is shown in Fig. 2. The pH in the reaction coil was varied by arbitrarily changing the NaOH concentration in the buffer and measuring the pH of the reaction line effluent. It may be seen that the yield of the reaction is fairly constant in the pH range 9.5—11.0. Above pH 11, the absorbance values increase rapidly, probably because of conversion of TNBS to picric acid which is known to occur at high pH [2]. A working pH in the range 10—10.5 was chosen, because small variations in pH would then have little effect on the results obtained. This pH is well above that recommended for the trinitrophenylation of amino acids (pH 7—8.5) by Sakate et al. [2]. Although these authors were aware of the faster reaction in more alkaline solutions, they avoided their use in view of the instability of the reagent and possible side-reactions at higher pH. In the present case it appears that this problem is insignificant because of the short reaction times employed.

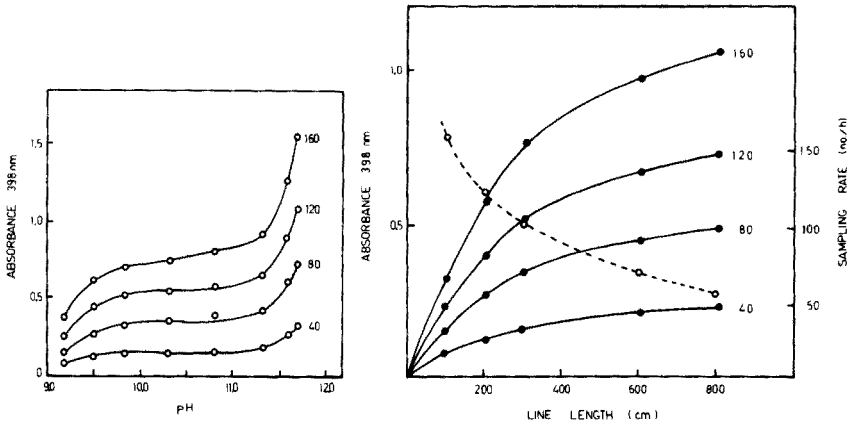

Fig. 2. Influence of pH on the TNBS reaction with amino acids. Samples were glycine solutions at 40, 80, 120 and 160 mg l^{-1}.

Fig. 3. Influence of line length (coil R) on absorbance readings. Samples were glycine solutions at 40, 80, 120 and 160 mg l^{-1}.

Line length

Absorbance readings showed a marked dependence on line length (Fig. 3). The fact that absorbance readings continued to increase up to the longest line length studied shows that the reaction was incomplete. Sensitivity to line length was greatest up to 300 cm. Above this length, absorbance readings increased more slowly, because the advantages of a longer reaction time were offset by dilution effects arising from dispersion of the sample zone. In any case, longer line lengths are undesirable because they diminish the sampling rate. With these factors in mind, a line length of 200 cm was chosen for routine use. With this line length the time taken from the injection of the sample to the appearance of the absorbance peak was just under 30 s. Since the absorbance fell to 1% of the peak value 17 s later, the next sample could be injected immediately after the peak (i.e. at 30-s intervals giving a sampling rate of 120 per h).

Sample volume

The relationship between sample volume and absorbance was established for volumes of 0.1—1.0 ml. The plot (Fig. 4) is almost linear up to a 0.4-ml sample volume, after which it curves so that above about 0.6 ml, readings are almost independent of sample volume. Although a large sample volume would need less precision in filling the sample injection syringe, it has the disadvantage that it is difficult to inject both quickly and evenly under hand pressure. In line with other work with this equipment [7] a 0.4-ml sample volume was selected as best in terms of sensitivity, reproducibility and ease of injection. With a rotary injection valve of 100-μl volume and a tube diameter of 0.5 mm, still slower pumping rates and proportionally shorter

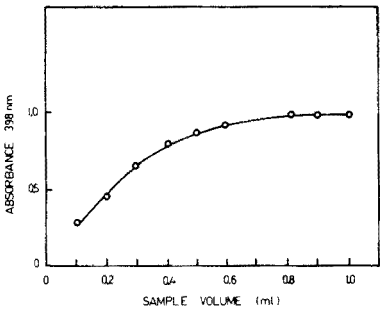

Fig. 4. Influence of sample volume on absorbance readings.

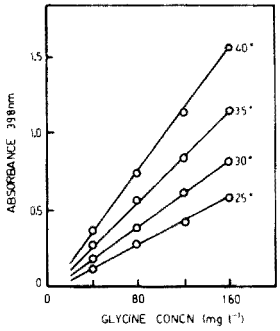

Fig. 5. Relationship between absorbance readings and glycine concentration at different temperatures.

coils N and R would yield comparable absorbances because of less dispersion of the sample zone [10]. Thus, either higher sensitivity could be gained by using higher reagent concentrations with reagent economy preserved, or lower reagent and sample consumption could be achieved, as required.

Effect of temperature

The speed of the reaction is increased by higher temperature. It is clear from Fig. 5 that much is to be gained in terms of sensitivity by using a higher temperature, and a temperature of 40°C was selected for routine work. A linear relationship was obtained between readings and concentration of amino acid in the sample at all temperatures studied.

TNBS concentration

The rate of reaction was increased by increasing the concentration of TNBS (Fig. 6). Although a great deal in terms of sensitivity could be gained by using high TNBS concentrations, 0.15% was chosen for routine work because of the high cost of this chemical. Replotting the data in Fig. 6 showed that the absorbance values are linear with increasing glycine concentration at all concentrations of TNBS.

Calibration of the method

Since the method was developed for possible use in programs where the screening for protein content in large numbers of samples is necessary, the method was calibrated against the universally accepted Kjeldahl method. For this purpose, 25 varieties of bean were selected with protein contents (as determined by the Kjeldahl method) covering as large a range as possible. Protein hydrolyzates of these samples were then analyzed by the flow injection method, and compared with the Kjeldahl values by regression analysis (Fig. 7). A good correlation (r = 0.98) was obtained between the

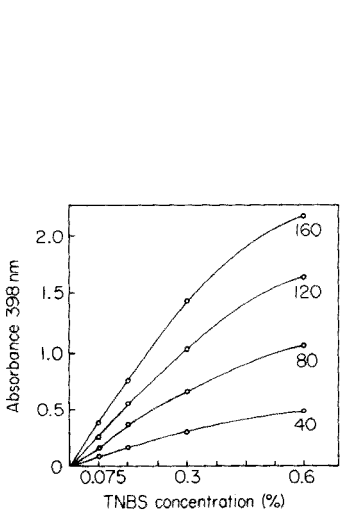

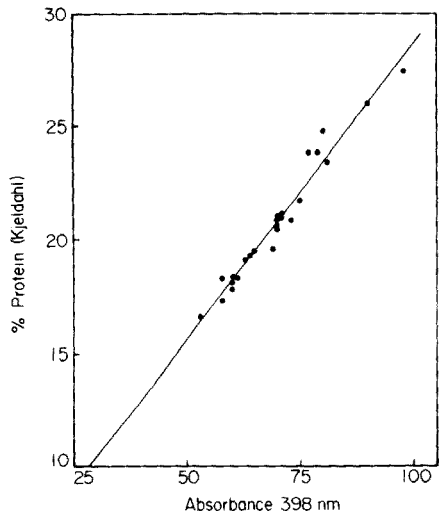

Fig. 6. Influence of TNBS concentration on absorbance readings with glycine concentrations of 40, 80, 120 and 160 mg l^{-1}.

Fig. 7. Calibration curve of the flow injection TNBS method for protein hydrolyzates of beans. Spectrophotometer readings are compared with % Kjeldahl protein of the bean samples. Regression analysis: $Y = 0.262X + 2.50$, $r = 0.98$, standard error of estimate (syx) = 0.55.

absorbance reading obtained by the flow injection method and the Kjeldahl protein values. The standard error of estimating percent (Kjeldahl) protein by the TNBS method was 0.55. It should be remembered however that the entity measured by the Kjeldahl method, namely total nitrogen, is somewhat different from that measured by TNBS, namely amino-nitrogen. Theoretically at least, the TNBS value should be closer to the figure that the plant breeder wants, i.e. total amino acid whether free or polymerized, without non-amino acid nitrogen.

Conclusions

The possibility of modifying an Autoanalyzer method for the determination of protein in grains to the flow injection system has been demonstrated. For routine analyses, the optimum parameters are: a pH (reaction coil) of 10—10.5, a TNBS concentration of 0.15%, a line length (coil R) of 200 cm, an injection volume of 0.4 ml, and a reaction temperature of 40° C. With the flow injection system described a sampling rate of 120 samples per h is possible, against 30 with the Autoanalyzer.

The influence of several parameters on the rate of colour formation shown above leaves several options open for bringing samples into the range of the spectrophotometer, if necessary. Temperature is the first variable to alter to obtain the desired sensitivity. Secondly, the line length of the reaction coil

may be varied, but this will, of course, affect the sampling rate. A third option is the TNBS concentration, although the high cost of this chemical would have to be considered when contemplating higher reagent concentrations. Following the approach outlined above, the reagent and sample consumption could be further reduced by the use of a miniaturized manifold furnished with a rotary injection valve [9, 10].

We are indebted to H. Bergamin and his staff for their helpful assistance and cooperation and to the International Atomic Energy Agency for its support by assigning two of the authors (J. R. and J. W. B. S.) as UNDP Experts to U.N. Project BRA/71/556, where this research took place. We also thank the Danish International Development Agency for partial material support.

REFERENCES

1 T. Okuyama and K. Satake, J. Biochem. (Tokyo), 47 (1960) 454.
2 K. Satake, T. Okuyama, M. Ohashi and T. Shinoda, J. Biochem. (Tokyo), 47 (1960) 654.
3 C. W. Gherke and L. L. Wall, Adv. in Automated Analysis, Vol. II, 93, Technicon International Congress 1970, Thurman Associates, 1971.
4 J. Růžička and E. H. Hansen, Anal. Chim. Acta, 78 (1975) 145.
5 J. Růžička and J. W. B. Stewart, Anal. Chim. Acta, 79 (1975) 79.
6 J. W. B. Stewart, J. Růžička, H. Bergamin Filho and E. A. G. Zagatto, Anal. Chim. Acta, 81 (1976) 371.
7 J. Růžička, J. W. B. Stewart and E. A. G. Zagatto, Anal. Chim. Acta, 81 (1976) 353.
8 J. W. B. Stewart and J. Růžička, Anal. Chim. Acta, 82 (1976) 137.
9 E. H. Hansen, F. J. Krugg, A. K. Ghose and J. Růžička, Analyst, 102 (1977) 218.
10 J. Růžička, E. Hansen, H. Mosbæk and F. J. Krugg, Anal. Chem., 49 (1977) 1858.
11 C. M. Johnson and A. Ulrich, Calif. Agric. Exp. St. Bull., (1959) 766.

Analytica Chimica Acta, 97 (1978) 335—342

SPECTROPHOTOMETRIC DETERMINATION OF NICKEL IN IRON AND STEEL WITH 2-NITROSO-1-NAPHTHOL-4-SULFONIC ACID. IMPROVEMENT OF SENSITIVITY BY EXTRACTING EXCESS OF REAGENT

SHOJI MOTOMIZU and KYOJI TÔEI*

Department of Chemistry, Faculty of Science, Okayama University, Tsushima, Okayama-shi (Japan)

(Received 27th September 1977)

SUMMARY

Removal of the excess of a reagent extracted into an organic phase in the solvent extraction of a metal complex anion with a quaternary ammonium ion can be helpful in improving spectrophotometric determinations of metals. The principle can be applied to the extraction with zephiramine of the nickel complex anion formed with 2-nitroso-1-naphthol-4-sulfonic acid. The exchange equilibrium constants for the nickel complex anion and monovalent anions (nitrate and halide) were determined. The proposed method was applied to the determination of nickel in iron and steel samples (NBS 55e, 19g, 101e and 126b).

With a given chelating ligand (HO-R-SO_3H), the order of extractability of ion-pairs formed with a quaternary ammonium ion is HO—R—SO_3^- or $M(O—R—SO_3)_n^{m-} > X^- > {}^-O—R—SO_3^-$, in the presence of a sufficient amount of a monovalent anion (X^-) which does not absorb at the maximum absorption wavelength of the complex [1]. If suitable amounts of anion (X^-) are added, only the excess of reagent in the organic phase can be exchanged by X^- and removed to the aqueous phase.

This paper describes this method of removing the excess of reagent from the organic phase as applied to the extraction system nickel(II)—2-nitroso-1-naphthol-4-sulfonic acid—tetradecyldimethylbenzylammonium salt. Several exchange equilibrium constants between chloroform and aqueous solution are reported, and the optimum conditions for removing the excess of reagent from the chloroform phase are described. The method was applied to the determination of nickel in iron and steel.

EXPERIMENTAL

Apparatus

A Shimadzu Model QV-50 spectrophotometer and a Hitachi Model EPS-3T recording spectrophotometer were used with 10-mm quartz cells. An Iwaki Model KM shaker was used.

Reagents

2-Nitroso-1-naphthol-4-sulfonic acid. The reagent (NNS) was obtained by nitrosation of the parent compound in aqueous solution with sodium nitrite; the crude nitroso compound was recrystallized twice from hydrochloric acid solution [2]. The crystals obtained were dried over calcium chloride in a vacuum desiccator for a week. Four molecules of water of crystallization were found by Karl Fisher's method. Thus, the compound is $C_{10}H_7NO_5S \cdot 4H_2O$ (m.w. 325.2). Aqueous solutions of recrystallized NNS were used.

Nickel(II) solution. Sponge nickel metal (99.999%, Mitsuwa Chemical Company, Inc.) was dissolved in hydrochloric acid solution. This solution was standardized by EDTA titration.

Tetradecyldimethylbenzylammonium chloride solution. Dotite zephiramine chloride (ZCl; Dojindo Co. Ltd., Research Laboratory) was used. The reagent was dried at reduced pressure (about 5 mm Hg) and 50—60 °C to constant weight, and dissolved in distilled water. This solution need not be standardized [3].

Other reagents used were of analytical-reagent grade.

Composition of the nickel complex in aqueous solution and in chloroform

The nickel : NNS ratio in the complex in aqueous solution and in the extracted complex in chloroform (with 10^{-3} M zephiramine) was found to be 1 : 3 by the mole ratio method (variable nickel concentration and 6.11×10^{-5} M NNS). The nickel : zephiramine ratio of the complex extracted into chloroform was found to be 1 : 4 by the mole ratio method (variable zephiramine concentration with 2×10^{-5} M nickel and 1×10^{-4} M NNS). The extracted species therefore contains nickel, NNS and zephiramine in the proportions of 1 : 3 : 4.

Determination of the equilibrium constants

The exchange equilibrium constant, $K_{An^-}^{nX^-}$, refers to the following reaction

$$A_{(a)}^{n-} + nZX_{(o)} \rightleftharpoons nX_{(a)}^{-} + Z_nA_{(o)}; \quad K_{An^-}^{nX^-} = [X^-]_a^n [Z_nA]_o / [A^{n-}]_a [ZX]_o^n$$

or

$$\log ([Z_nA]_o/[A^{n-}]_a) = \log D_A = \log K_{An^-}^{nX^-} - n \log ([X^-]_a/[ZX]_o)$$

where A^{n-}, Z^+ and X^- are the n-valent anion, the zephiramine cation and the monovalent anion (nitrate or halide), respectively, and the subscripts o and a refer to the organic and aqueous phases, respectively. The exchange equilibrium constants for A^{n-} and X^- were determined by extracting A^{n-} with ZX into chloroform from aqueous solutions containing various amounts of X^- and measuring the concentration of Z_nA in chloroform.

The exchange equilibrium constants for HR^- (the monovalent anion of NNS) and R^{2-} (the divalent anion of NNS) were determined previously [1]. In this work, the constants for the nickel complex, NiR_3^{4-}, were determined.

The plots of log D_{Ni} against log ($[X^-]_a/[ZX]_o$) for four monovalent anions are shown in Fig. 1, where $D_{Ni} = ([Z_4NiR_3]_o/[NiR_3^{4-}]_a)$. These plots are all linear and their slopes are almost −4. The constants determined for these anions (Table 1) indicate that chloride gives the highest concentration for the removal of the excess of reagent and therefore causes very effective salting-out. Figure 2 shows the percentage extraction for HR^-, R^{2-} and NiR_3^{4-}, which was calculated by using the exchange equilibrium constants for chloride listed in Table 1; obviously, it is much easier to remove reagent in the form R^{2-} than in the form HR^- from the organic phase. A study of the effect of chloride concentration on the removal of excess of reagent in the organic phase (Fig. 3) shows that when the chloride concentration exceeds 0.20 M, the absorbance of the reagent blank is small and virtually constant; with chloride concentrations above 0.4 M, the absorbance of the nickel complex decreases gradually. The optimal concentration of chloride is about 0.25 M. Figure 4 shows the absorbance spectra of the nickel complex and the reagent blank. When the excess of reagent in the organic phase is removed, the best sensitivity is obtained at 307.5 nm, at which the molar absorptivity is 5.3×10^4 l mol^{-1} cm^{-1}. The molar absorptivity at 480 nm is 2.4×10^4 l mol^{-1} cm^{-1}.

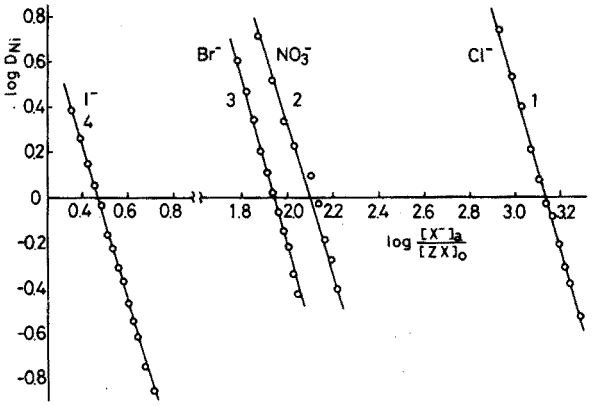

Fig. 1. The plot of log D_{Ni} against log ($[X^-]_a/[ZX]_o$). Curve 1, chloride. Curve 2, nitrate. Curve 3, bromide. Curve 4, iodide. $[NiR_3^{4-}]_{total} = 2 \times 10^{-5}$ M, $[\text{zephiramine}]_{total} = 5 \times 10^{-4}$ M, pH 8.6.

TABLE 1

The exchange equilibrium constants (25°C)

	Cl^-	NO_3^-	Br^-	I^-
log $K_{NiR_3}^{4X^-}$	12.53 ± 0.06	8.47 ± 0.05	7.76 ± 0.04	1.92 ± 0.06
log $K_{R^{2-}}^{2X^-}$	3.37 ± 0.05	1.30 ± 0.02	0.95 ± 0.05	−1.58 ± 0.10
log $K_{HR^-}^{X^-}$	2.49	1.46	1.28	0.01

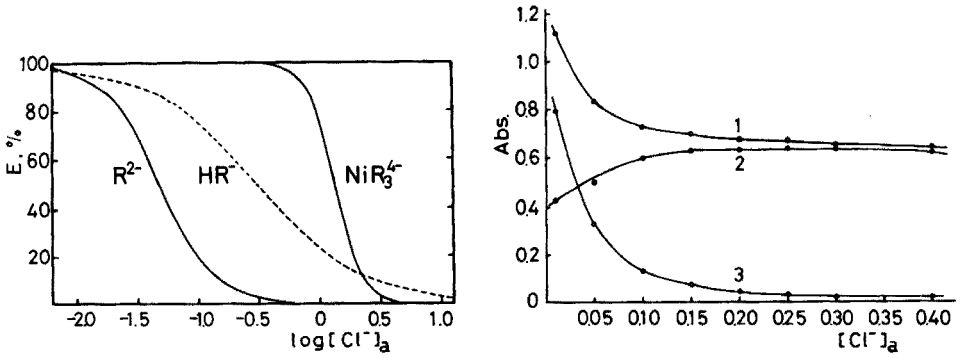

Fig. 2. Percentage extraction of HR^-, R^{2-} and NiR_3^{4-} against chloride concentration for 10^{-3} M zephiramine.

Fig. 3. Effect of chloride on the extraction of nickel and reagent. Curve 1, nickel (reference, chloroform). Curve 2, reagent blank (reference, chloroform). Curve 3, nickel (reference, reagent blank). $[Ni]_{total} = 1.2 \times 10^{-5}$ M. $[NNS]_{total} = 1.2 \times 10^{-4}$ M. $[zephiramine]_{total} = 10^{-3}$ M. pH 8.6; 307.5 nm.

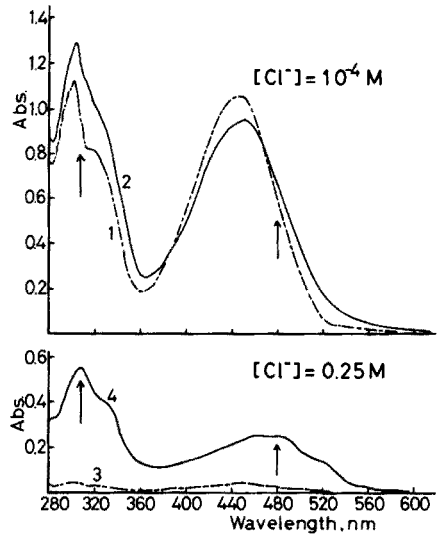

Fig. 4. Absorption spectra in chloroform. Curve 1, reagent blank. Curve 2, 10^{-5} M Ni. For curves 1 and 2, $[Cl^-] = 10^{-4}$ M at pH 8.6. Curve 3, reagent blank. Curve 4, 10^{-5} M Ni. For curves 3 and 4, $[Cl^-] = 0.25$ M at pH 8.6. In all cases, $[NNS]_{total} = 10^{-4}$ M, $[zephiramine]_{total} = 10^{-3}$ M.

Determination of nickel

General procedure (Method I). Pipette up to 5 ml of sample solution into a stoppered test tube, and dilute to 5 ml with distilled water. Add 0.1 ml of hydrogen peroxide (30%), 0.2 ml of trisodium citrate solution (0.15 M) and

0.1 ml of potassium pyrophosphate solution (0.5 M), and mix. Then add 0.5 ml of aqueous NNS solution (2×10^{-3} M), 0.5 ml of phosphate buffer solution (pH 8.6, 0.5 M) and 1 ml of sodium chloride solution (2 M). Shake with 5 ml of chloroform solution containing zephiramine (10^{-3} M) for 10 min. After the phases have separated, measure the absorbance of the organic phase at 307.5 nm against a reagent blank.

Effect of co-existing ions. The effect of co-existing ions was examined (see Table 2). In the general procedure, without addition of hydrogen peroxide, citrate and pyrophosphate, several metal ions at concentrations of 10^{-4} M cause errors; with addition of hydrogen peroxide and citrate, there are few interferences other than cobalt and copper(II). In the general procedure, concentrations of cobalt and copper above 5×10^{-6} M and iron at concentrations above 7.5×10^{-4} M cause positive errors. Cobalt reacts with NNS in the neutral pH region and is extracted into the organic phase even at about pH 2 with zephiramine; at this pH the nickel complex decomposes and is not extracted. Copper(II) can be reduced with reagents such as hydroxylamine, and copper(I) forms a very stable complex with pyrophosphate. These reactions were used to decrease the interference of cobalt and copper. The general procedure was modified as follows.

Improved method (Method II). Pipette the sample solution into a 10-ml volumetric flask, add 0.2 ml of hydrogen peroxide (30%), 0.4 ml of citrate

TABLE 2

Effect of diverse ions

Method	Ion	Maximum tolerable conc. (M)
Without H_2O_2, citrate and pyrophosphate		
	Alkali metal ions	0.4^a
	SO_4^{2-}, PO_4^{3-}	0.1^a
	Citrate	0.01
	NO_3^-, Br^-	5×10^{-3}
	Mg^{2+}, Ca^{2+}, Sr^{2+}	10^{-3} [a]
	Mn^{2+}, Pb^{2+}, Zn^{2+}, Ba^{2+}	10^{-4} [a]
	I^-	10^{-4}
Without pyrophosphate		
	Ba^{2+}	10^{-3} [a]
	Cr^{3+}, Al^{3+}, Cd^{2+}, Ag^+	10^{-4} [a]
	Fe^{2+}, Fe^{3+}	10^{-4}
	Cu^{2+}	10^{-5}
General procedure		
	Fe^{2+}, Fe^{3+}	7.5×10^{-4}
Improved method		
	Co^{2+}	10^{-3} [a]
	Cu^{2+}	5×10^{-5} [a]

[a]Maximum tested.

solution (0.15 M) and 0.2 ml of pyrophosphate solution (0.5 M). After mixing, add 1 ml of NNS (2×10^{-3} M) or an amount more than five-fold the molar equivalent of the cobalt content. Then add 1.0 ml of phosphate buffer (pH 8.6), mix and leave to stand for 10 min. Add 0.2 ml of sulfuric acid solution (6 M) and dilute to the mark with water. Transfer the solution to the separatory funnel and shake with 5 ml of zephiramine—chloroform solution (10^{-3} M) for 5 min. If excess of reagent or the cobalt complex still remains in the aqueous phase, again extract with further 5-ml portions of chloroform solution. After the phases have separated, pipette a 5-ml portion of the aqueous phase into a stoppered test tube. Add 0.5 ml of NNS solution and 1 ml of sodium hydroxide solution (1 M). Shake with 5 ml of zephiramine—chloroform solution (10^{-3} M) for 10 min. After the phases have separated, discard the aqueous phase, wash the organic phase with 5 ml of an aqueous solution containing citrate (0.003 M) and pyrophosphate (0.01 M) by shaking manually for about 5 s, and discard the aqueous phase. Shake the organic phase with 10 ml of washing solution (pH 8.6) containing hydroxylammonium chloride (0.0015 M), pyrophosphate (0.007 M) and sodium chloride (0.25 M) for 5 min. (In this process, copper extracted into the organic phase is reduced to copper(I) and transferred to the aqueous phase as the pyrophosphate complex; copper concentrations up to 5×10^{-5} M do not interfere.) Finally, measure the absorbance of the organic phase at 307.5 nm to obtain the nickel content.

Removal of large amounts of iron. Large amounts of iron in iron and steel samples are extracted with isobutyl methyl ketone (MIBK) from 5—6 M hydrochloric acid. When 10—20 ml of 0.25 M iron solution in 6 M HCl was shaken with three 5-ml portions of MIBK, the iron remaining in the aqueous phase was about 10^{-4} its initial concentration, the iron content being measured by the 2-nitroso-5-dimethylaminophenol method [4].

Preparation of iron and steel sample solutions. Weigh the required amounts of sample into a beaker. Add 3—5 ml of aqua regia and heat to dissolve. After dissolution, evaporation and dilution in the usual way, transfer the solution to a 25-ml stoppered test tube and, if necessary, add hydrochloric acid to give a 5—6 M solution. Shake with about 5 ml of MIBK for 30 s and discard the organic phase; repeat this extraction twice, discarding the organic phase. Transfer the aqueous phase to a beaker and evaporate nearly to dryness. Dilute with distilled water, transfer the solution to a suitable volumetric flask and dilute to the mark with water. When the iron concentration is less than 7.5×10^{-4} M in the sample solution, it need not be removed.

RESULTS

Nickel in iron and steel samples was determined by the following methods. Method I can be applied to samples which give copper and cobalt at concentrations below 10^{-5} and 10^{-7} M, respectively, in the final solution. Method II

can be applied to sample solution containing copper and cobalt at concentrations below about 5×10^{-5} and 10^{-3} M, respectively.

Calibration curves were prepared for Methods I and II. Both plots were straight lines in the nickel concentration ranges up to 1.6×10^{-5} M (307.5 nm), and the slopes of the plots were almost equal. The absorbances of the reagent blanks of Methods I and II were about 0.01 and 0.04, respectively.

The results obtained for four NBS samples are shown in Table 3.

DISCUSSION

The general method for the removal of the excess of reagent in the solvent extraction of a metal chelate anion with a quaternary ammonium cation [1] proved to be applicable to the extraction of nickel with 2-nitroso-1-naphthol-4-sulfonic acid and zephiramine. As almost all the excess of reagent in the organic phase was removed into the aqueous phase, the absorbances of the reagent blank at the maximum absorption wavelength of the nickel complex were very small and constant when 0.25 M chloride was added. Nickel could then be determined sensitively. The molar absorptivity of the nickel complex in chloroform is 5.3×10^4 l mol^{-1} cm^{-1} at 307.5 nm, which is 4 times larger than that at 520—530 nm. Methods I and II allowed nickel to be determined in iron and steel with satisfactory results.

TABLE 3

Determination of nickel in iron and steel

Sample[a]	Sample solution (mg/100 ml)	Method	Ni found[b,c] (%)
NBS 55e			
(Ni, 0.038%)	205.2[d]	II	0.0374 ± 0.0005
	199.0[d]	II	0.0387 ± 0.0004
NBS 19g			
(Ni, 0.066%)	202.3[d]	II	0.0678 ± 0.0008
	201.2[d]	II	0.0668 ± 0.0005
NBS 101e			
(Ni, 9.48%)	0.496	I	9.53 ± 0.13
	0.994	II	9.39 ± 0.13
NBS 126b			
(Ni, 35.99%)	0.206	I	35.61 ± 0.08

[a]Main constituents (%) are as follows: NBS 55e: Co 0.007, Cu 0.065, Cr 0.006, Mn 0.035. NBS 19g: Co 0.012, Cu 0.093, Cr 0.374, Mn 0.554. NBS 101e: Co 0.18, Cu 0.359, Cr 17.98, Mn 1.77. NBS 126b: Co 0.032, Cu 0.082, Cr 0.066, Mn 0.380.
[b]Mean values for four determinations.
[c]In all cases, 5 ml of the sample solution was used for the extraction procedures.
[d]Iron in sample solution was removed beforehand with MIBK.

TABLE 4

Molar absorptivities of nickel complexes extracted into chloroform with zephiramine

Reagents	λ (nm)	ε (10^4 l mol^{-1} cm^{-1})
2-Nitroso-1-naphthol-4-sulfonic acid	307.5 (480)	5.3 (2.4)
2-Nitroso-1-naphthol-5-sulfonic acid	313 (486)	5.1 (2.3)
1-Nitroso-2-naphthol-6-sulfonic acid	305 (460)	4.2 (1.5)
1-Nitroso-2-naphthol-7-sulfonic acid	309	2.8
	386 (454)	1.9 (1.6)
1-Nitroso-2-naphthol-3,6-disulfonic acid	310	3.7
	380 (466)	2.0 (1.9)
1-Nitroso-2,7-dihydroxynaphthalene-3,6-disulfonic acid	320.5 (413)	5.9 (2.9)

Table 4 shows a comparison with the molar absorptivities obtained for nickel complexes with other derivatives. The molar absorptivities of the 2-nitroso-1-naphthol derivatives are larger than those of the 1-nitroso-2-naphthol derivatives, except for 1-nitroso-2,7-dihydroxynaphthalene-3,6-disulfonic acid. This is the most sensitive reagent but it is very difficult to remove the excess of reagent from the organic phase, hence 2-nitroso-1-naphthol-4-sulfonic acid was preferred.

The proposed principle of removing the excess of reagent can be applied to many other solvent extraction systems involving chelating reagents which possess a chelate-forming hydroxyl group and a sulfonic acid group. In general, reagents possessing a sulfonic acid group should be removed at lower pH than reagents with no sulfonic acid group; effective removal is usually possible at pH values about 2 above the pK_a value of the hydroxyl group. For example, 2-nitroso-1-naphthol-4-sulfonic acid (pK_a: 6.16 [1]) can be removed from the organic phase at pH values above 8.2, whereas 2-nitroso-1-naphthol (pK_a: 7.41 [5]) in the organic phase is removed at pH values above 10, at which the nickel complex is decomposed to nickel hydroxide.

Such methods should lead to improved sensitivity and accuracy in many solvent extraction systems. Moreover, the addition of relatively large amounts of salt reduces the effect of co-existing anions in sample solutions and causes very effective salting-out, so that phase separation becomes faster.

REFERENCES

1 S. Motomizu and K. Tôei, Anal. Chim. Acta, 89 (1977) 167.
2 K. Tôei and S. Motomizu, Nippon Kagaku Zasshi, 92 (1971) 92.
3 K. Tôei and K. Kawada, Jpn. Anal., 21 (1972) 1510.
4 K. Tôei, S. Motomizu and T. Korenaga, Analyst, 100 (1975) 629.
5 S. Motomizu and K. Tôei, Analytical Instruments, 15 (1977) 1.

Analytica Chimica Acta, 97 (1978) 343—347

ULTRAMICRODETERMINATION OF CHOLESTEROL, TESTOSTERONE AND LSD BY FLUORESCENCE MEASUREMENTS OF TLC SPOTS

S. LEVI and R. REISFELD*

Department of Inorganic and Analytical Chemistry, The Hebrew University of Jerusalem, Jerusalem (Israel)

(Received 7th September 1977)

SUMMARY

Fluorescent derivatives of many organic materials adsorbed on t.l.c. plates are obtained by reaction with ammonia liberated by heating ammonium hydrogencarbonate. Spots whose fluorescence can be measured quantitatively with high sensitivity over wide ranges of concentrations can be obtained with testosterone (1—250 ng), LSD (2—150 ng) and cholesterol (4—150 ng).

Segura and Gotto [1] were the first to report the appearance of stable, highly fluorescent spots in t.l.c. after heating the plates in an atmosphere of ammonia liberated from ammonium hydrogencarbonate; many biological materials, including cholesterol and testosterone, were examined. After the chromatograms had been developed the fluorescent spots were scanned; a linear relation between the square root of the peak area of the spot and the concentration was obtained. The limit of determination was in the range 1—0.1 μg. The present work extends the sensitivity of the method to the nanogram range for the determination of cholesterol, testosterone, and LSD. This high sensitivity was obtained by direct measurement of the fluorescence of homogeneous, well-defined spots without any kind of scanning. This method can be used after separation of the materials by liquid chromatography or h.p.l.c. [2]. One of the most important advantages of this reaction is that the reagent is gaseous; an identical quantity of reagent is applied therefore to each spot, hence improving the reproducibility of the method. However, forming uniform t.l.c. layers (which is critical in this method) is not easy; the standard deviation of the results is caused mainly by the deviation of the layer thickness on the plates. How to overcome this difficulty is described under Experimental.

On heating, alumina and silica gel dehydrate molecules containing hydroxyl groups, thereby producing double bonds which increase the wavelength of excitation of the molecule and make those molecules available for fluorescence measurements. The ammonia in the system increases the fluorescence intensity by forming products in which the nitrogen atom is conjugated to the double bonds and its two free electrons participate in the π-electron

system. The reaction takes place with many organic materials, hence difficulties arise in getting a non-fluorescent background. To overcome this problem, the alumina and silica gel should be ultrapure. The level of the fluorescent background was minimized by heating the alumina and the silica (before making the suspension) and "washing", and by using pure solvents as described below.

As the wavelengths of excitation and emission differ only slightly from compound to compound, the same wavelengths have been used for all compounds. The wavelength of excitation was 405 nm (mercury source); emission was at 470 nm.

EXPERIMENTAL

Reagents

All chemicals were reagent grade. All the solvents were distilled before use. Alcoholic stock solutions (400 ppm) of the materials to be determined were diluted to the appropriate concentrations.

Preparation of the t.l.c. plates

Plastic strips were unsuccessful; their elastic property makes it difficult to keep spots in a constant position on the strip before reading the fluorescence. Small glass plates (7.5 × 2.5 cm) were optimal for the method. From stocks of glass plates (Chance Propper Ltd., Spon Lane, Smethwick, Warley, England) plates of 0.92 ± 0.01 mm thickness were selected with a micrometer. These small plates were put on moistened large plates (20 × 20 cm) which were placed on the plate holder; the small plates stick to the large plates and give a stable system. This makes the process of spreading easy and homogeneous plates are obtained.

A mixture of (1 + 2, w/w) of alumina gel (neutral, Merck) and silica gel (Merck) was prepared. The mixture was placed in a porcelain crucible and in an oven at 700°C for 4 h, and then cooled to room temperature. To 30 g of mixture, 70 ml of water, triply distilled, was added and mixed well for 10 min. The suspension was poured into a clean spreader (Desaga), adjusted to 0.25-mm thickness, and spread with constant rate of advance of the spreader. The plates were left to dry at room temperature for 6 h. The plates were removed carefully and "washed" 4 times by development with absolute methanol. After the final drying, a strip, 1 cm wide, from both edges of the layer was scraped off to allow the t.l.c. plates to enter the fluorimeter holder smoothly.

Apparatus

The fluorescence measurements were made with a Perkin-Elmer Fluorescence Spectrophotometer model 203, into which a holder for the t.l.c. plates was fitted as described previously [2].

Preparation of the spot on t.l.c. plates

The solutions were delivered from a motorized microsyringe (which can also be used manually) as described previously [2, 3]. The needle of the microsyringe permits delivery of 5-μl drops of the solutions onto the t.l.c. plates which are placed in a holder slightly modified from that described previously [2]. The size of the holder was adjusted to the size of the plates, 7.5 × 2.5 cm. Two spots are placed on every plate, one on each side, one as a blank and the other of the appropriate concentration. After drying, the t.l.c. plates are inserted into a tank of 2.5 l capacity to which 2.5 g of ammonium hydrogencarbonate are added. The sealed tank is put in an oven at 120°C for 3 h. The plates are removed carefully, inserted into the holder, and fluorescent readings are then taken. Two filters are used; one before the sample cuts out all radiation over 470 nm and the other, placed after the sample, passes all radiation over 480 nm. The fluorescence is viewed at 45°.

RESULTS AND DISCUSSION

The optimum fluorescence reaction takes place on heating at 120°C for 3 h. With longer heating the background becomes significant from the reaction of residual impurities with the ammonia.

Figure 1 shows the fluorescence spectrum of the testosterone derivative (after subtraction of the blank). The shape of the spectrum is not symmetrical because of the two filters used. The optimal emission wavelength for quantitative measurements was 470 nm. A linear dependence over a wide range was found between the concentration and the intensity of fluorescence (Fig. 2).

A theoretical treatment of fluorescent densitometry of thin layer chromatograms has been given by Goldman [4]. His mathematical treatment is based on the model and assumptions of the Kubelka—Munk theory. In this

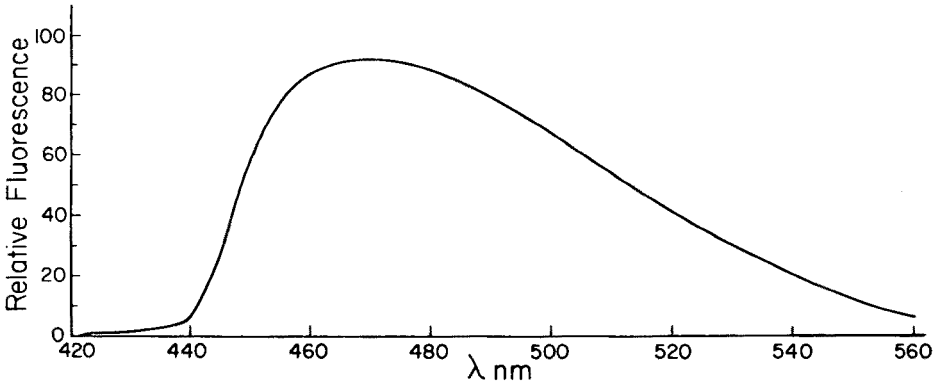

Fig. 1. Fluorescence spectrum of testosterone derivative excited at 405 nm (mercury source).

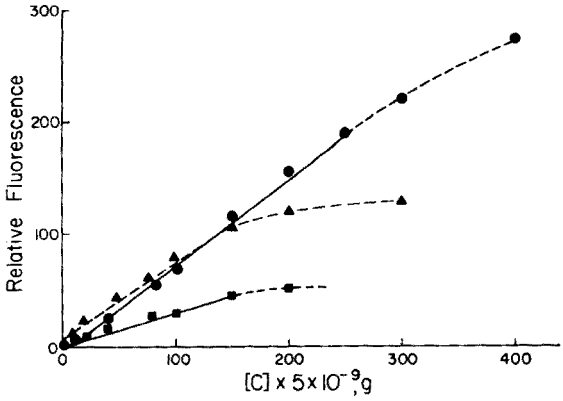

Fig. 2. Calibration curves for the testosterone (•), LSD (▲) and cholesterol (■) derivatives. Each point is the average for 4 spots after deduction of the blank.

case the phenomenon is more complicated because of the two kinds of light present in the solid medium: the incident light from outside the medium and fluorescent light produced inside the medium. The incident light undergoes absorption and scattering simultaneously; the fluorescent light is assumed to pass scattering only. For this operation Goldman derives two pairs of Kubelka–Munk differential equations:

$$-\mathrm{d}i/\mathrm{d}x = -(s + k)i + s_j;\ \mathrm{d}j/\mathrm{d}x = -(s + k)j + s_i \qquad (1)$$

$$-\mathrm{d}I/\mathrm{d}x = -SI + SJ + (i + j)\alpha k/2;\ \mathrm{d}J/\mathrm{d}x = -SJ + SI + (i + j)\alpha k/2 \qquad (2)$$

Equations (1) are for the incident light travelling in the transmission (i) and "reflection" (j) directions. Equations (2) are for the fluorescent light travelling in transmission (I) and reflection (J) directions, where x = thickness of the medium; s = scattering coefficient of the incident light; k = absorption coefficient of the incident light; S = scattering coefficient of the fluorescent light; and $I^+ = I$ at $x = 0$ and $J^+ = J$ at $x = X$, the fluorescence obtained in transmission and reflection, respectively. Solutions for these equations are complicated and a computer is required but, for low concentrations and high scattering power (SX) the solutions become simple:

$$\frac{I^+}{i_0} = \frac{1}{3}\,kX\left(1 - \frac{7}{30}\,sX \cdot kX\right);\ \frac{J^+}{i_0} = \frac{2}{3}\,kX\left(1 - \frac{4}{30}\,sX \cdot kX\right) \qquad (3)$$

where i_0 = the initial incident intensity and α = the conversion factor from incident to fluorescent light.

The reflected fluorescence, compared with the transmitted fluorescence, has the important advantages of higher intensity and of being unaffected by scattering power changes in the range 5–20. When the medium has some absorption, a correction for the layer width should be made. The following results help to confirm the theoretical treatment of Goldman [4].

TABLE 1

Equations of the straight lines obtained from linear regression, standard deviations, correlation coefficients and coefficients of variation

	Testosterone	LSD	Cholesterol
Range of conc. (ng)	1—250	2—150	4—150
Intensity of fluorescence	$0.764C - 1.722$	$0.715C + 3.425$	$0.270C + 4.598$
Correlation coefficient	0.99885	0.99795	0.97096
Standard deviation of the regression line (ng)	4.6	3.83	3.88
Coefficient of variation	1.84	2.55	2.59

In this work, simple linear dependence was achieved between the quantity of the fluorescent derivative adsorbed on the layers of the solid phase and the intensity of the fluorescence, when the spots had spherical symmetry and were all irradiated on the same part of the spot. The deviation from linearity in the work of Segura and Gotto [1] may be caused by deviation from spherical symmetry of the spots.

The precision of the method may be seen from 5 readings taken from 5 spots of 500 ng of the testosterone derivative; corrected values of 70, 76, 74, 72 and 75 units were obtained. The relative standard deviation is ca. 3% and is caused mainly by the slight variation of the layer thickness of the solid medium on the glass plate. Calibration curves should be prepared for each determination to minimize deviations arising from the process of preparing the t.l.c. plates. The limit of determination changes from material to material. The testosterone derivative gives the most intense fluorescence and can be determined in the range 5—250 ng; LSD can be determined in the range 25—150 ng; cholesterol gives less intensity but can be determined over the range of concentration, 5—150 ng (Table 1). Under the same conditions, oleic acid, methyl oleate, inolein, β-sitosterin, stigmasterol, lactose and phenylalanine also produce fluorescent products. The fluorescent derivatives are sensitive to sunlight and should be kept in a dark place.

The authors are grateful to Prof. R. Ikan for supplying the natural products. This work was supported by the Israel National Council of Research and Development.

REFERENCES

1 R. Segura and M. Gotto, Jr., J. Chromatogr., 99 (1974) 643.
2 R. Reisfeld and S. Levi, Anal. Lett., 10 (1977) 483.
3 R. Reisfeld, E. Greenberg and W. J. Levene, Anal. Chim. Acta, 74 (1975) 253.
4 J. Goldman, J. Chromatogr., 78 (1973) 7.

Analytica Chimica Acta, 97 (1978) 349—356

AQUEOUS PHASE SOLUBILITIES AND PARTITION DATA FOR COMMERCIAL COPPER EXTRACTANTS

H. J. FOAKES, J. S. PRESTON** and R. J. WHEWELL*

Schools of Chemical Engineering, University of Bradford (Gt. Britain)

(Received 10th October 1977)

SUMMARY

The aqueous solubilities of purified samples of several commercial metal extractants have been determined, and the influence of the important variables of temperature and aqueous phase pH value on the solubility has been studied. The distribution isotherm between n-heptane and an aqueous phase has been constructed for one of the reagents, and, by use of vapour-phase osmometry data relating to the degree of self-association in the organic phase, the partition coefficient of the monomeric form obtained. The presence of lower-molecular-weight oximes, which are not removed in the purification process, causes considerable experimental difficulty.

Considerable current research effort is being devoted to the investigation of mechanisms of solvent extraction processes, particular interest being centred on the determination of the nature and site of the mechanistic step which controls the overall reaction kinetics [1—4]. The outcome of such research is relevant not only to the theory of solvent extraction chemistry but also to the design of improved commercial processes. Of special interest, therefore, are systems involving β-hydroxyoxime reagents of the type

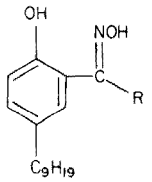

currently in large scale use for the extraction of copper from acidic leach liquors. Such reagents are supplied by General Mills Inc. (as LIX 65N with R = phenyl), by Shell Chemicals Ltd. (as SME 529 with R = methyl) and by Acorga Ltd. (as P17 with R = benzyl and as P50 with R = hydrogen). LIX 64N (General Mills Inc.), a mixture of LIX 65N and the α-hydroxyoxime catalyst LIX 63, has been used for the extraction—determination of copper(II) [5]. These reagents might be expected to differ in their aqueous

---

**Now at the School of Mathematical and Physical Sciences, Murdoch University, Western Australia.

solubilities and in view of the possible occurrence of a wholly aqueous phase reaction step between metal ion and extractant, a knowledge of such data is essential to the formulation of the extraction mechanism.

In selecting a method for the measurement of the extractant solubilities, however, it must be borne in mind that the commercial grades of reagent contain considerable amounts of both hydrocarbon diluent and nonylphenol [6]. Even after the removal of these contaminants there remains the possibility that lower-molecular-weight by-products are formed during manufacture, in which the t-nonyl substituent has been replaced by hydrogen or by an alkyl group derived by fission of the nonyl radical [7]. Such compounds might be expected to be more soluble in water than the major component. Thus, if the solubilities were to be measured by a method involving the equilibration of an aqueous phase with excess of oxime followed by the determination of the dissolved reagent (e.g. by spectrophotometry), misleading results would be produced by the presence of even relatively small amounts of more soluble oximes leached out of the excess of solute.

Solubilities have therefore been determined by a different approach [8], entailing the titration of a dilute ethanolic solution of the reagent into a known volume of aqueous phase, the presence of excess of reagent over the amount required to saturate the aqueous phase being signalled by the appearance of turbidity. The turbidity could be observed visually, but was better detected spectrophotometrically. Thus, while the initial section of a plot of absorbance against volume of titrant simply reflects the increase in absorption of radiation by the solution with reagent concentration according to Beer's Law, once the solubility limit has been reached the observed absorbance consists of the true absorption augmented by the light scattering effect of the dispersion. The nature of the latter is such that a linear relationship is maintained between absorbance and volume of titrant, but with increased gradient, enabling the solubility "end-point" to be located as a discontinuity in the plot. Clearly, such a procedure is not subject to disproportionate errors caused by traces of more soluble species.

MEASUREMENT OF AQUEOUS SOLUBILITIES

Experimental

Purified samples of the extractants were prepared as previously described [9, 10]. Analyses of the final products, obtained by non-aqueous titration [10] and copper loading [1] techniques, were in the range 97—101%.

Aqueous solubilities of the purified samples were determined by titrating an ethanolic solution of known oxime concentration (ca. 5 mg cm^{-3}) from an Agla microsyringe (0.5-cm^3 capacity) into 200 cm^3 of the well-stirred aqueous phase at 25.0°C. The absorbance of the solution was measured at suitable intervals with a Pye Unicam SP500 spectrophotometer (40-mm silica cells). Typical plots are illustrated in Fig. 1.

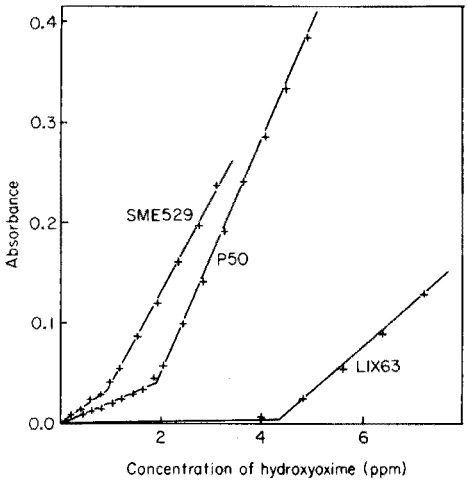

Fig. 1. Solubility titrations for hydroxyoximes in 0.018 mol dm^{-3} H_2SO_4, 0.032 mol dm^{-3} Na_2SO_4 at 25°C. Absorbance is measured at 285 nm.

Spectrophotometric measurements were made at 285 nm since this corresponds to an absorption minimum for β-hydroxyoximes and leads to an especially pronounced discontinuity in the gradient of the solubility plot. The apparent absorbance from light scattering by the dispersions is greater at shorter wavelength. When the chemical absorbance at 285 nm was substantial, however, it was preferable to select an alternative wavelength (600 nm).

The aqueous solution used was 0.018 mol dm^{-3} in sulphuric acid and 0.032 mol dm^{-3} in sodium sulphate (pH 1.78), corresponding approximately in pH value and ionic strength to aqueous phases employed in our kinetic studies of the solvent extraction of copper. In most cases, however, the omission of the sodium sulphate had a negligible effect on the measured solubilities. Similarly verified as having a negligible effect on the reagent solubility was the small volume of ethanol added to the aqueous phase during the titrations.

The validity of the technique was checked by measuring the solubility of biphenyl in distilled water. The value observed, 6.6 ± 0.5 ppm, compares adequately with values of 7.48 [11] and 5.94 [12] ppm, obtained by conventional methods. Maximum errors in the determination are estimated as 10% of the experimental value.

Solubilities of purified extractants

Solubilities at 25°C of the extractants in an aqueous phase of pH value 1.78 are shown in Table 1. LIX 63 is noticeably more soluble than the β-hydroxyoximes among which there is a trend of decreasing solubility with increasing molecular weight. Our value for LIX 63 agrees reasonably with that of Ashbrook [13], but β-hydroxyoxime solubilities are lower than might be inferred from Ashbrook's remaining measurements.

TABLE 1

Solubilities of purified extractants at 25°C in an aqueous phase of pH 1.78

Reagent	Solubility		Reagent	Solubility	
	(ppm)	(μmol dm^{-3})		(ppm)	(μmol dm^{-3})
LIX 65N *anti*	0.33	1.0	SME 529	0.84	3.0
LIX 65N *syn*	1.03	3.0	LIX 63	4.2	15.5
P17	0.36	1.0	Nonylphenol	7.8	35
P50	1.78	6.8	$Cu(LIX\ 65N)_2$	0.10	0.13

Solubility as a function of pH value

Table 2 shows the solubilities at 25°C of one oxime as the aqueous phase pH value is varied. Initial pH values are quoted, since the presence of even small concentrations of ethanol in the solutions during titration make pH values other than the initial pH difficult to interpret. The marked increase in solubility above a threshold pH parallels that noted for naphthenic acid [14].

The results are in accordance with a dissociation model for the aqueous oxime

$$HR_{aq} \rightleftharpoons H^+_{aq} + R^-_{aq} \qquad (1)$$

in which the undissociated oxime (HR) has a limited (1.8 ppm) aqueous solubility and the oxime anion (R^-) has a very much higher (>100 ppm) solubility. A previous measurement [10] gives $\log (K_1^H = [HR]_{aq}[H^+]^{-1}_{aq}[R^-]^{-1}_{aq}) \approx 9.5$ for P50, a value confirmed approximately by the present solubility measurements; in view of the potential errors in solubility measurements, however, it is not recommended that the solubility approach be used to determine $\log K_1^H$ values.

Solubility as a function of temperature

Table 3 shows the reduction in aqueous solubility of purified P50 as temperature is increased. Since the aqueous solubility properties of the oximes depend upon solvation by water molecules, an unfavourable entropy term will become of increasing importance as temperature rises, and the solubility will consequently decrease. The reduction of solubility with increasing temperature forms the basis of cloud point studies [15] of non-ionic detergents.

TABLE 2

Solubility of purified P50 at 25°C in aqueous phases of varying pH values

Initial pH value	1.0	1.8	5.8	8.4	9.5	10.5	11.5	≈12.5
Solubility (ppm)	1.56	1.78	1.82	2.04	2.48	10.4	37	>100

TABLE 3

Solubility of purified P50 at varying temperatures in a standard aqueous phase (pH value 1.78 at 25°C)

Temp. (°C)	15.0	25.0	30.0	35.0	40.0	45.0
Solubility	1.86	1.78	1.68	1.57	1.62	1.48
(ppm)		1.68		1.36	1.65	1.52

Solubility of mixed reagents

Studies related to real systems must consider several components simultaneously. Measurements of such systems are at a preliminary stage; when ethanolic P50 is added to an aqueous phase dosed previously with nonylphenol, a significant reduction in the oxime solubility is noted only when the aqueous nonylphenol concentration is high. Thus 2 ppm and 4 ppm solutions of aqueous nonylphenol have little effect on P50 solubility, but 6 ppm reduces the solubility by a factor of almost two.

MEASUREMENTS OF PARTITION COEFFICIENTS

The foregoing aqueous solubilities measure the limiting concentrations of oxime attainable in an aqueous phase, i.e. the concentrations at equilibrium with an organic phase of pure oxime. Of more direct interest in solvent extraction, however, is a knowledge of the concentration of reagent at equilibrium with a given organic phase containing both oxime and diluent.

Classical solvent extraction theory [16, 17] envisages that for acidic extractants HR there will be distribution of the reagent between aqueous and organic phases governed by a partition coefficient

$$P_{HR} = [HR]_{org}\,[HR]_{aq}^{-1} \tag{2}$$

together with dissociation (eqn. 1) and reaction between the metal cation and the ionized or unionized species R^- or HR in the aqueous phase. The extraction process is completed by the distribution of the uncharged metal complex (CuR_2 for the copper/oxime systems) between the two phases.

$$P_{CuR_2} = [CuR_2]_{org}\,[CuR_2]_{aq}^{-1} \tag{3}$$

Determination of P_{HR} is complicated by the existence of association equilibria in the organic phase [18],

$$j\,HR \rightleftharpoons (HR)_j \tag{4}$$

so that a clear distinction must be drawn between the partition coefficient of the monomeric extractant (eqn. 2) and the overall distribution "coefficient" for the extractant

$$D_{HR} = \Sigma j\,[(HR)_j]_{org}/\Sigma j\,[(HR)_j]_{aq} = \Sigma j\,[(HR)_j]_{org}/[HR]_{aq} \tag{5}$$

The latter equality is justified by the extreme dilution of the aqueous solution,

together with the exceptional hydrogen bonding capability of the aqueous medium, factors known to decrease the self-association of hydroxyoximes [18, 19].

If data are available to relate the total organic reagent concentration to the organic monomer concentration $[HR]_{org}$, then measurement of the distribution "coefficient" D_{HR} will permit the calculation of P_{HR}. Such data are provided by vapour-phase osmometry measurements and calculation as detailed elsewhere [18]; Table 4 shows monomer concentrations in the organic phase calculated from vapour-phase osmometry by two different models of complex formation. Monomer concentrations cannot be obtained without some assumption of the stoicheiometry of the aggregates; figures from the best two models are shown in Table 4 to avoid over-reliance on one model.

Experiments and results

In measuring the distribution coefficients of these reagents, the presence of lower-molecular-weight oximes again presents a problem which cannot be circumvented as in the case of the solubility measurements. However, provided that the proportion of such species is small, repeated aqueous washing of the organic phase should result in their selective removal, while loss of the major component to the aqueous phase will be slight. This procedure is illustrated in Fig. 2, where the u.v. spectra of aqueous phases (0.018 mol dm^{-3} sulphuric acid, 0.032 mol dm^{-3} sodium sulphate) obtained by successive equilibrations with a 0.20-mol dm^{-3} solution of purified SME 529 in n-heptane clearly show the progressive decrease in oxime content caused by the gradual removal of the more soluble species. Aqueous phases were centrifuged before the spectra were measured. With this material, prepared from an early batch of the SME 529 extractant, it was not possible to remove all such species. Even after 20 equilibrations, the aqueous phase spectrum still had not been reduced to that obtained by preparing a solution saturated with respect to the principal component by the technique employed for the solubility measurements.

For the reagent P50, however, after 15 washings of a 0.20-mol dm^{-3} solution in n-heptane with the standard aqueous phase at 1:20 organic:aqueous

TABLE 4

Total reagent concentrations and monomer concentrations for purified P50 in n-heptane, and equilibrium aqueous phase concentrations after twenty washings (pH 1.78)

Total [P50] organic (mol dm^{-3})	Organic [P50] monomer (mol dm^{-3})		[P50] aqueous (ppm)
	(Series)	(Tetramer)	
0.05	0.029	0.039	0.71, 0.80
0.10	0.043	0.056	1.07, 1.09
0.20	0.058	0.073	1.37, 1.39

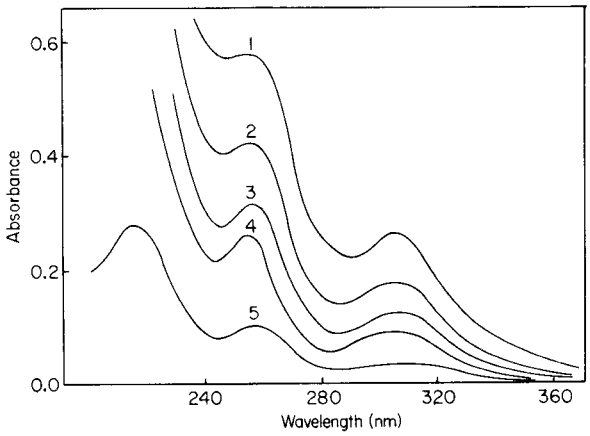

Fig. 2. U.v. absorption spectra of successive aqueous phases (0.018 mol dm^{-3} H_2SO_4, 0.032 mol dm^{-3} Na_2SO_4) equilibrated with 0.20 mol dm^{-3} purified SME 529 in n-heptane at 25°C. Curves 1, 2, 3 and 4 show the first, second, fifth and tenth equilibrations respectively; curve 5 shows the spectrum of a "saturated solution" prepared by microsyringe addition of ethanolic SME 529 to the aqueous phase.

volume ratio, the spectra of successive aqueous phases were identical. These spectra thus represent the equilibrium content of the pure extractant transferred into the aqueous phase; the concentration was determined from a calibration plot at 261 nm, obtained by the titration technique. Appropriate dilutions of the 0.20 mol dm^{-3} solution with n-heptane, followed by re-equilibration with fresh aqueous phases, allowed the distribution isotherm to be constructed. Some values are shown in Table 4.

A plot of the aqueous phase concentrations of oxime against the organic monomer concentrations resulted in the expected straight lines (eqn. 2). The slopes gave $P_{HR} = 1.05 \times 10^4$ and 1.38×10^4, respectively, for the two organic phase models based on series or tetramer aggregation.

CONCLUSION

The partition coefficient for one oxime has been obtained successfully, but the method is difficult to apply to other oximes because of interference by low-molecular-weight material or the relatively low aqueous solubilities of the reagents. Other approaches are being tried, in particular to measure partition coefficients for the neutral copper—oxime complexes, and to show the influence of the organic diluent on partition.

The authors thank Nchanga Consolidated Copper Mines (Zambia) for the financial support of this work.

REFERENCES

1 R. J. Whewell, M. A. Hughes and C. Hanson, J. Inorg. Nucl. Chem., 38 (1976) 2071.
2 D. S. Flett, D. N. Okuhara and D. R. Spink, J. Inorg. Nucl. Chem., 35 (1973) 2471.
3 R. L. Atwood, D. N. Thatcher and J. D. Miller, Met. Trans. A.I.M.E., 6B (1975) 465.
4 C. A. Fleming, National Institute for Metallurgy Report No. 1793, Johannesburg, 1976.
5 K. S. Koppiker and N. Maity, Anal. Chim. Acta, 75 (1975) 239.
6 C. Hanson, M. A. Hughes, J. S. Preston and R. J. Whewell, J. Inorg. Nucl. Chem., 38 (1976) 2306.
7 A. J. van der Zeeuw, Ger. Offen., 2, 510, 352 (1975).
8 P. J. Brooker and M. Ellison, Chem. Ind., (1974) 785.
9 T. A. B. Al-Diwan, M. A. Hughes and R. J. Whewell, J. Inorg. Nucl. Chem., 39 (1977) 1419.
10 J. S. Preston and R. J. Whewell, J. Inorg. Nucl. Chem., 39 (1977) 1675.
11 R. L. Bohon and W. F. Claussen, J. Am. Chem. Soc., 73 (1951) 1571.
12 L. J. Andrews and R. M. Keefer, J. Am. Chem. Soc., 71 (1949) 3645.
13 A. W. Ashbrook, Anal. Chim. Acta, 58 (1972) 115.
14 A. W. Ashbrook, Min. Sci. Eng., 5 (1973) 169.
15 K. Durham in K. Durham (Ed.), Surface Activity and Detergency, MacMillan, London, 1961.
16 I. M. Kolthoff and E. B. Sandell, J. Am. Chem. Soc., 63 (1941) 1906.
17 H. M. Irving and R. J. P. Williams, J. Chem. Soc., (1949) 1841.
18 R. J. Whewell, M. A. Hughes and C. Hanson, International Solvent Extraction Conference (ISEC '77), Toronto, September, 1977.
19 J. S. Preston, unpublished data.

Analytica Chimica Acta, 97 (1978) 357—363

AN H.P.L.C.—FLUORIMETRIC ANALYSIS FOR L-DOPA, NORADRENALIN AND DOPAMINE

PETER M. FROEHLICH* and THOMAS D. CUNNINGHAM**

Trace Analysis Research Centre, Department of Chemistry, Dalhousie University, Halifax, N.S. B3H 4J3 (Canada)

(Received 22nd August 1977)

SUMMARY

A rapid (10 min) and sensitive determination of 3,4-dihydroxyphenyl-L-alanine (L-dopa), noradrenalin and dopamine has been developed. The assay involves the separation of the compounds with a strong cation-exchange resin, followed by post-column derivatization with *o*-phthalaldehyde. The fluorescence of the derivative is measured in a flow-through fluorimeter and is linear over a concentration range of 500 times the lower detection limit (4.6 ng for L-dopa, 7.5 ng for noradrenalin and 9.3 ng for dopamine). The assay does not require the stringent removal of oxidizing materials which is necessary for electrochemical detection, and may be useful in the analysis of biological samples.

Analytical techniques for the catecholamines in tissues and body fluids are extremely useful in medicine and biochemistry. The catecholamines are neurotransmitters; analyses for compounds such as dopamine and 3,4-dihydroxyphenyl-L-alanine [L-dopa] in various tissues such as the brain are very important in the development of an understanding of the central nervous system. A number of diseases can be characterized by abnormal levels of catecholamines; for example, patients with Parkinson's disease have lower levels of dopamine than normal [1]. Parkinson's disease may be treated by administration of L-dopa [2]. (L-Dopa, a precursor of dopamine, can cross the blood/brain barrier, while the amine cannot.) The diagnosis of some tumors may be made via catecholamine analysis; a useful monitor for neuroblastoma is the increased secretion of dopamine or noradrenalin [3]. McMillan has suggested that the production of excessive dopamine is associated with malignancy [4].

Analyses for the catecholamine in biological samples must consider their low level (e.g. 0.33 mg of dopamine per g of rat cortex [5]) and their chemical similarities (e.g. dopamine and epinephrine differ only by a hydroxyl group on the aliphatic side-chain). The determination of

*Present address: Department of Chemistry, North Texas State University, Denton, TX 76203, U.S.A. All correspondence to this address.

**Present address: Experiment Station, Chemical Laboratories, Agriculture Building, University of Missouri, Columbia, MO 65201, U.S.A.

catecholamines often involves their separation on alumina, followed by formation of a fluorescent derivative by oxidation [6] to form the corresponding trihydroxyindole. Many variations on this theme have been reported [7] but the procedure is tedious. Other separation procedures involve boric acid as a chelating agent to elute the catecholamine from a cation-exchange resin [8] or involve a boric acid gel [9]. These procedures cannot isolate L-dopa, and the use of alumina appears to be a method of choice for biological samples.

Modern high-pressure liquid chromatography (h.p.l.c.) coupled with detection of the analyte (or a derivative thereof) in the eluant is an extremely powerful technique. Several analyses for the catecholamines with an h.p.l.c. cation-exchange resin have been reported; electrochemical detection [10—12], u.v. absorption [13] or post-separation formation of the fluorescent trihydroxyindole derivative [14] have been used. An analytical development of considerable utility has been the use of reagents which react rapidly with primary amines and amino acids to form fluorescent derivatives. Fluorogenic reagents such as fluorescamine [15] and *o*-phthalaldehyde [16] lead to very rapid and sensitive analyses for amino acids and primary amines.

It is possible to form a fluorescent derivative of an amino acid in the eluant stream from h.p.l.c.; such procedures lead to very rapid and sensitive assays [17, 18]. DeBelleroche and co-workers [19] have shown that an amino acid analyzer can be adapted to detect the *o*-phthalaldehyde derivatives of catecholamines.

A simple h.p.l.c.—fluorescence assay for catecholamines, capable of detecting ca. 30 pmol of dopamine, L-dopa or noradrenalin in less than 10 min by means of a cation-exchange resin and post-column derivatization has been developed.

EXPERIMENTAL

Reagents

L-Dopa, dopamine, and *o*-phthalaldehyde (Sigma Chemical Co., St. Louis, Mo.) and noradrenalin (Calbiochem, La Jolla, Cal.) were used. Salts used to prepare buffers (Fisher Scientific Co., Fairlawn, N.J.) were certified ACS grade. 2-Mercaptoethanol was obtained from Eastman (Rochester, N.Y.). These chemicals were used as received.

Hydrochloric acid (reagent grade) (Baker Chemical Co., Phillipsburg, N.J. or Allied Chemical Co., Morristown, N.J.) was diluted to 6 M and distilled from $K_2Cr_2O_7$ to oxidize primary amines which could result in high blanks and poor detection limits [20].

The elution buffer was an adaptation of that used [13] in the separation of catecholamines, and was obtained by diluting the buffer solution (10.5 g of citric acid, 2.1 ml of glacial acetic acid, 4.8 g of NaOH and 8.2 g of sodium acetate per liter) such that $[Na^+] = 0.04$ M; the pH was adjusted to 2.80 with distilled HCl.

Following separation, the eluant stream was mixed with a solution containing 0.2 g of *o*-phthalaldehyde in 2.5 ml of ethanol and 0.5 ml of 2-mercaptoethanol diluted to 250 ml with 0.05 M borax buffer (adjusted to pH 10.2 with 5 M NaOH).

All solutions were prepared from doubly distilled water and were degassed (by applying a slight vacuum and heating the solution) before use in the chromatograph.

Standard solutions of the biogenic amines, prepared daily, were protected from light by aluminum foil to prevent photodecomposition.

The separations were effected on 37—50-μm Bondapak SCX strong cation-exchange resin (Waters Associates, Milford, Mass.).

Apparatus

The separation was effected on the liquid chromatograph described below (see Fig. 1).

(a) Pump: Orlita kG constant flow diaphragm pump (Orlita Dossiertechnik, General Federal Republic).

(b) Injection port: Whitey ball valve No. 4356-346, Whitey Research Tool Co., Emeryville, Ca. as used by Cassidy and Frei [21]. Stopped flow on-column injection was made with a 10-μl syringe equipped with 10-cm replaceable needles (Hamilton Co., Reno, Nev.).

(c) Column: a precision-bore stainless steel column (29-cm long, 7-mm o.d., 3-mm i.d.; Analabs, Inc., North Haven, Conn.) was packed with the cation-exchange resin by the tap-fill method [22]. A glass wool plug was placed in one end and a fritted zero dead volume 1/4—1/16-in reducing union (Applied Science Lab., Inc., State College, Pa.) was connected to the detector end.

(d) Post-separation mixing system: a peristaltic pump (Polystaltic Pump, Model 2-6100, Buchler Instruments, Fort Lee, N.J.) was used to introduce the reagents and buffers, required to form the *o*-phthalaldehyde derivative, into the eluant stream. The mixing tee was connected to the detector by

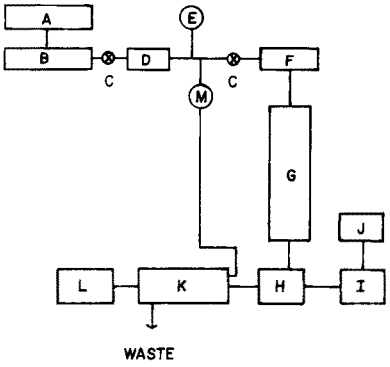

Fig. 1. Schematic diagram of the chromatograph. A, eluant reservoir; B, pump; C, ball valve; D, filter; E, pressure gauge; F, injection port; G, column; H, mixing tee; I, peristaltic pump; J, reagent reservoir; K, detector; L, recorder; M, micrometer metering valve.

Teflon tubing (20 cm × 0.018-in. i.d.) with heat shrinkable Teflon tubing (Penntube Plastics Co., Clifton Heights, Pa.).

(e) Detector: a fluoromonitor model 1209 (Laboratory Data Control, Inc., Riviera Beach, Fla.) was used for fluorescence detection. Preliminary experiments involved the use of a u.v. monitor (LDC Inc.) connected to the column outlet with 5 cm × 0.01-in. i.d. stainless steel tubing.

Manual fluorimetric measurements were made with a spectrophotofluorimeter (American Instrument Co., Silver Spring, Md.) equipped with a Hamamatsu P21 photomultipler and a Hanovia 901C Mercury—Xenon arc.

o-Phthalaldehyde derivatives were formed by mixing 0.1 ml of a solution of noradrenalin (151 mg in 1 l of 0.1 M hydrochloric acid) to 1.8 ml of either 0.05 M sodium pyrophosphate or sodium borate buffer, 1.0 ml of 2-mercaptoethanol (5 ml in 1 l of ethanol) and 0.1 ml of *o*-phthalaldehyde solution (51 mg of *o*-phthalaldehyde dissolved in 2.0 ml of methanol per 25 ml of 0.05 M sodium borate or sodium pyrophosphate buffer). The mixture was mixed on a vortex for 20 s. Fluorescence was measured at 455 nm (upon excitation at 340 nm).

RESULTS AND DISCUSSION

Chromatography

A separation of L-dopa, dopamine and noradrenalin was effected on the cation-exchange resin with the eluant buffer described. The concentration of Na^+ was lower than that used by Riceberg et al. [13] to make it easier to change the pH of the eluant to that required for the formation of the fluorescent derivative. McMurtrey et al. [23] have shown that the capacity factors for the compounds of interest are fairly independent of the molarity and the pH of the eluant over the range pH 3—7 and the 0.1 to 1.0 N concentration range. As indicated in Fig. 2, useful chromatograms were obtained with the modified buffer.

Formation of the fluorescent derivative

o-Phthalaldehyde derivatives were formed as described in the Experimental section. Maximum intensity was observed within 1 min after mixing. This observation is similar to that made by Benson and Hare [18] and contradicts the 5-min incubation time suggested by Roth [16].

Fluorescence detection with h.p.l.c. separation

Interfacing of the chromatographic separation with post-separation formation and detection of the *o*-phthalaldehyde derivative led to a satisfactory analytical procedure for the catecholamines. Consequently, experiments were performed to determine the sensitivity and limitations of the assay. An increase in the reaction temperature from 22 ± 1°C to 45 ± 1°C led to an enhancement of 50% in the signal from the L-dopa—*o*-phthalaldehyde derivative. (The temperature was changed by immersing the coil from the

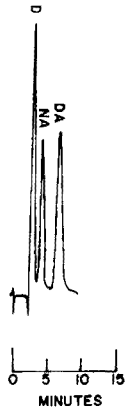

Fig. 2. Separation of biogenic amines with fluorescence detection of their *o*-phthalaldehyde derivatives. D = L-dopa, NA = noradrenalin, DA = dopamine.

mixing tee to the detector in a temperature-controlled water bath.) The reaction of *o*-phthalaldehyde with L-dopa probably does not go to completion at the lower temperature. An alternative to the use of the water bath might be to use a longer reaction coil; the only possible drawback to such an arrangement would be a loss in chromatographic resolution.

A typical chromatogram is presented in Fig. 2; 7 or 8 analyses per hour can be made. The linear range of the assay was ca. 500—1000, depending on the catecholamine, as indicated in Table 1. It may be possible to lower the absolute sensitivity to ca. 20 pmol by the use of highly purified *o*-phthalaldehyde (Durrum Chemical Co., Palo Alto, Calif.) which is considerably more expensive than the material used in routine work.

The reproducibility was studied. The standard deviation for the detection of a given metabolite (over a series of seven injections) was about 8%. A major cause of the variation is suspected to be the pulsation of the peristaltic pump used to feed the *o*-phthalaldehyde into the eluant stream.

This procedure will be especially valuable when catecholamines such as adrenalin or metanephrine (which are not primary amines) are present,

TABLE 1

Sensitivity of the assay

	Min. det.[a] (pmol)	Quantity (ng)	Upper limit of linear range (nmol)
L-Dopa	23.1	4.6	33
Noradrenalin	36.5	7.5	18
Dopamine	48.8	9.3	28

[a]Minimum detectable amount is defined as the quantity required to produce a peak with a height twice the baseline noise level.

because only primary amines will react with *o*-phthalaldehyde. An additional advantage in the use of fluorimetric derivatization accrues from the fact that the amine group is the functional group of interest. The electrochemical detection step involves oxidation of the catechol moiety of the compound of interest, and care must be taken that the *o*-quinone is not formed prior to detection. Some of the precautions required for electrochemical detection in which platinum needles are required for h.p.l.c. injection and all solutions used must be deoxygenated with purified nitrogen, have been described [8]; these steps were taken to ensure that iron or oxygen would not oxidize the catecholamines before their detection. An additional advantage in a fluorimetric analysis is that the presence of oxidizing compounds is not important in the work-up of biological samples. If the prime interest is in the catecholamines, as is usually the case [6—9], this procedure is more convenient than that of Belleroche et al. [19]. The analytical procedure outlined above can separate the compounds of interest in less than 10 min with a pellicular ion-exchange resin ambient temperature in an isocratic mode, in contrast to the gradient system used with a thermostated column [19].

The procedure described is similar to that of Schwedt [24] who condensed the amines with ethylenediamine, but the optimal conditions for the formation of the *o*-phthalaldehyde derivative are milder than those for the ethylenediamine derivatives. The procedure developed has high sensitivity, speed and ease of operation and should be useful for the routine measurement of primary catecholamines.

We thank the National Research Council of Canada for support. Special thanks are due to Drs. W. A. Aue and S. Kapila of Dalhousie University for their assistance.

[Note added in proof. The paper by G. Schwedt (Anal. Chim. Acta, 92 (1977) 337) which describes a somewhat similar procedure, appeared while this paper was in process of publication.]

REFERENCES

1 G. Curzon, in Cummings (Ed.), Biochemical Aspects of Nervous Disease, Plenum Press, New York, 1972, p. 151.
2 T. A. Hare, B. L. Beaseley, C. A. Chambers et al., Clin. Chim. Acta, 45 (1973) 273.
3 M. L. Vooheesin, in L. I. Gardner (Ed.), Endocrine and Genetic Diseases of Childhood, W. B. Saunders, Philadelphia, 1969, p. 781.
4 M. McMillan, Lancet, 2 (1956) 284.
5 R. F. Butterworth, F. Landreville, M. Guitard and A. Barbeau, Clin. Biochem., 8 (1975) 298.
6 A. H. Anton and D. F. Sayre, J. Pharmacol. Exp. Ther., 145 (1964) 326.
7 For example, H. Weil-Malherbe and L. B. Bigelow, Anal. Biochem., 22 (1968) 321; W. G. Wood and R. W. Mainwaring-Burton, Clin. Chim. Acta, 61 (1975) 297; and C. Valori, C. A. Brunori, V. Renizi and L. Corea, Anal. Biochem., 33 (1970) 158.
8 C. Refshauge, P. T. Kissinger, R. Dreiling, L. Blank, R. Freeman and R. N. Adams, Life Sci., 14 (1974) 311.

9 S. Higa, T. Suzuki, A. Hayashi, I. Tsuge and Y. Yamamura, Anal. Biochem., 77 (1977) 18.
10 F. N. Minard, J. C. Cain and D. S. Grant, J. Pharm. Pharmacol., 27 (1975) 288.
11 P. T. Kissinger, R. M. Riggin, R. L. Alcorn and L. D. Ran, Biochem. Med., 13 (1975) 299.
12 R. M. Riggin, R. L. Alcorn and P. T. Kissinger, Clin. Chem., 22 (1976) 782.
13 L. J. Riceberg, R. C. Abeles, H. Van Vunakis and A. Tashjian, Reprint no. DS048F, June 1974, Waters Assoc., Milford, Mass.
14 K. Mori, Rinsho Byori, 22 (1974) 304.
15 S. Udenfriend, S. Stein, P. Böhlen, W. Dairman, W. Leimgruber and M. Weigle, Science, 178 (1972) 871.
16 M. Roth, Anal. Chem., 43 (1971) 880.
17 S. Stein, P. Böhlen, J. Stone, W. Dairman and S. Udenfriend, Arch. Biochem. Biophys., 155 (1973) 203.
18 J. R. Benson and P. E. Hare, Proc. Nat. Acad. Sci., 72 (1975) 619.
19 J. DeBelleroche, C. R. Dykes and A. J. Thomas, Anal. Biochem., 71 (1976) 193.
20 C. Schwabe and J. C. Catlin, Anal. Biochem., 61 (1974) 302.
21 R. M. Cassidy and R. W. Frei, Anal. Chem., 44 (1972) 2250.
22 J. J. Kirkland, J. Chromatogr. Sci., 10 (1972) 129.
23 K. D. McMurtrey, L. R. Meyerson, J. L. Cashaw and V. E. Davis, Anal. Biochem., 72 (1976) 566.
24 G. Schwedt, Chromatographia, 10 (1977) 92.

Analytica Chimica Acta, 97 (1978) 365—372

COMPORTEMENT ELECTROCHIMIQUE DU MERCURE ET DU BISMUTH DANS L'ACÉTAMIDE FONDU A 98°C

M. POURNAGHI**

Laboratoire de Chimie, Institut National des Sciences et Techniques Nucléaires, Saclay (France)

J. DEVYNCK* et B. TRÉMILLON

Laboratoire d'Electrochimie Analytique et Appliquée (LA 216), Ecole Nationale Supérieure de Chimie de Paris, Université Pierre et Marie Curie 11, rue Pierre et Marie Curie, 75231 Paris Cedex 05 (France)

(Reçu le 24 octobre 1977)

RESUME

Le comportement acide des ions du mercure et du bismuth a été étudié dans l'acétamide fondu, à 98°C. Par voltammétrie et potentiométrie on a montré que seul le mercure au degré d'oxydation (2+) est stable et qu'une première réaction de solvolyse totale des ions Hg^{2+}, traduisant leur caractère mono-acide fort, peut être observée. A partir de titrages potentiométriques, on a déterminé la constante de la seconde acidité (faible) des ions Hg^{2+} (formation de $Hg(AcNH)_2$): pK_{A_2} = 4,8. On a montré également le caractère diacide fort de Bi^{3+} et on a mis en évidence le composé $Bi(AcNH)_3$ peu soluble, dont on a déterminé le produit de solubilité: pK_s = 7,9. Les propriétés du mercure et du bismuth sont traduites sous la forme de diagrammes potentiel—pH.

SUMMARY

The electrochemical behaviour of mercury and bismuth in molten acetamide at 98°C

The acidic behaviour of mercury and bismuth ions has been studied in molten acetamide at 98°C. Voltammetric and potentiometric measurements have shown that mercury is stable in solution only in the divalent state. Mercury(II) ions are strongly acidic, their solvolysis being complete. From potentiometric titrations, the acidity constant of the second (weak) acidity of Hg^{2+} was found to be pK_{A_2} = 4.8. It is also shown that Bi^{3+} is a strong diacid and that $Bi(AcNH)_3$ is only slightly soluble. The solubility product was found to be pK_s = 7.9. The properties of mercury(II) and bismuth are represented on potential—pH diagrams.

Les ions mercure(II) et bismuth(III) forment, dans l'acétamide fondu, à 98°C, des complexes acétamidure qui se traduisent par leur caractère acide. Le complexe $Hg(AcNH)_2$ avait été mis en évidence par Jander et Winkler [1]; plus récemment, l'utilisation d'une électrode de verre a permis de montrer que Hg^{2+} et Bi^{3+} possèdent un caractère acide fort, et de mettre en évidence

---

**Adresse actuelle: Faculté des Sciences, Université de l'Azarabadeghan, Tabriz (Iran).

les composés $Hg(AcNH)_2$ et $Bi(AcNH)_3$, qualitativement seulement par suite du mauvais fonctionnement de l'électrode de verre en milieu basique [2]. Nous avons donc repris l'étude du comportement acide de ces ions métalliques par polarographie, par voltammétrie avec une électrode de bismuth et par potentiométrie à courant nul. Nous avons confirmé les résultats obtenus avec l'électrode de verre et, de plus, déterminé les constantes de stabilité des complexes acétamidure formés.

PARTIE EXPERIMENTALE

Solvant

L'acétamide utilisé (Prolabo, Paris) était purifié par recristallisation dans le dioxanne absolu [3]. La teneur en eau, mesurée par la méthode de Karl Fisher, était inférieure à 10^{-3} mol kg^{-1}. L'une des princiaples impuretés du solvant est l'ion acétate provenant de l'hydrolyse partielle de l'acétamide, selon la réaction: $AcNH_2 + H_2O \rightleftharpoons AcO^- + NH_4^+$. Cet ion acétate fait apparaître en polarographie une vague d'oxydation du mercure, avec $E_{1/2} = + 0{,}350$ V, vague qui disparaît lors de l'addition d'un acide fort car l'acide acétique est un acide faible dans l'acétamide ($pK_A = 5{,}8$ [4]).

Solutés

Les acides et bases ont été préparés selon les diverses méthodes décrites précédemment [2].

Electrodes et appareillage

L'électrode de référence utilisant le système Ag/AgCl a été réalisée selon la méthode décrite par Guiot et Trémillon [4].

Les courbes voltammétriques ont été obtenues avec des microélectrodes tournantes de platine ($S = 2$ mm^2) ou de bismuth ($S = 2$ mm^2) et les courbes polarographiques ont été enregistrées en stillation forcée (temps de goutte: 1 s). L'appareillage était constitué d'un ensemble Tacussel comprenant: un potentiostat type PRT 20-2Z, un pilote Servovit 2, une unité d'adaptation UAP 1 et un enregistreur EPL 2.

Toutes les expériences ont été réalisées dans une cellule Tacussel type RM 01 à double paroi, thermorégulée à la température de 98°C ± 0,1°C.

RESULTATS EXPERIMENTAUX

Mercure

Degré d'oxydation. L'oxydation électrochimique du mercure en milieu neutre ou acide peut a priori conduire soit au mercure(I), soit au mercure(II). On peut montrer que, dans l'acétamide, Hg(I) n'est pas stable et subit une diminution: l'introduction de nitrate mercure(I) provoque en effet l'apparition d'un précipité noir et on observe une vague de réduction unique à une électrode de platine poli tournante, comme à l'électrode à gouttes de mercure. Le

mercure(II) présente une vague de réduction identique, aucun précipité n'apparaîssant alors.

L'augmentation de hauteur de la vague de réduction correspondant à l'addition de mercure(I) à une solution de mercure(II) est proportionnelle à la moitié de la concentration du mercure(I) ajouté. Ceci signifie que la moitié de celui-ci a été transformée en mercure(II). On peut donc conclure que le mercure(I) n'existe pas en solution dans l'acétamide fondu en milieu acide et qu'il est dismuté en mercure(II) et en mercure, qui constitue le précipité noir observé (en milieu acide nitrique concentré, le mercure formé est oxydé et disparaît après un court intervalle du temps).

Solvolyse des ions Hg^{2+}, en milieu neutre ou acide. Les ions Hg^{2+} provoquent une réaction de solvolyse totale que nous avions préalablement mise en évidence à l'aide d'une électrode de verre [2]. Les ions Hg^{2+} ont ainsi un comportement mono-acide fort: $Hg^{2+} + AcNH_2 \rightarrow Hg(AcNH)^+ + H^+$. L'oxydation du mercure en milieu acide ou neutre correspond donc à la réaction: $Hg + AcNH_2 - 2e^- \rightarrow Hg(AcNH)^+ + H^+$, et le potentiel d'équilibre E_{eq} d'une électrode de mercure est théoriquement défini par la relation.

$$E_{eq} = E^0_{Hg} - 0{,}037\ pH + 0{,}037 \log [Hg(AcNH)^+] \qquad (1)$$

Expérimentalement, la variation du potentiel à courant nul d'une électrode de mercure en fonction de la concentration des ions Hg^{2+} (en milieu acide fort $HClO_4$ 0,1 M) a été trouvée linéaire (pour. $10^{-3} < [Hg^{2+}] < 2.10^{-2}$ mol kg^{-1}); la pente de la droite (0,043 V) étant proche de la valeur théorique. L'extrapolation à concentration 1 mol kg^{-1} permet de déterminer la valeur du potentiel normal apparent: $E^0 = +0{,}752$ V (±5 mV).

Milieu basique. Comme en milieu acide, seul le degré d'oxydation 2+ est stable en présence d'ions acétamidure. Les complexes acétamidure du mercure(II) ont été mis en évidence par polarographie anodique et par potentiométrie à courant nul. Les courbes courant—potentiel d'oxydation d'une électrode à gouttes de mercure en présence d'acétamidure de sodium font apparaître deux vagues caractéristiques de la formation de complexes acétamidure de mercure. La première vague est caractérisée par la valeur $E_{1/2} = -300$ mV et une hauteur proportionnelle à la concentration d'acétamidure de sodium ajouté; la seconde vague est moins bien définie, située vers +300 mV avec une hauteur sensiblement égale à celle de la première (Fig. 1).

Ces courbes montrent donc qu'il existe deux complexes acétamidure du mercure. La première vague peut en effet être attribuée à la réaction électrochimique: $Hg + 2AcNH^- - 2e^- \rightarrow Hg(AcNH)_2$, et la seconde à la réaction: $Hg + Hg(AcNH)_2 - 2e \rightarrow 2Hg(AcNH)^+$. (2)

D'autre part, la courbe de titrage des ions $AcNH^-$ par Hg^{2+}, suivi par potentiométrie avec une électrode de mercure est représentée sur la Fig. 2. Elle présente deux parties bilogarithmiques.

La première partie correspond à la formation du complexe $Hg(AcNH)_2$ (soluble et incolore), pour $[Hg^{2+}]_{aj} < [AcNH^-]_{init}/2$, L'oxydation du mercure en milieu basique dans cette partie correspond donc bien à la

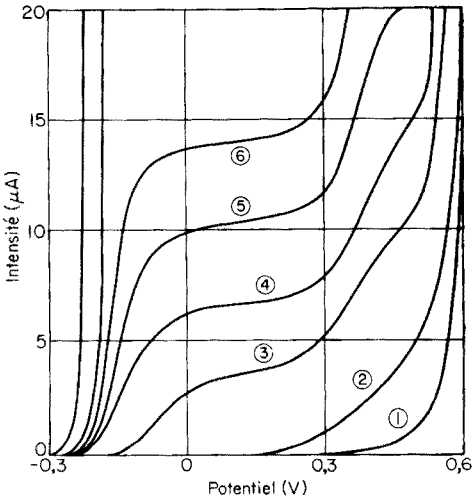

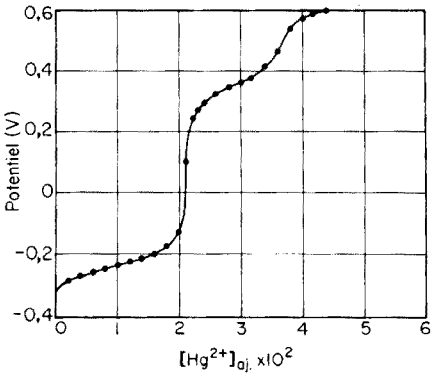

Fig. 1. Courbes polarographiques anodiques: (1) en milieu acide ($HClO_4$ 0,1 mol kg^{-1}); (2) en milieu neutre; en présence d'acétamidure de sodium: (3) $3{,}10^{-3}$; (4) 6.10^{-3}; (5) 9.10^{-3}; (6) $1{,}2.10^{-2}$; (7) 5.10^{-2}; (8) 0,1 mol kg^{-1}; Electrolyte support: $LiClO_4$ 1 mol kg^{-1}.

Fig. 2. Courbe de titrage potentiométrique des ions acétamidure (5.10^{-2} mol kg^{-1}) par les ions Hg(II) (ajoutés sous forme nitrate), électrode indicatrice de mercure.

réaction (2) ci-dessus. L'analyse de la courbe dans cette première partie vérifie la formule du complexe formé, la courbe: $E_{eq} = f(\log [Hg(AcNH)_2/]/[AcNH^-]^2)$ étant une droite de pente 0,043 V, valeur proche de la valeur théorique (0,037 V).

La deuxième partie de la courbe correspond à la formation du complexe $Hg(AcNH)^+$ à partir du complexe $Hg(AcNH)_2$, pour $[AcNH^-]_{init}/2 < [Hg^{2+}]_{aj} < [AcNH^-]_{init}$, selon la réaction $Hg(AcNH)_2 + Hg^{2+} \rightleftharpoons 2Hg(AcNH^+)$.

Le titrage inverse (titrage des ions Hg^{2+} par $AcNH^-$) présente également 2 points équivalents (Fig. 3): la première partie, monologarithmique, correspond à la neutralisation des ions H^+ libérés par la réaction de solvolyse, pour $[AcNH^-]_{aj} < [Hg(II)]_{init}$; la seconde partie de la courbe, entre le premier et le deuxième point équivalent, est bilogarithmique et correspond à la formation du complexe $Hg(AcNH)_2$ à partir de $Hg(AcNH)^+$, pour $[AcNH^-]_{aj} > [Hg^{2+}]_{init}$, selon la réaction: $Hg(AcNH)^+ + AcNH^- \rightleftharpoons Hg(AcNH)_2$.

Ceci confirme la réaction d'oxydation attribuée à la seconde vague polarographique précédente.

Constantes de formation des complexes acétamidure du mercure. Le comportement acide fort de Hg^{2+} ne permet pas de calculer la constante de formation du premier complexe $Hg(AcNH)^+$ mais permet de conclure que

$$K_1 = [Hg(AcNH)^+]/[Hg^{2+}]\,[AcNH^-] > 1/K_i = 10^{14,6} \qquad (3)$$

(K_i étant le produit ionique du solvant, égal à $10^{-14,6}$, déterminé par Guiot et Trémillon [4]).

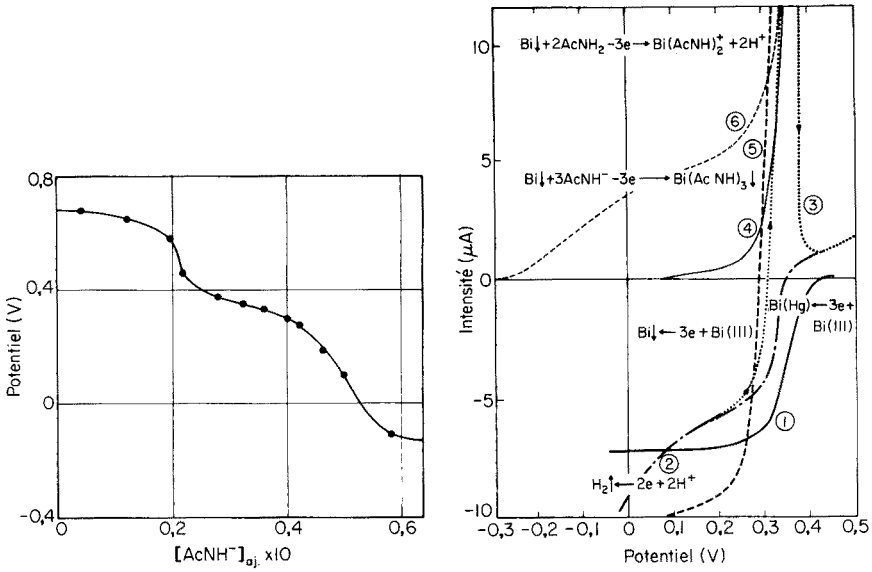

Fig. 3. Courbe de titrage potentiométrique des ions Hg(II) 2.10^{-2} mol kg^{-1} par les ions acétamidure (10^{-1} mol kg^{-1}) préparés par réduction coulométrique du solvant, électrode indicatrice de mercure.

Fig. 4. Courbes voltammétriques des systèmes du bismuth à différentes électrodes. Electrolyte support: $LiClO_4$ 1 mol kg^{-1}. (1) Réduction de Bi(III) (4.10^{-3} mol kg^{-1}) à l'électrode à gouttes de mercure; (2) à l'électrode de platine; (3) oxydation du bismuth, préablement déposé sur platine; (4) oxydation d'une électrode de bismuth en milieu $HClO_4$ 0,1 mol kg; (5) réduction de Bi(III) (4.10^{-3} mol kg^{-1}) à une électrode de bismuth; (6) oxydation du bismuth en milieu $AcNH^-$ 3.10^{-3} mol kg^{-1}.

De la première partie de la courbe de titrage de la Fig. 2 et de la seconde partie de celle de la Fig. 3, on peut tirer la valeur de la constante de formation de $Hg(AcNH)_2$

$$K_2 = [Hg(AcNH)_2]/[Hg(AcNH)^+]\ [AcNH^-] = 10^{9,8}\ mol^{-1}\ kg \qquad (4)$$

D'où: $pK_{A_2} = 14,6 - 9,8 = 4,8$.

Bismuth

Les ions Bi^{3+} manifestent en solution aqueuse un comportement acide que nous avons tenté de retrouver en solution dans l'acétamide fondu. Nous avons donc étudié les complexes acétamidure du bismuth par voltammétrie et par potentiométrie à une électrode de bismuth.

Degré d'oxydation. L'oxydation coulométrique du bismuth conduit au bismuth(III) qui est le seul degré d'oxydation stable dans l'acétamide fondu.

Voltammétrie et potentiométrie en milieu acide ou neutre. Les courbes voltammétriques d'une solution de Bi(III) à une électrode de platine font apparaître une seule vague de réduction (Fig. 4, courbe 2). Un pic de redissolution du bismuth déposé sur l'électrode peut également être observé

(Fig. 4, courbe 3). A l'électrode à gouttes de mercure, on obtient une vague polarographique (Fig. 4, courbe 1) qui correspond à la formation d'amalgame de bismuth. Enfin, l'oxydation d'une électrode de bismuth fournit la courbe 4 et la réduction de Bi(III) sur bismuth la courbe 5 (Fig. 4).

Comme dans le cas des ions Hg^{2+}, la solvolyse totale des ions Bi^{3+}, selon la réaction: $Bi^{3+} + 2AcNH_2 \rightarrow Bi(AcNH)_2^{+} + 2H^{+}$, avait été mise en évidence à partir de mesures effectuées à l'aide de l'électrode de verre [2].

Le système électrochimique du bismuth en milieu acide et neutre est donc le suivant: $Bi + 2AcNH_2 - 3e^{-} = Bi(AcNH)_2^{+} + 2H^{+}$, le potentiel d'équilibre répondant théoriquement à la formule

$$E_{eq} = E^0_{Bi} + 0{,}025 \log [Bi(AcNH)_2^{+}]\ [H^{+}]^2$$

$$= E^0_{Bi} - 0{,}049\ pH + 0{,}025 \log [Bi(III)] \qquad (5)$$

Nous avons étudié expérimentalement les variations du potentiel de l'électrode de bismuth en fonction de la concentration des ions Bi(III), le pH du milieu étant fixé par de l'acide perchlorique 0,2 mol kg^{-1} (concentration suffisante pour que les variations de pH provoquées par l'introduction de Bi^{3+} soient négligeables). Nous avons obtenu une droite dont la pente (0,025) est pratiquement égale à la valeur théorique. L'extrapolation à la concentration de Bi(III) 1 mol kg^{-1} conduit à la valeur du potentiel normal apparent: $E^0_{Bi} = 0{,}387$ V (±2 mV).

Milieu basique. L'oxydation d'une électrode de bismuth poli tournante, en milieu basique, fait apparaître une vague assez mal définie et peu reproductible (Fig. 4, courbe 6), qui doit correspondre à la réaction électrochimique: $Bi + 3AcNH^{-} - 3e^{-} \rightarrow Bi(AcNH)_3\downarrow$. La formation de précipité d'acétamidure de bismuth à l'électrode ne permet pas une interprétation quantitative de cette courbe.

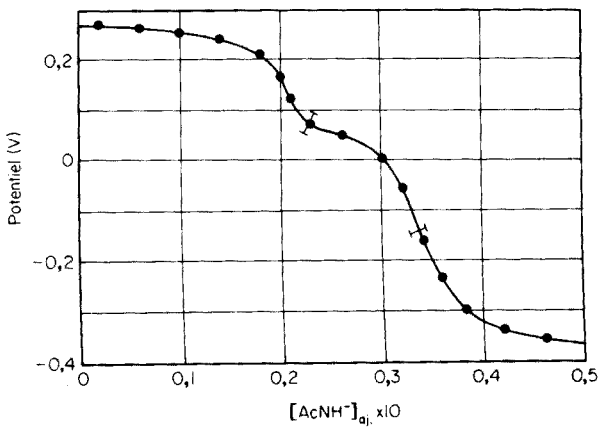

Fig. 5. Courbe de titrage potentiométrique des ions Bi(III) (2.10^{-2} mol kg^{-1}) par les ions acétamidure (0,1 mol kg^{-1}), électrode indicatrice de bismuth.

D'autre part, une courbe de titrage d'une solution de Bi(III) par l'acétamidure de sodium est représentée sur la Fig. 5. En effectuant ce titrage, nous avons constaté que la solution, initialement limpide, le demeure jusqu'au premier point équivalent; il apparaît ensuite un précipité blanc. Les courbes de titrage comprennent deux parties: la première, monologarithmique, correspond à la neutralisation des ions H^+ libérés par solvolyse, pour $[AcNH^-]_{aj} < 2[Bi(III)]_{init}$; la seconde, également monologarithmique, correspond à la formation de l'acétamidure de bismuth insoluble, selon la réaction: $Bi(AcNH)_2^+ + AcNH^- \rightarrow Bi(AcNH)_3\downarrow$.

Produit de solubilité de Bi(AcNH)$_3$. L'expression du potentiel d'équilibre de l'électrode de bismuth dans la seconde partie de la courbe de titrage peut être mise sous la forme

$$E_{eq} = E^0_{Bi} - 0{,}072\ V - 0{,}025\ pK_s - 0{,}025 \log [AcNH^-] \qquad (6)$$

K_s étant le produit de solubilité ($= [Bi(AcNH)_2^+]\ [AcNH^-]$).

L'analyse de la variation de E_{eq} en fonction de log $[AcNH^-]$ permet la détermination de $pK_s = -\log K_s/mol^2\ kg^{-2}$, soit: $pK_s = 7{,}9$ ($\pm 0{,}3$).

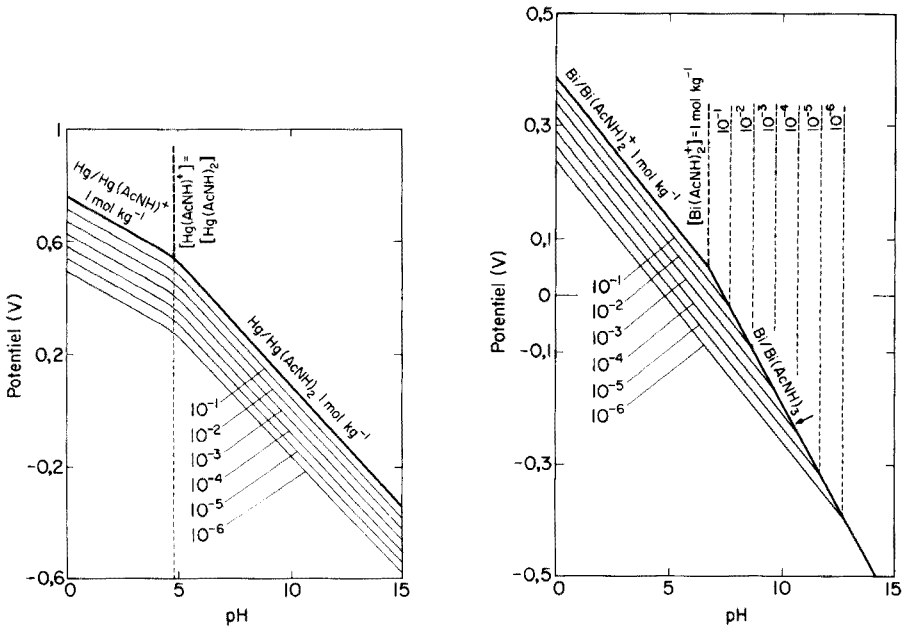

Fig. 6. Diagrammes d'équilibre potentiel—pH dans l'acétamide fondu, à 98° C pour différentes concentrations d'ions métalliques (les concentrations sont exprimées en mol kg^{-1}) (a) mercure; (b) bismuth.

CONCLUSION

Les résultats obtenus au cours de cette étude ont été les suivants. Les ions Hg^{2+} et Bi^{3+} n'existent pas dans l'acétamide puisqu'ils s'y comportent en acides forts, provoquant une solvolyse totale avec libération quantitative d'ions H^+. Hg^{2+} est mono-acide, Bi^{3+} est di-acide.

L'ion $Hg(AcNH)^+$ est, de plus amphotère: son caractère acide, qui résulte de l'équilibre suivant

$$Hg(AcNH)^+ + AcNH_2 \rightleftharpoons Hg(AcNH)_2 + H^+;\ pK_{A_2} = 4{,}8$$

fait que la forme $Hg(AcNH)^+$ prédomine jusqu'à pH = 4,8; au-delà, c'est la forme $Hg(AcNH)_2$ qui prédomine. La stabilité des complexes acétamidure du mercure(II) est responsable de la dismutation des ions mercure(I) (à tout pH).

L'ion $Bi(AcNH)_2^+$ possède, comme le composé correspondant du mercure, un caractère amphotère, selon l'équilibre

$$Bi(AcNH)_2^+ + AcNH_2 \rightleftharpoons Bi(AcNH)_3 + H^+;\ pK_{A_3} = -\log([H^+]/[Bi(AcNH)_2^+] = 6{,}87$$

Ainsi en milieu neutre (pH = 7,3), la concentration des ions $Bi(AcNH)_2^+$ ne peut dépasser $5 \cdot 10^{-2}$ mol kg^{-1}. Au-delà de cette valeur, $Bi(AcNH)_3$ précipite (et ne se redissout pas en milieu très basique, sous forme de complexes supérieurs).

L'influence de ces phénomènes d'acidobasicité sur le comportement électrochimique (à l'équilibre) du mercure et du bismuth (dont les systèmes sont rapides) est traduite par les diagrammes potentiel—pH de la Fig. 6, comparables à celui qui avait été établi pour l'argent [5].

BIBLIOGRAPHIE

1 G. Jander et G. Winkler, J. Inorg. Nucl. Chem., 9 (1959) 24.
2 M. Pournaghi, J. Devynck et B. Trémillon, Anal. Chim. Acta, 89 (1977) 321.
3 B. Gruttner, Z. Anorg. Allg. Chem., 270 (1952) 223.
4 S. Guiot et B. Trémillon, J. Electroanal. Chem. Interfacial Electrochem., 18 (1968) 261.
5 S. Guiot et B. Trémillon, J. Electroanal. Chem. Interfacial Electrochem., 22 (1969) 147.

Analytica Chimica Acta, 97 (1978) 373—383

STABILITE DE COMPLEXES ORGANOMETALLIQUES DANS LE CARBONATE DE PROPYLENE SATURE D'EAU
II. Complexes 1,10-Phénanthroline—Cuivre(II), Cadmium(II), Zinc(II) et Plomb(II)

F. QUENTEL, M. L'HER et J. COURTOT-COUPEZ*

Laboratoire de chimie analytique, E.R.A. CNRS 677, Université de Brest, 6, Avenue Victor Le Gorgeu, 29283 Brest-Cedex (France)

(Reçu le 3 octobre 1977)

RESUME

Dans le but d'utiliser le carbonate de propylène comme milieu d'extraction, la formation de complexes entre la 1,10-phénanthroline et différents cations métalliques (cuivre(II), cadmium(II), zinc(II) et plomb(II)) a été étudiée dans ce solvant saturé d'eau. Les études ont été effectuées par spectrophotométrie et potentiométrie à l'aide d'électrodes sélectives. Les complexes formés sont mononucléaires de type 1:1, 1:2 et 1:3 pour le cuivre(II), le cadmium(II) et le zinc(II); dans le cas du plomb seuls les composés de type 1:1 et 1:2 ont été mis en évidence. Les constantes de stabilité de ces différentes espèces à 25°C et à force ionique 0,1 M ont été déterminées.

SUMMARY

Stability of organometallic complexes in propylene carbonate saturated with water. Part 2. 1,10-Phenanthroline complexes of copper(II), cadmium(II), zinc(II) and lead(II)

Complex formation between 1,10-phenanthroline and copper(II), cadmium(II), zinc(II) and lead(II) has been studied in water-saturated propylene carbonate as a preliminary to extraction studies. The measurements are made spectrophotometrically or potentiometrically with selective electrodes. The complexes of copper(II), cadmium(II) and zinc(II) are mononuclear, of the 1:1, 1:2 and 1:3 types; in the case of lead(II) only 1:1 and 1:2 complexes exist. Stability constants for these different species at 25°C and 0.1 M ionic strength are reported.

La faible miscibilité à l'eau du carbonate de propylène jointe à son excellent pouvoir solvant vis-à-vis de nombreux composés a conduit un certain nombre d'expérimentateurs à utiliser cet ester cyclique comme agent d'extraction à partir de solutions aqueuses de divers complexes organométalliques [1]. Les caractéristiques du carbonate de propylène sont intéressantes à exploiter en vue de l'analyse des traces; elles permettraient d'atteindre grâce à la mise en oeuvre de méthodes électrochimiques au sein de la phase organique, une plus grande sensibilité dans l'analyse par extraction qu'avec les solvants actuellement employés. C'est en poursuivant ce but que nous avons été conduits à examiner le comportement de différents cations métalliques en présence de ligands types classiquement utilisés en extraction. Nous avons

dans un premier temps étudié le pouvoir complexant de l'hydroxy-8-quinoléine [2] dont la forme liée est l'anion oxinate, base relativement forte dans le carbonate de propylène saturé d'eau. Les résultats présentés ici concernent un ligand moléculaire, la 1,10-phénanthroline.

Le carbonate de propylène saturé d'eau offre un domaine d'acidité pratique de 14 unités de pH limité vers les milieux alcalins par la basicité de l'ion hydrogénocarbonate provenant de l'hydrolyse de l'ester [3]. Dans le mélange hydroorganique, l'électrode de verre aussi bien que l'électrode à hydrogène permettent la mesure du pH et par conséquent l'étude de nombreux équilibres en solution [2, 3].

PARTIE EXPERIMENTALE

Appareillage

Les spectres d'absorption électronique ont été obtenus à l'aide d'un appareil Beckman DK-2A. Les titrages spectrophotométriques ont été réalisés dans une cuve à circulation montée dans un spectrophotomètre Prolabo type Jean et Constant.

Toutes les mesures de pH ont été effectuées avec un millivoltmètre Tacussel type ISIS 20000 en utilisant une électrode de verre Radiometer type G202B et une électrode de référence Ag/AgCl (dans du chlorure de tétraéthylammonium 0,1 M). Cette dernière électrode est séparée du milieu à étudier par un pont liquide comportant un disque de verre fritté de porosité 4 à chacune de ses extrémités et contenant une solution de perchlorate de tétraéthylammonium 0,1 M. L'électrode de verre a été étalonnée à partir de solutions d'acide perchlorique de titre connu et de force ionique 0,1 M (Et_4NClO_4).

Le polarographe à trois électrodes utilisé comprend un potentiostat PRT-20-2 et une unité d'adaptation UAP1 Solea Tacussel ainsi qu'un enregistreur graphispot GRSO Sefram.

L'électrode à amalgame de cadmium a été préparée par dissolution directe du métal dans le mercure (environ 1% en poids). L'amalgame est ensuite lavé par de l'acide sulfurique dilué. L'électrode de cuivre est constituée par un fil de cuivre pur (99,99%), de 2 mm de diamètre. L'électrode sélective des ions Cu^{2+} est une électrode Orion type 94-29A.

Les mesures potentiométriques et polarographiques ont été effectuées dans des cellules classiques à double paroi reliées à un thermostat à circulation Haake type FE maintenant la température à 25 ± 0,1°C.

Réactifs et solutions

Les différents perchlorates métalliques (cuivre, zinc, cadmium, plomb) et le perchlorate de tétraéthylammonium sont des produits G. F. Smith. L'hydroxyde de tétrabutylammonium est un produit Fluka. Tous les autres produits utilisés sont des réactifs pour analyse.

Le perchlorate de bis(1,10-phénanthroline)argent(I) est préparé par précipitation à partir de perchlorate d'argent (G. F. Smith) et de la 1,10-phénanthroline, en milieu aqueux. Le solide est lavé à l'eau et séché sous vide.

Le perchlorate de bis(1,10-phénanthroline)mercure(I) est obtenu par addition d'une solution aqueuse acide ($HClO_4$) de perchlorate mercureux (G. F. Smith) à une solution de la 1,10-phénanthroline. Après lavage le précipité est séché sous vide.

Le carbonate de propylène utilisé (Hülls) est distillé sous pression réduite (environ 1 mm Hg). Les mélanges eau—carbonate de propylène (fraction molaire en solvant organique 0,7) sont préparés par pesée. L'eau utilisée est désionisée après distillation.

Le titre des solutions de la 1,10-phénanthroline a été déterminé par acidimétrie. Les titres des solutions des différents cations étudiés ont été déterminés par complexométrie à l'EDTA.

RESULTATS ET DISCUSSION

L'étude de la complexation proprement dite a été précédée par celle de l'influence de l'acidité du milieu sur la nature du ligand et des différentes espèces métalliques.

Comportement acido—basique de la 1,10-phénanthroline

Bien que la forme diprotonée de la 1,10-phénanthroline ait été mise en évidence par spectrophotométrie dans des solutions aqueuses très acides [4, 5], nous n'avons pas observé la fixation d'un second proton sur la molécule au sein des solutions acides que nous avons étudiées dans le carbonate de propylène saturé d'eau.

Le seul équilibre acido—basique intervenant dans le solvant est du type $L + H^+ \rightleftarrows HL^+$ (K_A). La courbe de neutralisation de la 1,10-phénanthroline par une solution d'acide perchlorique est typiquement celle d'une base faible par un acide fort. Les titrages ont été effectués sur des solutions 0,01 M en L et 0,1 M en Et_4NClO_4; leur exploitation au moyen de la méthode classique de Bjerrum et Anderson [6] conduit à la valeur de la constante d'acidité K_A.

Dans le Tableau 1 figurent les pK_A de la 1,10-phénanthroline dans l'eau [7], le mélange eau—dioxanne (1 + 1) [8] et le carbonate de propylène saturé d'eau.

La 1,10-phénanthroline se révèle être légèrement plus basique dans le mélange hydroorganique que dans l'eau. Nous avons déjà montré sur d'autres

TABLEAU 1

Constantes d'acidité de la 1,10-phénanthroline

Milieu	pK_A
Eau, $NaNO_3$ 0,1 M	4,95
Eau—dioxanne (1 + 1), KNO_3 0,1 M	4,53
CP saturé d'eau, Et_4NClO_4 0,1 M	5,7

exemples [3] que les valeurs de pK_A des couples HB^+/B sont peu différentes dans ces deux solvants.

Hydrolyse des ions métalliques

Les expériences réalisées n'avaient pour but que de déterminer la zone de pH la moins favorable à la formation des complexes cation-hydroxyle. Les résultats antérieurement présentés [2] conduisent à légitimement considérer l'hydrolyse des cations cuivre(II), zinc(II), plomb(II) et cadmium(II) négligeable en dessous de pH 6 pour des concentrations de l'ordre de 0,001 M.

Etude spectrophotométrique

Le spectre d'absorption électronique de la 1,10-phénanthroline est modifié aussi bien en présence d'acide perchlorique qu'en présence de perchlorate de cuivre(II), de plomb(II), de cadmium(II) et de zinc(II) (Tableau 2).

La spectrophotométrie d'absorption dans l'ultraviolet met donc en évidence la formation de complexes stables métal—1,10-phénanthroline en milieu neutre mais la forme protonée du ligand absorbant à des longueurs d'onde voisines de celles des complexes métalliques, la méthode spectrophotométrique ne peut dans ces conditions être employée de façon simple pour analyser en détails les réactions de complexation mises en oeuvre.

Seule la formation des complexes du cuivre(II) se traduit par une modification de l'absorption dans le domaine visible (apparition d'une coloration verte).

Sur la Fig. 1 sont présentés les résultats du titrage spectrophotométrique d'une solution de perchlorate du cuivre(II) 0,04 M par une solution de 1,10-phénanthroline; le titrage est suivi à 670 nm, correspondant au maximum d'absorption de l'un des complexes formés. En milieu neutre (courbe 1) trois points équivalents bien définis correspondant respectivement à des rapports ligand/métal égaux à 1, 2 et 3 mettent en évidence l'existence des trois complexes CuL^{2+}, CuL_2^{2+} et CuL_3^{2+}. En présence d'acide perchlorique 0,1 M (courbe 2) seuls les complexes 1:1 et 1:2 sont formés, ce qui indique une relative instabilité du complexe 1:3.

Etude polarographique

Dans notre précédent travail relatif aux complexes de l'hydroxy-8-quinoléine, la méthode polarographique nous avait fourni des résultats exploitables seulement dans le cas du cadmium(II) et du plomb(II), la réduction du

TABLEAU 2

Spectres d'absorption de la 1,10-phénanthroline et de ses complexes métalliques

	L	HL^+	Cu—L	Pb—L	Zn—L	Cd—L
λ_{max} (nm)	263	272	272	272	270	270
λ_{max} (nm)			294	293	291	291

cuivre(II) n'étant pas réversible et celle du zinc(II) pas suffisamment distincte de celle des protons.

Les polarogrammes correspondant à la réduction des complexes cadmium(II)—1,10-phénanthroline présentent tous un maximum que nous n'avons pu supprimer. Dans le cas du plomb(II), il y a chevauchement des vagues de réduction du ligand et du complexe. Une étude correcte de la stabilité des complexes formés par polarographie n'est donc pas possible.

Etude protométrique

Les réactions entre un cation métallique et un coordinat basique peuvent souvent être analysées en étudiant la différence d'affinité du proton et du cation à l'égard du ligand caractérisée par un équilibre du type $M^{2+} + nHL^{+} \rightleftarrows ML_n + nH^{+}$.

Dans le cas des cations étudiés, la faible basicité de la 1,10-phénanthroline et la relativement grande stabilité des complexes formés ont pour effet de déplacer pratiquement totalement cet équilibre vers la droite sauf dans le cas du plomb(II). La méthode classique de Bjerrum [9] ne peut donc être valablement employée que pour atteindre les constantes d'équilibre des complexes plomb(II)—1,10-phénanthroline.

Néanmoins, l'exploitation des courbes de titrage potentiométrique de mélanges équimoléculaires d'acide perchlorique et de perchlorate métallique 0,002 M par une solution de 1,10-phénanthroline 0,04 M conduisent à des résultats intéressants (Fig. 2). Dans le cas du cuivre(II), du cadmium(II) et du zinc(II) quatre équivalents de ligand sont nécessaires pour neutraliser

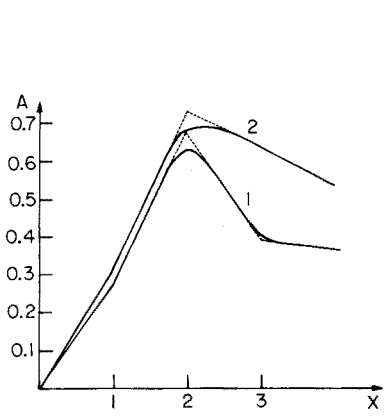

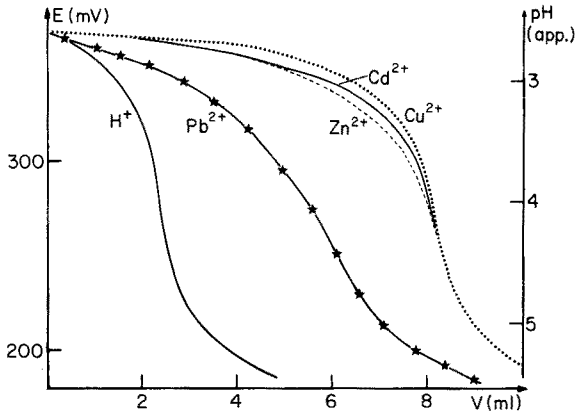

Fig. 1. Titrages spectrophotométriques de perchlorate de cuivre 0,04 M par une solution de la 1,10-phénanthroline 0,4 M. Courbe 1: milieu neutre non tamponné; courbe 2: milieu acide perchlorique 0,1 M.

Fig. 2. Titrages potentiométriques à l'électrode de verre de perchlorate métallique 0,002 M et d'acide perchlorique 0,0023 M par une solution de la 1,10-phénanthroline 0,04 M. Milieu Et_4NClO_4 0,1 M.

la solution, ce qui correspond à un rapport de chélation maximum L/M égal à trois. Dans le cas du plomb(II) (courbe 2), trois équivalents seulement sont utilisés, ce qui conduit à un rapport au plus égal à deux. Par ailleurs, les complexes formés avec Pb^{2+} sont moins stables; les mesures potentiométriques permettent alors de déterminer $\bar{n}$ la fonction de formation de Bjerrum [9] égale au nombre moyen de ligands liés au cation métallique. L'analyse des variations de $\bar{n}$ au cours du titrage par la méthode de Rossotti et Rossotti [10] fournit la formule des complexes PbL^{2+} et PbL_2^{2+} ainsi que la valeur de leur constante de stabilité: $\log \beta_1 = 5{,}4$ et $\log \beta_2 = 10{,}4$. En solution aqueuse ($NaNO_3$ 0,1 M 20°C) Anderegg [11] a obtenu $\log \beta_1 = 4{,}65$.

Etude au moyen d'électrodes sélectives

Ne pouvant déterminer par des mesures de pH la nature et la stabilité des complexes métal—1,10-phénanthroline dans le cas du cadmium, du cuivre et du zinc, nous avons tenté d'obtenir les résultats recherchés en mesurant une autre caractéristique du milieu réactionnel, l'activité du cation ou celle du ligand.

Electrodes indicatrices de l'activité du cation. Dans un premier temps, nous avons retenu les électrodes à amalgame. En milieu $HClO_4$ 0,1 M dans le carbonate de propylène saturé d'eau, l'électrode à amalgame de cadmium est indicatrice de l'activité des ions Cd^{2+} (pente de 29 mV/pCd à 25°C). Son utilisation et celle des autres amalgames sont néanmoins inadaptées à l'étude des complexes de la 1,10-phénanthroline, le ligand permettant l'oxydation rapide du mercure de l'électrode. Un phénomène analogue se produit avec une électrode de cuivre métallique indicatrice de l'activité des ions Cu^{2+} en milieu acide. En effet, en présence de la 1,10-phénanthroline le cuivre métallique est oxydé par le cuivre(II) grâce à la formation de complexes cuivre(I)—1,10-phénanthroline.

Nous avons eu alors recours à une électrode sélectif du cuivre(II) constituée d'une membrane cristalline de Ag_2S et CuS; ce type d'électrode n'a été utilisé que dans un nombre restreint de cas pour déterminer des constantes de formation de complexes [12, 13]. Son comportement dans le carbonate de propylène saturé d'eau est satisfaisant en milieu $HClO_4$ 0,1 M (pente de 34 mV/pCu).

Les courbes de titrage potentiométrique de solutions de la 1,10-phénanthroline 0,02 M par du perchlorate de cuivre obtenues en milieu neutre (Fig. 3A) et en milieu acide (Fig. 3B) font apparaître que les complexes les plus stables dans ces conditions sont respectivement CuL_3^{2+} et CuL_2^{2+}. Ces indications nous ont permis de choisir les conditions expérimentales d'acidité les plus favorables à leur étude.

La constante de stabilité du complexe 1:3 a été déterminée à partir des résultats du titrage potentiométrique d'une solution de perchlorate du cuivre 0,0001 M et de la 1,10-phénanthroline 0,002 M par de l'acide perchlorique; lors de ce titrage le pH et le pCu de la solution ont été simultanément mesurés. Seuls les points correspondant à des pH supérieurs

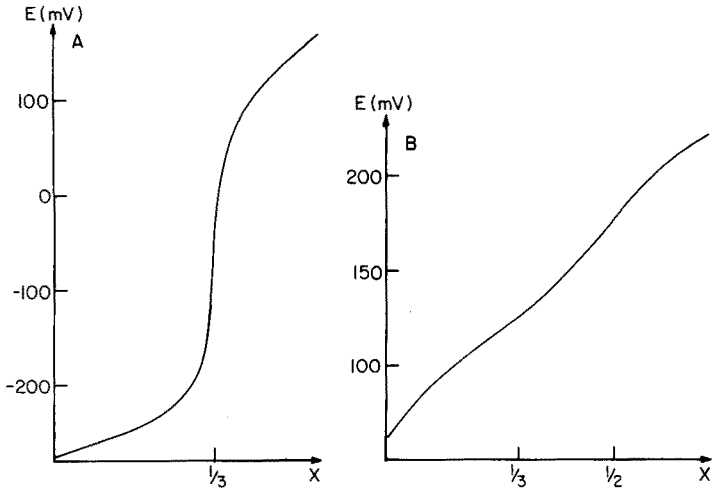

Fig. 3. Titrage potentiométrique à l'électrode sélective des ions Cu^{2+}. A, Titrage de la 1,10-phénanthroline 0,02 M par une solution de perchlorate de cuivre 0,11 M. B, Titrage de la 1,10-phénanthroline 0,0283 M et d'acide perchlorique 0,04 M par une solution de perchlorate de cuivre 0,11 M. Milieu Et_4NClO_4 0,1 M.

à 4, pour lesquels les variations de pCu en fonction de pL sont linéaires et démontrent la présence quasi exclusive de CuL_3^{2+}, ont été considérés.

La constante de stabilité du complexe 1:2 a été déterminée à partir des résultats du titrage potentiométrique d'une solution de perchlorate de cuivre 0,0001 M et de la 1,10-phénanthroline 0,002 M par de l'hydroxyde de tétrabutylammonium. Seuls les points correspondants à des pH inférieurs à 4,5 ont été retenus, la présence prépondérante de CuL_2^{2+} ayant été vérifiée: $\log \beta_3 = 22{,}4$ et $\log \beta_2 = 17{,}2_5$. Dans l'eau ($NaNO_3$ 0,1 M, 20°C), Anderegg [11] a obtenu $\log \beta_3 = 21{,}5$ et $\log \beta_2 = 16{,}00$.

Nous n'avons pu étudier la stabilité de CuL^{2+} par cette méthode; en effet, pour éviter la formation des complexes supérieurs, il est nécessaire de diminuer l'activité du ligand libre et donc d'augmenter l'acidité ($pH \simeq 1$). Dans ces conditions particulières, l'électrode sélective ne fonctionne pas correctement; il y a attaque des sulfures métalliques qui la constituent par action conjointe de l'acidité (formation de H_2S) et de la complexation (action du ligand en excès sur les ions métalliques de la membrane).

La poursuite de ce travail sur la détermination des constantes de stabilité des complexes de la 1,10-phénanthroline a nécessité la mise en oeuvre d'une électrode sélective de l'activité du ligand.

Electrode indicatrice de l'activité du ligand. Une électrode du métal M en présence d'une solution d'activité constante en un composé ML_nA du cation M^+ peut constituer un système indicateur de l'activité du ligand en solution. C'est ainsi que des systèmes Ag/AgL_2NO_3 (s) [14—16] ou $Hg/Hg_2L_2(NO_3)_2$ (s) [7] ont déjà été employés en solution aqueuse pour

mesurer l'activité de la 1,10-phénanthroline et ont permis la détermination de la stabilité de certains complexes.

Nous avons étudié le comportement d'une électrode d'argent en présence d'une suspension de perchlorate de bis(1,10-phénanthroline)argent(I) dans le carbonate de propylène saturé d'eau. La réaction de titrage analysée en sa présence était celle de neutralisation d'une solution de perchlorate de 1,10-phénanthrolinium 0,01 M par de l'hydroxyde de tétrabutylammonium, le pH du milieu étant mesuré à l'aide d'une électrode de verre et le pL correspondant calculé. Les variations du potentiel de l'électrode Ag/AgL_2ClO_4 (s) en fonction de la concentration caractéristique en ligand sont linéaires (pente de 118 mV/pL), ce qui indique son fonctionnement correct. Nous n'avons pu cependant utiliser cette électrode pour étudier les complexes de la 1,10-phénanthroline avec le cuivre(II), le cadmium(II) et le zinc(II) car en présence de ces cations le perchlorate de bis(1,10-phénanthroline)argent(I) se dissout, les complexes formés étant plus stables que celui de l'argent.

Nous avons alors envisagé l'emploi d'une électrode de mercure en présence d'une suspension de perchlorate de bis(1,10-phénanthroline)mercure(I). En opérant dans les mêmes conditions que pour l'argent (cf. plus haut), on constate que le précipité se dissout et que les variations linéaires de potentiel de l'électrode ne sont pas celles attendues pour le cas du complexe insoluble (pente de 87 mV pour pL 3—5) mais correspondent à la formation d'une espèce soluble du type $Hg_2L_3^{2+}$. Lorsque le titrage du ligand protoné est effectué en remplaçant le complexe du mercure(I) par une faible quantité de perchlorate de mercure(II) (5×10^{-4} M), les résultats obtenus sont identiques, les ions Hg^{2+} étant réduits par le mercure de l'électrode. C'est dans les conditions de concentration ci-dessous décrites que nous avons utilisé le système $Hg/Hg_2L_3^{2+}$ pour déterminer l'activité de la 1,10-phénanthroline en solution.

Les constantes de stabilité des différents complexes du cuivre(II), du zinc(II), du cadmium(II) et de la 1,10-phénanthroline ont été obtenues en exploitant les courbes de titrage par la 1,10-phénanthroline de solutions de perchlorate métallique 0,004 M en présence d'acide perchlorique 0,005 M et du complexe $Hg_2L_3^{2+}$ 6×10^{-5} M (Fig. 4); outre le potentiel de l'électrode de mercure, celui d'une électrode de verre a été également mesuré au cours de ces titrages. Ces données ont permis le calcul de la fonction de formation $\bar{n}$ (Fig. 5) ainsi que celui des constantes globales β_1, β_2 et β_3 à partir de la résolution d'un système d'équations linéaires simultanées à trois inconnues par la méthode de triangularisation de Gauss—Jordan. Dans le cas du cuivre(II) les constantes des réactions successives K_2 et K_3 peuvent être calculées plus simplement à partir de la courbe de formation (Fig. 5) mais β_1 n'est pas accessible par cette méthode, le complexe 1:1 étant trop stable.

L'ensemble des résultats est donné dans le Tableau 3 où figurent également les valeurs publiées par Anderegg [11] dans le cas de l'eau à 20°C et à force ionique 0,1 M ($NaNO_3$). Les valeurs des constantes retenues pour les complexes du plomb(II) ont été obtenues à partir des titrages protométriques.

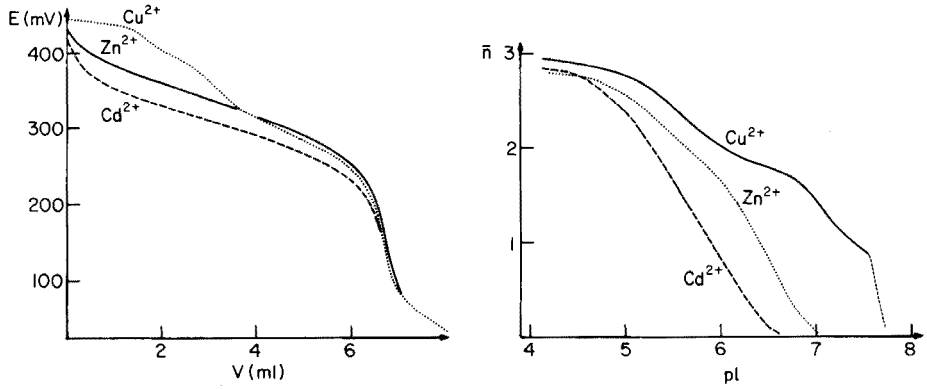

Fig. 4. Titrages potentiométriques à l'électrode de mercure de perchlorate métallique 0,004 M et d'acide perchlorique 0,005 M par une solution de 1,10-phénanthroline 0,100 M en présence de $Hg_2L_3^{2+}$ 6.10^{-5} M. Milieu Et_4NClO_4 0,1 M.

Fig. 5. Variations de $\bar{n}$ en fonction de la concentration caractéristique du ligand lors du titrage en milieu acide de perchlorates métalliques par la 1,10-phénanthroline.

TABLEAU 3

Constantes de stabilité des complexes de la 1,10-phénanthroline

	Carbonate de propylène saturé Cation d'eau pK_A = 5,7					Eau pK_A = 4,95				
	$\log \beta_1 = \log K_1$	$\log \beta_2$	$\log K_2$	$\log \beta_3$	$\log K_3$	$\log \beta_1 = \log K_1$	$\log \beta_2$	$\log K_2$	$\log \beta_3$	$\log K_3$
Cu^{2+}	10,0	17,0	7,0	22,4	5,4	9,25	16,00	6,75	21,35	5,35
Zn^{2+}	6,5	12,8	6,3	$17,9_5$	$5,1_5$	6,55	12,35	5,80	17,55	5,20
Cd^{2+}	6,0	11,7	5,7	16,7	5,0	5,78	10,82	5,04	14,92	4,10
Pb^{2+}	5,4	10,4	5,0			4,65				

Pour les autres cations, les constantes sont celles qui ont été déterminées après mesure de l'activité du ligand en solution à l'aide de l'électrode de mercure. Cependant, dans le cas du cuivre(II) la constante K_1 n'est pas accessible par cette dernière méthode; elle a été calculée à partir de K_2, K_3 et de la valeur de β_3 résultant de l'étude potentiométrique à l'aide de l'électrode sélective des ions cuivriques.

Dans les deux solvants, l'ordre de stabilité des complexes est le même, à savoir $Cu^{2+} > Zn^{2+} > Cd^{2+}$, ordre d'affinité proposé par Irving et Williams [17]. On constate que le complexe 1:1 du cuivre(II) est beaucoup plus stable que les complexes 1:2 et 1:3 ce qui n'est pas le cas pour le zinc(II), le cadmium(II) et le plomb(II). Le passage de l'eau au solvant hydroorganique ne modifie pas de façon importante les stabilités des complexes de la 1,10-phénanthroline. Néanmoins, on peut remarquer que dans le carbonate de propylène

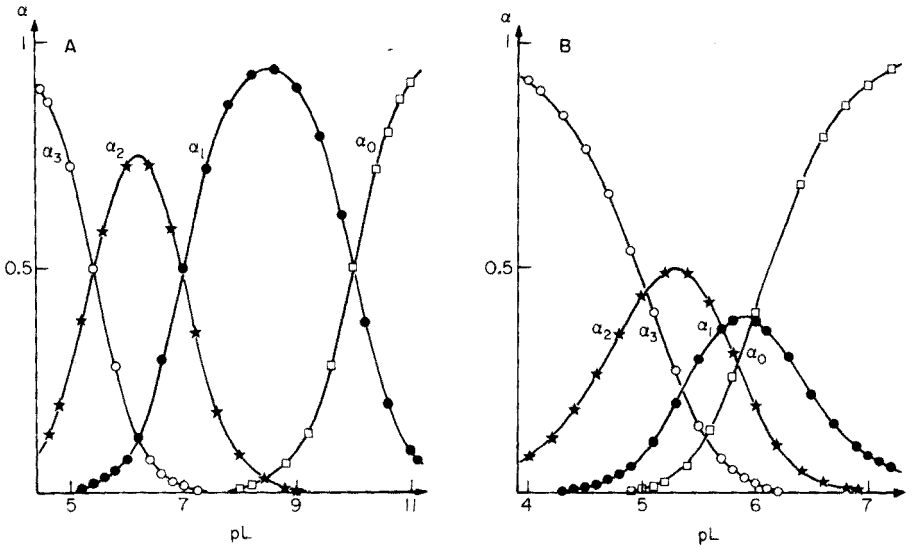

Fig. 6. Diagramme de répartition des espèces en fonction de la concentration caractéristique de la 1,10-phénanthroline dans le milieu. A, Cu^{2+} (α_0), CuL^{2+} (α_1), CuL_2^{2+} (α_2), et CuL_3^{2+} (α_3). B, Cd^{2+} (α_0), CdL^{2+} (α_1), CdL_2^{2+} (α_2) et CdL_3^{2+} (α_3).

saturé d'eau, le complexe 1:3 du cadmium(II) est plus stable que dans l'eau et qu'il existe un chélate 1:2 du plomb(II).

La connaissance des constantes de stabilité des différents complexes permet de calculer le diagramme de répartition des espèces en solution en fonction de la concentration du ligand libre dans le milieu. Si on note α_i la proportion du complexe ML_i, la grandeur $\alpha_i = [ML_i]/[M^{2+}]$ peut être facilement exprimée en fonction de la concentration en ligand L qui elle-même dépend du pH et des concentrations totales des produits mis en oeuvre. Ces courbes de répartition qui permettent en particulier de prévoir les conditions les plus favorables à la présence d'un complexe donné dans le milieu sont représentées pour le cuivre(II) et le cadmium(II) (Fig. 6).

Nous tenons à remercier la Délégation générale à la recherche scientifique et technique pour l'aide dont elle nous a fait bénéficier.

BIBLIOGRAPHIE

1 B. G. Stephens et H. L. Felfel, Anal. Chem., 47 (1975) 1676.
2 F. Quentel, J. Y. Cabon, M. L'Her et J. Courtot-Coupez, Anal. Chim. Acta, 96 (1978) 133.
3 F. Quentel, J. Y. Cabon, M. L'Her et J. Courtot-Coupez, C.R. Acad. Sci. Ser. C, 284 (1977) 917.
4 D. W. Margerum, R. I. Bystroff et C. V. Banks, J. Am. Chem. Soc., 78 (1956) 4211.
5 R. G. Linnell et A. Kaczmarczyck, J. Phys. Chem., 65 (1961) 1196.
6 J. Bjerrum et P. L. Anderson, Kgl. Danske. Vid., 7 (1945) 1.
7 G. Anderegg, Helv. Chim. Acta, 42 (1959) 344.

8 B. R. James et R. J. P. Williams, J. Chem. Soc., (1961) 2007.
9 J. Bjerrum, Metal ammine formation in aqueous solution, Haase and Son, Copenhague, 1941.
10 F. J. C. Rossotti et J. S. Rossotti, Acta Chem. Scand., 9 (1955) 1166.
11 G. Anderegg, Helv. Chim. Acta, 46 (1963) 2397.
12 H. Wada et Q. Fernando, Anal. Chem., 43 (1971) 751.
13 G. Nakagawa, H. Wada et T. Hayakawa, Bull. Chem. Soc. Jpn., 48 (1975) 424.
14 P. G. Grimes, Ph.D. Thesis, Iowa State University, 1958.
15 R. Fullerton, Ph.D. Thesis, Iowa State University, 1959.
16 M. J. Fahsel et C. Banks, J. Am. Chem. Soc., 88 (1966) 878.
17 H. Irving et R. J. P. Williams, J. Chem. Soc., (1953) 3192.

Analytica Chimica Acta, 97 (1978) 385—389

NAPHTHIDINES AS REDOX INDICATORS IN TITRATIONS WITH VANADATE

H. SANKE GOWDA* and R. SHAKUNTHALA

Department of Postgraduate Studies and Research in Chemistry, Manasa Gangotri, University of Mysore, Mysore (India)

(Received 7th October 1977)

SUMMARY

Naphthidine, naphthidinedisulphonic acid, 3,3'-dimethylnaphthidine and 3,3'-dimethylnaphthidinedisulphonic acid have been studied as redox indicators in titrations with vanadate. Sharp colour changes are obtained at the equivalence points in titrations of 0.05—0.01 N solutions of iron(II), hydroquinone, molybdenum(V) and uranium(IV) under appropriate conditions of acidity with oxalic or phosphoric acid as indicator catalyst. The transition potentials are reported.

Naphthidine [1] was first used as indicator in the titration of iron(II) with dichromate. Belcher et al. [2—5] investigated the indicator properties of naphthidines and compared naphthidine, naphthidinedisulphonic acid (NDS), dimethylnaphthidine (DMN) and dimethylnaphthidinedisulphonic acid (DMNS) in titrations of iron(II) with dichromate. Naphthidine, NDS and DMNS were also employed in titrations of iron(II), hydroquinone, molybdenum(V) and uranium(IV) with cerium(IV) sulphate [6]. Suitable conditions for the use of naphthidine, NDS, DMN and DMNS indicators in titrations with vanadate are described in this paper.

EXPERIMENTAL

Reagents

Solutions (0.2% w/v) of naphthidine, NDS, DMN and DMNS were prepared [4, 5]. Approximately 0.05 N solutions of hydroquinone, molybdenum(V), uranium(IV), iron(II) ammonium sulphate and sodium vanadate were prepared and standardized as described previously [6, 7]. Other working solutions were made by suitable dilution of these solutions.

Procedures

The transition potentials of naphthidine, DMN and DMNS. These potentials were determined in the titration of iron(II) with vanadate as described previously [8].

Titration of 0.05—0.01 M iron(II). Iron(II) solution (20 ml), 0.25 ml of 0.2% indicator solution, 4 ml of syrupy phosphoric acid (*d*, 1.75) and 3 ml of 1 M oxalic acid (no oxalic acid for NDS) were diluted to 40 ml with enough sulphuric or hydrochloric acid to give a 1 N concentration of the acid at the end-point. The mixture was titrated with 0.05 N sodium vanadate solution to the appearance of a red or red-violet colour. In the titration of 0.01 M iron(II) (10 ml), 0.1 ml of indicator solution, 2 ml of syrupy phosphoric acid and 0.5 ml of 1 M oxalic acid were diluted to 25 ml and titrated with 0.01 N sodium vanadate.

Titration of 0.05—0.01 N hydroquinone. An aliquot of 0.05 N hydroquinone solution, 2 ml of 1 M oxalic acid or 3 ml of syrupy phosphoric acid and 0.25 ml of naphthidine, NDS or DMNS indicator solution were diluted with sulphuric or hydrochloric acid and titrated with 0.05 N vanadate as described for iron(II). In the titration of 0.01 N hydroquinone solution (10 ml), 0.5 ml of 1 M oxalic acid or 1 ml of syrupy phosphoric acid and 0.1 ml of the indicator were diluted to 25 ml and titrated with 0.01 N vanadate.

Titration of 0.05—0.01 N molybdenum(V). Molybdenum(V) solution (20 ml), 0.25 ml of indicator solution and 2 ml of 1 M oxalic acid (2 ml of syrupy phosphoric acid for NDS) were diluted with hydrochloric or sulphuric acid and titrated as described for iron(II). In the titration of 0.01 N molybdenum(V) (10 ml), 1 ml of 1 M oxalic acid (1 ml of syrupy phosphoric acid for NDS) and 0.1 ml of the indicator were diluted to 25 ml to give an overall acidity of 0.5 N at the end-point and titrated with vanadate.

Titration of 0.05—0.01 N uranium(IV). Uranium(IV) solution (20 ml), 1 ml of 1 M oxalic acid (1 ml of syrupy phosphoric acid is added towards the end-point in titrations with NDS indicator) and 0.25 ml of indicator solution (not DMN) were mixed with acid and titrated with vanadate, as described for molybdenum(V).

RESULTS AND DISCUSSION

The formal redox potentials of DMN, DMNS [4], naphthidine and NDS [6] have already been determined. The transition potentials for naphthidine, DMN and DMNS in the titration of iron(II) with vanadate were noted when the potentials had stabilized after about 2 min (Table 1). The transition potential of NDS could not be determined because the colour of the oxidized form disappeared after 2 min.

Titration of iron(II)

The mechanism of the action of naphthidine, NDS, DMN and DMNS in the titration of iron(II) with vanadate is similar to that described recently [6]. The indicators do not give end-points in sulphuric or hydrochloric acid media (0.4—5.0 N) in the absence of phosphoric or oxalic acid; the red or red-purple colour of the oxidized form appears prematurely because

TABLE 1

Transition potentials (vs. NHE) of naphthidine, DMN and DMNS in varying concentrations of sulphuric acid at 28°C

Indicator	H_2SO_4 (M)	Transition potential (mV)	Indicator	H_2SO_4 (M)	Transition potential (mV)
Naphthidine	0.25	769.6	DMNS	0.25	766.3
	0.50	788.4		0.50	781.0
	0.75	802.6		0.75	801.0
	1.00	808.6		1.00	804.6
DMN	0.25	728.1			
	0.50	743.4			
	0.75	770.1			
	1.00	801.0			

of oxidation by iron(III). The end-points are sluggish with naphthidine, DMN and DMNS, but sharp with NDS, in the presence of phosphoric acid. Sharp end-points are also obtained with naphthidine, DMN and DMNS in the presence of both phosphoric and oxalic acids.

Naphthidine and DMNS give sharp colour changes from parrot green through blue to red or red-purple at the end-point in media containing 0.4—5.0 N H_2SO_4 or 0.4—1.5 N HCl and 3—8 ml of syrupy phosphoric acid with 1—5 ml of 1 M oxalic acid in a total volume of 60 ml of titration mixture. DMN gives detectable end-points in 0.4—2.0 N H_2SO_4 or 0.4—1.0 N HCl solutions containing these quantities of phosphoric acid and oxalic acid. The end-point colours of these three indicators are stable for 10—15 min and can be reversed within 3 min by a drop of iron(II). NDS gives sharp end-points from parrot green through blue to pinkish blue in 1—3 N H_2SO_4 or HCl containing 2—8 ml of syrupy phosphoric acid. The end-point colour is stable for about 2 min and can be reversed immediately by a drop of iron(II). Higher acidities cause premature end-points in all these cases.

All four indicators give sharp end-points in the titration of 0.01 M iron(II) in 0.4—1.5 N H_2SO_4 or HCl containing 1—4 ml of syrupy phosphoric acid and 0.5—2 ml of 1 M oxalic acid (no oxalic acid for NDS) in a total volume of 35 ml. The colour change is from almost colourless to light pink.

At least 0.2 ml of 0.2% naphthidine, NDS, DMN or DMNS is necessary in a total volume of 60 ml for proper indicator action. More than 0.6 ml of the indicator gives sluggish end-points. The indicator correction is almost negligible in the titration of 0.05 M iron(II).

In the titration of iron(II), NDS is superior to the other three indicators; it gives sharper and more reversible end-points and does not require the use of oxalic acid.

Under the recommended conditions, iron(II) in the range 4—40 mg could be determined without significant errors.

Titration of hydroquinone

Preliminary experiments showed that quinone and vanadium(IV) retard the oxidation of naphthidine, NDS and DMNS by vanadium(V); the effect increases with increasing concentrations of quinone and vanadium(IV), the combined effect being synergic. Oxalic or phosphoric acid counteracts the retardation and acts as indicator catalyst. The speed of oxidation of the indicator also increases with increasing concentration of phosphoric or oxalic acid. DMN was found to be of no value in this titration.

Naphthidine and DMNS give sluggish end-points in 0.5—4.0 N H_2SO_4 or HCl, but very sharp, correct end-points from parrot green through pinkish green to red or red-purple, when 2—6 ml of syrupy phosphoric acid or 1.0—4.0 ml of 1 M oxalic acid is also present. The end-point colour is stable for 10—15 min and can be reversed immediately by a drop of hydroquinone. NDS gives reasonable end-points from parrot green through blue to bluish pink in 2—5 N H_2SO_4 or HCl, but end-points are sharper in 1—3 N H_2SO_4 or HCl containing 1—5 ml of syrupy phosphoric acid in a total volume of 60 ml. The end-point colour is stable for about 2 min and is immediately reversible. Higher acidities give premature end-points in all these cases.

These three indicators function well in the titration of 0.01 N hydroquinone, with sharp end-points from almost colourless to pink in 0.5—2 N H_2SO_4 or HCl containing 1—4 ml of syrupy phosphoric acid or 0.5—2 ml of 1 M oxalic acid (no oxalic acid for NDS) in a total volume of 35 ml.

In this titration, DMNS proved to be the most sensitive reversible indicator. Excellent results were obtained over the range 5—22 mg of hydroquinone.

Titration of molybdenum(V)

Phosphoric and oxalic acids catalyse the oxidation of naphthidine, DMN and DMNS by vanadium(V) in the presence of molybdenum(VI) and vanadium(IV) in hydrochloric acid medium. The oxidized indicators are reduced quickly by molybdenum(V) in less than 2 N HCl, but slowly at higher acidities; oxalic acid catalyses this reduction, whereas phosphoric acid retards it. End-points with naphthidine, DMN and DMNS are poor in 0.5—4 N H_2SO_4 or HCl, unless oxalic acid is present; phosphoric acid is not a satisfactory additive.

Naphthidine and DMNS give sharp end-points in 0.25—1.5 N H_2SO_4 or HCl containing 1—5 ml of 1 M oxalic acid in a total volume of 60 ml. DMN functions satisfactorily in 0.25—2 N H_2SO_4 or HCl containing 1—3 ml of 1 M oxalic acid. NDS gives sharp end-points in 1—3 N H_2SO_4 or HCl containing 1—3 ml of syrupy phosphoric acid. The colour change is from parrot green through blue to red or red-purple and is easily reversible with molybdenum(V). Higher concentrations of acid give premature end-points. The end-points with naphthidine, DMN and DMNS are stable for 8—12 min, and that with NDS for about 2 min.

All four indicators also function satisfactorily in the titration of 0.01 M molybdenum(V) solution with vanadate in 0.5—1.5 N H_2SO_4 or HCl containing 0.5—1.5 ml of 1 M oxalic acid (0.5—2 ml of syrupy phosphoric acid with NDS).

All four compounds show very satisfactory reversibility in this titration. Very good results were obtained for 5—60 mg of molybdenum(V). DMNS was found to be the most sensitive indicator.

Titration of uranium(IV)

Preliminary experiments with naphthidine, NDS, and DMNS in this titration showed that the uranium(IV)—vanadium(V) reaction induces the reaction between uranium(IV) and the oxidized indicator, particularly in the presence of oxalic or phosphoric acid. DMN is of no value in this titration.

Naphthidine and DMNS give sharp, correct end-points from parrot green to red-purple in 0.4—1 N H_2SO_4 or HCl containing 0.5—2.0 ml of 1 M oxalic acid, but sluggish end-points in the presence of phosphoric acid. The end-point colour is stable for about 5—10 min and can be reversed immediately with uranium(IV). NDS gives very sharp end-points in 1.0—2.0 N H_2SO_4 or HCl containing 0.2—0.5 ml of 1 M oxalic acid, but the end-point colour is stable only for 20—30 s; addition of 1—2 ml of syrupy phosphoric acid near the end-point improves the stability to 2 min. Sluggish and premature end-points are obtained at higher acidities. Of the three indicators, DMNS is the most sensitive.

Naphthidine, NDS and DMNS give satisfactory colour changes from light green to pink in titrations of 0.01 N uranium(IV) with vanadate in 0.5—1 N H_2SO_4 or HCl containing 0.2—1.0 ml of 1 M oxalic acid (0.5—1.0 ml of syrupy phosphoric acid for NDS). With these indicators, very satisfactory results can be obtained for 7.5—55 mg of uranium(IV).

The results obtained in the titration of iron(II), hydroquinone, molybdenum(V) and uranium(IV) with vanadate compare favourably with those obtained with prochlorperazine maleate indicator [7].

The authors thank Dr. W. I. Stephen, Department of Chemistry, University of Birmingham, for the supply of pure indicators.

REFERENCES

1 L. E. Straka and R. E. Oesper, Ind. Eng. Chem. Anal. Ed., 6 (1934) 405.
2 R. Belcher and A. J. Nutten, J. Chem. Soc., (1951) 547.
3 R. Belcher, A. J. Nutten and W. I. Stephen, J. Chem. Soc., (1951) 1520, 3444.
4 R. Belcher, A. J. Nutten and W. I. Stephen, J. Chem. Soc., (1952) 1269, 3857.
5 R. Belcher, S. J. Lyle and W. I. Stephen, J. Chem. Soc., (1958) 3243, 4454.
6 H. Sanke Gowda and R. Shakunthala, Anal. Chim. Acta, 91 (1977) 399.
7 H. Sanke Gowda and R. Shakunthala, Ind. J. Chem., 14A (1976) 431.
8 H. Sanke Gowda and R. Shakunthala, Talanta, 13 (1966) 1375.

Analytica Chimica Acta, 97 (1978) 391—394

Short Communication

POTENTIOMETRIC DETERMINATION OF IODINE VALUES OF OILS WITH AN IODIDE-SELECTIVE ELECTRODE

AKIKO HONDA* and MACHIKO KASHIMOTO
Department of Nutrition, Koshien University, Takarazuka, Hyogo-ken (Japan)
SUSUMU HONDA
Faculty of Pharmaceutical Sciences, Kinki University, Kowakae, Higashi-osaka (Japan)
(Received 7th October 1977)

There are many potentiometric determinations of inorganic ions by means of ion-selective electrodes, but very few applications to the analysis of organic compounds. Examples of such applications are the analysis of halogenated pharmaceuticals [1], and an indirect determination of carbohydrates with an iodide-selective electrode [2]. This communication reports a convenient method for the determination of iodine values of oils. These values, designated as the total halogens absorbed by oils but expressed as the equivalent amount of iodine, are nutritionally as well as pharmaceutically important indices of oils. They are usually determined by iodimetric titration of halogens with thiosulfate [3, 4], but these analyses are laborious because the sample and titrant solutions are immiscible, so that colour changes near the end-points are slow.

The potentiometric method described herein is simpler and more efficient, especially for rapid routine analysis. The oil sample is treated with iodine monobromide in carbon tetrachloride, then the mixture is shaken with arsenite solution and the concentration of the iodide in the aqueous layer is measured directly.

Experimental

Materials. Iodine monobromide (Nakarai Chemicals, Karasuma, Kyoto), arsenic trioxide and unsaturated fatty acids (Wako Pure Chemical Industries, Doshomachi, Osaka) were of reagent grade. Solvents were of spectroscopic grade.

Apparatus. A temperature-compensating Toa-dempa IM-1B ion meter was equipped with an I-125 iodide-selective electrode and a standard calomel electrode.

Recommended procedure. Dissolve a sample of an oil or a fatty acid in carbon tetrachloride (1 ml). (The recommended sample size (w) is 30—50 mg for expected iodine values above 100, and 80—100 mg for expected values below 100.) Add a 2% carbon tetrachloride solution (5 ml) of iodine mono-

bromide, and place the mixture for 1 h in the dark. Then add 25.0 ml of 0.05 M sodium arsenite (prepared by dissolution of arsenic trioxide in an equivalent volume of 1 M sodium hydroxide, and adjusted to pH 8.0 with sodium hydrogencarbonate). Shake the mixture until the colour of the reagent disappears. Measure the potential of the aqueous layer with the iodide-selective electrode, and read the concentration of iodide (a) from a calibration curve obtained with standard solutions of potassium iodide in 0.05 M sodium arsenite. Repeat this procedure without addition of the sample to obtain the concentration of iodide (b) for the blank. Calculate the iodine value from the formula, $6.35 \times 10^5 \times (b - a)/w$.

Results and discussion

Halogen reagents for the determination of iodine values include iodine monochloride (Wijs method) and iodine monobromide (Hanus method). The latter reagent was preferred here, as it is less hygroscopic and more stable. Carbon tetrachloride proved to be a satisfactory solvent for the samples used, and there was no change of volume on shaking with the aqueous arsenite solution. In contrast, methylene chloride and chloroform showed volume changes of ca. +3% and −1%, respectively, after shaking with equal volumes of the arsenite solution.

Electrode response. The calibration curve for electrode response was linear for iodide concentrations of 10^{-5}—10^{-1} M. The response was not affected by addition of equimolar amounts of bromide, and aqueous and 0.05 M sodium arsenite solutions containing the same concentrations of iodide showed the same potentials (Table 1). However, the electrode response was strongly affected by addition of sodium thiosulfate. The potentials of aqueous solutions of iodide did not change after extraction with carbon tetrachloride.

Amount of sample. On the basis of these results, the recommended procedure for iodine values was devised. Table 2 shows the results for three model olefins which have different iodine values. The effect of the

TABLE 1

Effects of other ions and extraction on electrode response

Concentration of KI (M)	Potential of aq. solution (mV vs. SCE)	ΔV (mV)		
		Aq. solution containing equimol. KBr	0.05 M arsenite solution	Aq. solution extracted with CCl_4
10^{-1}	−277	+1	0	0
10^{-2}	−218	+1	0	−1
10^{-3}	−159	0	−1	−1
10^{-4}	−100	0	−1	0
10^{-5}	−41	−1	0	0
10^{-6}	+14	−3	−1	−9
10^{-7}	+59	−11	−24	—

TABLE 2

Determination of iodine values of unsaturated fatty acids

Fatty acid	Amount of sample (mg)	No. of detns.	Iodine value	
			Theoretical	Found
Oleic acid	60—70	3	89.9	77.0 ± 1.82
	70—80	6		80.4 ± 2.15
	80—90	5		87.8 ± 2.34
	90—100	7		91.5 ± 1.56
	100—110	6		87.6 ± 0.61
	110—120	2		87.2
Undecylenic acid	30—40	1	137.7	141
	40—50	1		140
	50—60	1		133
	60—70	1		125
Linoleic acid	30—40	1	181.0	181
	40—50	1		176
	50—60	1		172

amount of sample on the percentage reagent uptake was not negligible in these estimations, and the most appropriate sample size differed with the expected iodine value. Accordingly, the amount of sample taken should be adjusted as indicated in the Procedure.

TABLE 3

Accuracy and precision of the determination of oleic acid

Method	Iodine value[a]	Yield (%)
Modified Wijs method	95.5 ± 0.79	106 ± 0.88
Modified Hanus method	87.0 ± 0.55	96.8 ± 0.91
Potentiometry	91.5 ± 1.56	101 ± 1.72

[a]Theoretical value, 89.9; 7 determinations were done by each method.

TABLE 4

Estimation of iodine values of various oils

Oil	Iodine value found		Oil	Iodine value found	
	Potentiometry	Titration		Potentiometry	Titration
Olive oil	81.0	80.7	Rapeseed oil	118	121
Caster bean oil	87.9	88.7	Corn oil	120	122
Peanut oil	99.8	98.6	Peppermint oil	120	122
Sesame oil	109	107	Soybean oil	126	127

The iodine value for oleic acid obtained under these conditions was closer to the theoretical value than those obtained by the classical methods, although reproducibility was poorer (Table 3).

Measurement of iodine values of oils. Table 4 gives the iodine values of various oils measured by the present potentiometric method. All these values agreed well with those determined by titration of the same reaction solutions with sodium arsenite.

REFERENCES

1 Y. M. Dessouky, K. Tóth and E. Pungor, Analyst, 95 (1970) 1027.
2 S. Honda, K. Sudo, K. Kakehi and K. Takiura, Anal. Chim. Acta, 77 (1975) 274.
3 Standard Methods of Analysis of Oils, Japanese Association of Oils, 1969, p. 147.
4 Official Methods of Analysis, Association of Official Analytical Chemists, 12th ed., (1975) p. 488.

Analytica Chimica Acta, 97 (1978) 395—398

Short Communication

THE USE OF A SLOTTED TUBE FOR THE DETERMINATION OF LEAD, ZINC, CADMIUM, BISMUTH, COBALT, MANGANESE AND SILVER BY ATOMIC ABSORPTION SPECTROMETRY

R. J. WATLING

Applied Spectroscopy Division, National Physical Research Laboratory, Council for Scientific and Industrial Research, P.O. Box 395, Pretoria 0001 (South Africa)

(Received 21st September 1977)

Since the inception of atomic absorption spectrometry as an analytical tool [1], accessories such as heated graphite atomizers [2], tantalum filaments [3], Delves cups [4] and long path-length tubes [5, 6] have been developed in order to increase the detection power of the technique. All of these accessories, while substantially lowering analytical limits, suffer from being more cumbersome than a conventional flame or from an increase in time of analysis.

This communication describes the use of a slotted tube [7] which is positioned on top of a conventional atomic absorption burner head. It is used in conjunction with an air-acetylene flame to give increased sensitivity for seven elements. Precision of analysis is also significantly improved at low element concentrations. The tube can be made either of quartz or stainless steel, is inexpensive and can be manufactured in most workshops.

Experimental

Composite multi-element standards containing lead, zinc, cadmium, bismuth, cobalt, manganese and silver were prepared in the range 0.01—50.00 μg ml^{-1}. These solutions were sprayed into a premixed air-acetylene flame, and instrument and flame conditions were optimized for each element to give maximum absorbance signals. The same solutions were then sprayed into the tube which was aligned in the optical path, using burner alignment controls. Instrument and flame conditions were again optimized and the new absorbance signals recorded. A Varian-Techtron AA6 atomic absorption spectrometer and BC6 hydrogen background corrector were used with a Hitachi flatbed recorder.

Results and discussion

Sensitivity. The calibration curves which were obtained by spraying directly into the air-acetylene flame (F) and into the slotted tube (T) are plotted for bismuth, cadmium, silver and lead in Fig. 1.

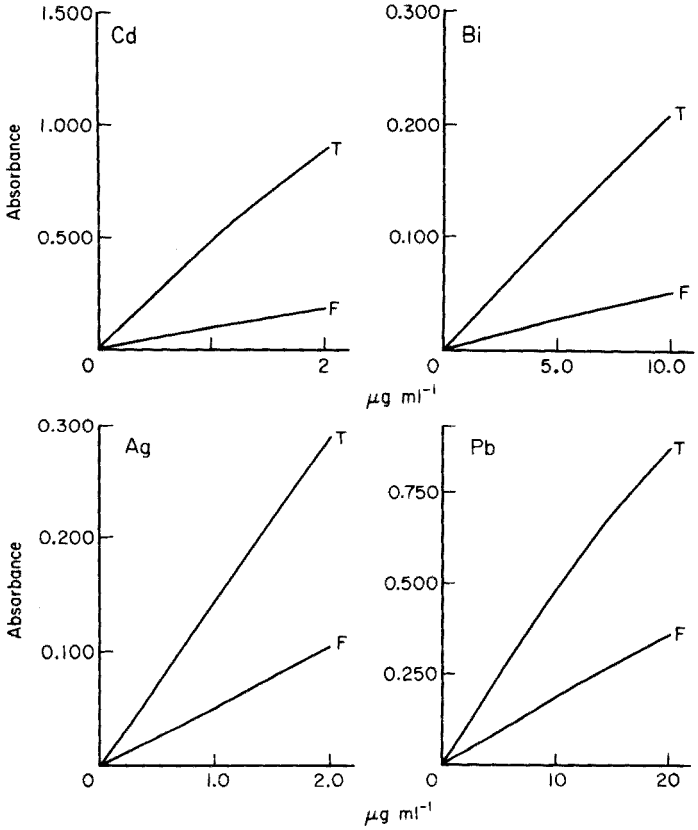

Fig. 1. Absorbance signal enhancement with the slotted tube.

Characteristic concentrations [8] (concentrations giving 0.004 absorbance) obtained by direct nebulization of the seven elements under the conditions of these experiments are compared with those determined by the slotted tube in Table 1. The improved sensitivity which is observed with the slotted tube is probably due to increased residence time of atoms in the optical path. This in turn is due to the slower flame speed and the longer optical path through which the atoms pass. The partial exclusion of entrained air also affects the chemical environment in the tube, as that portion of the flame which burns inside the tube probably consists largely of interconal gases and contains fewer oxidizing species. As a consequence, the chemical environment is more stable and the concentration of neutral atoms in the optical path is increased.

Precision. Much better analytical precision was obtained with the slotted tube. The results for four elements are shown in Fig. 2 and data for all seven elements are summarized in Table 2. In all cases there is an improvement in precision at low concentrations when the slotted tube is used. The improve-

TABLE 1

Characteristic concentrations obtained with an air-acetylene flame directly and with the slotted tube

Element	Flame (μg ml^{-1})	Slotted tube (μg ml^{-1})	Element	Flame (μg ml^{-1})	Slotted tube (μg ml^{-1})
Zn	0.01	0.003	Bi	0.40	0.10
Cd	0.02	0.005	Pb	0.25	0.08
Ag	0.09	0.01	Mn	0.10	0.06
Co	0.15	0.08			

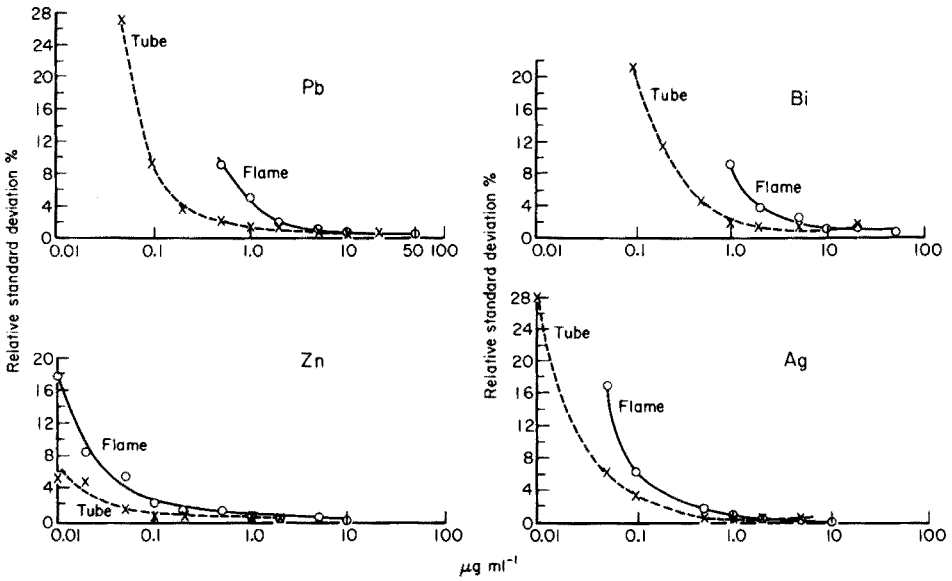

Fig. 2. Relative standard deviation—concentration graphs for lead, zinc, bismuth and silver.

ment is apparently related to the degree of thermolability of the metal and the ease with which atoms are formed. All comparative results were obtained from absorbance values in the linear portion of the calibration curve.

Interference studies. For these studies three new series of standards were prepared, one containing 1.00 μg ml^{-1} lead, bismuth, cobalt and manganese, another 1.00 μg ml^{-1} silver and the third 0.01 μg ml^{-1} zinc and cadmium. All of these standards, excepting silver, were made up in solutions containing interfering chlorides as well as nitrates. The silver standard was only made up with nitrate salts of interfering ions. The solutions tested were sodium and potassium chlorides, sodium, potassium, calcium, magnesium and strontium nitrates, and the final interferent concentrations ranged from 0 to 1000 μg ml^{-1}.

The effects of these salts on the absorbance signal values were investigated

TABLE 2

Comparisons of precisions near the analytical limits for the flame and the slotted tube

Element	Flame		Slotted tube	
	Concentration (μg ml^{-1})	s_r (%)[a]	Concentration (μg ml^{-1})	s_r (%)[a]
Zn	0.01	18.0	0.01	5.2
Cd	0.05	14.4	0.05	1.9
			0.01	10.9
Ag	0.05	16.6	0.05	6.2
			0.01	28.3
Co	0.1	28.4	0.1	5.4
			0.05	18.0
Bi	1.0	9.1	1.0	1.9
			0.1	21.0
Pb	0.5	9.0	0.5	2.3
			0.05	27.0
Mn	0.05	23.4	0.05	13.2

[a]For 20 determinations.

for each element. The study indicated that certain of the solutions investigated did affect the absorbance signal values for some elements with either the flame or the slotted tube. While it was apparent that some of the effects were specific to the slotted tube, others were reduced by its use, notably calcium and magnesium enhancement of lead absorbance signal values. In general, however, interference effects were minimal.

The proposed slotted tube gives a significant increase in sensitivity and precision for all the elements studied. The tube is inexpensive and easily manufactured in a laboratory workshop.

REFERENCES

1 A. Walsh, Spectrochim. Acta, 7 (1955) 108.
2 H. Massmann, Rev. GAMS, 4 II (1968) 193.
3 M. R. Sensmeier, W. F. Wagner and G. D. Christian, Fresenius Z. Anal. Chem., 277 (1975) 19.
4 H. T. Delves, Analyst, 95 (1970) 431.
5 K. Fuwa and B. L. Vallee, Anal. Chem., 35 (1963) 942.
6 J. W. Robinson, Anal. Chim. Acta, 27 (1962) 465.
7 R. J. Watling, CSIR FIS 108 Special Report (1977).
8 B. M. Gatehouse and J. B. Willis, Spectrochim. Acta, 17 (1961) 710.

Analytica Chimica Acta, 97 (1978) 399—403

Short Communication

A TUNGSTEN CARBIDE-COATED CRUCIBLE FOR ELECTROTHERMAL ATOMIZATION. DETERMINATION OF COPPER IN SOME BIOLOGICAL STANDARDS

E. NORVAL

National Physical Research Laboratory, C.S.I.R., P.O. Box 395, Pretoria 0001, (South Africa)

(Received 10th October 1977)

A new tungsten crucible with tungsten carbide coating, designed to replace standard pyrolytically-coated graphite crucibles in conventional flameless atomizers of the smaller type, has been developed. Unlike conventional cups, the tungsten crucible is heated by conduction of heat from the supporting rods and therefore does not attain atomizing temperatures as quickly. For this reason, applied voltage must be increased to obtain a maximum absorbance signal.

Precision of results for aqueous standards was examined for both types of crucible, and in both the atomic absorption and atomic fluorescence modes the tungsten crucible compares well with the standard cup. In addition, as the coating of the tungsten crucible is composed of a pyrolytic form of tungsten carbide with a small percentage of entrained graphite, the cup is far more resistant to breakdown. It is inexpensive and has a lifetime greatly in excess of conventional graphite or pyrolytically coated cups.

The graphite components of the conventional atomization systems have recently received considerable attention, as they deteriorate on ageing [1]. Furthermore, the particles likely to be ejected from carbon crucibles cause spurious reflection signals when flameless atomization is used for atomic fluorescence. Even when the crucibles are repeatedly given pyrolytic coatings, signs of ageing are apparent after about 150—300 firings.

The poor sensitivity obtained for elements which form thermally stable carbides has been attributed to carbide formation, and a 20-fold improvement in the sensitivity for barium has been reported when the tube was lined with tantalum foil [2]. However, Runnels et al. [3] pointed out that carbide formation may also play a part in the atomization of elements readily determined with a graphite atomizer. Stiefel et al. [4] extended the $ZrOCl_2$ treatment described by Runnels et al. [3] to obtain an inner carbide coating, so as to have a coating on the outside as well.

Since the characteristics of the carbon rod arrangement are such that copper atomization requires the maximum attainable temperature, the

determination of this element in biological samples was chosen to illustrate the application of the tungsten crucible.

Experimental

Apparatus. The atomization system used was the Techtron CRA63. The light beam from a copper hollow-cathode lamp was mechanically modulated at 285 Hz. Because fluorescence measurements were also to be undertaken, the beam was focussed immediately above the crucible. It was then refocussed on the entrance slit of a Zeiss PMQ II monochromator, the photomultiplier of which was connected to a Techtron phase-sensitive amplifier. The fluorescence radiation was observed by a photomultiplier which had a narrow-band interference filter in front of it, was screened from the intense radiation emitted by the heated crucible, and was connected directly to the amplifier. A fast-response recorder was used.

Crucibles. Crucibles were machined from a thoriated tungsten rod to the same dimensions as the standard (Mini-Massmann) graphite crucibles, but without the two holes through which the light beam normally passes. As tungsten carbide forms between 1600 and 1700°C [5], the crucible was fired in a flow of methane at an atomizing voltage setting of 8 (Table 1). The crucible was sheathed in argon at a flow rate of 2.5 l min^{-1} to defer burning of the methane until the last 2 or 3 s, and an independent methane flow of 0.75 l min^{-1} was used. The initial coating was obtained with 12 firings of 10 s each. For all but the last two of these, the methane flow was directed into the crucible via a quartz tube with capillary tip about 8 mm in length. For the last two firings, a quartz tube of about 6 mm inner diameter, which just covered the crucible, was used to direct the methane flow around and into the latter. This removed the pentoxide which had formed to a small extent on the outside. During the process, any carbon particles which formed, aggregated around the tube, and the portions of the supporting electrodes nearest the crucible received a coating of pyrolytic carbon, mixed with some tungsten carbide. One of the electrodes usually tended to weld to the crucible so that the vertical position was fixed and reproducibility was consequently improved. Any small deposit remaining after the final firing was blown out with methane. The required coating is black and slightly lustrous on the outside and grey or greyish black on the inside. A recording on an x-ray diffracto-

TABLE 1

Temperatures (°C) obtained 5 s after onset of atomization stage

Voltage setting	Tungsten crucible	Graphite crucible
8	1665	1760
8.5	1760	1875
9	1892	2025
9.5	1930	2100
10	1972	2170

meter of scrapings from the outer coating, indicated that the covering layer consisted of a pyrolytic form of tungsten carbide and entrained graphite. With continuous use, a deposit of a carbon/tungsten oxide mixture may accumulate on the grid of the gas inlet. This is removed by firing an old graphite crucible at maximum temperature for 5 s in an argon flow of 10 l min^{-1}.

Graphite crucibles were pyrolytically coated using the same gas flows at 2170°C. With repeated treatments these cups may eventually coat unevenly and may become very thin in parts.

Procedure. High-purity argon was used as purge gas at a flow rate of 4 l min^{-1}. Bleeding in of methane during the measuring process is not recommended, particularly for fluorescence measurements, as the carbon particles formed on decomposition of the gas, cause reflection signals.

Four biological standards were analyzed by atomic absorption spectrometry. Samples (10 μl) were placed in the crucible with an Eppendorf pipette. During the drying stage of the temperature programme, the droplet was inspected by shining a torch into the crucible to ensure that there was no boiling and that it evaporated smoothly and completely. It is important that no residual moisture is present during the higher temperature stages, as this can cause formation of tungsten oxides which may either depress the signal by reacting with the analyte, or enhance it when the condensed oxide vapour partially shields the light beam. When this occurs, it is easily detected by the state of the crucible after atomization. It should preferably show no colour change, or only a slight dark blue tinge. The optimum voltage setting for drying should be determined precisely at the start of a series of determinations. Optimum results in this study were obtained when the drying time was set at maximum. An ashing stage of 10 s with the voltage setting at 5 was incorporated, to stabilize the atomizing temperature for which a voltage setting of 10 was used.

After the initial coating of the crucible, one treatment after each determination was sufficient. This replaced the firing to clean the crucible which is normally used. With acid concentrations of 5% and less, a treatment time of 6 s was adequate. For higher acid concentrations, 10-s treatment periods were necessary, and at the start of a series, two such treatments may be desirable. With 10-s treatment periods, the crucible was resistant to acid concentrations of 12.5% and lower. (The use of higher concentrations was not tested.)

Reagents and sample preparation. High-purity acids were used throughout. A 1000-ppm copper(II) stock solution was diluted with 5% (v/v) nitric acid for the standard solutions. Four biological standards from the International Atomic Energy Agency were analysed.

The dried blood and fish solubles were dried to constant weight at 100°C. Six solutions were made of each sample, 0.5 g of the dried blood being used and 1.0 g of the other samples. All the samples were covered with concentrated nitric acid in silica crucibles, dried and ashed overnight at 450°C.

The fish solubles and wheat flour samples were dried and remoistened with nitric acid twice and the blood six times before the overnight ashing.

After the ashing, the calcined bone samples were heated in 4% (v/v) nitric acid and cooled. After addition of 1.5 ml of concentrated hydrochloric acid, these samples were made up to 20 ml with 3% (v/v) nitric acid. The blood residues were dissolved in about 10 ml of 3% (v/v) nitric acid containing 2 ml of concentrated hydrochloric acid and then diluted to 25 ml with the 3% HNO_3. After the overnight ashing, the fish solubles and wheat flour samples were again moistened with concentrated nitric acid, dried, ashed at 550°C for 20 min and finally dissolved in 20 ml of 5% (v/v) nitric acid.

No signals were obtained for 12.5% (v/v) nitric acid blank solutions.

Results and discussion

Atomization temperatures were measured with an optical pyrometer. Those obtained with the tungsten crucible are compared in Table 1 with those obtained with a pyrolytically-coated graphite crucible. The atomizing stage was preceded by a 10-s ashing stage (at setting 5).

Nine atomic absorption and six atomic fluorescence measurements were recorded for 1-ppm copper with each type of crucible. Relative standard deviations obtained with the tungsten and graphite cups, respectively, were 1.9% and 2.7% (atomic absorption) and 3.0% and 2.6% (atomic fluorescence). The precision of results obtained with the graphite crucible decreased with ageing. The tungsten crucible, although it eroded gradually with continued use, showed no signs of ageing after more than 1000 firings.

The tungsten crucible attained maximum atomization temperature slightly more slowly than did the graphite cup. However, this did not unduly affect the sensitivity, the average peak height for 1-ppm copper being 93% of the average peak height obtained with a coated graphite cup.

Small tungsten tubes suitable for use with the rod atomization system could be fabricated in the same way as the crucible, and a faster temperature rise could be obtained if the walls of the crucible and tube were to be

TABLE 2

Copper concentrations (ppm) in international biological standards

	IAEA values	IAEA standard deviation (absolute)	Values obtained with tungsten crucible (atomic absorption)	Standard deviation (absolute)
Fish solubles	5.25	1.2	5.8	—[a]
Wheat flour	5.8	1.1	6.5	0.6[b]
Calcined animal bone	6.8	2.3	7.3	1.0[b]
Dried animal whole blood	45.0	3.0	44.5	2.9[b]

[a] 3 determinations only (5.5, 5.5, 6.4).
[b] 6 determinations.

machined to dimensions thinner than those of their graphite counterparts. The tungsten tubes and crucibles could be coated on a large scale with the use of an induction furnace.

Determination of copper in biological samples. The atomic absorption calibration curve was linear up to 1.25-ppm copper — higher concentrations were not examined. Values obtained by the method described here are compared in Table 2 with the mean value supplied by the International Atomic Energy Agency.

REFERENCES

1 C. W. Fuller, Electrothermal Atomization for Atomic Absorption Spectrometry, Analytical Sciences Monograph No. 4, Chemical Society, London, 1977.
2 G. D. Renshaw, At. Absorpt. Newsl., 12 (1973) 158.
3 J. H. Runnels, R. Merryfield and H. B. Fisher, Anal. Chem., 47 (1975) 1258.
4 Th. Stiefel, K. Schulze and G. Tölg, Anal. Chim. Acta, 87 (1976) 67.
5 G. V. Samsonov (Ed.), Handbook of Physicochemical Properties of the Elements, IFI-Plenum, New York, 1968.

Analytica Chimica Acta, 97 (1978) 405—408

Short Communication

FLUORIMETRE DIFFERENTIEL DE FAIBLE COUT. APPLICATION A LA MESURE DE LA CONCENTRATION DE TRACEURS EN HYDROLOGIE

J. C. ANDRE* et M. NICLAUSE

I.N.P.L., Laboratoire de Chimie Générale, E.R.A. n° 136 du C.N.R.S., 1, rue Grandville, 54042 Nancy Cedex (France)

(Reçu le 15 juillet 1977)

L'utilisation de traceurs fluorescents en hydrogéologie est une technique répandue; ces traceurs servent à la détection de communication directe entre deux points, à l'évaluation des vitesses de circulation et de débit de rivières, à des études de pollution, etc. L'emploi des traceurs a trouvé dans le domaine du karst un champ d'action important lié essentiellement au développement de la spéléologie [1]. Les conceptions de circulation des eaux dans le calcaire donnaient une place de choix à la recherche de grands réseaux d'ecoulement recherche dans un but d'identification spéléologique de ces réseaux, ou dans l'optique d'un captage nécessitant la détection de sources de contamination possibles [1, 2].

En France, ce sont les résultats de traçages effectués par les spéléologues qui sont les plus nombreux. Le traceur employé a été la fluorescéine ou plus précisément sa forme dianionique l'uranine. Ce traceur présente l'avantage d'être décelable à l'oeil nu pour des concentrations $\geqslant$100 ppb [1]. Depuis quelques années, d'autres colorants fluorescents sont utilisés, il s'agit de la sulforhodamine G, de l'éosine et des rhodamines B et WT [3].

Si l'analyse qualitative permettant la détection de telles substances à l'oeil nu requiert des concentrations faibles ($\geqslant$100 ppb), elle nécessite souvent des injections massives de traceurs difficilement dégradables à l'obscurité (plusieurs kg voire même plusieurs dizaines de kg). Il peut en découler une certaine forme de pollution et d'erreurs importantes de mesure (qualitatives et quantitatives) dues à la présence dans l'eau de traceurs provenant d'expériences réalisées préalablement [4].

L'analyse quantitative, permettant de déterminer le fonctionnement d'un système hydrodynamique souterrain, ne peut être réalisée pour l'instant qu'au laboratoire à l'aide de la technique proposée en [4, 5], à partir de prises d'échantillons prélevées sur place. Il en est de même pour l'analyse semi-quantitative de Lallemand et Paloc [6].

L'emploi de spectrofluorimètres ou fluorimètres commerciaux étant exclu pour des raisons évidentes de danger de destruction, de difficultés de

déplacement des matériels et des alimentations en milieu souterrain, etc., une analyse qualitative, de plus faibles concentrations de traceur (< 10 ppb) et quantitative ne pourrait être réalisée sur place. Pour ces deux raisons, nous avons été amenés à réaliser un appareil de fluorimétrie robuste, de faible encombrement, sans électronique qui puisse être déplacé facilement en milieu souterrain, qui fournit des mesures quantitatives avec une précision raisonnable (de l'ordre de 10%) et qui possède une sensibilité de détection satisfaisante (environ 2 ppb de fluorescéine).

Principe de l'appareil

En général, on utilise un photo-multiplicateur sur un spectrofluorimètre ou fluorimètre [7]; il nécessite une alimentation haute tension stabilisée et un micro-ampèremètre. Cependant, compte tenu de la robustesse et de l'absence de haute tension exigées pour un emploi souterrain, nous avons préalablement porté notre choix sur d'autres photorécepteurs (photo-diodes, photo-résistances, cellules photo-électriques, etc.). Or, lors des expériences réalisées dans une pièce obscure, ces photorécepteurs nous sont apparus moins ou aussi performants que l'oeil de l'expérimentateur. Nous avons donc réalisé un fluorimètre à filtres dont l'oeil est l'instrument de mesure.

Or dans le cas des traceurs fluorescents utilisés où la fluorescence est émise dans un domaine de longueurs d'onde comprises entre 400 et 700 nm [3, 4], l'observation par l'oeil peut être effectuée directement. L'oeil ne peut cependant pas constituer directement un instrument de mesure absolu. Pour pallier ce défaut, nous avons cherché à comparer deux intensités de fluorescence: l'intensité de fluorescence provenant de la solution à étudier, et l'intensité de fluorescence provenant d'une solution étalon. Dans ce cas, l'oeil est capable d'estimer l'égalité ou l'inégalité des deux intensités lumineuses observées. La modification de l'intensité de la lumière excitatrice pénétrant dans la solution étalon (supposée plus concentrée que la solution à étudier) à l'aide d'un obturateur mécanique permet d'obtenir deux intensités lumineuses égales. On relie alors le déplacement de l'obturateur mécanique à la concentration en produit fluorescent de la solution à étudier.

Le schéma de l'appareil est présenté sur la Fig. 1. Par simplicité, les deux cellules (échantillon et référence) sont placées à la suite l'une de l'autre. L'obturateur mécanique sépare les deux cellules. Ce système simple limite l'appareil à l'étude de solutions de faible densité optique (en pratique, inférieure à 0,1) car l'intensité lumineuse qui pénètre dans la cellule de référence devient par trop inférieure à celle pénétrant dans la cellule de mesure.

La lampe utilisée sur notre prototype est une lampe à iode de projecteur, alimentée sous 12 V et de puissance 50 W. Elle peut être alimentée au laboratoire en courant alternatif à l'aide d'un transformateur, sur le terrain à l'aide d'une batterie portable cadmium—nickel. Les filtres utilisés sont des filtres du commerce provenant de divers fabricants.

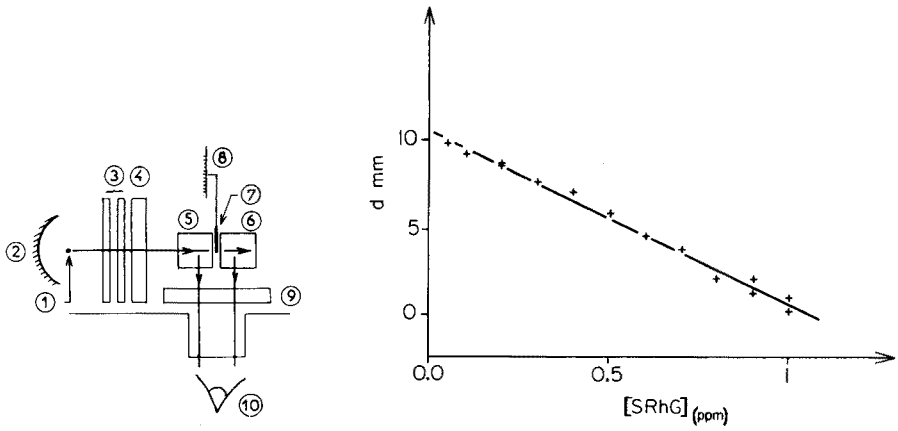

Fig. 1. Principe de l'appareil. 1 Lampe à iode, 50 W. 2 Miroir cylindrique. 3 Filtres thermiques. 4 Filtre optique primaire. 5 Echantillon. 6 Référence. 7 Obturateur mécanique. 8 Mesure du déplacement de l'obturateur. 9 Filtre optique secondaire. 10 Détecteur oculaire.

Fig. 2. Relation entre déplacement *d* de l'obturateur et concentration en corps fluorescent. Référence: Sulforhodamine G à la concentration [S Rh G] de 1,5 ppm.

Mesures

La cellule de référence doit contenir une concentration suffisante pour que l'oeil soit susceptible d'observer la luminescence. Compte tenu de la nature de la lampe et des filtres utilisés, nous avons obtenu les résultats limites d'observation présentés dans le Tableau 1.

La Fig. 2 représente les variations de la distance *d*, représentative des déplacements de l'obturateur en fonction de la concentration de sulforhodamine G. On observe sur cette figure que *d* varie de façon sensiblement linéaire avec la concentration en traceur fluorescent. La mesure peut être obtenue avec une précision pouvant atteindre sensiblement 10%.

TABLEAU 1

Limites de détection

Substance	Filtres	Limite de détection (ppb)
Fluorescéine	Kodak	2
Rhodamine B	Turner, Kodak	2
Sulforhodamine G	Turner, Kodak	2
Rhodamine WT	Turner, Kodak	5
Sulfate de quinine	Turner	100
Anthracène[a]	Turner	5×10^4

[a]En solution non dégazée dans le benzène.

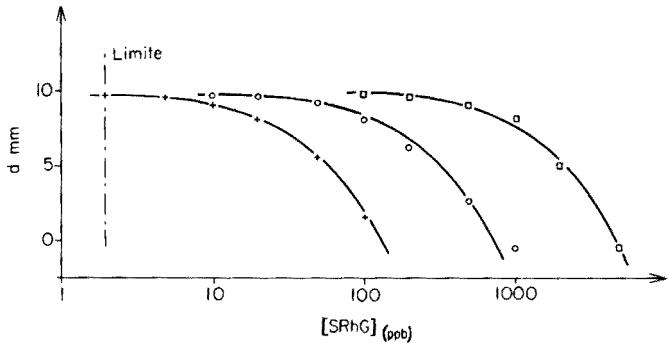

Fig. 3. Relation entre déplacement *d* de l'obturateur et concentration en corps fluorescent selon la concentration de la solution de référence. Référence: Sulforhodamine G [S Rh G]; + 0.2 p.p.m. ○ 1 p.p.m. □ 10 p.p.m.

La Fig. 3 montre que dans le cas particulier de la sulforhodamine G, la détermination d'une concentration peut être réalisée dans un domaine de concentration important [entre 2 et 10^4 p.p.b. de solution]. Il suffit pour cela de changer la concentration de la solution de référence. Des courbes similaires de celles présentées sur la Fig. 3 ont pu être obtenues avec d'autres substances fluorescentes (fluorescéine, rhodamine B, rhodamine WT.).

Limites de l'appareil

Avec la lampe à iode utilisée, l'excitation peut être réalisée dans un domaine de longueur d'onde compris entre 350 et 700 nm; l'analyse ne peut être réalisée qu'entre 400 et 700 nm.

Le remplacement de la lampe à iode par une lampe à vapeur de mercure, par exemple, permettrait une excitation en u.v. Si la fluorescence est émise aussi dans le domaine de l'ultra-violet, l'interposition entre le filtre d'analyse et l'oeil d'une solution de rhodamine B, absorbant les radiations émises et restituant une luminescence dans le domaine du visible permettrait la mesure [8]. Un tel dispositif autoriserait l'emploi de nouveaux traceurs qui sont actuellement étudiés au Laboratoire [9].

Les auteurs remercient très sincèrement MM. P. Pommier et S. Joly pour leur collaboration efficace dans la réalisation du prototype.

BIBLIOGRAPHIE

1 A. Mangin, J. Molinari et H. Paloc, La Houille Blanche, 3 (1976) 261.
2 E. A. Martel, Nouveau traité des eaux souterraines, Doin Ed., Paris, 1921.
3 J. C. Andre et J. Molinari, J. Hydrology, 30 (1976) 257.
4 J. C. Andre, M. Bouchy, Ph. Baudot et M. Niclause, Anal. Chim. Acta, 92 (1977) 369.
5 J. C. Andre, M. Bouchy, Ph. Baudot et M. Niclause, C.R. Acad. Sci., 284 (1977) 667.
J. C. Andre, Ph. Baudot et M. Niclause, Clin. Chim. Acta, 76 (1977) 55.
6 A. Lallemand et H. Paloc, Mémoires Réunions AIH, 7 (1967) 220.
7 C. A. Parker, Photoluminescence of solutions, Elsevier, Amsterdam, 1968.
E. L. Wehry, Modern Fluorescence Spectroscopy, Vols. 1 et 2, Plenum, New York, 1976.
8 J. Yguerabide, Rev. Sci. Inst., 39 (1968) 1048.
9 J. C. Andre, M. L. Viriot, J. Molinari et M. Niclause, Travaux en cours.

Analytica Chimica Acta, 97 (1978) 409—413

Short Communication

EXTRACTION OF TANTALUM BY POLAR SOLVENTS FROM MIXED MEDIA

A. HAGGAG*, W. SANAD and N. TADROS

Atomic Energy Authority, Cairo (Egypt)

(First received 30th November 1976; in revised form 18th July 1977)

Polar organic solvents, especially nitrobenzene, have been used for the extraction of many metals that form anionic halide complexes, e.g. HMX_4, where M = Fe, Ga, Au, Tl or In [1]. The present communication reports some investigations on the extraction of tantalum from aqueous solutions of mineral acids and mixed media by nitrobenzene and 20% n-nonanol.

Experimental

Apparatus and reagents. An Ekco Scintillation counter type N664C (with a well-type, 3 × 3-in., NaI(Tl) crystal) was connected to an Ekco automatic scaler type N610B for activity measurements.

Nitrobenzene, n-nonanol, methanol, ethanol, n-propanol and acetone were reagent-grade products (B.D.H., Fluka, Carlo Erba and Merck). Benzene was used for the dilution of nitrobenzene and n-nonanol. Analytical-grade acids and double-distilled water were used.

The ^{182}Ta tracer was obtained by irradiation of Specpure Ta_2O_5 in the research reactor at a neutron flux of 1×10^{12} n cm^2 s^{-1} for 48 h. After 120 days, Ta_2O_5 was dissolved in warm (2 + 1) 11 M HCl and 40% HF. The radiochemical purity was checked by means of a 4096-channel analyzer, with a PDP/11 computer, and was found satisfactory.

Procedure. Extraction experiments were carried out in polyethylene tubes (20 ml). Sulphuric acid solutions were prepared by adding the concentrated acid to water or aqueous solutions of other additives, and cooling to room temperature (18 ± 4°C). Equal volumes (4 ml) of the phases were shaken for 30 min. The aqueous phase contained TaF_5 or $TaCl_5$ (1×10^{-4} M) labelled with ^{182}Ta (0.001 μCi ml^{-1}). The distribution ratio (D) was determined from the ratio of the activity of 2 ml of the organic phase to that of 2 ml of the aqueous phase.

Results and discussion

Tantalum ions are strongly hydrolyzed, even in acidic solutions; thus their extraction behaviour may change on aging. However, if the solutions contain a F:Ta ratio exceeding 7, then the mononuclear complex species are stable in solutions [2, 3].

Extraction from pure halogen acid solutions. The distribution ratio D of freshly prepared TaF_5 and $TaCl_5$ was determined for nitrobenzene and 20% nonanol from 0.004 M HF and 0.004 M HCl, respectively, as a function of HCl and HBr concentrations. The results are shown in Fig. 1. Figure 1(A) shows that the extraction of TaF_5 from HCl solutions with nitrobenzene (curve a) increases with increasing acidity and passes through a flat maximum at 3—7.5 M HCl; the extraction of $TaCl_5$ (curve b) first decreases and passes through a shallow minimum at 2—6.5 M HCl. The extraction of TaF_5 with nonanol (curve c) increases steadily with increasing acidity, but extraction of $TaCl_5$ is negligible at any acidity. The extraction of both TaF_5 and $TaCl_5$ from HBr solutions (Fig. 1B) with the two solvents was similar to that from HCl solutions, except that with nitrobenzene there was no extraction above 3.2 M HBr.

Extraction from sulphuric acid solutions. The effect of H_2SO_4 concentration on the extraction of TaF_5 and $TaCl_5$ from 0.004 M HF and 0.004 M HCl, respectively, with nitrobenzene and nonanol is shown in Fig. 1(C). For TaF_5 with nitrobenzene, D is maximal at 4.2 M H_2SO_4 (curve a), whereas it is maximal at 11 M H_2SO_4 with nonanol (curve c); for $TaCl_5$ with nitrobenzene, D decreases rapidly (curve b), but with nonanol D is negligible at all H_2SO_4 concentrations. Figure 1 shows that TaF_5 is more readily extracted with nonanol from H_2SO_4 solutions than from HCl or HBr solutions, whereas the opposite is true for nitrobenzene.

At an otherwise constant composition of the aqueous phase, the effect of H_2SO_4 concentration on the D value of TaF_5 with nitrobenzene is shown in Fig. 2. In the presence of HF (curve a) and KI (curve b), the maximal D

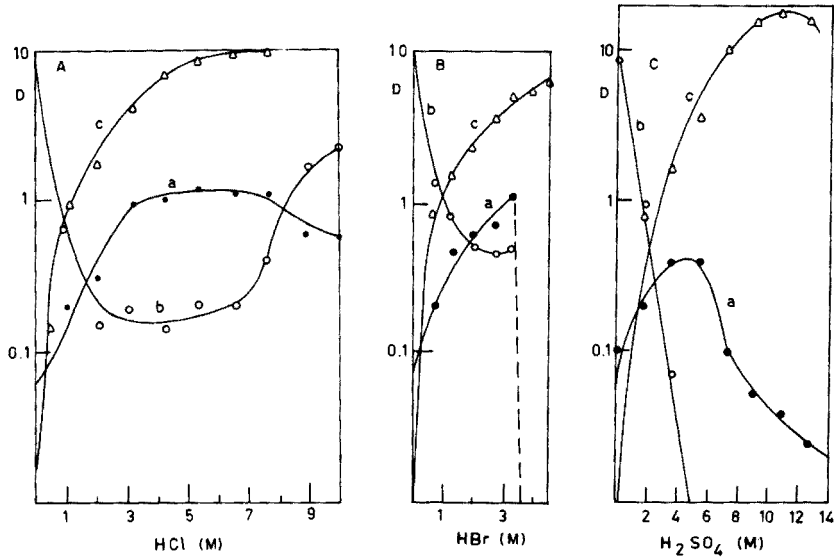

Fig. 1. Effect on D of tantalum of acid concentration. A, HCl. B, HBr. C, H_2SO_4. Curves: (a) TaF_5—nitrobenzene, (b) $TaCl_5$—nitrobenzene, (c) TaF_5—nonanol.

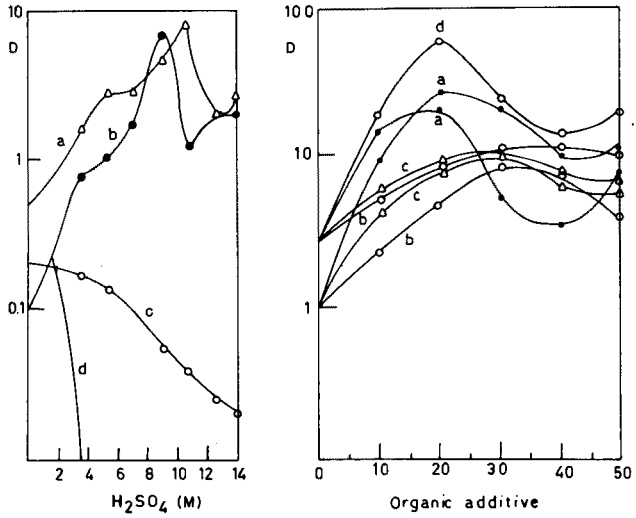

Fig. 2. Effect of H_2SO_4 concentration on D of TaF_5 in the presence of 0.004 M HF with other acids added. Curves: (a) 0.27 M HF, (b) 0.1 M KI, (c) 1.2 M HCl, (d) 0.64 M HBr.

Fig. 3. Effect of organic additives on D of TaF_5. Upper group of curves for 5.4 M H_2SO_4—0.27 M HF and lower group for 5.4 M H_2SO_4—0.1 M KI. Curves: (a) acetone, (b) methanol, (c) ethanol, (d) n-propanol.

values appear at 10.8 and 9 M H_2SO_4, respectively. In the cases of HCl (curve c) and HBr (curve d), there is a considerable decrease in D.

Effect of water-miscible organic solvents. The effects of 10—50% methanol, ethanol, n-propanol or acetone in the aqueous phase on the extraction of TaF_5 and $TaCl_5$ from 5.4 M H_2SO_4 and 3.4 M HCl with nitrobenzene were examined. For TaF_5, the D values were not appreciably affected by the additives and lay in the range 0.1—1, except in the case of acetone—HCl where D increased with increasing acetone percentage. Extraction of $TaCl_5$ was negligible in all cases. Figure 3 shows the effect of these miscible organic solvents on the extraction from 5.4 M H_2SO_4—0.27 M HF or 0.1 M KI with nitrobenzene. Generally, the curves show a broad maximum for D.

Effect of solvent concentration. The plots of log D vs. log solvent concentration at constant composition of the aqueous phase were studied. For TaF_5 in 5.4 M H_2SO_4, the slope was 2.8 for nitrobenzene (Fig. 4, curve a) and 2.4 for nonanol (Fig. 5, curve d); the slope was 3 in 3.6 M H_2SO_4 for the di(2-ethylhexyl)phosphoric acid [4], which proved that the extracted species is TaF_2^{3+}. The other slopes, and a slope of 3 for the anion-exchanger Amberlite LA2 from 0.02 M H_2SO_4 indicate that the extracted species in $H_n\,TaF_{5+n}^{-n}$. These results indicate that the tantalum fluoride complexes in solutions containing up to 6 M H_2SO_4 are mainly $H_n\,TaF_2 \cdot F_{3+n}^{-n}$. As the H_2SO_4 concentration increases, stepwise formation of stable $H_n\,TaF_{5+n}^{-n}$ takes place by removal of water molecules surrounding TaF_2^{3+} and other fluoride ions.

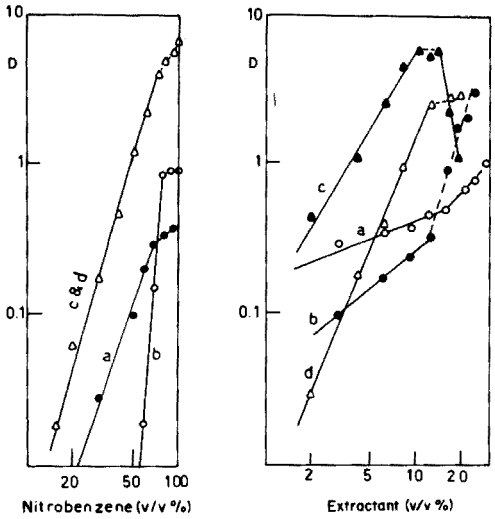

Fig. 4. Effect of nitrobenzene concentration on D at constant composition of the aqueous phase. Curves: (a) at 5.4 M H_2SO_4, (b) at 3.36 M HCl, (c) at 9.9 M H_2SO_4—0.27 M HF, (d) at 9.9 M H_2SO_4—0.1 M KI.

Fig. 5. Effect of solvent concentration on D at constant composition of the aqueous phase. Curves: (a) 5.4 M H_2SO_4—0.27 M HF—30% acetone—(nitrobenzene), (b) 5.4 M H_2SO_4—0.27 M HF—30% n-propanol—(nitrobenzene), (c) 5.4 M H_2SO_4—0.27 M HF—$TaCl_5$—(nonanol), (d) 5.4 M H_2SO_4—TaF_5—(nonanol).

The slopes of the other curves in Fig. 4 are 14 (curve b) and 3.5 (curves c and d); in Fig. 5 the slopes of curves a and b are 0.4 and 1, respectively. The slopes higher than 3 may be explained by extraction of excess acid. The slopes lower than 3 may be due to organic additive interactions similar to those found with thorium [5].

$TaCl_5$ is not extracted by nonanol, but when the solution is made 0.27 M in HF, tantalum is readily extracted, indicating that Ta—fluoride complexes are formed. Comparison of the slope 1.7 (Figure 5, curve c) from 5.4 M H_2SO_4—0.27 M HF with the slope 2.4 (curve d), indicates that Ta—fluoro—chloro complexes are the extracted species.

Purification and separation of tantalum from other elements. As, In, Sn, Sb, Se and Hg are extracted from above 7 M H_2SO_4 in the presence of a little HCl or HBr by benzene, xylene and other solvents [6]. From the same medium, Fe, Ga, Au, Tl and Ge, which form halo complexes, are completely extracted by nitrobenzene [7, 8]. Several useful separations from tantalum may therefore be possible.

In the presence of 0.27 M HF mixed with H_2SO_4 solutions above 7 M, tantalum can be extracted with nitrobenzene, and separated from Th, Co, Zn, U and rare earths [5, 9].

REFERENCES

1 L. R. L. Randall, Erickson and R. L. McDonald, J. Am. Chem. Soc., 88 (1966) 2099.
2 F. Fairbrother, The Chemistry of Niobium and Tantalum, Elsevier, 1967.
3 Y. Marcus and A. S. Kertes, Ion Exchange and Solvent Extraction of Metal Complexes, Wiley-Interscience, London, 1967.
4 W. Sanad, A. Haggag and N. Tadros, J. Radioanal. Chem., in print.
5 A. Haggag, S. A. El-Fekey, M. El-Mamoon Yehia and W. Sanad, J. Radioanal. Chem., 33 (1976) 139.
6 A. Alian, W. Sanad and M. Nofal, J. Inorg. Nucl. Chem., 37 (1975) 297.
7 A. Haggag, W. Sanad, A. Alian and N. Tadros, J. Radioanal. Chem., 35 (1977) 253.
8 A. Alian, A. El-Kot, A. Haggag, W. Sanad and N. Tadros, J. Radioanal. Chem., 26 (1975) 39.
9 A. Alian, A. Haggag and W. Sanad, J. Radioanal. Chem., 20 (1974) 559.

Analytica Chimica Acta, 97 (1978) 415—418

Short Communication

DEGRADATION OF COUMAPHOS IN DISTILLED WATER AS A FUNCTION OF pH

V. N. MALLET* and Y. VOLPE

Department of Chemistry, Université de Moncton, Moncton, New Brunswick (Canada)

(Received 5th October 1977)

The analytical techniques for determining organophosphorus pesticides have been reviewed [1, 2]. The most commonly used quantitative method of analysis is gas—liquid chromatography (g.l.c.), largely because of the selectivity of the flame photometric detector and its inherent sensitivity [3—7]. Unfortunately, not all pesticides can be determined easily by g.l.c., some because of their instability to heat, others because of their lack of volatility. This is the case with coumaphos.

In an earlier article [8] a technique for the detection of coumaphos on a silica-gel thin-layer chromatogram (t.l.c.) was described. The pesticide was made fluorescent simply by heating the chromatogram at an optimum temperature for a definite time; a few nanograms per spot could be detected [9]. The detection technique was applied successfully to the determination of coumaphos and its oxygen analog, coroxon, in water and eggs [10, 11].

Recently [12], a simple method was proposed for the identification and determination of Potasan in technical coumaphos. In addition, it was established that, in water, coumaphos degrades primarily into coroxon the oxygen analog and chlorferone, which is the hydrolysis product and also the fluorescent species resulting from the heat-treatment of coumaphos.

In this work the effect of pH on the stability of coumaphos in water is studied by t.l.c. and in situ fluorimetry for detection and determination. This was undertaken primarily to determine the degradation rate and establish the pH value at which the stability of coumaphos is at a maximum.

Experimental

Chemicals and apparatus. Solvents were of pesticide-grade quality. Coumaphos (*O*, *O*-diethyl-*O*-(3-chloro-4-methyl-7-coumarinyl)phosphorothioate); coroxon (*O*, *O*-diethyl-*O*-(3-chloro-4-methyl-7-coumarinyl)phosphate) and chlorferone (3-chloro-4-methyl-7-hydroxycoumarin) were obtained as analytical standards (Chemagro Corp., Kansas City, U.S.A.).

T.l.c. plates (20 × 20 cm, 250 μm thick) were prepared with Silica-Gel H (Brinkmann Instruments, Rexdale, Canada) with a Desaga spreader.

The fluorescence was measured with a Turner fluorimeter, Model III, with t.l.c. attachment and filters 7-60 and 2A for excitation and emission, respectively.

Extraction of coumaphos and related compounds from water. A 100-ml sample of distilled water, spiked with 10 μg of coumaphos, was extracted with chloroform (3 × 75 ml), shaking each time for 3 min. The chloroform extract was dried with 10 g of anhydrous sodium sulphate and evaporated to ca. 15 μl in the usual way [9].

Degradation of coumaphos in water. The acidity of 600 ml of distilled water was adjusted to pH 4 or 5.5 with a buffer of pH 3, (potassium hydrogenphthalate—HCl) and adjusted to pH 6.3, 7.0 or 8.5 with a buffer of pH 9 (boric acid—KOH). The water was then spiked with 60 μg of coumaphos. A 100-ml aliquot was taken at the desired time and the pH re-adjusted to 5.5 with the buffer pH 9 for acidic water and with buffer pH 3 for basic water. Extraction from water was as described earlier.

Thin-layer chromatography and fluorimetric analysis. The concentrate was spotted on a plate along with appropriate standards and the plate was developed in carbon tetrachloride: methanol (100:7). Visualization was obtained by heating the chromatogram in an oven at 200°C for 20 min [9].

Results and discussion

The in situ fluorimetric method of analysis mentioned in this paper and described previously [12] is straightforward for the simultaneous determination of coumaphos, coroxon and chlorferone in water; percentage recoveries are always ca. 95%. This makes it possible to determine the concentration of each individual compound at a particular time in the reaction medium.

The behavior of coumaphos in distilled water has been studied. The results presented in Table 1 for various pH values show that degradation of coumaphos occurs and that the compound is more stable at neutral pH than it is in either acidic or basic media. Table 1 also shows the half-lives calculated from the recovery data. The degradation rate was assumed to be first order.

TABLE 1

Recovery (%) of coumaphos[a] from distilled water and half-lives[b] of coumaphos in distilled water

pH	Time (h)					k_1 (d^{-1})	Half-life (d)
	0	24	48	72	96		
4.0	94.5	93.0	90.8	88.8	87.0	0.021	33
5.5	95.9	94.3	93.9	93.0	92.1	0.010	67
6.3	96.2	95.7	95.2	94.6	94.0	0.0056	124
7.0	95.8	95.8	95.4	95.1	95.0	0.0020	347
8.5	94.5	92.5	90.0	88.0	86.0	0.024	29

[a]The initial concentration of coumaphos was 10 μg. The data are the averages of 3 t.l.c. analyses from a single extraction.
[b]Assuming first-order degradation.

TABLE 2

Recovery (μg) of coroxon and chlorferone from distilled water

pH	Time (h)					pH	Time (h)				
	0	24	48	72	96		0	24	48	72	96
Coroxon						*Chlorferone*					
4.0	0	0.0043	0.0100	0.0138	0.0192	4.0	0	0.0073	0.0152	0.0220	0.0300
5.5	0	0.0018	0.0049	0.0068	0.0100	5.5	0	0.0032	0.0060	0.0103	0.0140
6.3	0	0.0016	0.0035	0.0056	0.0073	6.3	0	0.0025	0.0045	0.0065	0.0083
7.0	0	0.0005	0.0010	0.0015	0.0019	7.0	0	0.0012	0.0020	0.0025	0.0035
8.5	0	0.0070	0.0130	0.0215	0.0280	8.5	0	0.0080	0.0150	0.0235	0.0305

TABLE 3

Degradation of coumaphos and formation of coroxon and chlorferone (after 96 h)

pH	Quantity of coumaphos degraded (μ mol)	Total quantity of coroxon and chlorferone (μ mol)	Total quantity produced (%)
4.0	2.10	2.00	95
5.5	1.10	0.96	87
6.3	0.62	0.61	98
7.0	0.22	0.23	104
8.5	2.40	2.30	96

Coumaphos in water degrades first into coroxon and then to chlorferone [12]. The quantities of these compounds produced by the degradation of coumaphos (see Table 1) were measured (Table 2).

From these results, the loss in coumaphos can be attributed quantitatively to the formation of coroxon and chlorferone; the results of calculations are presented in Table 3. The quantities not accounted for may be attributed to experimental error inherent in the analytical technique (i.e., 95% recovery for each compound) rather than to further degradation of coroxon or chlorferone, as suggested by earlier authors [13].

The authors thank the National Research Council of Canada and the "Conseil de Recherche" of this University for financial support.

REFERENCES

1 E. D. Chilwell and G. S. Hartley, Analyst, 86 (1961) 148.
2 D. C. Abbott and H. Egan, Analyst, 92 (1967) 475.
3 I. H. Williams, R. Kore and D. G. Finlayson, J. Agric. Food Chem., 19 (1971) 452.
4 M. C. Bowman and K. R. Hill, J. Agric. Food Chem., 19 (1971) 342.

5 C. W. Miller and A. F. M. Funes, J. Chromatogr., 59 (1971) 73.
6 W. E. Westlake, M. E. Dusch and L. R. Jeppson, J. Agric. Food Chem., 19 (1971) 1191.
7 R. Greenhalgh, J. Doklodalova and W. O. Haufe, Bull. Environ. Contamin. Toxicol., 7 (1972) 237.
8 G. L. Brun, D. Surette and V. Mallet, Int. J. Environ. Anal. Chem., 3 (1973) 61.
9 G. L. Brun and V. Mallet, J. Chromatogr., 80 (1973) 117.
10 J. G. Zakrevsky and V. Mallet, J. Ass. Offic. Anal. Chem., 58 (1975) 554.
11 V. Mallet and G. L. Brun, Bull. Environ. Contam. Toxicol., 12 (1974) 739.
12 Y. Volpé and V. N. Mallet, Anal. Chim. Acta, 81 (1976) 111.
13 F. A. Gunther (Ed.), Residue Rev., 46 (1973) 54.

Analytica Chimica Acta, 97 (1978) 419—421

Short Communication

A SEPARATION METHOD FOR SECOND PHASES FROM IRON MATRICES IN AQUEOUS SOLUTIONS ABOVE pH 6

ROBERT POMPE

Department of Inorganic Chemistry, Chalmers University of Technology and University of Technology, P.O. Box, S-402 20 Göteborg 5 (Sweden)

(Received 11th October 1977)

The properties of steels are profoundly influenced by the presence of second phases such as oxides, carbides, nitrides etc. embedded in the iron matrix. In order to identify and determine these phases, they have to be separated from the iron metal. The separation methods commonly used are: (a) oxidation of the iron matrix by a halogen (Br, I)—ester solution [1] and (b) anodic dissolution of iron in an electrolytic cell [2] with neutral or acidic aqueous electrolytes and low current density. These and other methods have been reviewed by Scholes and White [3].

Nitrides, carbides and carbonitrides of iron and alloying elements are very common second phases in steels. Many of them are known to be unstable at low pH values and/or susceptible to oxidation. This sets limitations on possible separation methods with regard to the phases recoverable from steel samples and the dissolution rate of the iron matrix.

In this communication, a separation method is proposed in which the iron matrix is dissolved indirectly; the dissolution rate is rapid compared to the methods generally used. The method consists of two steps: (1) the iron is dissolved by treatment with a copper(II) solution [$Fe(s) + Cu^{2+} \rightarrow Fe^{2+} + Cu(s)$] and (2) the copper precipitated is dissolved in aqueous ammonia in the presence of ammonium salts and an oxidant. The residue then contains the second phases and other substances insoluble in these reagents.

Dissolution of the iron matrix

Steel samples are frequently covered by a thin oxide layer. This layer must be removed before precipitation of copper starts. Copper(II) is a weak acid, so that the Cu^{2+} salts of strong acids form solutions with low pH values (e.g. for a saturated solution of $CuSO_4$ at 25°C, the pH is about 2.5); this may be enough to dissolve the oxide layer. However, these salt solutions can be employed only when acid-resistant phases (such as Si_3N_4, BN) are present. In most other cases, the salts of organic acids, e.g. a saturated solution of copper acetate at 25°C (pH ≈ 6), have been found to be suitable.

To remove the oxide layer, the steel samples have then to be treated very briefly with dilute acid. For the copper precipitation to proceed rapidly, the sample should be in the form of a powder, but compacted samples may also be used. The copper precipitated on the surface is removed by scraping and/or by ultrasonic action.

Dissolution of the copper

The precipitated copper is dissolved in ammonia mainly as the $Cu(NH_3)_4^{2+}$ complex. The solution formed is the well-known Schweizer's reagent [4]. The metal is dissolved only in the presence of oxygen or oxidizing agents; as reported, copper powder in an ammoniacal solution can be oxidized by direct action of oxygen or, more suitably, by ammonium persulphate. The excess of oxygen may oxidize the solution itself (nitrite formation). The solution can be stabilized against oxidation by addition of sucrose (ca. 1 g l^{-1}), which is reported also to increase the rate of dissolution of copper. Generally, the solution can be further stabilized by excess of ammonia and by decreased temperature. The solubility of copper in aqueous ammonia increases with decreasing temperature. At 15°C, ca. 5—12 M NH_3 solution seems to give highest solubility (about 10 g Cu l^{-1} for 11.5 M NH_3 [4]). Addition of ammonium salts increases the solubility considerably. The ammoniacal copper solution is of course less basic than concentrated alkali or alkaline earth hydroxide solutions. Most of the second phases should not be attacked by this solution to any significant extent.

Separation of an Mn—Si—Fe alloy

The method was tested on a powdered 10Mn—10Si—Fe alloy (typical grain size, ca. 20 μm) nitrided for ca. 20 h in pure nitrogen. The phases identified by x-ray analysis after nitriding were α-Fe and orthorhombic $MnSiN_2$; some unreacted manganese and silicon were also present. More details on the nitriding process will be given elsewhere.

The powder (ca. 1 g) was treated with either saturated copper sulphate or copper acetate solution at room temperature for ca. 1 h. During the precipitation of copper, the solutions were kept continuously in an ultrasonic cleaner (Sharp UT-52) to remove copper deposited on the grains of the alloy. The precipitate (copper and the second phases) were then washed with distilled water.

To dissolve the copper metal, an ammoniacal solution was prepared by dissolving ammonium nitrate (ca. 15 M) in ammonia liquor at about 15°C; considering the data for the system NH_4NO_3—NH_3—H_2O [5], the solution was made ca. 12 M with respect to ammonia. A saturated solution of ammonium persulphate (15°C) in ca. 12 M ammonia proved a suitable oxidant; during the copper dissolution, the temperature was kept below 15°C to prevent the spontaneous decomposition of the oxidant and to stabilize the solution. The copper precipitate could be dissolved completely within 30—60 min. It also proved possible to use a ca. 1 M hydrogen peroxide

solution. The solution then had to be kept in an ice bath to minimize decomposition of the peroxide in contact with the fine precipitate. Complete dissolution of copper was then achieved within ca. 3 h.

The residue was washed repeatedly with distilled water. The unreacted silicon present in the alloy appeared to have been oxidized to SiO_2, which formed a stable suspension easily separated from the nitride phase residue by a series of sedimentation—decantation steps. The residue was dried at 140°C. Examination under an optical microscope showed that it was a homogeneous phase with a grain size of about 1 μm. X-ray diffraction analysis indicated orthorhombic $MnSiN_2$. The amount of the residue corresponded to 97 ± 2% of the nitrogen bound as $MnSiN_2$ which was originally taken up by the alloy. The nitride phase could thus be recovered quantitatively from this alloy.

Another powdered alloy (typical grain size, 200 μm, i.e. about ten times larger than the previous one) was also nitrided, and the same isolation procedure was employed. Examination by x-ray diffraction, i.r. spectroscopy and optical microscopy suggested the presence of grains of amorphous silica in the residue. The silica phase may be difficult to separate from the second nitride phases. In such cases, thermal methods of analysis [3] seem to be suitable for determination of the nitrogen in the residue.

This work formed part of a project on nitrides in steel supported financially by the Swedish Board for Technical Development (Contr. No. EKB-U-287-76/77).

REFERENCES

1 H. F. Beeghly, Anal. Chem., 21 (1949) 1513.
2 W. Koch and H. Sundermann, Arch. Eisenh., 38 (1957) 557.
3 P. H. Scholes and G. White, Steel Times Ann. Rev., (1970) 172.
4 Gmelin, Syst. nr. 60, Kupfer, 8:e Aufl., Teil B, Lief. 1, 118.
5 Gmelin, Syst. nr. 23, Ammonium. 8:e Aufl., 131.

Analytica Chimica Acta, 97 (1978) 423—426

Short Communication

THE COMPLEX EQUILIBRIA BETWEEN BERYLLIUM(II) AND 5-HYDROXYSALICYLIC ACID IN AQUEOUS SOLUTION

LAURI H. J. LAJUNEN* and MIKKO KARVO
Department of Chemistry, University of Oulu, SF-90100 Oulu 10 (Finland)
(Received 24th October 1977)

Salicylic acid and its derivatives are classical ligands in research on complex equilibria, but there are few reports on the complex formation of the 3-, 4-, 5-, and 6-hydroxy derivatives of salicylic acid [1]. The present communication describes a study of beryllium(II) complex formation with 5-hydroxysalicylic acid in aqueous solution under constant conditions, $I = 0.5$ ($NaClO_4$) and 25°C, by a potentiometric method. In addition, the protonation of the ligand anion has been examined.

Experimental

Reagents. 5-Hydroxysalicylic acid (99.9%; E. Merck) was recrystallized several times from hot water before use.

Be^{2+} solutions were prepared from the corresponding nitrate (E. Merck).

Apparatus and methods. The titrations were carried out with an automatic digital titration system (Radiometer), in which a TTT61 digital titrator was connected to a PHM64 pH meter and an ABU13 Autoburette. A Beckman N40495 glass electrode was used as indicator electrode with a calomel reference electrode, in which the electrolyte was 0.5 M NaCl solution. The pure concentration titrations were carried out automatically and the titrations for calculating the constants manually.

The concentrations of the ligand acid and beryllium(II) ions were varied between 1×10^{-3} and 1×10^{-2} M. Several different titrations were carried out, in which the titrant was either 0.1 M NaOH or partly neutralized 5-hydroxysalicylic acid solution. Both the titrant solutions were 0.5 M in $NaClO_4$.

Further details of the methods (including the calibration of the potentiometer) are reported elsewhere [2].

Calculations. The protonation constants of the ligand anion and the stability constants of the beryllium(II) complexes were computed with the programme MINIQUAD [3] as overall stability constants β_{qpr}. The stability constant of a general binary complex $M_qH_pL_r$ is defined by

$$\beta_{qpr} = [M_qH_pL_r]/[M]^q[H]^p[L]^r \quad (1)$$

where square brackets indicate the concentrations of the free metal, hydrogen and ligand ions.

By a least-squares refinement, the stability constants with their standard deviations were obtained along with an agreement index R

$$R = [\sum_i (f_i^{obs} - f_i^{calc})^2 / \sum_i (f_i^{obs})^2]^{1/2} \quad (2)$$

In addition, the calculations also gave a χ^2 statistic which is a measure of the conformity to normal distribution of the residuals $(f_i^{obs} - f_i^{calc})$.

All the data pertain to an aqueous solution of ionic strength 0.5 (total perchlorate) at 25.0 ± 0.1°C.

Results

It is well known that salicylic acid dimerizes in concentrated aqueous solutions. Dimerization begins [4] when the total concentration exceeds 0.01 M (at I = 3 ($NaClO_4$) and 25°C). It is chemically quite reasonable that 5-hydroxysalicylic acid should also dimerize in aqueous solution. In the present titrations, the concentration of the ligand acid was limited to 0.001—0.010 M. The possible polymerization of 5-hydroxysalicylic acid in this concentration range was checked via the experimental values of the $\bar{n}_H$ function [5]. Figure 1 shows that $\bar{n}_H$ is a function of $-\log[H^+]$ under the conditions used; thus dimerization is negligible and the protonation of 5-hydroxysalicylic acid can be described by three parameters, K_1, K_2 and K_3, when the concentration does not exceed 0.01 M.

Okac et al. [6] studied the protonation of 5-hydroxysalicylic acid potentiometrically in an aqueous solution at ionic strength 0.1, and reported the following values for the protonation constants: $\log K_1 > 12$,

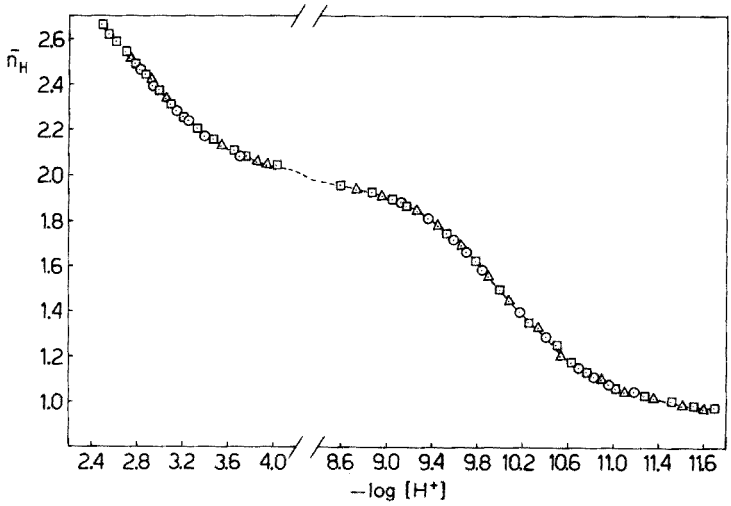

Fig. 1. Some experimental values of $\bar{n}_H$ versus $-\log[H^+]$ for 5-hydroxysalicylic acid at I = 0.5 ($NaClO_4$) and 25°C. $\bar{n}_H$ (expl.) = $[C_H - ([H^+] - K_w[H^+]^{-1})]/C_L$. C_L = 2.67 mM (○), 5.34 mM (△) or 13.34 mM (□).

log K_2 = 10.50, and log K_3 = 2.97. In the present work the values log K_1 = 12.74 (±0.02), log K_2 = 9.995 (±0.004), and log K_3 = 2.731 (±0.002) were obtained at I = 0.5 ($NaClO_4$) and 25°C (the values in parentheses are the standard deviations for 5 determinations).

At pH values below 7, the formation of beryllium complexes with 5-hydroxysalicylic acid greatly resembles that of Be^{2+} ions with salicyclic acid [7], and can be described successfully by two parameters, β_{111} and β_{122}. The corresponding complexation reactions are

$$Be^{2+} + H_3L = BeHL + 2H^+ \quad (3)$$

$$BeHL + H_3L = BeH_2L_2^{2-} + 2H^+ \quad (4)$$

Above pH 7, the dissociation of the protons of the hydroxyl groups in the C-5 position begins, and the following reactions can be assumed to occur

$$BeHL = BeL^- + H^+ \quad (5)$$

$$BeH_2L_2^{2-} = BeHL_2^{3-} + H^+ \quad (6)$$

$$BeHL_2^{3-} = BeL_2^{4-} + H^+ \quad (7)$$

The amount of the species BeL^- was so small in the titrations that the equilibrium of reaction (5) could not be determined. Reactions (6) and (7) occurred at pH values above 7, when an excess of the ligand was present in the solution. The formation of beryllium(II)—5-hydroxysalicylate complexes is illustrated in Fig. 2, for three different pH values.

The values log β_{111} = 21.839 (±0.002), log β_{122} = 41.347 (±0.004), log β_{112} = 31.409 (±0.017), and log β_{102} = 20.972 (±0.012), were obtained for the logarithms of the overall stability constants of the $BeHL$, BeH_2L_2, $BeHL_2$, and BeL_2 complexes, respectively, at I = 0.5 ($NaClO_4$) and 25°C. The criterion of the validity of these constants is based on the smallness of the standard deviations, the agreement index R, and the χ^2 statistics. The inclusion of any species other than the four reported in the calculations was unsuccessful.

β_{111} and β_{122} were computed from about 50 points of each titration curve where pH was between 3.5 and 6.5, and β_{112} and β_{102} similarly from about 50 points where the pH was between 8.5 and 11. The values of R and χ^2 varied in the first set of calculations between 0.0003 and 0.0005, and 2.5 and 8.6, respectively, and in the second set of calculations between 0.001 and 0.003, and 5.4 and 11.6, respectively. The values of χ^2 should be less than 12.6 at the 95% confidence level for 6 degrees of freedom [8].

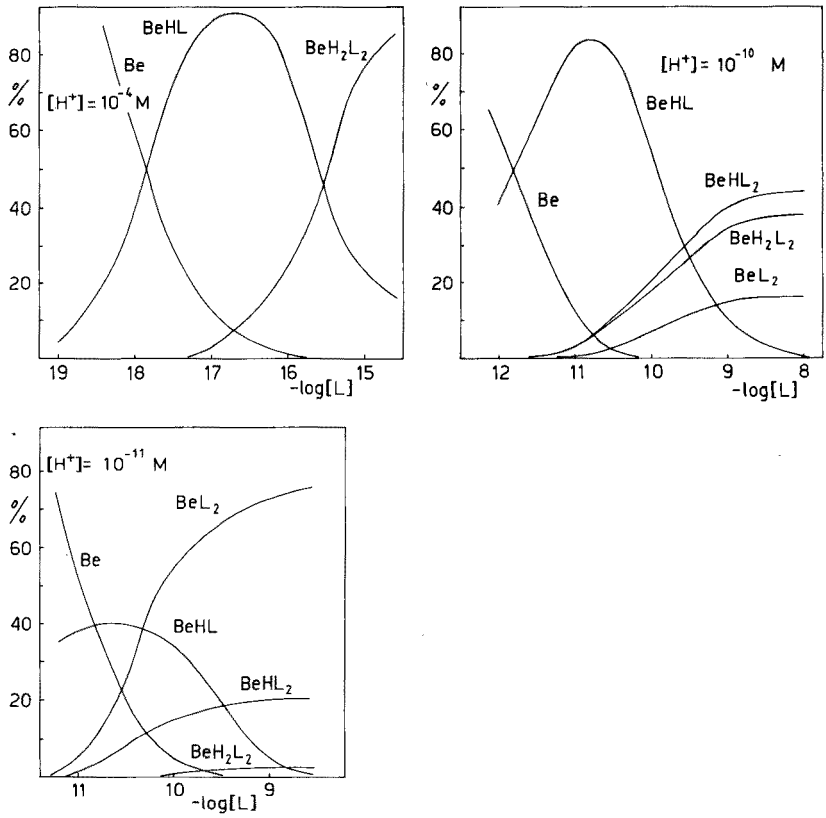

Fig. 2. The relative amounts of the different complex species in the beryllium(II)–5-hydroxysalicylic acid system at three different values of free hydrogen ion concentration.

The financial support of the Magnus Ehrnrooth Foundation is gratefully acknowledged by L. L.

REFERENCES

1 Stability Constants of Metal Ion Complexes, Spec. Publ. No. 25, The Chemical Society, London, 1971.
2 L. H. J. Lajunen, Ann. Acad. Sci. Fenn. Ser., A II 179 (1976).
3 A. Sabatini, A. Vacca and P. Gans, Talanta, 21 (1974) 53.
4 Y.-H. Lee and G. Lundgren, Contributions to Coordination Chemistry in Solution, Transactions of the Royal Institute of Technology, Stockholm, Sweden, 1972, p. 247.
5 H. S. Rossotti, Talanta, 21 (1974) 813.
6 J. Tsin-jao, L. Sommer and A. Okac, Collect. Czech. Chem. Commun., 27 (1962) 1171.
7 H. J. DeBruin, D. Kaitis and R. B. Temple, Aust. J. Chem., 15 (1962) 457.
8 A. Sabatini and A. Vacca, Coord. Chem. Rev., 16 (1975) 161.

Analytica Chimica Acta, 97 (1978) 427—431

Short Communication

A NEW DEVICE FOR IMPROVING SENSITIVITY AND STABILIZATION IN FLOW-INJECTION ANALYSIS

H. BERGAMIN F°*, B. F. REIS and E. A. G. ZAGATTO

Centro de Energia Nuclear na Agricultura, Cx. Postal 96, 13400 Piracicaba, S.P. (Brasil)

(Received 26th August 1977)

The flow-injection approach to automation of chemical analyses, based on the original idea of Růžička and Hansen [1], has been successfully applied to determinations of phosphate [2], nitrogen [3], chloride [4], nitrite [5] and sulphate [6] in natural waters or predigested plant material. Good sensitivity, high speed and reproducibility are the main advantages of the technique. Up to 250 determinations per hour have been attained in the routine analysis of waters and plant material in this laboratory.

In flow-injection analysis, an aqueous sample is injected into a continuously moving carrier stream of reagent; the sample, in a well-defined zone, reacts in the carrier stream to form a species which is quantitatively measured in a flow-through detector. However, if the sample injection is done by forcing the liquid into the carrier stream, the regularity of the flow is disturbed momentarily. Thus, there is a temporary difference in mixing ratios at those points in the manifold where two streams meet; this can cause a change in the blank values (a) when the difference in refractive index between the reagent and sample is high, and (b) when the reagent absorbs significantly at the wavelength used. In case (a), the mixing boundary formed will cause a high blank value [3, 5, 6]. In case (b), peaks corresponding to very dilute samples will be distorted or even negative peaks may appear [7]. To minimize these phenomena while increasing sensitivity, a confluence manifold [7] was used for the spectrophotometric and/or turbidimetric determination of nitrite, sulphate and chloride in natural waters. In this communication, an injection pulse dampener is reported; this device is particularly recommended when flow-injection confluence systems are employed for analysis of very dilute samples.

Experimental

Instrumentation. The samples were injected manually with 1-ml plastic syringes without needles. The injection valve had a dead volume of 3 μl [4] and was included on a plastic tube through which the carrier stream was pumped. This valve and the Y-shaped or straight connectors were made from perspex blocks. The manifolds were made of polyethylene (0.85-mm i.d.)

tubing of the non-collapsible wall type. The resistor coil had an internal diameter of 0.5 mm. Mixing coils were made by winding the required lengths of plastic tube round a suitable support. All components were fixed on a baseplate by means of plastic blocks [1].

The injection pulse dampener (Fig. 1) was made from glass and had an inner volume of ca. 25 cm^3. During operation, the bulb remains partly filled with air, which acts as a damper.

The apparatus consisted of a Technicon AA II peristaltic pump with tygon tubes, a model 25 spectrophotometer connected to a model 24 25 ACC recorder (both Beckman Inc. Fullerton) with a Hellma flow-through cuvette, type 178, light path 10 mm, volume 0.08 ml. The dual beam mode was used with the reagent solution serving as a blank. Absorbances were measured at 535 nm and 480 nm for the nitrite and chloride determinations respectively; turbidity was measured at 480 nm.

The flow-injection systems for chloride [4], nitrite [5] and sulphate [6] determinations are all limited in sensitivity by the characteristics mentioned above. The flow diagrams of the systems used for this work are presented in Fig. 2.

Reagents. All chemicals used were analytical grade. The carrier stream reagents and the standard solutions were the same as used previously [4–6].

Results and discussion

Straight configuration. When a very dilute sample is injected into an absorbing carrier stream reagent, distorted or even negative peaks can occur. Figure 3a shows such peaks for aqueous samples containing less than 5 ppm of chloride, injected into the chloride colour reagent, which absorbs significantly at 480 nm. An example of high blanks arising from a mixing boundary when the sample and reagent have different refractive indexes is shown in Fig. 4, curve a; here the high blank is due mainly to the phosphoric acid in the nitrite colour reagent [5]. A similar phenomenon appears in the turbidimetric sulphate procedure [6], the high blank value arising from the barium chloride in the carrier stream. The straight configuration

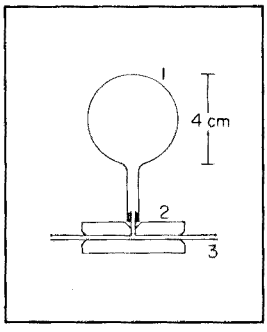

Fig. 1. Schematic representation of the injection pulse dampener. Numbers 1, 2 and 3 correspond to glass, perspex and polyethylene respectively.

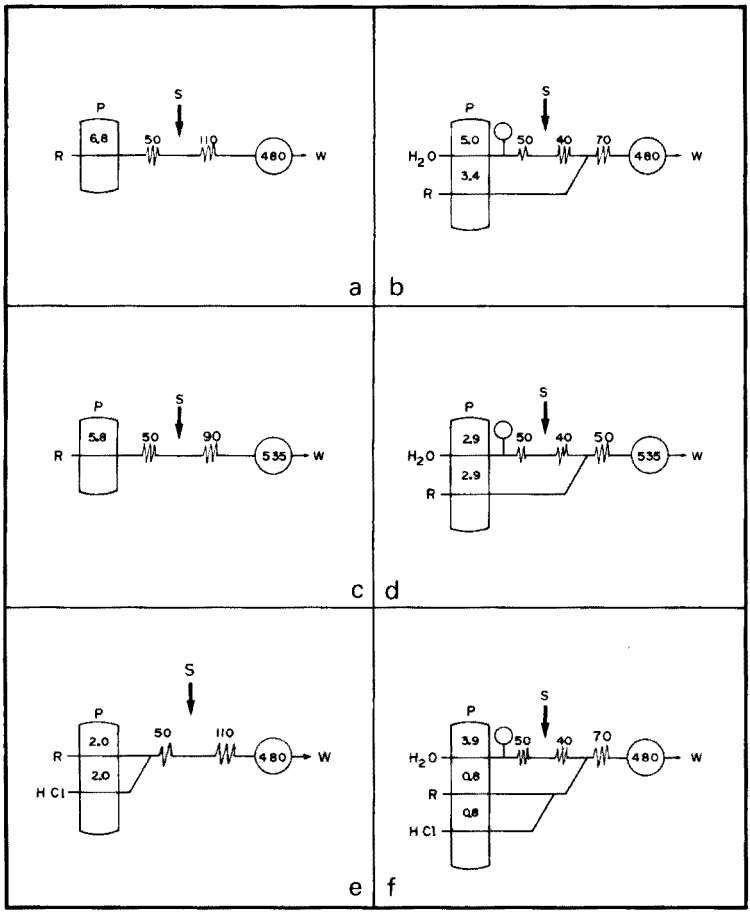

Fig. 2. Flow diagrams for chloride (a, b), nitrite (c, d) and sulphate (e, f) determinations, in normal (a, c, e) and confluence (b, d, f) configuration. R is the reagent used, P is the peristaltic pump with indication of the flow in ml min^{-1}, S is the point of sample injection (0.4 ml), and W denotes waste. The numbers on the coils represent lengths in cm and the numbers inside the flow cell indicate wavelength (nm). In the confluence system the injection pulse dampener is placed immediately after the pump and the resistor coil immediately after the injection point.

is thus recommended only when the samples are sufficiently concentrated or when the reagent does not show the above-mentioned characteristics.

Confluence configuration. Figure 3b shows that better peak shape is obtained with the confluence configuration. The blank values decrease (cf. Fig. 4, curve b), mainly because the very dilute aqueous samples are injected into water, and not into the reagent flow. At the confluence point, the dilution effect is attenuated by the better conditions of mixing between sample and reagent. The slopes of the nitrite calibration curves remain

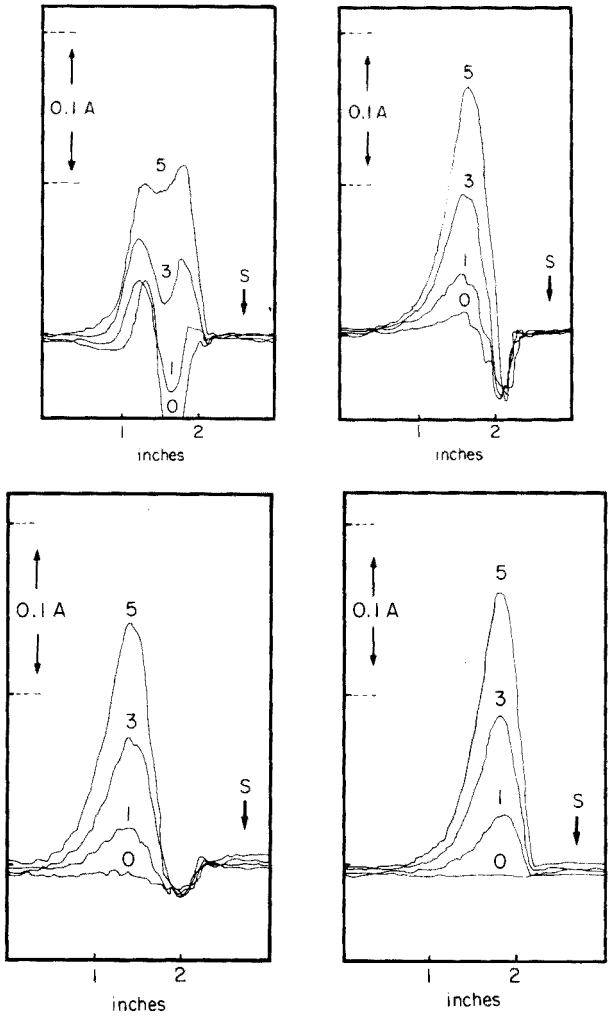

Fig. 3. Recorded high speed peaks for aqueous standards containing 5, 3, 1 and 0 ppm of chloride. (a) Straight configuration. (b—d) Simple confluence configuration. The action of the injection pulse dampener alone and together with the resistor coil is shown in (c) and (d), respectively. Paper speed: 12s/in. S represents sample injection.

much the same when the configuration is changed (Fig. 4). Of course, the ratio of the two confluent flows can be controlled, but a compromise is always needed.

Injection pulse dampener. The injection of a sample causes a transient change in the ratio of the confluent fluxes, resulting in a sharp irreproducible peak just before the main peak. This initial peak — negative for an absorbing reagent (Fig. 3b) or positive in the case of nitrite and sulphate — makes measurement of the sample peak difficult. The decrease in this initial peak when the injection pulse dampener is used in the chloride determination, is

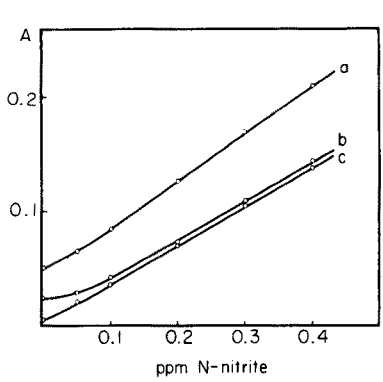

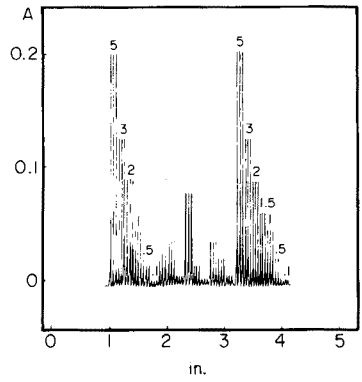

Fig. 4. Standard curves for the nitrite flow-injection systems. a relates to the straight configuration, and b and c to the confluence configuration without (b) or with (c) the use of the injection pulse dampener.

Fig. 5. Routine run for chloride in nine rain waters. The samples were preceded and succeeded by standards; all determinations were made in triplicate. The calibration curve was prepared for the flow diagram depicted in Fig. 2b. The numbers correspond to ppm of chloride. Paper speed: 0.1 in/min.

shown in Fig. 3c. This device also improves the nitrite determination; the blank value reading nearly disappears (Fig. 4c).

Resistor coil. The transient increase in the pressure caused by injection is distributed along the flow, and despite the pressure dampener, reaches the cuvette causing a small disturbance (Fig. 3c and Fig. 4c). To avoid this disturbance and to improve the sensitivity, it was decided to increase the resistance to the flow in the coil after the injection point, directing the volume of the injected sample towards the injection pulse dampener. This was done using a 0.5-mm i.d. tubing instead of the normal 0.85 mm i.d. in the 40-cm coil. Figure 3d shows the effect of the resistor coil in the chloride determination. In the nitrite and sulphate determinations, use of this coil gave little practical benefit, because in these cases the blank reading was already close to zero.

The system described is being used in routine determinations of chloride, nitrite and sulphate in water. Figure 5 shows a routine run of several rain water samples for chloride. Obviously, levels of chloride below 1 ppm can be measured with very good reproducibility.

REFERENCES

1 J. Růžička and E. H. Hansen, Anal. Chim. Acta, 78 (1975) 145.
2 J. Růžička and J. W. B. Stewart, Anal. Chim. Acta, 79 (1975) 79.
3 J. W. B. Stewart, J. Růžička, H. Bergamin F° and E. A. G. Zagatto, Anal. Chim. Acta, 81 (1976) 371.
4 J. Růžička, J. W. B. Stewart and E. A. G. Zagatto, Anal. Chim. Acta, 81 (1976) 387.
5 S. S. Jorgensen, H. Bergamin F°, E. A. G. Zagatto, F. J. Krug and S. R. B. Bringel, Bol. Cient. 047 CENA (1977).
6 F. J. Krug, H. Bergamin F°, E. A. G. Zagatto and S. S. Jorgensen, Analyst, 102 (1977) 503.
7 J. Růžička, E. H. Hansen and E. A. G. Zagatto, Anal. Chim. Acta, 88 (1977) 1.

ANALYTICA CHIMICA ACTA, VOL. 97 (1978)

AUTHOR INDEX

(continued from outside of cover)

Short Communications

Printed in The Netherlands

VOL. 97 No. 2 ANALYTICA CHIMICA ACTA APRIL 1, 1978

CONTENTS

(continued on inside of cover)